

Kinematic Wave Models of Network Vehicular Traffic

By

Wenlong Jin

B.S. (University of Science and Technology of China, Anhui, China) 1998

M.A. (University of California, Davis) 2000

DISSERTATION

Submitted in partial satisfaction of the requirements for the degree of

DOCTOR OF PHILOSOPHY

in

APPLIED MATHEMATICS

in the

OFFICE OF GRADUATE STUDIES

of the

UNIVERSITY OF CALIFORNIA

DAVIS

Approved:

Dr. H. Michael Zhang

Dr. Elbridge Gerry Puckett

Dr. Zhaojun Bai

Committee in Charge

September 2003

Wenlong Jin
September 2003
Applied Mathematics

Kinematic Wave Models of Network Vehicular Traffic

Abstract

The kinematic wave theory, originally proposed by (Lighthill and Whitham, 1955b; Richards, 1956), has been a good candidate for studying vehicular traffic. In this dissertation, we study kinematic wave models of network traffic, which are expected to be theoretically rigorous, numerically reliable, and computationally efficient.

For inhomogeneous links, we reformulate the Lighthill-Whitham-Richards model into a nonlinear resonant system. In addition to shock and rarefaction waves, standing (transition) waves appear in the ten basic wave solutions. The solutions are consistent with those by the supply-demand method (Daganzo, 1995a; Lebacque, 1996).

For merging traffic, we examine existing supply-demand models and, particularly, distribution schemes. Further, we propose a new distribution scheme, which captures key merging characteristics and leads to a model that is computationally efficient and easy to calibrate.

For diverging traffic, we propose an instantaneous kinematic wave model, consisting of nonlinear resonant systems. After studying the seven basic wave solutions, we show that this model is equivalent to a supply-demand model with modified definitions of traffic demands.

For traffic with mixed-type vehicles, we show the existence of contact waves. Using simulations by the developed Godunov method, we demonstrate that First-In-First-Out (FIFO) principle is observed in this model.

For network traffic flow, we propose a multi-commodity kinematic wave (MCKW) model, in which we combine kinematic wave models of different network components and a commodity-based kinematic wave theory. We also propose an implementation of the MCKW simulation and carefully design the data structure for network topology, traffic characteristics, and simulation algorithms. The solutions are consistent with FIFO principle in the order of a time interval.

For a road network with a single origin-destination (O/D) pair and two routes, we first demonstrate the formation of an equilibrium state and find multiple equilibrium status for different route distributions. We then show the formation of periodic oscillations and discuss their structure and properties.

Finally, we summarize our work and discuss future research directions.

Acknowledgements

I owe many thanks to my wife, Ling. Her selfless support and encouragement is indispensable to the completion of this dissertation. In particular, she brings me the best gift for ever, our baby Laurel, who makes my life more joyful than ever. I also want to thank my family in China, including my parents, sister, and brothers. They have been a constant source of encouragement and support for me.

I'm very grateful to my advisor, Dr. Michael Zhang, for his financial support and academic guidance. Four years ago, he introduced me to the wonderful land of transportation studies. Since then, I've worked on several projects on traffic flow models and ramp metering methods. I always enjoy discussing research questions with him and have been inspired by his advices all the time. During these years when I work with him, he gave me many helpful suggestions on research and career development.

I'm also grateful to Dr. Elbridge Gerry Puckett, my academic advisor and a committee member of my dissertation. He spent a great deal of time in answering all kinds of questions about study and research. His careful revisions to my master thesis and this dissertation have helped me a lot on efficient technical writings. His comments on my research and career development will continue to influence my research in the future. He also introduced me to his colleagues, including Dr. Randall J. LeVeque and Dr. Phillip Colella, to whom I also owe my thanks for their interests

in my research.

I'm also grateful to Dr. Zhaojun Bai for serving on the committee of this dissertation and his supportive and encouraging comments on my career development.

I'd like to thank Dr. John Hong for introducing the concept of resonant nonlinear waves, which form a foundation of the kinematic wave theories of inhomogeneous links (Chapter 2) and diverges (Chapter 4). I'd also like to thank Dr. Blake Temple, who generously offered many suggestions on my studies of vacuum problems and merging and diverging models. His research results in resonant nonlinear waves is a key reference in my studies.

Thanks go to Dr. Albert Fannjiang, for his comments and suggestions on my study, research and career, and Dr. Carlos Daganzo, for his suggestions on my research directions.

Thanks go to my fellow classmate, Scott Beaver, for his friendliness and help.

I also owe my thanks to many other colleagues who are not mentioned above but have also contributed to this dissertation in different aspects.

Finally, I offer my sincere thanks the University of California Transportation Center for their financial support through a dissertation grant.

Contents

1	Introduction	1
1.1	Background	1
1.1.1	Traffic congestion	1
1.1.2	The role of traffic models	2
1.1.3	Traffic models and simulation packages	5
1.2	Continuum models	6
1.2.1	Kinematic wave models	6
1.2.2	Higher-order models	10
1.3	Fundamental diagrams	12
1.4	Motivation for the dissertation research	14
2	Kinematic wave traffic flow model of inhomogeneous links	17
2.1	Introduction	17
2.2	Properties of the inhomogeneous LWR model as a resonant nonlinear system	21
2.3	Solutions to the Riemann problem	23
2.3.1	Solutions of the boundary fluxes	25
2.3.2	Summary	40
2.4	Simulation of traffic flow on a ring road with a bottleneck	43
2.4.1	Solution method	43

2.4.2	Numerical results	44
2.5	Concluding remarks	49
3	Kinematic wave traffic flow model of merging traffic	51
3.1	Introduction	51
3.2	The discrete kinematic wave model of merges with the supply-demand method	55
3.2.1	The discrete LWR model in the supply-demand framework . .	56
3.2.2	The kinematic wave model of merging traffic in the supply-demand framework	59
3.3	Investigation of various distribution schemes	63
3.3.1	Discussion of existing distribution schemes	64
3.3.2	A simple distribution scheme and its interpretation	66
3.3.3	Properties of the discrete kinematic wave model of merges with the simplest distri	
3.4	Numerical simulations	71
3.4.1	Simulation of merging traffic without control	74
3.4.2	Simulation of merging traffic when the on-ramp is controlled .	76
3.4.3	Computation of convergence rates	78
3.5	Discussions	79
4	Kinematic wave traffic flow model of diverging traffic	83
4.1	Introduction	83
4.2	A kinematic wave theory for diverges	86
4.2.1	The kinematic wave theory of single-commodity traffic flow . .	87
4.2.2	The kinematic wave theory of multi-commodity traffic flow . .	88
4.2.3	A kinematic wave theory of diverging traffic	89
4.3	The instantaneous kinematic waves	91
4.3.1	The properties of Equation 4.12 as a nonlinear resonant system	93
4.3.2	The instantaneous kinematic waves of Equation 4.12 with Equation 4.13	95

4.4	The supply-demand method with a new definition of traffic demand	103
4.5	Numerical simulations	106
4.5.1	Simulation I: A general case	108
4.5.2	Simulation II: An extreme case	110
4.6	Discussions	112
5	Kinematic wave traffic flow model for mixed traffic	113
5.1	Background	113
5.2	The extended KW model for mixed traffic	116
5.3	The Riemann problem and basic wave solutions	119
5.4	Fundamental diagrams for mixed traffic	121
5.5	Numerical solution method and simulations	123
5.5.1	The Godunov method	123
5.5.2	Numerical simulations	125
5.6	Concluding remarks	127
6	Kinematic wave simulation model for multi-commodity network traffic flow	132
6.1	Introduction	132
6.2	Underlying theories of the MCKW simulation model	136
6.2.1	Kinematic wave theories at the aggregate level	136
6.2.2	Commodity-based kinematic wave theories	140
6.3	Network structure, data structure, and program flow-charts in the MCKW simulation pla	
6.3.1	Network structure	144
6.3.2	Data structure	145
6.3.3	Program flow-chart	150
6.4	Cumulative flow, travel time, and other properties of a road network	153
6.4.1	Cumulative flow and vehicle identity	153

6.4.2	Travel time	154
6.5	Numerical simulations	157
6.5.1	Simulation set-up	157
6.5.2	Traffic patterns on the road network	158
6.5.3	Convergence of the MCKW simulation model	162
6.6	Discussions	164
7	Studies of network vehicular traffic with kinematic wave simulations	165
7.1	Introduction	165
7.2	Equilibrium states of a road network and preliminary examination of traffic assignment	166
7.2.1	The simulated network	167
7.2.2	Equilibrium states	168
7.2.3	Travel times at equilibrium states	172
7.2.4	Discussions	174
7.3	The formation and structure of periodic oscillations in the kinematic wave model of road	
7.3.1	Network for studying periodic solutions	176
7.3.2	Periodic oscillations	178
7.3.3	The structure of periodic solutions	182
7.3.4	Discussions	184
7.4	Conclusions	185
8	Conclusions	187
8.1	Summary	187
8.2	Future research directions	190
8.2.1	Further investigations of the kinematic wave theories	190
8.2.2	Calibration, validation, and enhancement of the MCKW simulation model	191
8.2.3	Applications of the MCKW simulation model	192

List of Tables

1.1	Traditional speed-density relationship functions	14
2.1	Solutions of the boundary fluxes f_0^*	41
2.2	Comparison with Lebacque's results	42
3.1	Convergence rates of the discrete merge model	80
4.1	Solutions of the boundary flux $q(x = 0, t > 0)$	106
5.1	Shock wave solutions in mixed traffic	124
5.2	Rarefaction wave solutions in mixed traffic	125
6.1	Total travel time (TTT) and average travel time (ATT) for two commodities	161
6.2	Convergence rates for the MCKW simulation platform	163
7.1	Equilibrium density and flow-rate v.s. ξ	172
7.2	Equilibrium speed and travel times v.s. ξ	174
7.3	Constraints on equilibrium states	178

List of Figures

1.1	The definition and role of traffic models in traffic studies	4
1.2	A typical occupancy-flow rate relationship (Hall et al., 1986)	13
2.1	Integral curves	24
2.2	The Riemann problem for U_L left of Γ	26
2.3	The Riemann problem for U_L right of Γ	27
2.4	An example for wave solutions of type 1 for Equation 2.5 with initial conditions Equation	
2.5	An example for wave solutions of type 2 for Equation 2.5 with initial conditions Equation	
2.6	An example for wave solutions of type 3 for Equation 2.5 with initial conditions Equation	
2.7	An example for wave solutions of type 4 for Equation 2.5 with initial conditions Equation	
2.8	An example for wave solutions of type 5 for Equation 2.5 with initial conditions Equation	
2.9	An example for wave solutions of type 6 for Equation 2.5 with initial conditions Equation	
2.10	An example for wave solutions of type 7 for Equation 2.5 with initial conditions Equation	
2.11	An example for wave solutions of type 8 for Equation 2.5 with initial conditions Equation	
2.12	An example for wave solutions of type 9 for Equation 2.5 with initial conditions Equation	
2.13	An example for wave solutions of type 10 for Equation 2.5 with initial conditions Equatio	
2.14	The Kerner-Konhäuser model of speed-density and flow-density relations	45
2.15	Initial condition Equation 2.33 with $\rho_h = 28$ veh/km and $\Delta\rho_0 = 3$ veh/km	46
2.16	Solutions of the homogeneous LWR model with initial condition in Figure 2.15	47

2.17	Initial condition Equation 2.33 with $\rho_h = 28$ veh/km/lane and $\Delta\rho_0 = 3$ veh/km/lane	48
2.18	Solutions of the inhomogeneous LWR model with initial condition in Figure 2.17	50
3.1	Feasible solutions in Daganzo's supply-demand method	61
3.2	Feasible solutions in Lebacque's supply-demand method	62
3.3	Solutions of flows in Daganzo's distribution scheme	65
3.4	Solutions of flows in the simple distribution scheme	67
3.5	The triangular fundamental diagrams for the mainline freeway and the on-ramp	73
3.6	Simulation of merging traffic without control	76
3.7	Simulation of merging traffic with on-ramp control	77
4.1	Integral curves in (ρ, k) -space	96
4.2	The Riemann solutions when U_L is UC	97
4.3	The Riemann solutions when U_L is OC	98
4.4	An example for wave solutions of type 1 for Equation 4.12 with initial conditions Equation	
4.5	An example for wave solutions of type 2 for Equation 4.12 with initial conditions Equation	
4.6	An example for wave solutions of type 3 for Equation 4.12 with initial conditions Equation	
4.7	An example for wave solutions of type 4 for Equation 4.12 with initial conditions Equation	
4.8	An example for wave solutions of type 5 for Equation 4.12 with initial conditions Equation	
4.9	An example for wave solutions of type 6 for Equation 4.12 with initial conditions Equation	
4.10	An example for wave solutions of type 7 for Equation 4.12 with initial conditions Equation	
4.11	The Newell model of speed-density and flow-density relations	107
4.12	Simulation I: A general case	109
4.13	Simulation II: An extreme case	111
5.1	Phase diagram for determining elementary and simple waves	122
5.2	Wave solutions to the Riemann problem: Shock + Contact wave (left) and Expansion wa	
5.3	The extended triangular fundamental diagram	129

5.4	Contour plots of solutions on the $x - t$ space with the extended triangular fundamental d	
5.5	Contour plot of ρ_2/ρ_1 on the $x - t$ space with the extended triangular fundamental diagram	
6.1	A demonstration road network	144
6.2	Data structure in the MCKW mckw platform	146
6.3	The program flow chart in the MCKW simulation	151
6.4	Cumulative flows and travel time	155
6.5	Contour plots of network traffic flow	159
6.6	N-curves and travel times of each commodity in the road network . .	162
7.1	Network for studying equilibrium state and traffic assignment	167
7.2	Solutions when $\xi = 0.5$	170
7.3	Solutions when $\xi = 0.6$	171
7.4	Solutions when $\xi = 0.4$	173
7.5	Travel times at equilibrium states v.s. proportion ξ	175
7.6	Network for studying periodic oscillations	177
7.7	Contour plots of periodic oscillations	180
7.8	Density, flow-rate, and speed at the end of link 2, start of link 3, and start of link 4	181
7.9	Periodic solutions at the end of link 2, start of link 3, and start of link 4 in the (ρ, q) -plane	
7.10	Structure of periodic solutions on link 2	184

Chapter 1

Introduction

1.1 Background

1.1.1 Traffic congestion

As the backbone of the intermodal transportation network in the United States, road networks - consisting of highways, arterial roads, surface streets, and other kinds of roadways - connect air, transit, rail, and port facilities and terminals. In particular, highways carry 90 percent of passenger travel and 72 percent value of freight. Therefore, the performance of its road networks largely defines the mobility of the nation and affects economic and social activities in the United States. However, traffic conditions on road networks in many metropolitan areas are becoming increasingly congested: in 68 major American urban areas, the percentage of un-congested periods was two thirds of the whole peak period in 1982, while the percentage drops to one third in 1997 (Schrank and Lomax, 1999).

In a road network, traffic congestion can be recurrent and non-recurrent. Recurrent traffic congestion is generally caused by limited physical infrastructure, increasing

travel demand, rush hours, and toll booths. Non-recurrent congestion is associated with accidents, work zones, and weather. Traffic congestion increases travel delay and fuel consumption and adversely affects safety, mobility, productivity, the human and natural environment. As a result, increasing delay has seriously damaged the speed and reliability of road networks, which are vital to emerging industries, like warehousing and logistics.

It has been a major goal of transportation scientists and engineers to alleviate traffic congestion. Many strategies have been pursued to achieve this goal. One method is to expand existing road facilities by adding new roads or lanes, rebuilding key network components, and enhancing the physical condition of roadways. Another method is to apply traffic management and operation technologies, including automatic highways, travel demand management, freeway management, incident management, emergency response management, weather response management, value pricing, arterial signal control, on-ramp metering, traveler information, changeable message signs, and so on.

All these approaches are intended to either increase the capacity of road networks or reduce their load. Among them, the method of expanding existing road networks has seen limited use due to huge construction costs and the difficulty of addressing public and environmental concerns. Therefore, the idea of using existing infrastructure more efficiently by building Intelligent Transportation Systems (ITS) is a more preferable option.

1.1.2 The role of traffic models

Whichever of the aforementioned strategies are taken to improve the mobility of a road network, their success relies on a better understanding of the properties of congestion and the overall performance of the road network. Widely available sensing,

information and communication technology has had a major influence in detecting traffic conditions in a timely manner. However, collecting meaningful traffic data is not an easy job. Moreover, many management and control decisions are grounded on an estimate of traffic conditions in the near or long-term future. Thus, it is essential to accurately estimate traffic conditions in a road network during certain time periods and understand the evolution pattern of traffic conditions, i.e., the traffic dynamics. This calls for the development of traffic models.

A traffic model is a function which relates the movement of a vehicle to driver's behavior, vehicle type, network characteristics, weather conditions, traffic signals, guidance information, and interaction with other vehicles. The movement of a vehicle can be represented by its position at any time, i.e., its trajectory, from which its speed and acceleration rate can be obtained. Given all vehicles' trajectories, one can measure the performance of a road network, e.g., travel time, level of service, congestion level, etc. As shown in Figure 1.1, traffic models can be considered as a theoretical substitution of a real traffic system.

Besides the constraints in Figure 1.1, traffic models are also subject to both space and time limitations, i.e., initial traffic conditions and boundary conditions. Moreover, all traffic models are subject to calibration and validation. In calibration, parameters in a traffic model are adjusted so that it acts as closely to the real traffic system as possible. In validation, the output of a traffic model is compared with observation of real traffic.

The role of traffic models in transportation engineering is two-fold. First, they provide better understanding of traffic dynamics, in particular the formation and propagation of traffic congestion. Hence, traffic researchers can use traffic models to identify possible bottlenecks. Second, they can serve as a simulation platform, on which different strategies for improving mobility, as shown in Figure 1.1, can be

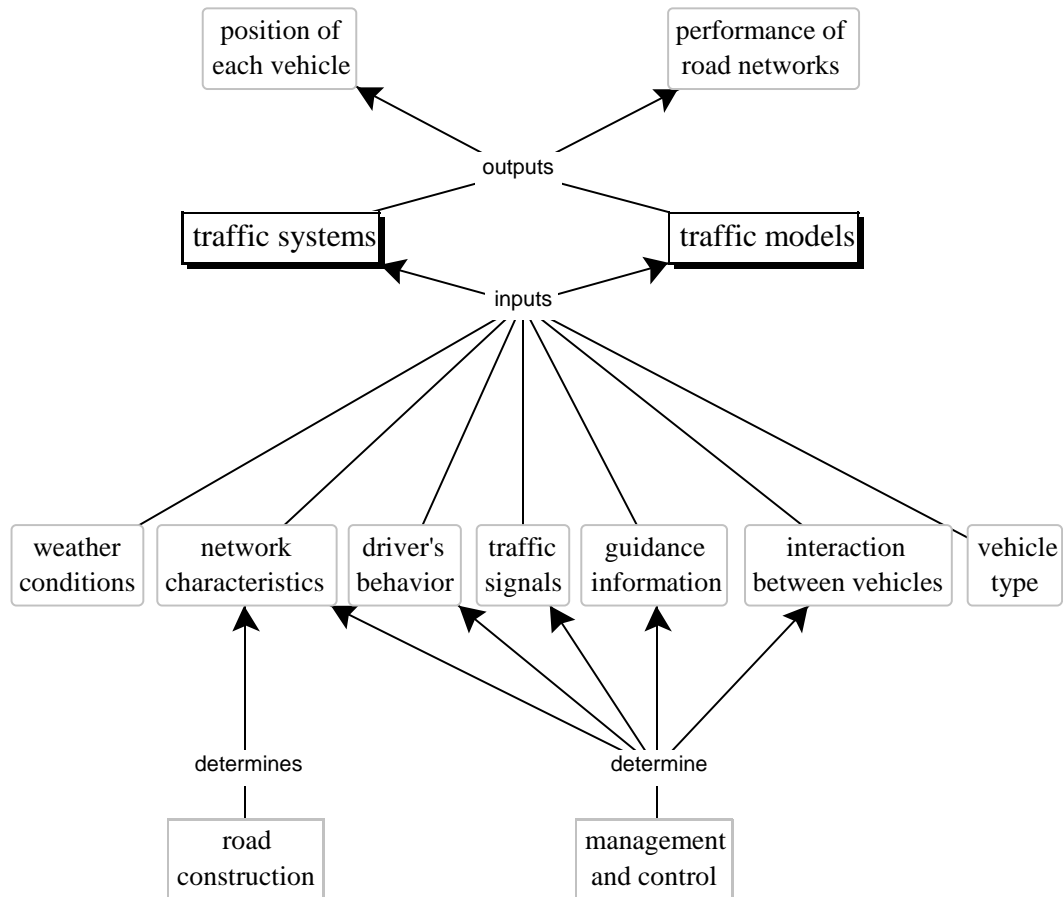


Figure 1.1: The definition and role of traffic models in traffic studies

developed and evaluated. For example, in the plan for expanding a road network, traffic models can be used to simulate proposed expanded networks and help choose the most cost-effective strategy. For another example, they are also helpful in determining the best location of tolling booths, which are designed to divert traffic away from busy roads by charging fees. Finally, traffic models can be used to evaluate previously implemented strategies.

1.1.3 Traffic models and simulation packages

In a vehicular traffic system, a number of trips - defined by their origin/destination, departure time/arrival time and travel route - interact on the road network and generate various dynamics and phenomena. To study these traffic phenomena and the corresponding applications, many traffic models and simulation packages have been proposed in literature.

From a microscopic point of view, a stream of vehicular traffic is the combination of the movements of all vehicles. In a microscopic model of traffic, the movement of each vehicle and interactions between the vehicle pairs are studied. Three types of microscopic models have been suggested. One approach is the GM family of car-following models developed in the 1960's (e.g., (Gazis et al., 1961)). In these models, the movement of a vehicle is described by an ordinary differential equation in time. In another approach, known as coupled-map lattice models, a vehicle's movement is defined by equations that are discrete in time (Chowdhury et al., 2000). Yet another approach, cellular automata (CA) models are based on the framework of statistical physics, in which not only independent variables (space and time) but also descriptive variables (speed and acceleration) are discrete (Chowdhury et al., 2000).

From a macroscopic point of view, one approach to modeling traffic is to treat the traffic as it were a gas of interacting particles, in which each particle represents a vehicle. The resulting model is called a kinetic model of vehicular traffic. Another approach is to consider traffic flow as a compressible fluid (continuum). Such models are known as continuum models, or fluid-dynamical models. In continuum models, the basic characteristics are flow rate q , traffic density ρ , and travel speed v , which are all functions in time and space. The first-order continuum models are generally called kinematic wave models, in which traffic dynamics are regarded as a combination of "kinematic" waves in these quantities.

Based on the aforementioned theoretical models of vehicular traffic, many simulation packages have been developed; for example, the PASSER series (Texas Transportation Institute, 1991), TRANSYT (Courage and Wallace, 1991), INTEGRATION (Van Aerde and the Transportation Research Board, 1995), DYNASMART (Jayakrishnan et al., 1994), NETSIM (Federal Highway Administration, 1998), FRESIM (Smith and Noel, 1995), FREFLO (Payne, 1979), MITSIM (Massachusetts Institute of Technology, 1999), TRANSIMS (TRANSIMS), and PARAMICS (Cameron and Duncan, 1996). In some simulation packages, however, the underlying traffic flow theories lack mathematical rigor, particularly for traffic dynamics at highway junctions. Furthermore, numerical methods used in some simulations have not been well justified and may cause numerical instability. Another common drawback with many simulation packages is their enormous computational cost. Therefore, many of these simulation packages have serious limitations in applications. That said, continuing efforts to develop theoretically rigorous, numerically sound, and computationally effective models are still necessary, in particular for applications to dynamic traffic assignment and other advanced traffic engineering strategies.

1.2 Continuum models

1.2.1 Kinematic wave models

In the kinematic wave models, traffic is viewed as a continuous media and characterized by traffic density (ρ), travel speed (v), and flow-rate (q). The movements of vehicles on a road network are considered as combinations of kinematic waves in either of these three quantities.

The different types of kinematic waves are associated with different components of a traffic system. For example, on a homogeneous link with uniform conditions

in vehicles, drivers, weather, etc., one can observe two basic waves: decelerating shock waves, generally seen when lights turn red, and accelerating rarefaction waves, generally seen when lights turn green. In a traffic system with inhomogeneous links, merges, diverges, or different vehicle types, more complicated waves can be observed, such as standing transitional waves, contact waves, and periodic waves.

In kinematic wave models, a hyperbolic conservation law is derived from traffic conservation:

$$\rho_t + q_x = 0. \quad (1.1)$$

A fundamental assumption in kinematic wave models is that the flow-rate q is a function of the traffic density ρ ; i.e., $q = Q(\rho)$, which is called the fundamental diagram. Hence, $v = V(\rho) \equiv Q(\rho)/\rho$. Generally, flow-rate is a concave function in density and retains its maximum, the capacity, at the critical density ρ_c . When traffic density is higher than the critical density, it is in the over-critical region and in the under-critical region, otherwise. The fundamental diagram, or the speed-density relation, varies with link characteristics, vehicle types, and so on.

Lighthill and Whitham (1955b) and Richards (1956) first proposed and analyzed kinematic waves on homogeneous links. The corresponding model is known as the LWR model and is described by a first-order, nonlinear PDE:

$$\rho_t + Q(\rho)_x = 0. \quad (1.2)$$

This model is an hyperbolic conservation law, whose Riemann problems ¹ can be analyzed using well developed tools (e.g., Lax, 1972; Smoller, 1983). Analysis shows that solutions to Equation 1.2, where $f(x, \rho) = \rho V(\rho)$, have wave properties analogous

¹In a Riemann problem, the initial traffic conditions are described by a Heaviside function or step function.

to those of water flow in channels (Lighthill and Whitham, 1955a). In other words, the Riemann problem consists of either shock or rarefaction waves.

Numerically, the LWR model can be solved with a first-order Godunov method (Godunov, 1959), in which a link is partitioned into a number of cells, a time duration into a number of time steps, and traffic conditions in each cell at a time step are uniform. In a Godunov method, traffic conditions are updated according to the conservation equation, Equation 1.2; i.e., during a time interval, the increasing number of vehicles in a cell are the difference between the in-flow through its upstream boundary and the out-flow through its downstream boundary. Traditionally (LeVeque, 2002), flows through cell boundaries are computed from wave solutions of Riemann problems.

As an alternative of the Godunov method, the celebrated supply-demand method was first proposed in (Daganzo, 1995a; Lebacque, 1996). In this intuitive, engineering method, the flow through a boundary equals the minimum of the traffic demand of its upstream cell and the traffic supply of the downstream cell. Here the traffic demand (Lebacque, 1996), called sending flow in (Daganzo, 1995a), of a cell is defined as its flow-rate when traffic is under-critical or its capacity when over-critical, and its traffic supply (Lebacque, 1996), receiving flow in (Daganzo, 1995a), is the capacity when traffic is under-critical or the flow-rate when under-critical. Since one does not have to understand wave solutions of Riemann problems, this method has been widely applied in traffic studies.

Many attempts have been made to model more complicated traffic systems under the framework of the LWR model. For example, Lighthill and Whitham (1955b) discussed the kinematic wave theory of traffic dynamics on an inhomogeneous link with lane-drops or curvatures. Lately, Lebacque (1996) gave a detailed analysis of the kinematic wave solutions of such a traffic system and summarized the solutions into the supply-demand method. In (Daganzo, 1995a), the concepts of sending flow (traffic

supply) and receiving flow (traffic demand) was intuitively extended for simulating traffic on an inhomogeneous link.

Another attempt is to model traffic dynamics on a highway network, where the focus is on highway junctions, including merges, diverges, and other intersections. Holden and Risebro (1995) studied kinematic waves initiated at highway junctions, by assuming the existence of an optimization problem at each junction and excluding route choice behavior. Without route choice, this model sees limited applications in reality. In the network traffic flow model by Kuhne and Michalopoulos (1992), on-ramps and off-ramps are considered as sources and sinks respectively. Although including the influence of ramps on mainline freeways, this model omits the other side: the influence of mainline freeways on ramps. Thus it also has limitations without giving a full picture of traffic dynamics. To capture overall traffic phenomena in a traffic system, (Daganzo, 1995a; Lebacque, 1996) proposed some discrete models, in which traffic demands and supplies for cells around an intersection are defined the same as those for cells inside a link, and route choice behavior and certain optimization rules for flows are incorporated in order to determine unique flows through the intersection. In literature, there have been little progress in analyzing the kinematic waves initiated at a highway junction considering route choice behavior, mainly due to the difficulties in formulating them into a system of continuous partial differential equations as in the LWR model.

In the framework kinematic wave theories, other extensions have been proposed for addressing different concerns in traffic systems. In (Daganzo, 1997; Daganzo et al., 1997), traffic on special lanes is investigated. In (Daganzo, 2002), driver behavior are incorporated. Wong and Wong (2002) discuss differentiated vehicle types. Other interesting studies can be found in (Vaughan et al., 1984; Newell, 1993, 1999; LeVeque, 2001; Lebacque, 2003)

Compared to other traffic models, kinematic wave models have the following appealing features. First, they have inherit compliance with many applications in large-scale road networks, in which aggregate quantities such as traffic counts, flows, and space-mean travel speed are more important than characteristics of individual vehicles. Second, kinematic wave models can generally be written into a system of hyperbolic partial differential equations, or hyperbolic conservation laws. Thus, one can better understand the formation and structure of a traffic phenomenon on a road network through theoretical analysis of these equations. Finally, there exist many sound, efficient numerical methods for solving hyperbolic conservation laws, and one can carry out efficient and trustful simulations of large-scale road networks.

1.2.2 Higher-order models

Among many efforts to extend the LWR theory to capture instabilities in practical traffic flow, one direction leads to higher-order, or nonequilibrium, models. Payne (1971) and Whitham (1974) introduced a momentum equation to capture the change in travel speed in addition to the traffic conservation equation, Equation 1.1:

$$v_t + vv_x + \frac{c_0^2}{\rho} \rho_x = \frac{V(\rho) - v}{\tau}. \quad (1.3)$$

Here the constant c_0 is the traffic sound speed, the source term $\frac{V(\rho) - v}{\tau}$ is called a relaxation term, and τ is the relaxation time. With the momentum equation, the PW model attempts to model driver behavior by accounting for drivers' anticipation and inertia. One can show that the LWR model is an asymptotic approximation of the PW model (Schochet, 1988).

The PW model, as a second-order system of hyperbolic conservation laws with a source term, can be numerically solved by Godunov methods (Jin and Zhang, 2001b). With simulations it was shown that, in addition to modeling stable traffic like the

LWR model, the PW model is capable of modeling the formation of vehicle clusters (Jin and Zhang, 2003a). However, the PW model has drawn some criticism since it allows wave solutions with speed higher than vehicle travel speed and may yield back-traveling (or negative-speed) results (Daganzo, 1995c).

Another nonequilibrium traffic flow model is due to (Zhang, 1998, 1999, 2000, 2001a). In this model, a modified momentum equation is included,

$$v_t + vv_x + \frac{(\rho V'(\rho))^2}{\rho} \rho_x = \frac{V(\rho) - v}{\tau}. \quad (1.4)$$

This model bears shortcomings similar to the PW model, yet differs from the latter in that the sound speed $c = \rho V'(\rho)$ varies with respect to traffic density ρ . Moreover, it is always stable and therefore acts like the LWR model (Li, 2003).

In order to avoid the negative-speed drawbacks of the PW model, Aw and Rascle (2000) identified a number of principles and proposed a satisfactory momentum equation in the following form:

$$v_t + (v - \rho p'(\rho))v_x = \frac{V(\rho) - v}{\tau}, \quad (1.5)$$

where $p(\rho)$ is a pressure law and is increasing. Further, the Riemann problems were discussed for the model. However, how $p(\rho)$ is related to driver-behavior was not specified in their study.

In the same spirit, Zhang (2002) derived a model similar to Aw and Rascle's model from a car-following model:

$$v_t + (v + \rho V'(\rho))v_x = \frac{V(\rho) - v}{\tau}, \quad (1.6)$$

which is in the framework of Equation 1.5 with $p(\rho) = -V(\rho)$. In this model, the definition of $p(\rho)$ is derived from a car-following model. Both models, Equation 1.5 and Equation 1.6, no longer admit wave solutions faster than traffic and avoids back-traveling (Aw and Rascle, 2000; Zhang, 2002). However, they are always stable (Li,

2003) and, therefore, lose the PW model's ability to simulate unstable traffic and vehicle clusters.

Also in the framework of Equation 1.5, another model was proposed in (Jiang et al., 2002) as

$$v_t + (v - c_0)v_x = \frac{V(\rho) - v}{\tau}, \quad (1.7)$$

where the pressure function $p(\rho) = c_0 \ln \rho$. Like the PW model, this model is unstable under some traffic conditions, but yields non-physical solutions when traffic is in unstable region (Jin and Zhang, 2003d).

More complicated traffic systems, for example, with highway junctions (Liu et al., 1996; Lee et al., 2000), have been studied with non-equilibrium models, primarily the PW model. Moreover, several simulation packages are also based on the PW model. In this dissertation, however, we focus on the LWR model, i.e., the first-order continuum model.

1.3 Fundamental diagrams

In the kinematic wave models, fundamental diagrams capture constraints on a traffic system such as road characteristics, vehicle type, driver's behavior, weather conditions, and traffic rules. Therefore, the success of such models rely on the accuracy of the fundamental diagram.

One typical relationship that has been observed between flow rate and occupancy is shown in Figure 1.2 from (Hall et al., 1986). It's generally assumed that the equilibrium travel speed $V(\rho)$ is decreasing with respect to traffic density; i.e., $V'(\rho) < 0$, and the fundamental diagram $Q(\rho) \equiv \rho V(\rho)$ is concave; i.e., $Q''(\rho) < 0$.

Due to their importance, many fundamental diagrams have been proposed since

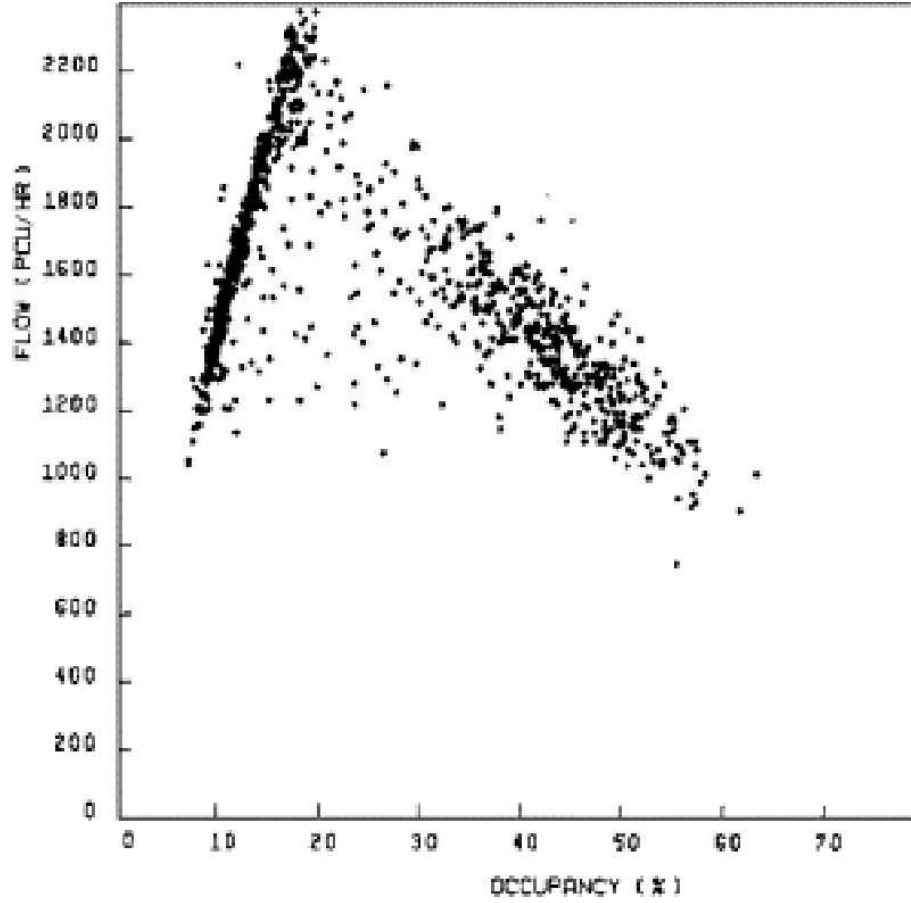


Figure 1.2: A typical occupancy-flow rate relationship (Hall et al., 1986)

the early era of traffic engineering practice. Some traditional speed-density relations are listed in Table 1.1.

More recent examples are the following: the triangular fundamental diagram (Newell, 1993),

$$V(\rho) = \begin{cases} v_f & \text{when under-critical,} \\ v_f \frac{\rho_c}{\rho_j - \rho_c} \left(\frac{\rho_j}{\rho} - 1 \right) & \text{otherwise,} \end{cases} \quad (1.8)$$

a non-convex fundamental diagram (Kerner and Konhäuser, 1994; Herrmann and Kerner, 1998),

$$V(\rho) = 5.0461 \left[(1 + \exp\{[\rho/\rho_j - 0.25]/0.06\})^{-1} - 3.72 \times 10^{-6} \right] l/\tau, \quad (1.9)$$

Functions	$V(\rho)$
Greenshields (1935)	$v_f(1 - \rho/\rho_j)$
Greenberg (1959)	$v_0 \ln(\rho_j/\rho)$
Newell (1961)	$v_f \left[1 - \exp \left(\frac{ c_j }{v_f} (1 - \rho_j/\rho) \right) \right]$
Underwood (1961)	$v_f \exp(-\rho/\rho_j)$
Drake et al. (1967)	$v_f \exp \left[-\frac{1}{2} \left(\frac{\rho}{\rho_j} \right)^2 \right]$
Pipes (1967)	$v_f \left(1 - \frac{\rho}{\rho_j} \right)^n, n > 1$

Table 1.1: Traditional speed-density relationship functions

and the exponential form (Del Castillo and Benitez, 1995a,b),

$$V(\rho) = v_f \left\{ 1 - \exp \left[1 - \exp \left(\frac{|c_j|}{v_f} \left(\frac{\rho_j}{\rho} - 1 \right) \right) \right] \right\}. \quad (1.10)$$

The aforementioned fundamental diagrams are all continuous functions. In addition, to capture “two-capacity” phenomena (Banks, 1991), a discontinuous fundamental diagram in “reverse-lambda” shape has been proposed (e.g., Koshi et al., 1983). Finally, Daganzo (1997) has proposed a novel, two-regime fundamental diagram for differentiated road and vehicle types.

In this dissertation, we focus on studying network inhomogeneities such as merges, diverges, and other junctions. Thus, we will consider continuous fundamental diagram, mostly of the triangular shape.

1.4 Motivation for the dissertation research

While driving in “stop and go” traffic, many people may have wondered how such congestion is formed, propagated, and diffused. As we know, the network structure is an important factor in determining the characteristics of traffic congestion. For

example, congestion generally forms at merging junctions and propagates through diverges. Therefore, traffic conditions on a road network have to be considered as a whole.

The kinematic wave theory is a good candidate for studying vehicular traffic dynamics due to its theoretical rigor, numerical soundness, and computational efficiency. However, its potential has yet to be fully explored. Theoretically, there has been little progress in finding kinematic waves in network traffic systems since (Lighthill and Whitham, 1955b; Richards, 1956), and traffic congestion in road networks has not been well understood in the framework of kinematic waves. Numerically, little attention is paid to the stability and convergence of solution methods. Computationally, many simulation models based on kinematic wave theory still keep track of individual vehicles and lose a part of the kinematic wave models' efficiency. Due to the aforementioned limitations, kinematic wave theories of network traffic flow have yet to be improved so that they can be applied in solving practical problems, e.g., in Intelligent Transportation Systems.

In the framework of kinematic wave theories, we study network traffic dynamics and provide a theoretically rigorous, numerically reliable, and computationally efficient simulation model for understanding and mitigating congestion in large-scale road networks. In order to fully explore the advantages of the kinematic wave theory, we consider the following four aspects of traffic modeling in this dissertation. First, we study traffic dynamics at crucial components of a road network, such as link bottlenecks, merges, and diverges, as well as different types of vehicles. In addition, we consider the dynamics of additive multi-commodity traffic. These studies will offer a more rigorous understanding of traffic dynamics in terms of kinematic waves. Second, we discuss systematically with numerical methods for computing commodity-specified fluxes through junctions in the framework of supply-demand

method (Daganzo, 1995a; Lebacque, 1996). Third, we develop a macroscopic simulation platform of multi-commodity traffic on a road network. Finally, we apply this simulation model to study traffic on a road network and probe traffic phenomena related to network topology and route choice behavior.

The structure of this dissertation is as follows. In Chapter 2, we study the kinematic waves on inhomogeneous links. In Chapter 3, we discuss kinematic wave models of merging traffic, which are based on the supply-demand method. In Chapter 4, we propose a new kinematic wave theory for diverging traffic. In Chapter 5, we discuss theoretical and numerical solutions for mixed-type traffic. In Chapter 6, we develop a the multi-commodity kinematic wave simulation platform for network traffic flow. In Chapter 7, we apply this simulation model to study some traffic phenomena in road networks. Finally, we summarize our research results and present future research plans in Chapter 8.

Chapter 2

Kinematic wave traffic flow model of inhomogeneous links

2.1 Introduction

The kinematic wave traffic flow model of LWR was introduced by Lighthill and Whitham (1955b) and Richards (1956) for modeling dense traffic flow on crowded roads, where the evolution of density $\rho(x, t)$ and flow-rate $q(x, t)$ over time is described by equation,

$$\rho_t + q_x = 0. \tag{2.1}$$

This equation follows conservation of traffic that vehicles are neither generated nor destroyed on a road section with no entries and exits.

The conservation equation alone is not sufficient to describe traffic evolution, because it does not capture the unique character of vehicular flow—drivers slow down when their front spacing is reduced to affect safety. The LWR model addresses this issue by assuming a functional relationship between local flow-rate and density, i.e., $q = f(x, \rho)$. This flow-density relation, also known as the fundamental diagram of

traffic flow, is often assumed to be concave in ρ and is a function of the local characteristics of a road location, such as the number of lanes, curvature, grades, and speed limit, as well as vehicle and driver composition. When a piece of roadway is homogeneous; i.e., the aforementioned characteristics of the road are uniform throughout the road section, the fundamental diagram is invariant to location x and the LWR model becomes

$$\rho_t + f(\rho)_x = 0. \quad (2.2)$$

In contrast, if a section of a roadway is inhomogeneous, the LWR model is

$$\rho_t + f(x, \rho)_x = 0. \quad (2.3)$$

Here we introduce a more explicit notation, an inhomogeneity factor $a(x)$, into the flux function $f(x, \rho)$ and obtain the following equivalent LWR model for an inhomogeneous road

$$\rho_t + f(a, \rho)_x = 0. \quad (2.4)$$

This equation is particularly suited for our later analysis of the LWR model for inhomogeneous roads (We shall hereafter call Equation 2.2 the homogeneous LWR model and Equation 2.4 the inhomogeneous LWR model).

Both the homogeneous and inhomogeneous LWR models have been studied by researchers and applied by practitioners in the transportation community. Note that the homogeneous version Equation 2.2 is nothing more than a scalar conservation law. Therefore, its wave solutions exist and are unique under the so-called ‘‘Lax entropy condition’’ (Lax, 1972). These solutions are formed by basic solutions to the Riemann problem of Equation 2.2, in which the initial conditions jump at a boundary and are constant both upstream and downstream of the jump spot. Nevertheless,

because analytical solutions are difficult to obtain for Equation 2.2 with arbitrary initial/boundary conditions, numerical solutions have to be computed in most cases. The most often used approximation of Equation 2.2 is perhaps that of Godunov. In the Godunov method, a roadway is partitioned into a number of cells; and the change of the number of vehicles in each cell during a time interval is the net inflow of vehicles from its boundaries. The rate of traffic flowing through a boundary is obtained by solving a Riemann problem at this boundary. Besides the Godunov method, there are other types of approximations of the homogeneous LWR model, and some of them are shown to be variants of Godunov's method (Lebacque, 1996).

In contrast to the well researched homogeneous LWR model, the inhomogeneous model is less studied and less understood. Of the few efforts to rigorously solve the inhomogeneous LWR model, the works of Daganzo (1995a) and Lebacque (1996) should be mentioned. In his cell transmission model, Daganzo started with a discrete form of the conservation equation and suggested that the flow through a boundary connecting two cells of a homogeneous road is the minimum of the “sending flow” from the upstream cell and the “receiving flow” of the downstream cell. The “sending flow” is equal to the upstream flow-rate if the upstream traffic is undercritical (UC) or the capacity of the upstream section if the upstream traffic is overcritical (OC); on the other hand, the “receiving flow” is equal to the capacity of the downstream section if the downstream traffic is UC or the downstream flow-rate if the downstream traffic is OC. In the homogeneous case, the boundary flux computed from the “sending flow” and the “receiving flow” is the same as that computed from solutions of the associated Riemann problem. Since the definitions of “sending flow” and “receiving flow” can be extended to inhomogeneous sections, Daganzo's method can also be applied to the inhomogeneous LWR model. Different from Daganzo, Lebacque started his method with the solution of the “generalized” Riemann problem for Equation

2.3. In this work, Lebacque came up with some rules for solving the “generalized” Riemann problem. These rules play the same role as entropy conditions. Moreover, Lebacque found that the boundary flux obtained from solving the Riemann problem is consistent with that from Daganzo’s method, and he called Daganzo’s “sending flow” demand and “receiving flow” supply.

The methods of Daganzo and Lebacque are streamlined versions of Godunov’s method for the inhomogeneous LWR model. They hinge upon the definitions of the demand and supply functions, which can be obtained unambiguously when $f(a, \rho)$ is unimodal. When $f(a, \rho)$ has multiple local maximum, or when the traffic flow model is of higher order, it is yet to be determined if equivalent demand/supply functions exist. Thus, these two methods may not be applicable to solve the LWR model that has multiple critical points on its fundamental diagram, nor higher-order models of traffic flow, such as the Payne-Whitham (Payne, 1971; Whitham, 1974) model and a model by (Zhang, 1998, 1999, 2000, 2001a). Note that, however, these higher-order models for homogeneous roads can still be solved with Godunov’s method (Zhang, 2001a).

In this chapter, we present a new method for solving the Riemann problem for Equation 2.4, which can be extended to solve higher-order models. By introducing an additional conservation law for $a(x)$, we consider the inhomogeneous LWR model as a resonant nonlinear system and study its properties (Section 2.2). We also solve the Riemann problem for Equation 2.4 and show that the boundary flux at the location of the inhomogeneity is consistent with the one given by Lebacque and Daganzo for the same initial condition (Section 2.3). Finally, we demonstrate our method through solving an initial value problem on a ring road with a bottleneck, and draw some conclusions from our analyses.

2.2 Properties of the inhomogeneous LWR model as a resonant nonlinear system

Instead of directly study the inhomogeneous LWR model described by Equation 2.4, we augment Equation 2.4 into a system of conservation laws through the introduction of an additional conservation law $a_t = 0$ for the inhomogeneity factor $a(x)$, which leads to

$$U_t + F(U)_x = 0, \quad (2.5)$$

where $U = (a, \rho)$, $F(U) = (0, f(a, \rho))$, $x \in R, t \geq 0$. Without loss of generality, we assume the inhomogeneity is the drop/increase of lanes at a particular location, and write the fundamental diagram as $f(a, \rho) = \rho V(\frac{\rho}{a})$, where $v = V(\frac{\rho}{a})$ is the speed-density relation. The results obtained hereafter apply to other types of inhomogeneities, such as changes in grades.

The inhomogeneous LWR model Equation 2.5 can be linearized as

$$U_t + \partial F(U)U_x = 0, \quad (2.6)$$

where the differential $\partial F(U)$ of the flux vector $F(U)$ is

$$\partial F = \begin{bmatrix} 0 & 0 \\ -\frac{\rho^2}{a^2}V'(\frac{\rho}{a}) & V(\frac{\rho}{a}) + \frac{\rho}{a}V'(\frac{\rho}{a}) \end{bmatrix}. \quad (2.7)$$

The two eigenvalues of ∂F are

$$\lambda_0 = 0, \quad \lambda_1 = V(\frac{\rho}{a}) + \frac{\rho}{a}V'(\frac{\rho}{a}). \quad (2.8)$$

The corresponding right eigenvectors are

$$\mathbf{R}_0 = \begin{bmatrix} V(\frac{\rho}{a}) + \frac{\rho}{a}V'(\frac{\rho}{a}) \\ (\frac{\rho}{a})^2V'(\frac{\rho}{a}) \end{bmatrix}, \quad \mathbf{R}_1 = \begin{bmatrix} 0 \\ 1 \end{bmatrix},$$

and the left eigenvector of $\partial f/\partial \rho$ as $\mathbf{l}_1 = 1$.

System Equation 2.5 is a non-strictly hyperbolic system, since it can happen that $\lambda_1 = \lambda_0$. We consider a traffic state $U_* = (a_*, \rho_*)$ in this system as critical if

$$\lambda_1(U_*) = 0; \quad (2.9)$$

i.e., at critical states, the two wave speeds are the same and system Equation 2.5 is singular. For a critical traffic state U_* we also have

$$\frac{\partial}{\partial \rho} \lambda_1(U_*) = f_{\rho\rho} < 0 \quad (2.10)$$

since flow-rate is concave in traffic density, and

$$\frac{\partial}{\partial a} f(U_*) = -\left(\frac{\rho}{a}\right)^2 V'\left(\frac{\rho}{a}\right)|_{U_*} = \frac{\rho}{a} V\left(\frac{\rho}{a}\right)|_{U_*} > 0. \quad (2.11)$$

A consequence of properties Equation 2.10 and Equation 2.11 is that the linearized system Equation 2.6 at U_* has the following normal form

$$\begin{bmatrix} \delta a \\ \delta \rho \end{bmatrix}_t + \begin{bmatrix} 0 & 0 \\ 1 & 0 \end{bmatrix} \begin{bmatrix} \delta a \\ \delta \rho \end{bmatrix}_x = 0. \quad (2.12)$$

System Equation 2.12 has the solution $\delta \rho(x, t) = \delta a'(x)t + c$, and the solution goes to infinity as t goes to infinity. Therefore Equation 2.12 is a linear resonant system, and the original inhomogeneous LWR model Equation 2.5 is a nonlinear resonant system.

For Equation 2.5, the smooth curve Γ in U -space formed by all critical states U_* are named a transition curve. Therefore Γ is defined as

$$\Gamma = \{U | \lambda_1(U) = 0\}.$$

Since $\lambda_1(U) = V(\frac{\rho}{a}) + \frac{\rho}{a} V'(\frac{\rho}{a})$, we obtain

$$\Gamma = \left\{ (a, \rho) \middle| \frac{\rho}{a} = \alpha, \text{ where } \alpha \text{ uniquely solves } V(\alpha) + \alpha V'(\alpha) = 0 \right\}; \quad (2.13)$$

i.e., the transition curve for Equation 2.5 is a straight line passing through the origin in U -space. In Equation 2.13, α is unique since $f(a, \rho)$ is concave in ρ .

The entropy solutions to a nonlinear resonant system are different from those to a strictly hyperbolic system of conservation laws. Isaacson and Temple (1992) proved that solutions to the Riemann problem for system Equation 2.5 exist and are unique with the conditions Equation 2.9-Equation 2.11. Lin et al. (1995) presented solutions to a scalar nonlinear resonant system, which is similar to our system Equation 2.5 except that f is convex in their study. In the next section we apply those results to solve the Riemann problem for the inhomogeneous LWR model.

2.3 Solutions to the Riemann problem

In this section we study the wave solutions to the Riemann problem for Equation 2.5 with the following jump initial conditions

$$U(x, t = 0) = \begin{cases} U_L & \text{if } x < 0 \\ U_R & \text{if } x > 0 \end{cases}, \quad (2.14)$$

where the initial values of U_L, U_R are constant. For computational purposes, we are interested in the average flux at the boundary $x = 0$ over a time interval Δt , which is denoted by f_0^* and defined as

$$f_0^* = \frac{1}{\Delta t} \int_0^{\Delta t} f(U(x = 0, t)) dt. \quad (2.15)$$

The augmented inhomogeneous LWR model Equation 2.5 has two families of basic wave solutions associated with the two eigenvalues. The solutions whose wave speed is λ_0 are in the 0-family, and the waves are called 0-waves. Similarly the solutions whose wave speed is λ_1 are in the 1-family, and the waves are called 1-waves. The 0-wave is also called a standing wave since its wave speed is always 0. The 1-wave solutions are

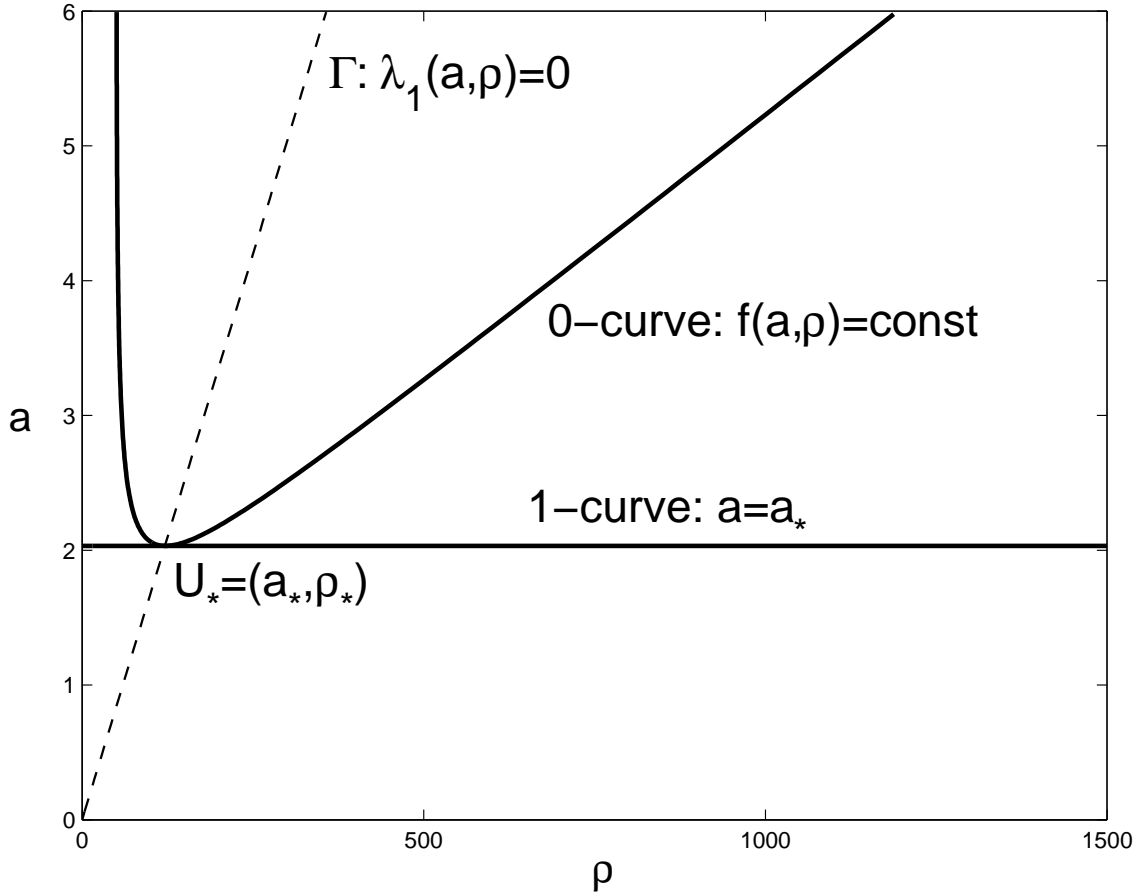


Figure 2.1: Integral curves

determined by the solutions of the scalar conservation law $\rho_t + f(\bar{a}, \rho)_x = 0$, where \bar{a} is a constant. Corresponding to the two types of wave solutions, the integral curves of the right eigenvectors \mathbf{R}_0 and \mathbf{R}_1 in U -space are called 0- and 1-curves respectively. Hence the 0-curves are given by $f(U)=\text{const}$, and the 1-curves are given by $a = \text{const}$. A 0-curve, a 1-curve, and the transition curve Γ passing through a critical state U_* are shown in Figure 2.1, where a is set as the vertical axis and ρ the horizontal axis.

As shown in Figure 2.1, the 0-curve is convex, and the 1-curve is tangent to the 0-curve at the critical state U_* . The transition curve Γ intersects the 0- and 1-curves

at U_* , and there is only one critical state on one 0-curve or 1-curve. For any point U , only one 0-curve and one 1-curve pass it. In Figure 2.1, the states left to the transition curve are undercritical (UC) since $\rho/a < \alpha$; and the states right to the transition curve are overcritical (OC) since $\rho/a > \alpha$.

The wave solutions to the Riemann problem for Equation 2.5 are combinations of basic 0-waves and 1-waves. Since Equation 2.5 is a hyperbolic system of conservation law, its wave solutions must satisfy Lax's entropy condition that the waves from left (upstream) to right (downstream) should increase their wave speeds so that they don't cross each other. For Equation 2.5 as a resonant nonlinear system, an additional entropy condition is introduced by Isaacson and Temple,

$$\text{The standing wave can NOT cross the transition curve } \Gamma. \quad (2.16)$$

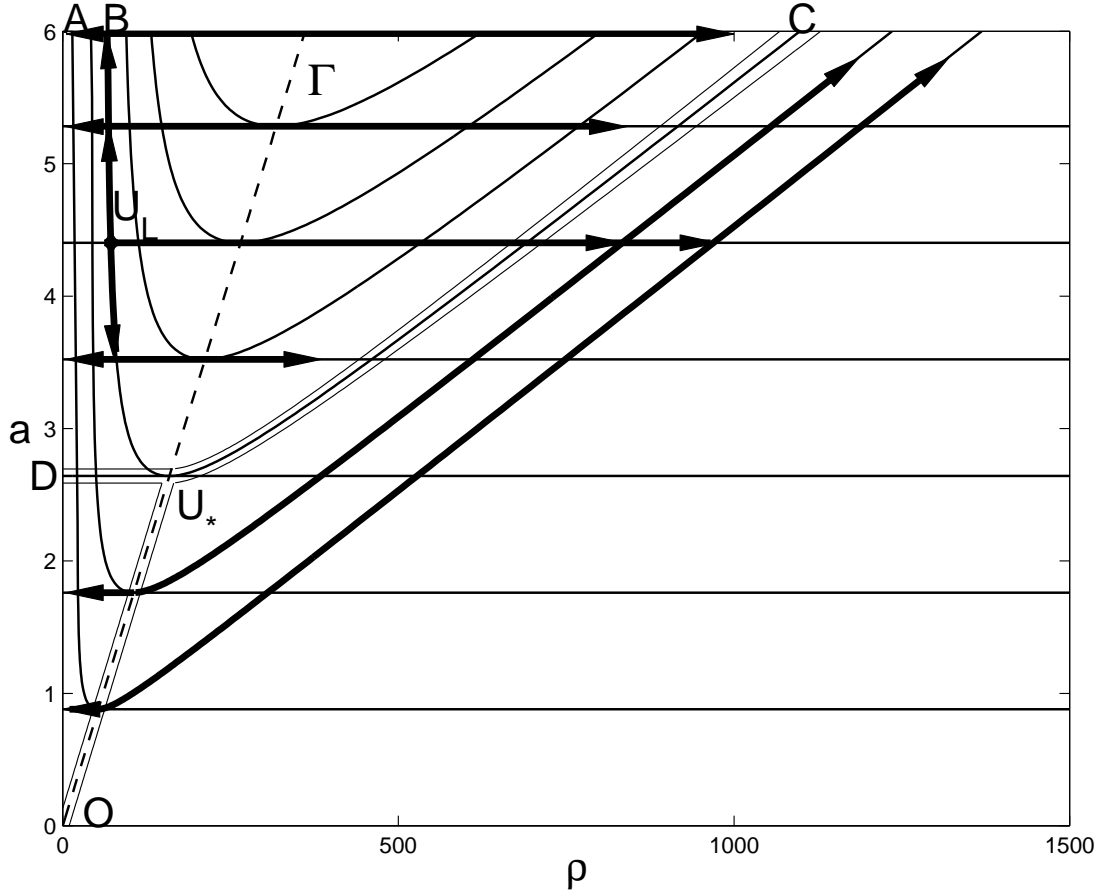
This entropy condition is equivalent to saying that, relative to the apexes of the fundamental diagrams, traffic conditions upstream and downstream of inhomogeneities are on the same side. That is, they should be either both UC or both OC.

With the two entropy conditions, the solutions to the inhomogeneous LWR model exist and are unique. The wave solutions for UC left state U_L are shown in Figure 2.2, and those for OC left state U_L are shown in Figure 2.3.

In the remaining part of this section, we discuss wave solutions to the Riemann problem for Equation 2.5, present the formula for the boundary flux f_0^* related to each type of solution, summarize our results and compare them with those found in literature.

2.3.1 Solutions of the boundary fluxes

When $U_L = (a_L, \rho_L)$ is UC; i.e., $\rho_L/a_L < \alpha$, where α is defined in Equation 2.13, we denote the special critical point on standing wave passing U_L as U_* . Thus, as

Figure 2.2: The Riemann problem for U_L left of Γ

shown in Figure 2.2, the U -space is partitioned into three regions by DU_* , OU_* and U_*C , where $DU_* = \{(a, \rho) | a = a_*, \rho < \rho_*\}$, $OU_* = \Gamma \cap \{0 \leq \rho \leq \rho_*\}$ and $U_*C = \{(a, \rho) | f(a, \rho) = f(U_L), \rho > \rho_*\}$. Related to different positions of the right state U_R in the U -space, the Riemann problem for Equation 2.5 with initial conditions Equation 2.14 has the following four types of wave solutions. For each type of solutions we provide formula for calculating the associated boundary flux f_0^* .

Type 1 When U_R is in region ABU_LU_*DA shown in Figure 2.2; i.e.,

$$f(U_R) < f(U_*) = f(U_L), \quad \rho_R/a_R < \alpha \text{ and } a_R \geq a_*, \quad (2.17)$$

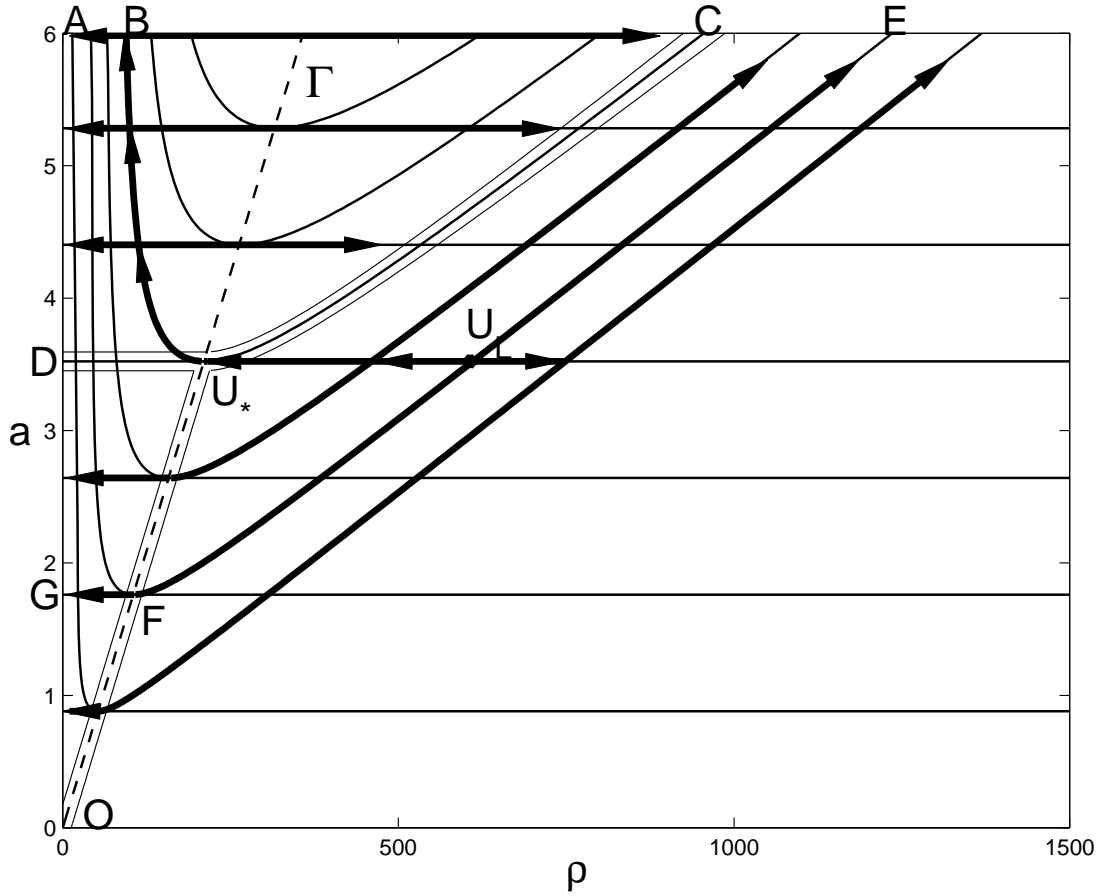


Figure 2.3: The Riemann problem for U_L right of Γ

wave solutions to the Riemann problem are of type 1. These solutions consist of two basic waves with an intermediate state $U_1 = (a_R, \rho_1 |_{f(a_R, \rho_1) = f(U_*) = f(U_L)})$. Of these two waves, the left one (U_L, U_1) is a standing wave, and the right one (U_1, U_R) is a rarefaction wave with characteristic velocity $\lambda_1(a, \rho) > 0$.

From Figure 2.2, we can see that the Riemann problem may admit this type of solutions when $a_L > a_R$ or $a_L \leq a_R$; i.e., when the road merges or diverges at $x = 0$. Here we present an example of this type of solutions in Figure 2.4, where the roadway merges at $x = 0$. In the case when the roadway diverges at

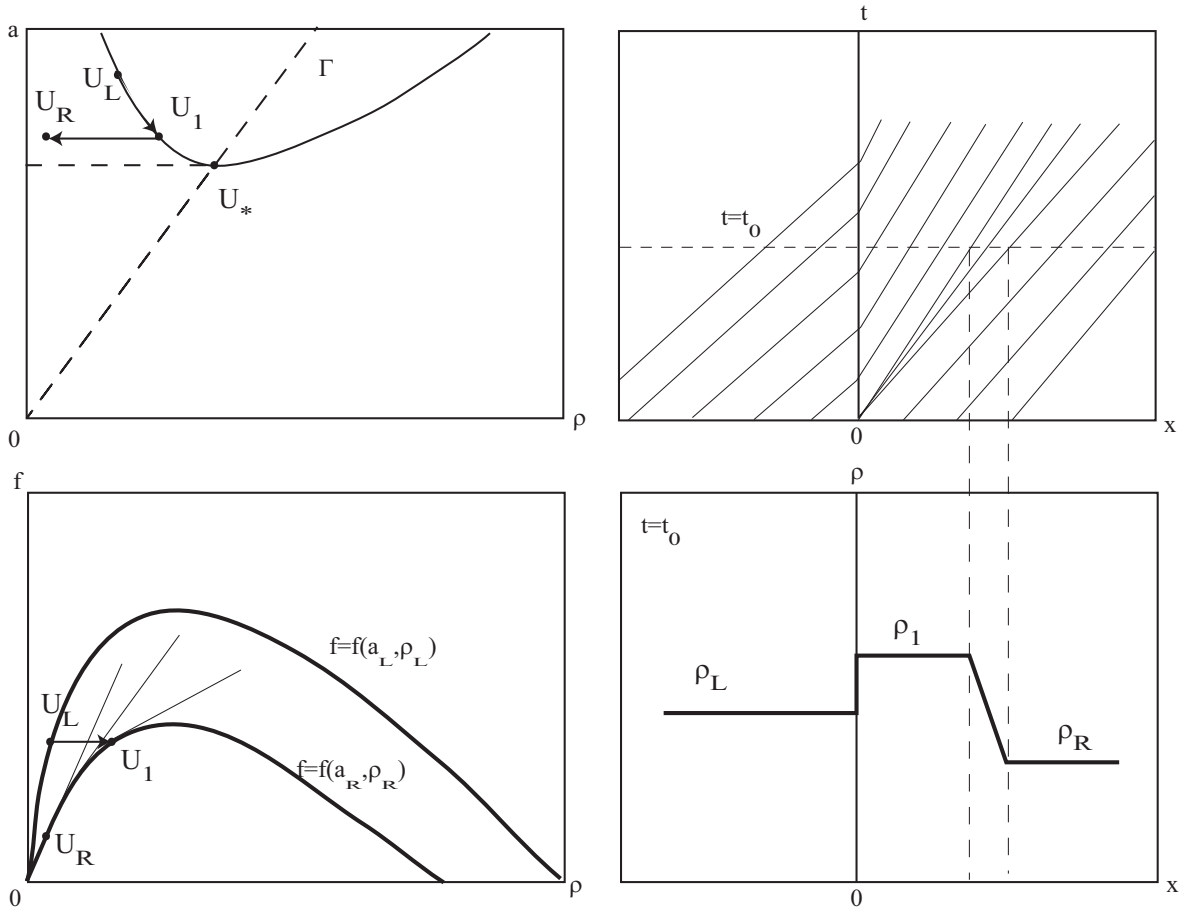


Figure 2.4: An example for wave solutions of type 1 for Equation 2.5 with initial conditions Equation 2.14

$x = 0$, we can find similar solutions.

From Figure 2.4, we obtain the boundary flux $f_0^* = f(U_L) = f(U_*)$ for wave solutions of type 1.

Type 2 When U_R is in region BU_LU_*CB shown in Figure 2.2; i.e.,

$$f(U_R) \geq f(U_*) = f(U_L), \tag{2.18}$$

wave solutions to the Riemann problem are of type 2. These solutions consist

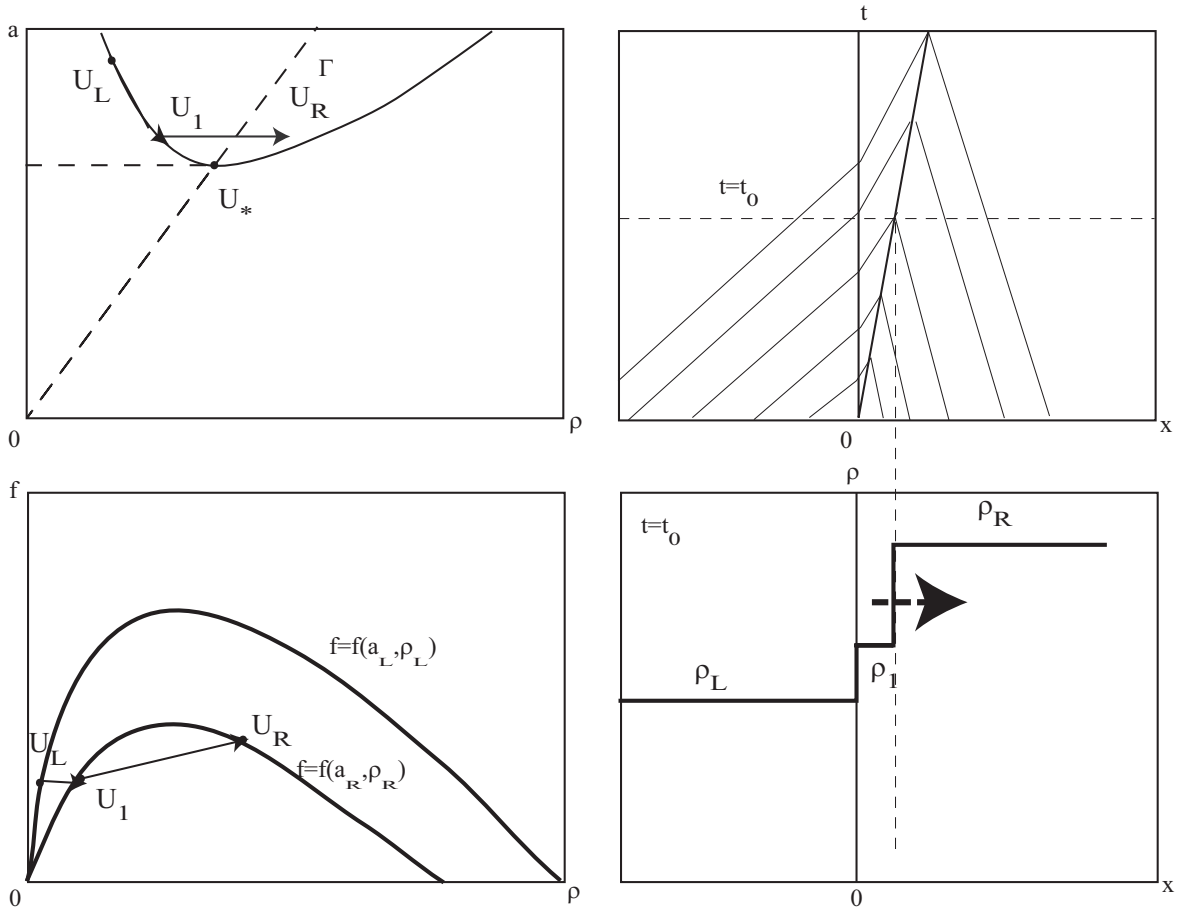


Figure 2.5: An example for wave solutions of type 2 for Equation 2.5 with initial conditions Equation 2.14

of two basic waves with an intermediate state $U_1 = (a_R, \rho_1 |_{f(a_R, \rho_1) = f(U_*) = f(U_L)})$. Of these two waves, the left (U_L, U_1) is a standing wave, and the right (U_1, U_R) is a shock wave with positive speed $\sigma = \frac{f(U_R) - f(U_*)}{\rho_R - \rho_1} > 0$.

From Figure 2.2, we can see that the Riemann problem may admit this type of solutions when the downstream traffic condition U_R is UC or OC, or the roadway merges or diverges at $x = 0$. Here we present an example of this type of solutions in Figure 2.5, where the downstream traffic condition is OC and the

roadway merges at $x = 0$. Similar solutions can be found for other situations that satisfy Equation 2.18.

From Figure 2.5, we obtain the boundary flux $f_0^* = f(U_L) = f(U_*)$ for wave solutions of type 2. Here we have the same formula as that for wave solutions of type 1.

Type 3 When U_R is in region OU_*CO shown in Figure 2.2; i.e.,

$$f(U_R) < f(U_*) = f(U_L), \quad \rho_R/a_R \geq \alpha, \quad (2.19)$$

wave solutions to the Riemann problem are of type 3. These solutions consist of two basic waves with an intermediate state $U_1 = (a_L, \rho_1 |_{f(a_L, \rho_1) = f(U_R)})$. Of these two waves, the left one (U_L, U_1) is a shock wave with negative speed $\sigma = \frac{f(U_1) - f(U_L)}{\rho_1 - \rho_L} < 0$, and the right one (U_1, U_R) is a standing wave.

From Figure 2.2, we can see that the Riemann problem may admit this type of solutions when the roadway merges or diverges at $x = 0$. Here we present an example of this type of solutions in Figure 2.6, where the roadway merges at $x = 0$. In the case when the roadway diverges at $x = 0$, similar solutions can be found.

From Figure 2.6, we obtain the boundary flux $f_0^* = f(U_R)$ for wave solutions of type 3.

Type 4 When U_R is in region OU_*DO shown in Figure 2.2; i.e.,

$$f(U_R) < f(U_*) = f(U_L), \quad \rho_R/a_R < \rho_*/a_* \text{ and } a_R < a_*, \quad (2.20)$$

wave solutions to the Riemann problem are of type 4. These solutions consist of three basic waves with two intermediate states: $U_1 = (a_L, \rho_1 |_{f(a_L, \rho_1) = f(U_2)})$ and $U_2 = (a_R, \rho_2 |_{\rho_2/a_R = \alpha})$. Of these three waves, the left one (U_L, U_1) is a shock

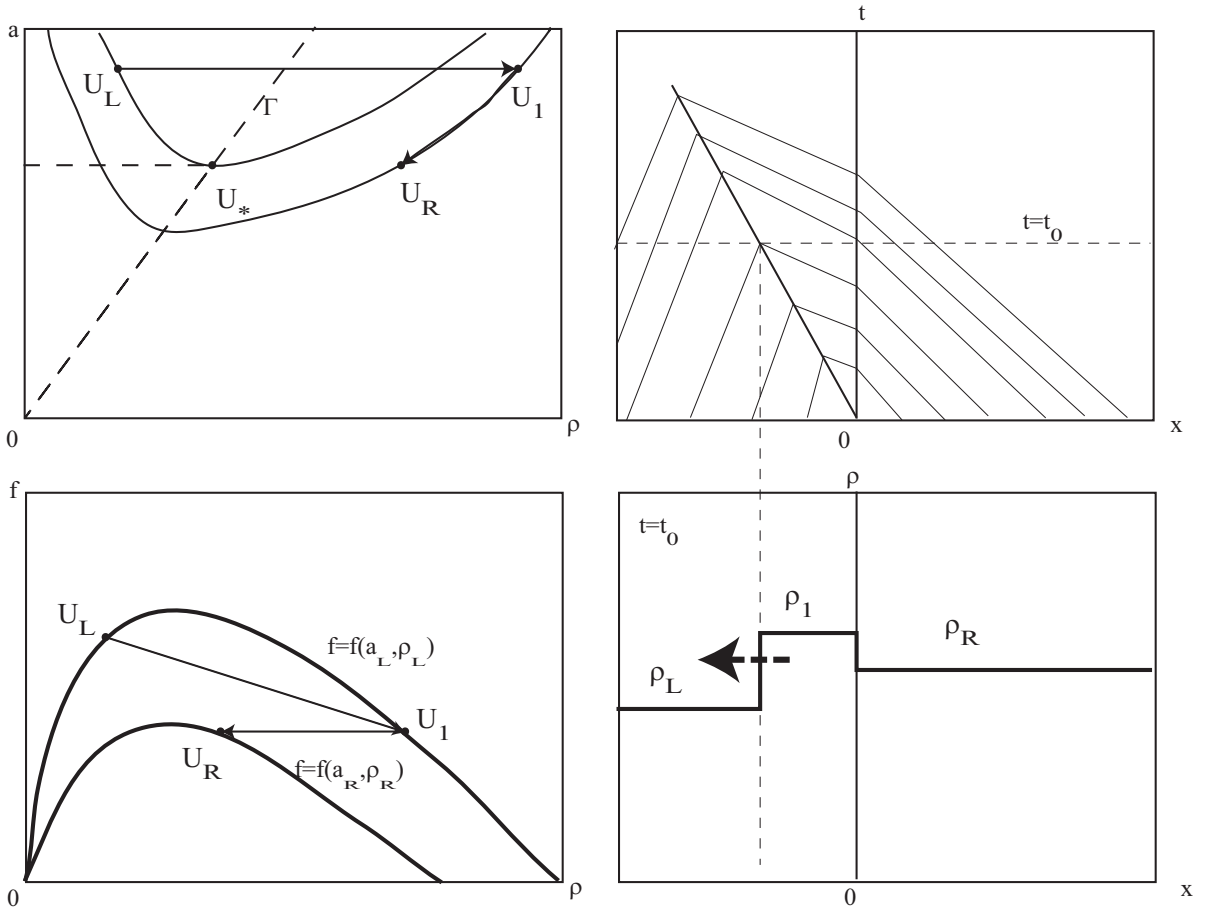


Figure 2.6: An example for wave solutions of type 3 for Equation 2.5 with initial conditions Equation 2.14

wave with negative speed $\sigma = \frac{f(U_1)-f(U_L)}{\rho_1-\rho_L} < 0$, the middle one (U_1, U_2) is a standing wave with zero speed, and the right one (U_2, U_R) is a rarefaction wave with characteristic velocity $\lambda_1(a, \rho) > 0$.

From Figure 2.2, we can see that this type of solutions are admitted only when the roadway merges at $x = 0$. Here we present an example of this type of solutions in Figure 2.7.

From Figure 2.7, we obtain the boundary flux $f_0^* = f(U_2)$ for wave solutions of

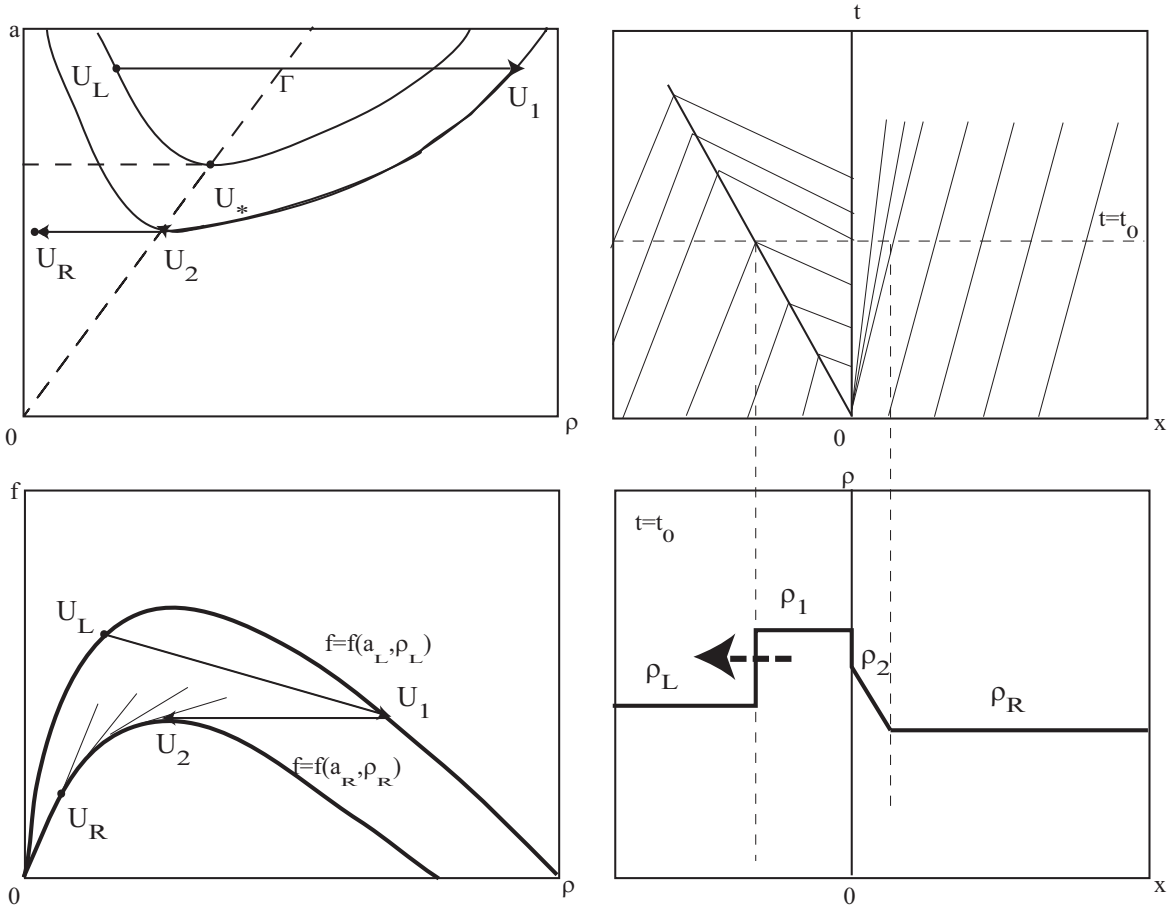


Figure 2.7: An example for wave solutions of type 4 for Equation 2.5 with initial conditions Equation 2.14

type 4.

When $U_L = (a_L, \rho_L)$ is OC; i.e., $\rho_L/a_L > \alpha$, we denote the special critical point on 1-wave curve passing U_L as U_* ; i.e., $U_* = (a_L, \rho_*|_{\rho_*/a_L=\alpha})$. Thus, as shown in Figure 2.3, the U -space is partitioned into three regions by three curves $DU_* = \{a = a_* = a_L, 0 \leq \rho \leq \rho_*\}$, $OU_* = \{0 \leq a \leq a_*, \rho = a\alpha\}$ and $U_*C = \{a \geq a_*, f(a, \rho) = f(U_*)\}$. Related to different positions of the right state U_R in the U -space, the Riemann problem for Equation 2.5 with initial conditions Equation 2.14 has the following six

types of wave solutions. For each type of solutions we provide formula for calculating the associated boundary flux f_0^* .

Type 5 When U_R resides in region ABU_*DA shown in Figure 2.3; i.e.,

$$f(U_R) < f(U_*), \quad \rho_R/a_R < \alpha \text{ and } a_R \geq a_* = a_L, \quad (2.21)$$

wave solutions to the Riemann problem are of type 5. These solutions consist of three basic waves with two intermediate states: $U_1 = U_*$ and $U_2 = (a_R, \rho_2|_{f(U_2)=f(U_*)})$. Of these three waves, the left one (U_L, U_1) is a rarefaction wave with negative characteristic wave velocity $\lambda_1(a, \rho)$, the middle one (U_1, U_2) is a standing wave and the right one (U_2, U_R) is a rarefaction wave with positive characteristic velocity $\lambda_1(a, \rho)$.

From Figure 2.3, we can see that this type of solutions are admitted only when the roadway diverges at $x = 0$. Here we present an example of this type of solutions in Figure 2.8.

From Figure 2.8, we obtain the boundary flux $f_0^* = f(U_2)$ for wave solutions of type 5.

Type 6 When U_R resides in region BU_*CB shown in Figure 2.3; i.e.,

$$f(U_R) \geq f(U_*), \quad (2.22)$$

solutions to the Riemann problem are of type 6. These solutions consist of three basic waves with two intermediate states: $U_1 = U_*$ and $U_2 = (a_R, \rho_2|_{f(U_2)=f(U_*)})$. Of these three waves, the left one (U_L, U_1) is a rarefaction wave with negative characteristic velocity $\lambda_1(a, \rho)$, the middle one (U_1, U_2) is a standing wave and the right one (U_2, U_R) is a shock wave with positive speed $\sigma = \frac{f(U_R)-f(U_2)}{\rho_R-\rho_2}$.

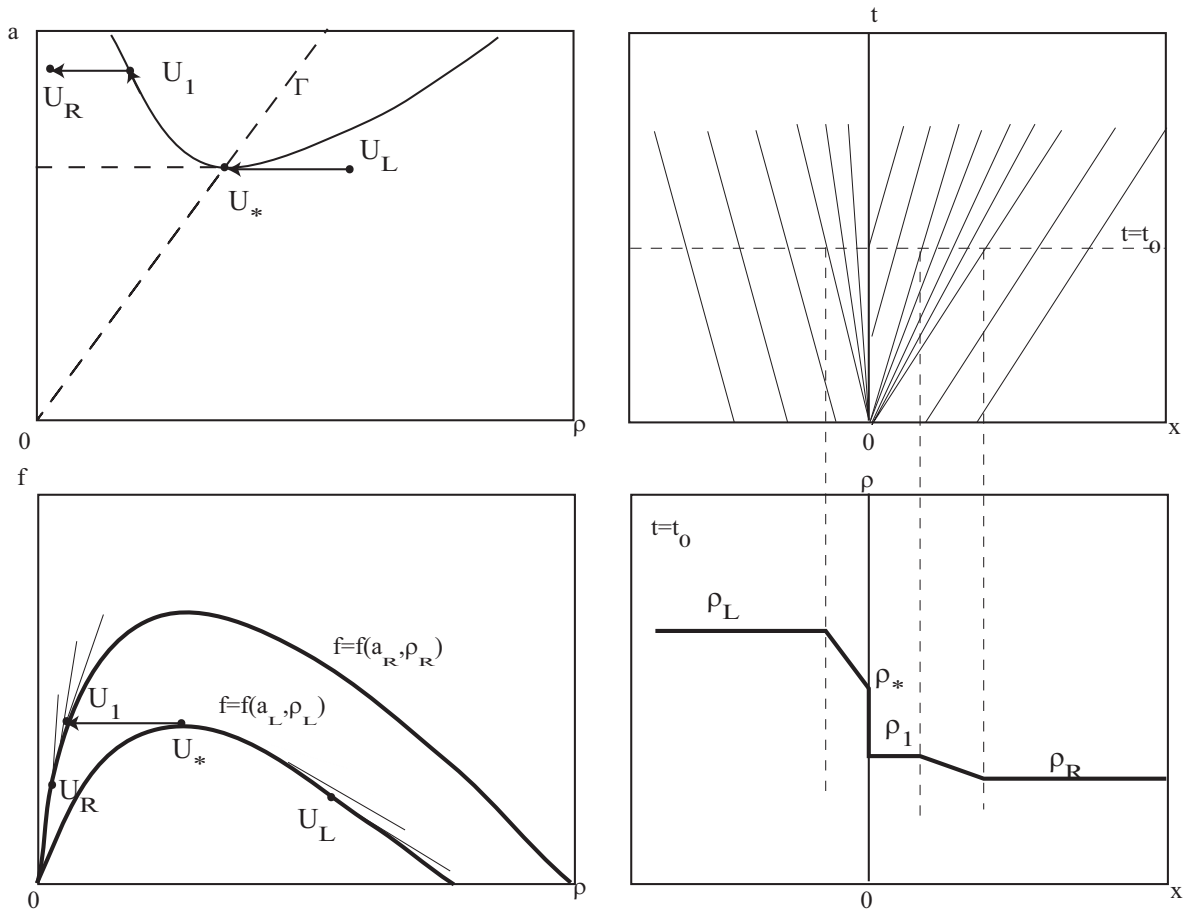


Figure 2.8: An example for wave solutions of type 5 for Equation 2.5 with initial conditions Equation 2.14

From Figure 2.3, we can see that this type of solutions may be admitted when the downstream traffic condition is UC or OC; However, they are admitted only when the roadway diverges at $x = 0$. Here we present an example of this type of solutions in Figure 2.9, where the downstream traffic condition is OC. In the case when the downstream traffic condition is UC, we can find similar solutions. From Figure 2.9, we obtain the boundary flux $f_0^* = f(U_2)$ for this type of wave solutions. Here we have the same formula as that for wave solutions of type 5.

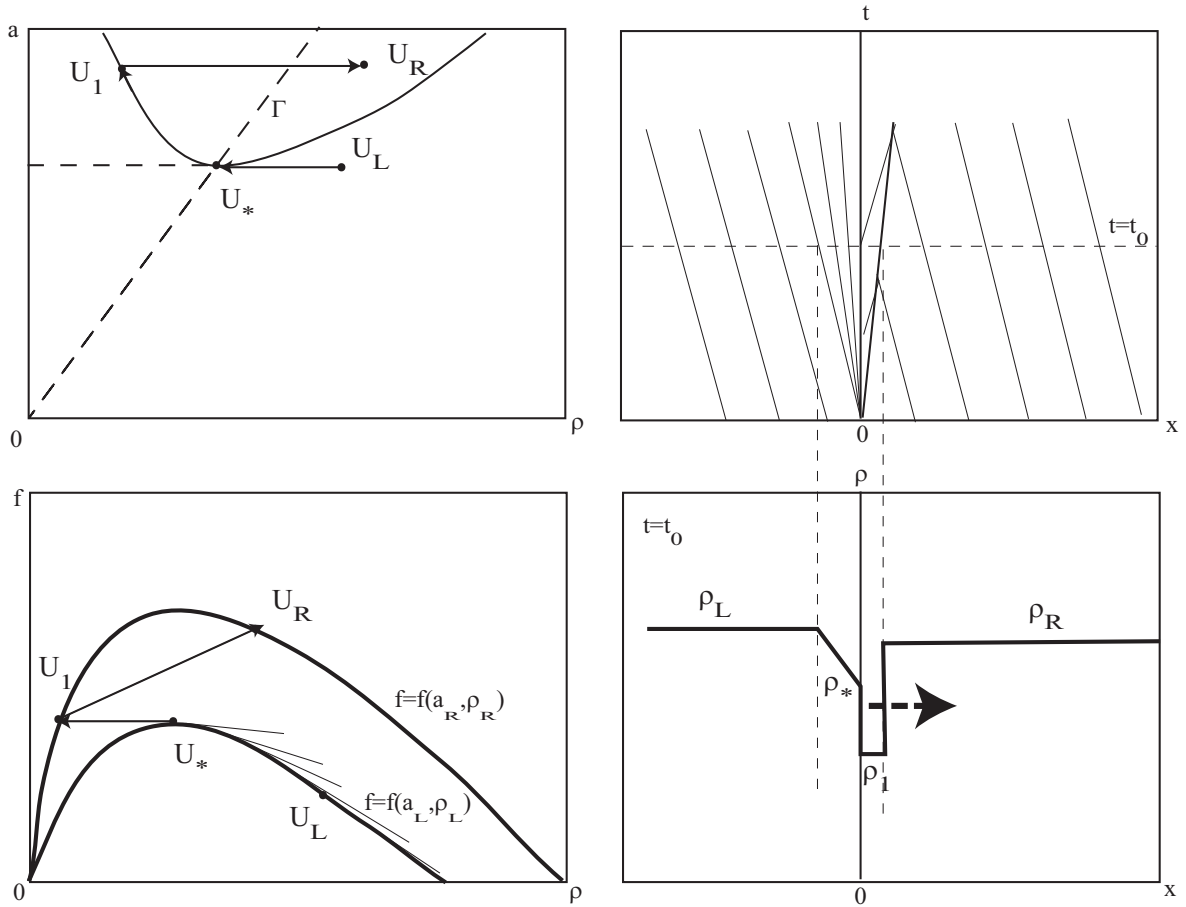


Figure 2.9: An example for wave solutions of type 6 for Equation 2.5 with initial conditions Equation 2.14

Type 7 When U_R resides in region $CU_*FU_L EC$ shown in Figure 2.3; i.e.,

$$f(U_L) \leq f(U_R) < f(U_*) \text{ and } \rho_R/a_R \geq \alpha, \tag{2.23}$$

wave solutions to the Riemann problem are of type 7. These solutions consist of two basic waves with an intermediate state $U_1 = (a_L, \rho_1 |_{f(U_1)=f(U_R)})$. Of these two waves, the left one (U_L, U_1) is a rarefaction with negative characteristic velocity $\lambda_1(a, \rho)$, and the right one (U_1, U_R) is a standing wave.

From Figure 2.3, we can see that the Riemann problem may admit this type of

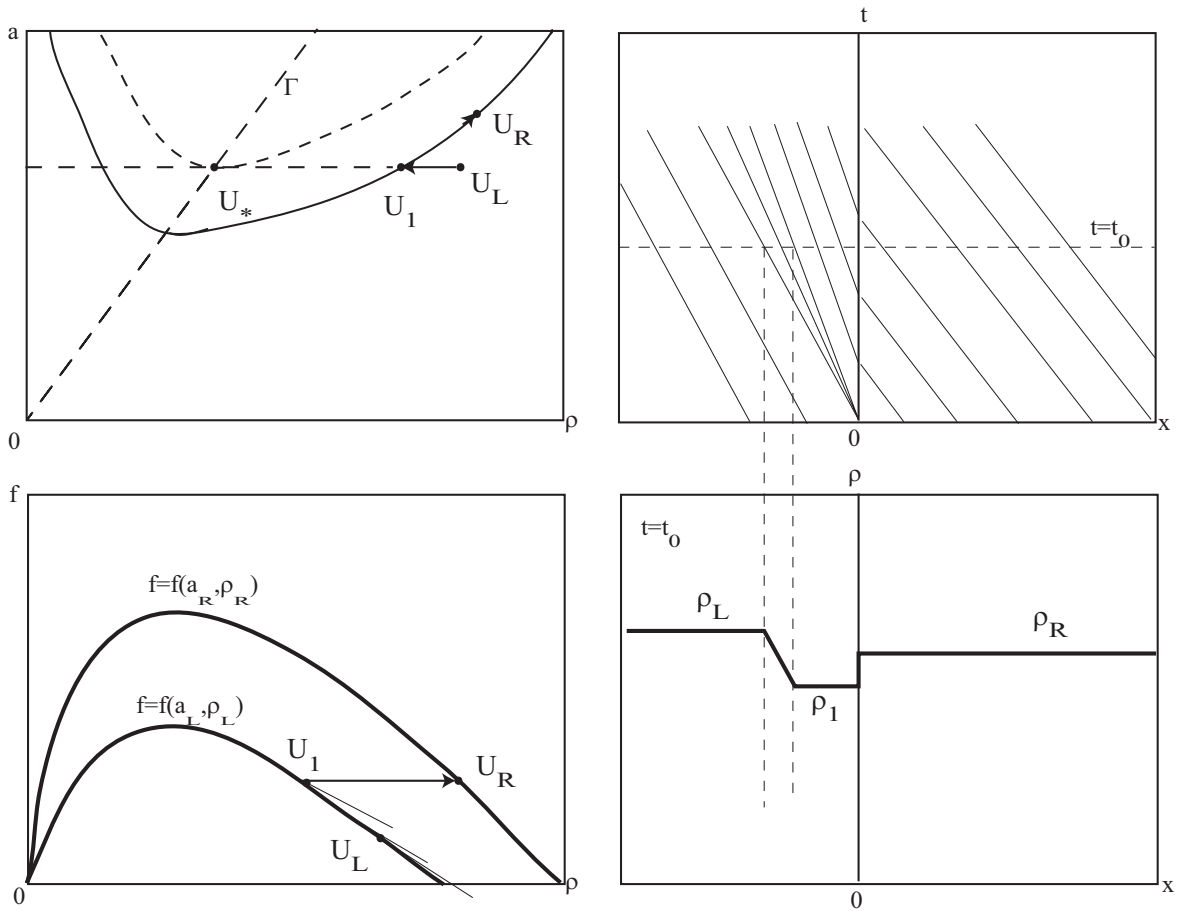


Figure 2.10: An example for wave solutions of type 7 for Equation 2.5 with initial conditions Equation 2.14

solutions when the roadway merges or diverges at $x = 0$. Here we present an example of this type of solutions in Figure 2.10, where the roadway diverges at $x = 0$. In the case when the roadway merges, we can find similar solutions.

From Figure 2.10, we obtain the boundary flux $f_0^* = f(U_R)$ for wave solutions of type 7.

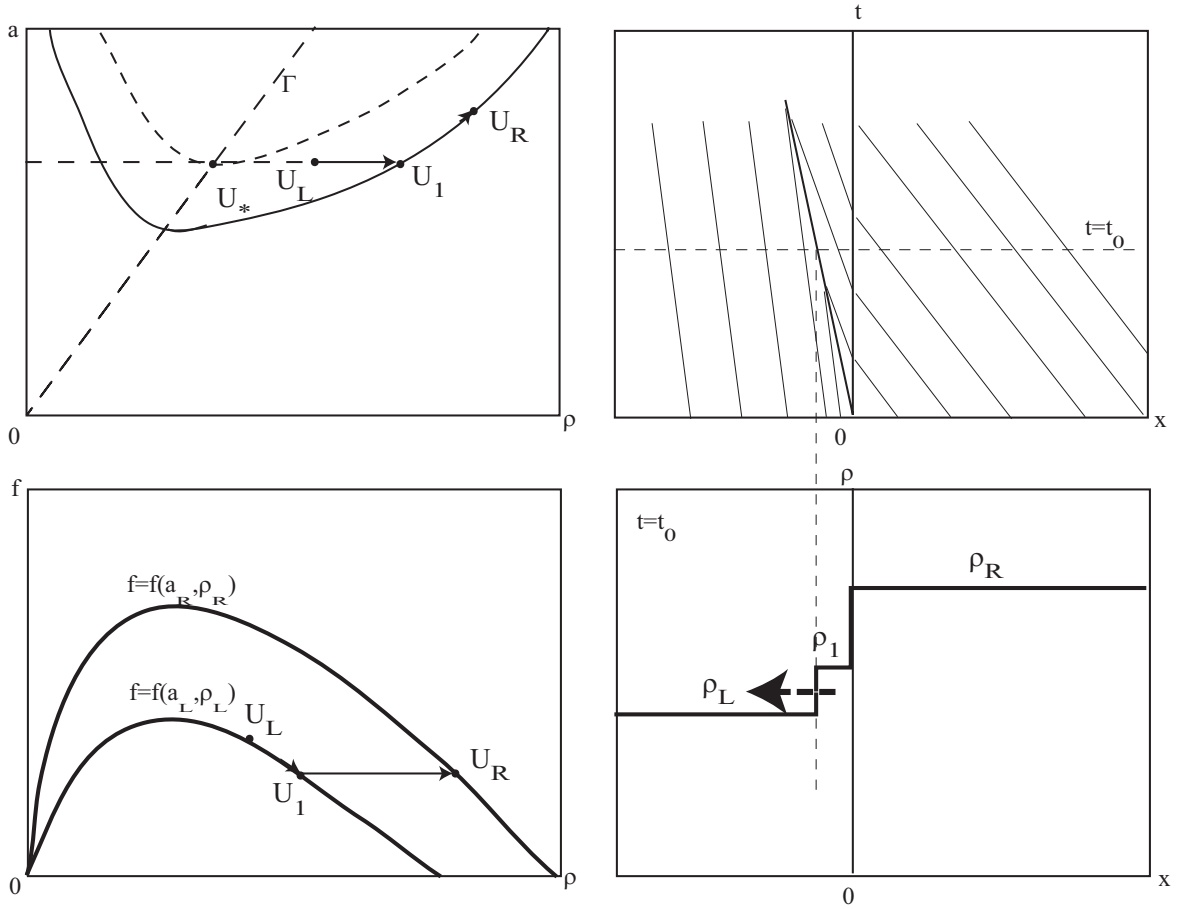


Figure 2.11: An example for wave solutions of type 8 for Equation 2.5 with initial conditions Equation 2.14

Type 8 When U_R locates in region $FU_L EOF$ shown in Figure 2.3; i.e.,

$$f(U_R) < f(U_L) < f(U_*) \text{ and } \rho_R/a_R \geq \alpha, \tag{2.24}$$

wave solutions to the Riemann problem are of type 8. These solutions consist of two basic waves with an intermediate state $U_1 = (a_L, \rho_1 |_{f(U_1)=f(U_R)})$. Of these two waves, the left one (U_L, U_1) is a shock with negative speed $\sigma = \frac{f(U_L)-f(U_1)}{\rho_L-\rho_1}$, and the right one (U_1, U_R) is a standing wave.

Like in the previous case, the Riemann problem may admit this type of solutions

when the roadway merges or diverges at $x = 0$. Here we present an example of this type of solutions in Figure 2.11, where the roadway diverges at $x = 0$. In the case when the roadway merges, we can find similar solutions.

From Figure 2.11, we obtain the boundary flux $f_0^* = f(U_R)$ for wave solutions of type 8. The formula is the same as that for wave solutions of type 7.

Type 9 When U_R resides in region DU_*FGD shown in Figure 2.3; i.e.,

$$f(U_L) \leq f(U_R) < f(U_*), \quad \rho_R/a_R < \alpha \text{ and } a_R < a_* = a_L, \quad (2.25)$$

wave solutions to the Riemann problem are of type 9. These solutions consist of three basic waves with two intermediate states: $U_1 = (a_L, \rho_1|_{f(U_1)=f(U_2)})$ and $U_2 = (a_R, \rho_2|_{\rho_2/a_R=\alpha})$. Of these three waves, the left one (U_L, U_1) is a rarefaction with negative characteristic velocity $\lambda_1(a, \rho)$, the middle one (U_1, U_2) is a standing wave, and the right one (U_2, U_R) is a rarefaction with positive speed $\lambda_1(a, \rho)$.

From Figure 2.3, we can see that this type of solutions are admitted only when the roadway merges at $x = 0$. Here we present an example of this type of solutions in Figure 2.12.

From Figure 2.12, we obtain the boundary flux $f_0^* = f(U_2)$ for wave solutions of type 9.

Type 10 When U_R resides in region $GFOG$ shown in Figure 2.3; i.e.,

$$f(U_R) < f(U_L) < f(U_*), \quad \rho_R/a_R < \alpha \text{ and } a_R < a_* = a_L, \quad (2.26)$$

wave solutions to the Riemann problem are of type 10. These solutions consist of three basic waves with two intermediate states: $U_1 = (a_L, \rho_1|_{f(U_1)=f(U_2)})$ and $U_2 = (a_R, \rho_2|_{\rho_2/a_R=\alpha})$. Of these three waves, the left one (U_L, U_1) is a shock

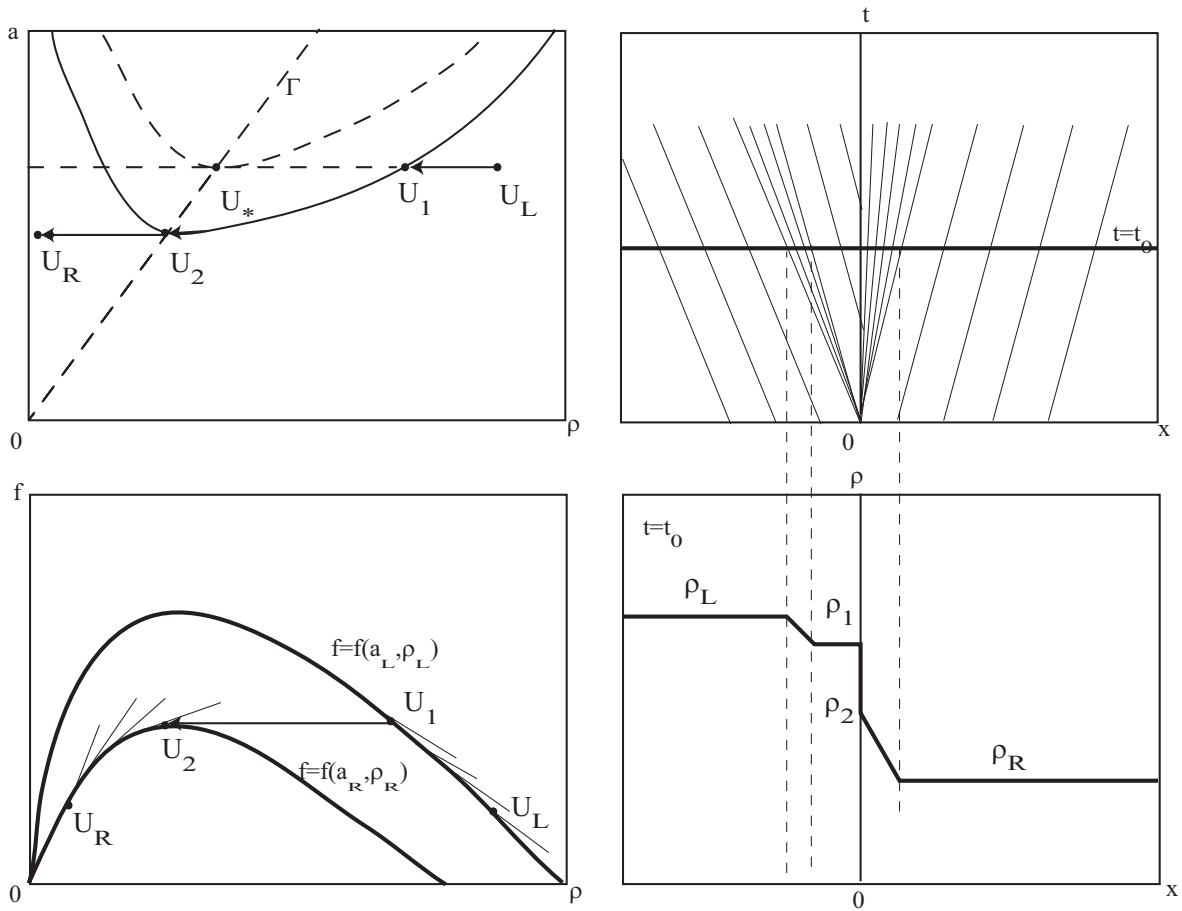


Figure 2.12: An example for wave solutions of type 9 for Equation 2.5 with initial conditions Equation 2.14

with negative speed, the middle one (U_1, U_2) is a standing wave, and the right one (U_2, U_R) is a rarefaction wave with positive characteristic velocity $\lambda_1(a, \rho)$.

Like in the previous case, this type of solutions are admitted only when the roadway merges at $x = 0$. Here we present an example of this type of solutions in Figure 2.13.

From Figure 2.13, we obtain the boundary flux $f_0^* = f(U_2)$ for wave solutions of type 10. Here we have the same formula as that for wave solutions of type 9.

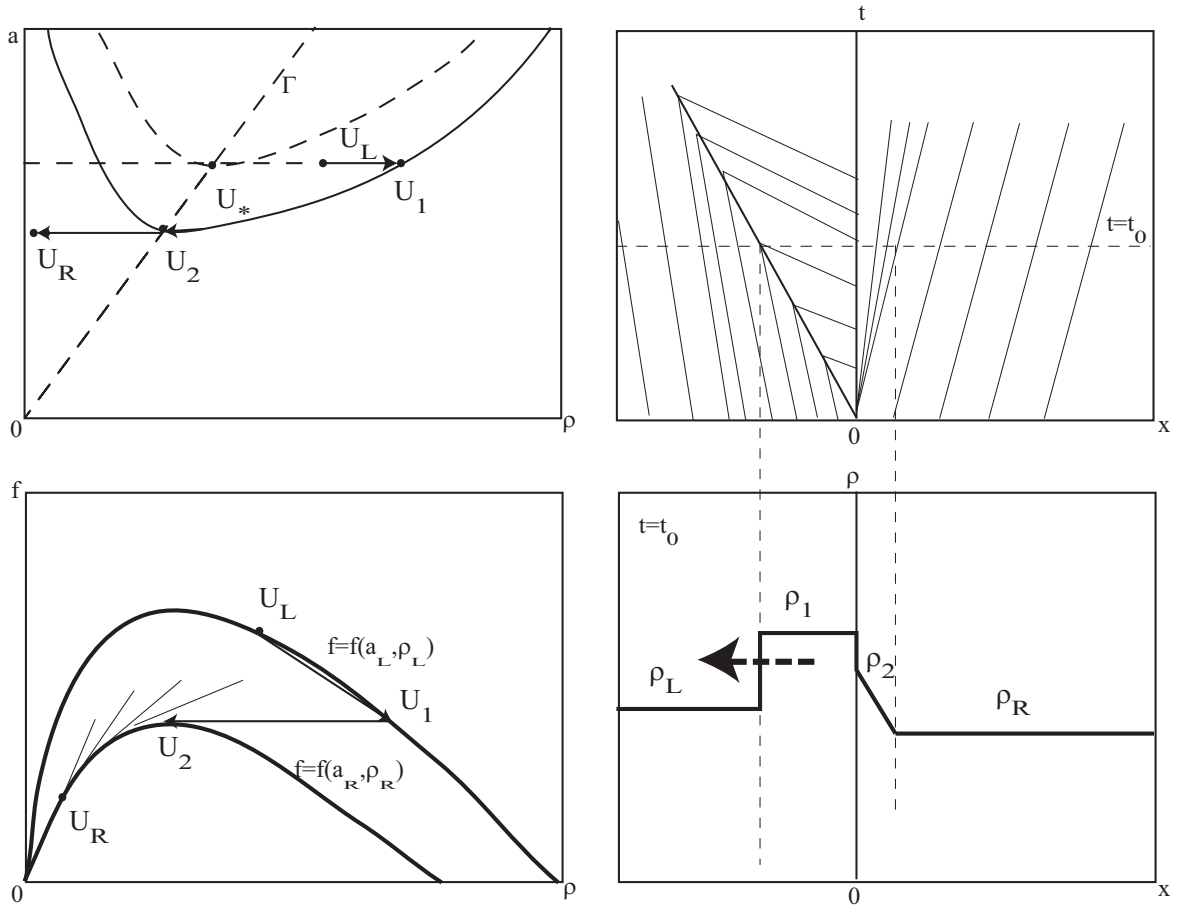


Figure 2.13: An example for wave solutions of type 10 for Equation 2.5 with initial conditions Equation 2.14

2.3.2 Summary

In each of the 10 cases discussed above, the boundary flux f_0^* is equal to one of the following four quantities: the upstream flow-rate $f(U_L)$, the downstream flow-rate $f(U_R)$, the capacity of the upstream roadway f_L^{max} and the capacity of the downstream roadway f_R^{max} . For wave solutions of type 1 and 2, the boundary flux is equal to the upstream traffic flow-rate; i.e., $f_0^* = f(U_L)$. For wave solutions of type 3, 7 and 8, the boundary flux is equal to the downstream traffic flow-rate; i.e.,

No.	left state U_L	right state U_R	f_0^*
1	UC	$f(U_R) < f(U_L), a_R > a_*, \rho_R/a_R < \alpha$	$f(U_L)$
2	UC	$f(U_R) > f(U_L)$	$f(U_L)$
3	UC	$f(U_R) < f(U_L), \rho_R/a_R > \alpha$	$f(U_R)$
4	UC	$f(U_R) < f(U_L), \rho_R/a_R < \alpha, a_R < a_*$	f_R^{max}
5	OC	$f(U_R) < f_L^{max}, a_R > a_L, \rho_R/a_R < \alpha$	f_L^{max}
6	OC	$f(U_R) > f_L^{max}$	f_L^{max}
7	OC	$f(U_L) < f(U_R) < f_L^{max}, \rho_R/a_R > \alpha$	$f(U_R)$
8	OC	$f(U_R) < f(U_L), \rho_R/a_R > \alpha$	$f(U_R)$
9	OC	$f(U_L) < f(U_R) < f_L^{max}, \rho_R/a_R < \alpha, a_R < a_L$	f_R^{max}
10	OC	$f(U_R) < f(U_L), \rho_R/a_R < \alpha, a_R < a_L$	f_R^{max}

Table 2.1: Solutions of the boundary fluxes f_0^*

$f_0^* = f(U_R)$. For wave solutions of type 4, 9 and 10, the boundary flux is equal to the capacity of the downstream roadway; i.e., $f_0^* = f_R^{max}$. For wave solutions of type 5 and 6, the boundary flux is equal to the capacity of the upstream roadway; i.e., $f_0^* = f_L^{max}$. In Table 2.1, the boundary fluxes are listed for the 10 types of wave solutions to the Riemann problem, as well as the conditions when the Riemann problem admit those solutions.

Note that when $a_L = a_R$; i.e., when Equation 2.4 becomes a homogeneous LWR model, wave solutions and the solutions of the boundary fluxes provided here are the same as those for the homogeneous LWR model.

Lebacque (1996) studied the Riemann problem of the inhomogeneous LWR for Equation 2.3. He classified the problem according to two criteria. The first criterion is to compare capacity of the upstream cell and that of the downstream cell. For the roadway with variable number of lanes, it is equivalently to compare the number of

Conditions	Solutions by Lebacque	Types	Our solutions
$a_L \leq a_R, U_L \text{ UC}, U_R \text{ UC}$	$f(U_L)$	1	$f(U_L)$
$a_L \leq a_R, U_L \text{ UC}, U_R \text{ OC}$	$\min\{f(U_L), f(U_R)\}$	2 or 3	$f(U_L)$ or $f(U_R)$
$a_L \leq a_R, U_L \text{ OC}, U_R \text{ UC}$	f_L^{max}	5 or 6	f_L^{max}
$a_L \leq a_R, U_L \text{ OC}, U_R \text{ OC}$	$\min\{f_L^{max}, f(U_R)\}$	6, 7 or 8	f_L^{max} or $f(U_R)$
$a_L \geq a_R, U_L \text{ UC}, U_R \text{ UC}$	$\min\{f_R^{max}, f(U_L)\}$	1 or 4	$f(U_L), f_R^{max}$
$a_L \geq a_R, U_L \text{ UC}, U_R \text{ OC}$	$\min\{f(U_L), f(U_R)\}$	2 or 3	$f(U_L)$ or $f(U_R)$
$a_L \geq a_R, U_L \text{ OC}, U_R \text{ UC}$	f_R^{max}	9 or 10	f_R^{max}
$a_L \geq a_R, U_L \text{ OC}, U_R \text{ OC}$	$f(U_R)$	7 or 8	$f(U_R)$

Table 2.2: Comparison with Lebacque's results

lanes of the upstream cell and that of the downstream cell. The second criterion is to consider whether the upstream and downstream traffic conditions are UC or OC. With these criteria, he discussed 8 types of waves solutions to the Riemann problem and obtained the formula for the boundary flux related to each type of solutions. The conditions for those types of wave solutions as well as the formulas related to those types of solutions are listed in Table 2.2. Under each of those conditions, the Riemann problem may admit different types of solutions discussed in Section 2.3.1. The types of solutions and our related formulas for the boundary flux are also presented in Table 2.2. From this table, we can see that our results are consistent with those provided by Lebacque, although the Riemann problem is solved through different approaches.

The consistency of our results with existing results can also be shown by introducing a simple formula for the boundary flux. If we define the upstream demand as

$$f_L^* = \begin{cases} f(U_L), & \rho_L/a_L < \alpha \\ f_L^{max}, & \rho_L/a_L \geq \alpha \end{cases} \quad (2.27)$$

and define the downstream supply as

$$f_R^* = \begin{cases} f_R^{max}, & \rho_R/a_R < \alpha \\ f(U_R), & \rho_R/a_R \geq \alpha \end{cases} \quad (2.28)$$

then the boundary flux can be simply computed as

$$f_0^* = \min\{f_L^*, f_R^*\}. \quad (2.29)$$

Note that $f_L^* = f(U_*)$. Formula Equation 2.29 was also provided by Daganzo (1995a) and Lebacque (1996).

2.4 Simulation of traffic flow on a ring road with a bottleneck

2.4.1 Solution method

The augmented inhomogeneous LWR model, expressed in conservation form Equation 2.5, can be solved efficiently with Godunov's method under general initial and boundary conditions. In Godunov's method, the roadway is partitioned into N cells and a duration of time is discretized into M time steps. In a cell i , we approximate the continuous equation Equation 2.5 with a finite difference equation

$$\frac{U_i^{m+1} - U_i^m}{\Delta t} + \frac{F_{i-1/2}^* - F_{i+1/2}^*}{\Delta x} = 0, \quad (2.30)$$

whose component for ρ is

$$\frac{\rho_i^{m+1} - \rho_i^m}{\Delta t} + \frac{f_{i-1/2}^* - f_{i+1/2}^*}{\Delta x} = 0, \quad (2.31)$$

where ρ_i^m denotes the average of ρ in cell i at time step m , similarly ρ_i^{m+1} is the average at time step $m + 1$; $f_{i-1/2}^*$ denotes the flux through the upstream boundary

of cell i , and similarly $f_{i+1/2}^*$ denotes the downstream boundary flux of cell i . In Equation 2.31, the boundary flux $f_{i-1/2}^*$ is related to solutions to a Riemann problem for Equation 2.5 with the following initial conditions:

$$U(x = x_{i-1/2}, t = t_m) = \begin{cases} U_{i-1}^m & x < x_{i-1/2} \\ U_i^m & x > x_{i-1/2} \end{cases}, \quad (2.32)$$

which have been discussed in Section 2.3.

2.4.2 Numerical results

We use the approximation developed earlier to simulate traffic on a ring road. The length of the ring road is $L = 800l = 22.4$ km. The simulation time is $T = 500\tau = 2500$ s = 41.7 min. We partition the road $[0, L]$ into $N = 100$ cells and the time interval $[0, T]$ into $K = 500$ steps. Hence, the length of each cell is $\Delta x = 0.224$ km and the length of each time step is $\Delta t = 5$ s. Since $|\lambda_*| \leq v_f = 5l/\tau$, we find the CFL (Courant et al., 1928) condition number

$$\max |\lambda_*| \frac{\Delta t}{\Delta x} \leq 0.625 < 1.$$

Moreover, we adopt in this simulation the fundamental diagram used in (Kerner and Konhäuser, 1994; Herrmann and Kerner, 1998) with the following parameters: the relaxation time $\tau = 5$ s; the unit length $l = 0.028$ km; the free flow speed $v_f = 5.0l/\tau = 0.028$ km/s = 100.8 km/h; the jam density of a single lane $\rho_j = 180$ veh/km/lane. The equilibrium speed-density relationship is therefore

$$v_*(\rho, a(x)) = 5.0461 \left[\left(1 + \exp\left\{ \left[\frac{\rho}{a(x)\rho_j} - 0.25 \right] / 0.06 \right\} \right)^{-1} - 3.72 \times 10^{-6} \right] l/\tau,$$

where $a(x)$ is the number of lanes at location x . The equilibrium functions $V(\rho, a(x))$ and $f(\rho, a(x))$ are given in Figure 2.14.

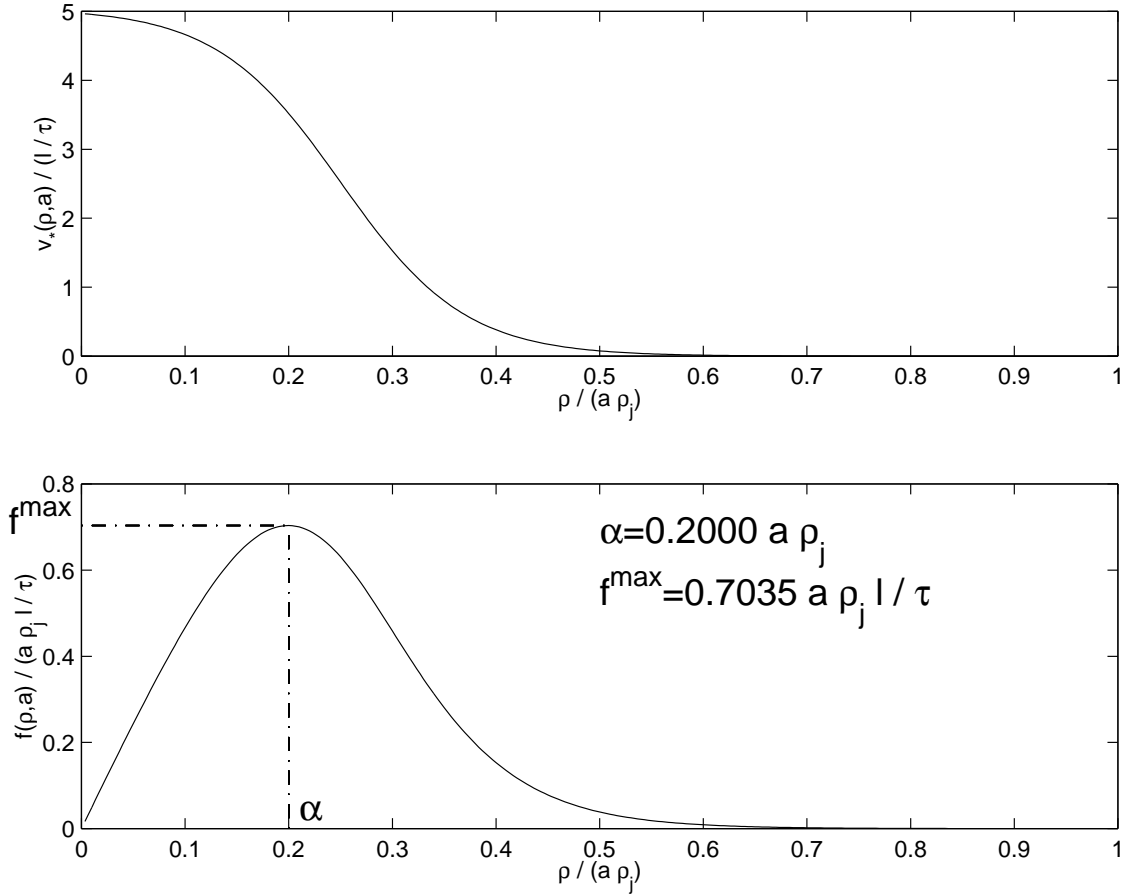


Figure 2.14: The Kerner-Konhäuser model of speed-density and flow-density relations

The first simulation is about the homogeneous LWR model. Here we assume that the ring road has single lane everywhere; i.e., $a(x) = 1$ for any $x \in [0, L]$, and use a global perturbation as the initial condition

$$\begin{aligned} \rho(x, 0) &= \rho_h + \Delta\rho_0 \sin \frac{2\pi x}{L}, \quad x \in [0, L], \\ v(x, 0) &= v_*(\rho(x, 0), 1), \quad x \in [0, L], \end{aligned} \tag{2.33}$$

with $\rho_h = 28$ veh/km and $\Delta\rho_0 = 3$ veh/km (the corresponding initial condition Equation 2.33 is depicted in Figure 2.15).

The results are shown in Figure 2.16, from which we observe that initially wave

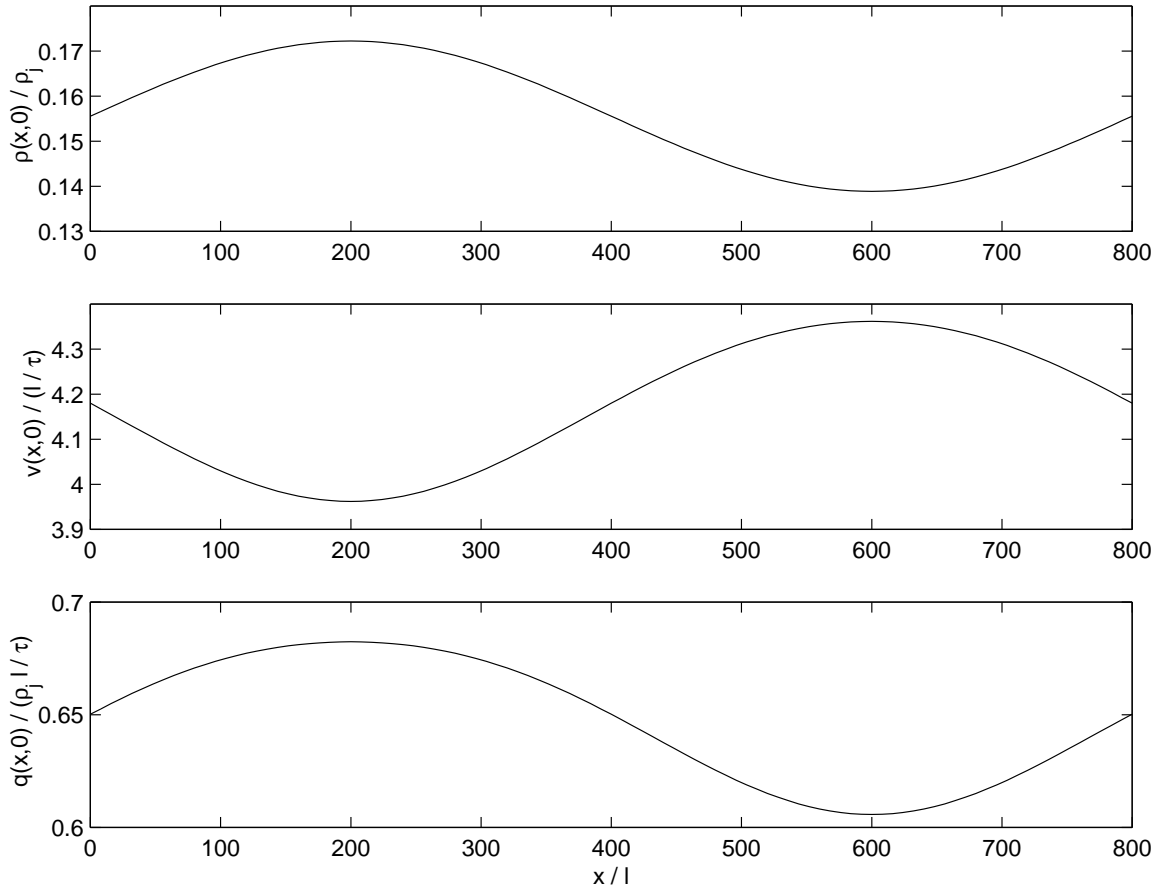


Figure 2.15: Initial condition Equation 2.33 with $\rho_h = 28$ veh/km and $\Delta\rho_0 = 3$ veh/km

interactions are strong but gradually the bulge sharpens from behind and expands from front to form a so-called N -wave that travels around the ring with a nearly fixed profile.

In the second simulation we created a bottleneck on the ring road with the following lane configuration:

$$a(x) = \begin{cases} 1, & x \in [320l, 400l), \\ 2, & \text{elsewhere} . \end{cases} \quad (2.34)$$

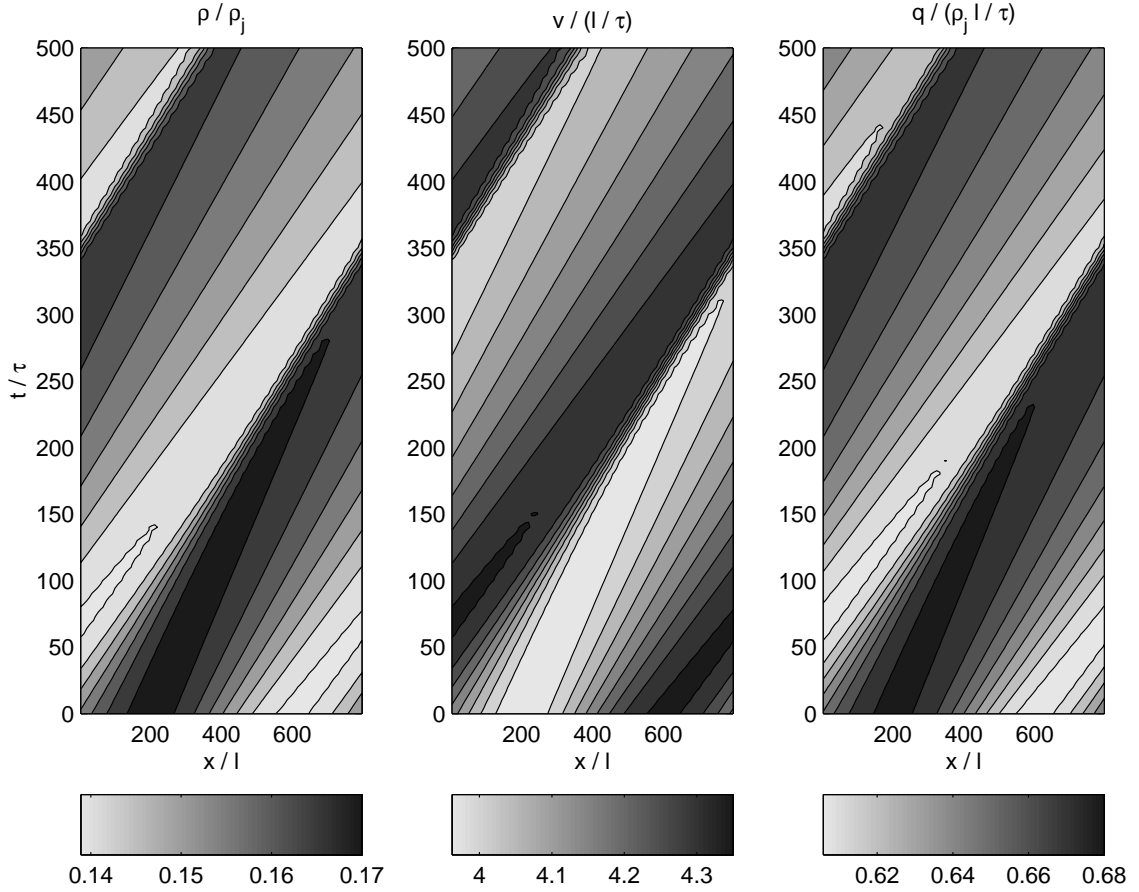


Figure 2.16: Solutions of the homogeneous LWR model with initial condition in Figure 2.15

As before, we also use a global perturbation as the initial condition

$$\begin{aligned}
 \rho(x, 0) &= a(x)(\rho_h + \Delta\rho_0 \sin \frac{2\pi x}{L}), & x \in [0, L], \\
 v(x, 0) &= v_*(\rho(x, 0), a(x)), & x \in [0, L],
 \end{aligned}
 \tag{2.35}$$

with $\rho_h = 28$ veh/km/lane and $\Delta\rho_0 = 3$ veh/km/lane (the corresponding initial condition Equation 2.35 is depicted in Figure 2.17).

The results for this simulation are shown in Figure 2.18, and are more interesting. We observe from this figure that at first flow increases in the bottleneck to make

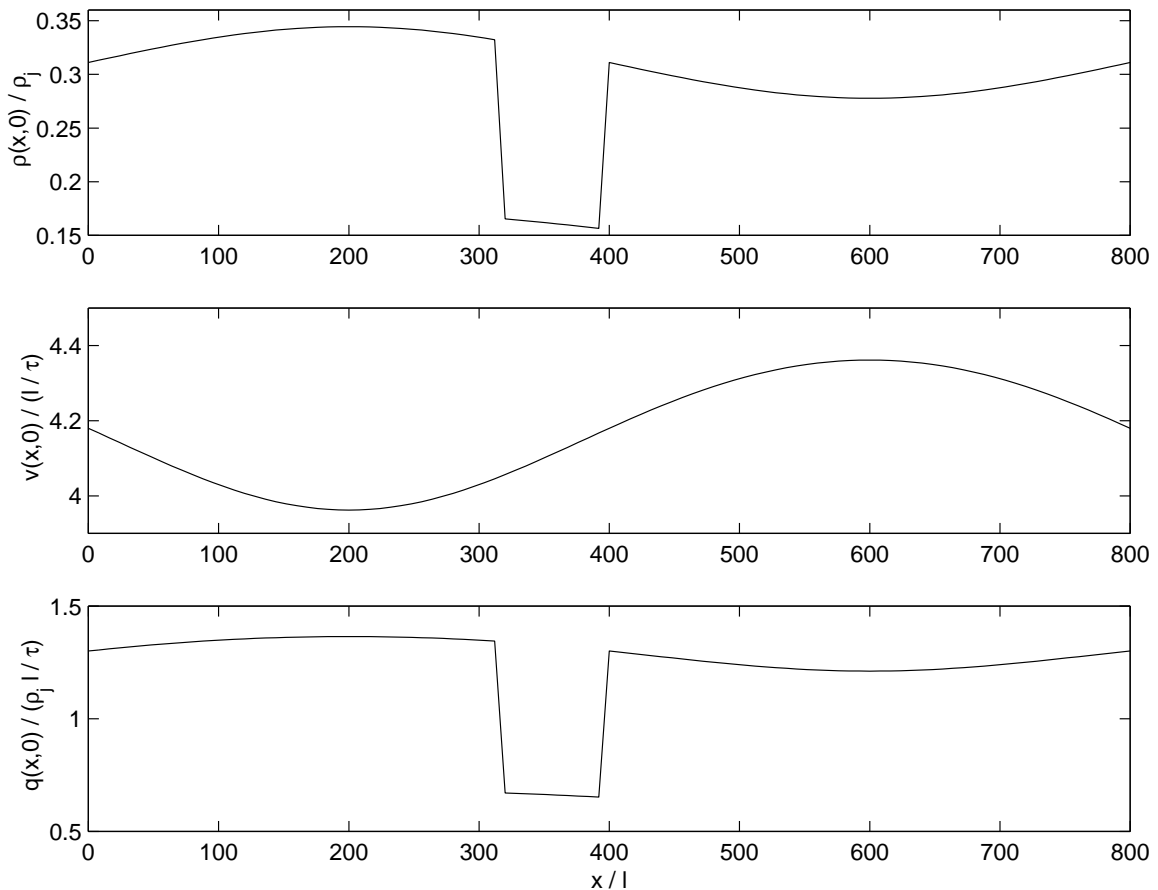


Figure 2.17: Initial condition Equation 2.33 with $\rho_h = 28$ veh/km/lane and $\Delta\rho_0 = 3$ veh/km/lane

the bottleneck saturated, then a queue forms upstream of the bottleneck, whose tail propagates upstream as a shock. At the same time, traffic emerging from the bottleneck accelerates in an expansion wave. After a while, all the commotion settles and an equilibrium state is reached, where a stationary queue forms upstream of the bottleneck, whose in/out flux equals the capacity of the bottleneck. Similar situations can be observed in real world bottlenecks, although queues formed at such bottlenecks rarely reach equilibrium because, unlike in the ring road example, their

traffic demands change over time. Therefore, we observe queues forming, growing, and dissipating at locations with lane drops, upward slopes, or tight turns. Sometimes queues formed at a bottleneck can grow fairly long, to the extent that they entrap vehicles that do not use the bottleneck. Under such situations, we can implement various types of control strategies, such as ramp metering, to control the extent of the bottleneck queues so that they do not block vehicles that wish to exit upstream of the bottleneck. For this purpose the numerical method presented here can be used to help model and design effective control.

2.5 Concluding remarks

We studied the inhomogeneous LWR model as a nonlinear resonant system. The nonlinear resonance arises when the two characteristics of the augmented LWR model coalesce. Critical states and a transitional curve Γ can be defined in the U space based on the behavior of these characteristics, which are in turn used to solve the Riemann problem for the inhomogeneous LWR model. It is found that, under the entropy conditions of Lax and of Isaacson and Temple, there exist ten types of wave solutions. Formulas for computing the boundary fluxes related to different types of wave solutions were also obtained. These formulas, after translated into the supply/demand framework, are found to be consistent with those found in literature. For problems with general initial/boundary conditions, the method of Godunov was applied to solve the inhomogeneous model numerically.

The method presented here can be extended easily to model more complicated situations, such as multiple inhomogeneities. Suppose at location x , there are $i = 1, \dots, n$ types of inhomogeneities, such as changes in number of lanes, grade, and curvature. We introduce an inhomogeneity vector $\vec{a}(x) = (a_1(x), a_2(x), \dots, a_n(x))^T$, and

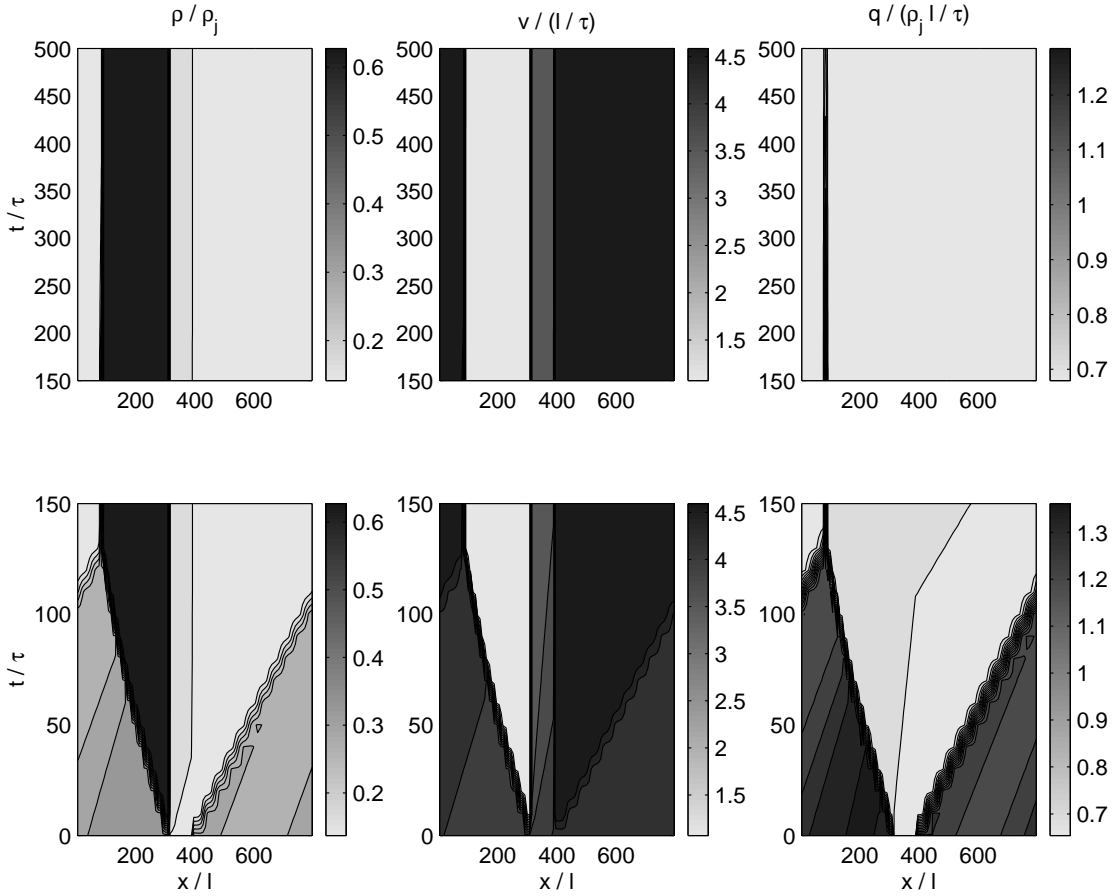


Figure 2.18: Solutions of the inhomogeneous LWR model with initial condition in Figure 2.17

express the flow-density function as $f(\vec{a}(x), \rho)$. Then the conservation law becomes

$$\begin{cases} \rho_t + f(\vec{a}(x), \rho)_x = 0, \\ \vec{a}(x)_t = 0, \end{cases}$$

and this higher-dimensional nonlinear resonant system can be solved in a similar way.

It is worth mentioning that the augmentation approach taken in this chapter also applies to higher-order traffic flow models for inhomogeneous roads.

Chapter 3

Kinematic wave traffic flow model of merging traffic

3.1 Introduction

For developing advanced traffic control strategies, dynamic traffic assignment (DTA) algorithms, and other technologies in Advanced Traffic Management Systems (ATMS) and Advanced Traveler Information Systems (ATIS), traffic engineers need the assistance of network traffic flow models that can capture system-wide features of traffic dynamics and are computationally efficient for a network of realistic size. The kinematic wave model is a promising candidate for these tasks since it provides a realistic description of dynamic traffic phenomena in the aggregate level in terms of expansion and shock waves and as such is highly efficient for simulating traffic dynamics in a large network.

In the seminal kinematic wave model by Lighthill and Whitham (1955b) and Richards (1956), a.k.a. the LWR model, how a disturbance in traffic propagates through a link was thoroughly studied. To model traffic dynamics on a network with

the kinematic wave model, however, one needs to carefully study traffic dynamics at a merge, a diverge, or other components of a network. The kinematic wave models of merging traffic have been studied by Daganzo (1995a), Holden and Risebro (1995), and Lebacque (1996). In the model by Holden and Risebro, traffic flows through a merge are determined by an optimization problem. However, the physical meaning and the objective function of the optimization problem are not known or supported by observations. On the other hand, the models by Daganzo and Lebacque are based on the definitions of the local traffic supply and demand and can be considered as reasonable extensions of the kinematic wave model of link traffic flow. In this chapter, we will examine the latter models so that they can be better understood, more easily calibrated, and more efficiently applied in simulation.

As we know, the LWR model, in which the evolution of traffic density $\rho(x, t)$, flow-rate $q(x, t)$, and travel speed $v(x, t)$ is studied in space x and time t , can be written as a partial differential equation based on the fact of traffic conservation and the adoption of a fundamental diagram. For the purpose of simulation, the LWR model is generally written in a discrete form: a link and a duration of time are partitioned into a number of cells and time steps respectively, and the increment of the number of vehicles in a cell at each time step equals to the difference between the inflow into and outflow from that cell during the time step. In the discrete LWR model, to solve the flow through a boundary (i.e., the inflow into the downstream cell and the outflow from the upstream cell), two equivalent approaches can be used: in the mathematical approach, one solves the Riemann problem at that boundary (Lebacque, 1996; Jin and Zhang, 2003b); in the engineering approach, a.k.a. the supply-demand method, the supply of the upstream cell and the demand of the downstream cell are computed first and the boundary flow is taken as their minimum. Here the concepts of supply and demand were first introduced by Daganzo (1995a), but using the terms of “sending flow” and

“receiving flow” instead; the terms of “supply” and “demand” were first used by Lebacque (1996). The definitions of demand and supply are as follows: the demand of a cell is equal to its flow-rate when the traffic condition is under-critical (i.e., free flow) and its flow capacity when overcritical (i.e., congested); the supply is equal to the flow capacity of the cell when the traffic condition is under-critical and the flow-rate when overcritical.¹

For computing flows through a merge, including the outflows from the upstream cells and the inflow into the downstream cell, Daganzo (1995) extended the supply-demand method as follows: the outflow from an upstream cell is smaller than or equal to its demand, the inflow to the downstream cell is smaller than or equal to its supply, and the inflow is equal to the sum of the outflows in order to preserve traffic conservation. In this supply-demand method, the inflow is unique since it is equal to the minimum of the supply and total demand. But the outflow from each upstream cell may not be unique. Thus one has to find a way to distribute to each upstream cell a fraction of the total outflow, which is equal to the inflow. Here we call such a way of determining the distribution fractions *the distribution scheme*.

Lebacque proposed another extension of the supply-demand method: the supply of the downstream cell is first distributed as a virtual supply to each upstream cell, the outflow from each upstream cell is the minimum of its demand and virtual supply, and the inflow into the downstream cell is equal to the sum of the outflows. Thus the distribution scheme in Lebacque’s method is used to determine the fractions of virtual supplies, and is more general since more feasible solutions of flows can be found in this method.

Both Daganzo and Lebacque provided general formulations of the kinematic wave

¹From the definitions of demand and supply, we can see that the flow through a boundary is bounded by the capacity.

model of merges. Here, we do not intend to extend these formulations. Rather, we are interested in the distribution schemes used in these models since a distribution scheme is the key to uniquely determine flows through a merge. Since in possible applications of a merge model one wants to obtain unique flows under a given situation, the distribution schemes are worth a thorough examination.

At a first glance, the determination of distribution fractions seems to be complicated since they may be affected by travelers' merging behavior, the geometry of the studied merge, traffic capacities, differences between the upstream cells, traffic conditions, and traffic control. Considering part of these factors, both Daganzo (1995) and Lebacque (1996) provided some suggestions on the distribution fractions: Lebacque suggested that the distribution fraction of an upstream cell is proportional to its number of lanes; Daganzo considered that upstream cells bear different priorities and hence introduced parameters for priorities in his distribution fractions. Both suggestions have their limitations: Lebacque's distribution scheme is very coarse and fails under certain situations, while Daganzo's scheme becomes very complicated for a merge with three or more upstream links. Moreover, priorities in Daganzo's distribution scheme vary with flow levels, which seems to be counter intuitive. Therefore, we devote this study to the better understanding of various distribution schemes in a merge model, and propose a new distribution scheme which is well-defined, computationally efficient, and capable of capturing the characteristic differences between different branches of the merge.

In this chapter, we first review the discrete kinematic wave model of merges and discuss different formulations of the supply-demand method for computing flows through a merge (Section 3.2). In Section 3.3.2, after discussing existing distribution schemes, we propose a simple distribution scheme, which incorporates the "fairness" condition. In this scheme, the distribution fractions are proportional to traffic de-

mands of upstream cells. This scheme is shown to work well in simulations due to its many merits: 1) it is capable of capturing the characteristic differences between upstream cells (e.g. the speed difference between the upstream freeway and on-ramps); 2) it is easy to calibrate because additional parameters such as priorities do not need to be explicitly introduced; and 3) it is computationally efficient. In Section 3.4, we present an example of two merging flows and demonstrate in numerical simulations that the discrete kinematic wave merge model incorporating the “fairness” condition is well-defined and converges in first order. In the conclusion part, we present the supply-demand method for computing flows through a diverge and a general junction for single-commodity traffic flow, and discuss related future research.

3.2 The discrete kinematic wave model of merges with the supply-demand method

In the kinematic wave traffic flow model of a road network with a merge, the LWR model can be used to describe traffic dynamics of each branch, for which flows through the merge can be considered as boundary conditions. Thus, in this section, we first review the discrete LWR model, the definitions of supply and demand, and the supply-demand method for computing flows through link boundaries. After reviewing the models of merges under the supply-demand framework by Daganzo (1995) and Lebacque (1996), we then demonstrate the importance of distribution schemes. At the end of this section, we will discuss the properties of existing distribution schemes.

3.2.1 The discrete LWR model in the supply-demand framework

In the LWR model for each branch of a merge, traffic dynamics are governed by a traffic conservation equation,

$$\rho_t + q_x = 0, \quad (3.1)$$

and an equilibrium relationship between ρ and q , also known as the fundamental diagram,

$$q = Q(a, \rho), \quad (3.2)$$

where $a(x)$ is an inhomogeneity factor, depending on road characteristics, e.g., the number of lanes at x . Since $q = \rho v$, we also have a speed-density relation: $v = V(a, \rho) \equiv Q(a, \rho)/\rho$. For vehicular traffic, generally, v is non-increasing and q is concave in ρ . Examples of empirical models of speed- and flow-density relations can be found in (Newell, 1993; Kerner and Konhäuser, 1994). Related to the fundamental diagram, the following definitions are used in this chapter: the maximum flow-rate at x is called the traffic capacity, and the corresponding density is called the critical density; traffic flow is overcritical when its density is higher than the critical density, and under-critical conversely.

From Equation 3.1 and Equation 3.2, the LWR model can be written as

$$\rho_t + Q(a, \rho)_x = 0, \quad (3.3)$$

where $0 \leq \rho \leq \rho_j$ (ρ_j is the jam density). When $a(x)$ is uniform with respect to location x , the LWR model is called homogeneous. Otherwise it is called inhomogeneous. Both the homogeneous and inhomogeneous models are hyperbolic systems of conservation laws. Actually the former, which is a strict hyperbolic conservation law (Lax,

1972), is a special case of the latter, a non-strictly hyperbolic system of conservation laws and a resonant nonlinear system (Isaacson and Temple, 1992). Therefore, the following discussions for the inhomogeneous LWR model are valid for any kind of links.

With jump initial conditions, the LWR model Equation 3.3 is solved by shock waves, expansion waves, and standing waves. These wave solutions are unique under the so-called “entropy” conditions. However, solutions of the LWR model with general initial and boundary conditions can not be expressed in analytical form, which calls for approximate solutions with numerical methods. One efficient numerical method for solving Equation 3.3 is due to Godunov (1959). In the Godunov method, the link is partitioned into N cells, a duration of time is discretized into M time steps, and the discretization of space and time satisfies the Courant-Friedrichs-Lewy (Courant et al., 1928) (CFL) condition so that a vehicle is not allowed to cross a cell during a time interval. Assuming that the spacing Δx and the time step Δt are constant, ρ_i^m is the average of ρ in the cell i at time step m , $q_{i-1/2}^{m+1/2}$ and $q_{i+1/2}^{m+1/2}$ are the inflow into and the outflow from cell i from time step m to $m+1$ respectively, the LWR model Equation 3.3 for cell i can be approximated with a finite difference equation:

$$\frac{\rho_i^{m+1} - \rho_i^m}{\Delta t} + \frac{q_{i-1/2}^{m+1/2} - q_{i+1/2}^{m+1/2}}{\Delta x} = 0. \quad (3.4)$$

In Equation 3.4, the flow through the link boundary $x_{i-1/2}$, i.e., $q_{i-1/2}^{m+1/2}$, can be computed in two approaches. One is from the wave solutions of the Riemann problem for Equation 3.3 with the following initial conditions (Jin and Zhang, 2003b):

$$U(x = x_{i-1/2}, t = t_m) = \begin{cases} U_{i-1}^m & x < x_{i-1/2} \\ U_i^m & x > x_{i-1/2} \end{cases}, \quad (3.5)$$

where $U = (a, \rho)$. Another is the supply-demand method (Daganzo, 1995a; Lebacque, 1996), in which the flow through a link boundary is the minimum of the traffic demand

of its upstream cell and the traffic supply of its downstream cell. The two approaches were shown to be equivalent (Jin and Zhang, 2003b). However, the method of solving the Riemann problem and the supply-demand method have different fates for studying traffic dynamics through a merge: there has been no formulation of the Riemann problem for merging dynamics in literature, but the supply-demand method has been extended and applied in the discrete kinematic wave models of merges.

In the following, we describe in detail the supply-demand method. Considering the link boundary at $x_{i-1/2}$, whose upstream and downstream cells are respectively denoted by cell $i - 1$ and cell i , supposing that the traffic densities of the two cells are ρ_{i-1}^m and ρ_i^m at time step m , Daganzo (1995) and Lebacque (1996) suggested the following supply-demand method for computing $q_{i-1/2}^{m+1/2}$. First, traffic demand of the cell $i - 1$ (called “sending flow” by Daganzo), $D_{i-1}^{m+1/2}$, and traffic supply of the cell i (called “receiving flow” by Daganzo), $S_i^{m+1/2}$, are defined by

$$D_{i-1}^{m+1/2} = \begin{cases} Q_{i-1}^m, & \text{cell } i - 1 \text{ is under-critical,} \\ Q_{i-1}^{max}, & \text{otherwise;} \end{cases} \quad (3.6)$$

$$S_i^{m+1/2} = \begin{cases} Q_i^{max}, & \text{cell } i \text{ is under-critical,} \\ Q_i^m, & \text{otherwise;} \end{cases} \quad (3.7)$$

where Q_i^{max} is the capacity of cell i , and Q_i^m the flow-rate of cell i at time step m . The demand can be considered as the maximum flow that can be discharged by the cell $i - 1$ from time step m to $m + 1$; the supply $S_i^{m+1/2}$ is the maximum flow that can be received by the cell i . Thus, the boundary flow satisfies (all superscripts will be suppressed hereafter)

$$\begin{aligned} q_{i-1/2} &\leq D_{i-1}, \\ q_{i-1/2} &\leq S_i. \end{aligned} \quad (3.8)$$

Note that Equation 3.8 admits multiple solutions. To identify the unique boundary flow, an additional “optimality” condition, that the actual boundary flow always

reaches its maximum, is assumed. Hence, the boundary flow can be simply computed by

$$q_{i-1/2} = \min\{D_{i-1}, S_i\}. \quad (3.9)$$

Here the “optimality” condition can be considered as an entropy condition, which helps to choose a physical solution out of all feasible solutions.

3.2.2 The kinematic wave model of merging traffic in the supply-demand framework

In this subsection, we review the kinematic wave model of merging traffic in the supply-demand framework. In this type of models, the supply-demand method is used to compute flows through a merge. Without loss of generality, we consider a merge that connects two upstream cells to one downstream cell. Furthermore, we assume that, at time step m , traffic demands of the two upstream cells and the traffic supply of the downstream cell are D_1 , D_2 , and S_d respectively. We denote the outflows from the upstream cells by q_1 and q_2 and the inflow into the downstream cell by q from time step m to $m + 1$. Then, according to traffic conservation, we have $q = q_1 + q_2$.

The basic assumption in the supply-demand method for computing the flows through a merge is that the flows, q_1 , q_2 , and q , are determined by traffic conditions D_1 , D_2 , S_d , and/or other characteristics of the merge. Another assumption, as in the supply-demand method for computing the flow through a link boundary, is the optimality condition. Two types of optimality conditions have been proposed: one is that the total flow q reaches its maximum, and the other is that both q_1 and q_2 reaches their individual maximums. Following the first assumption leads to Daganzo’s merge model (1995), and following the second leads to Lebacque’s (1996).

In Daganzo's supply-demand method, we have the following optimization problem:

$$\begin{aligned}
 \max q &= q_1 + q_2 \\
 \text{s.t.} & \\
 q_1 &\leq D_1, \\
 q_2 &\leq D_2, \\
 q_1 + q_2 &\leq S_d, \\
 q_1, q_2 &\geq 0,
 \end{aligned} \tag{3.10}$$

from which we can find the total flow,

$$q = \min\{D_1 + D_2, S_d\}.$$

However, (q_1, q_2) may have multiple feasible solutions. This can be shown with Figure 3.1: when $S_d \geq D_1 + D_2$, the solution is unique and at point Q ; i.e., $(q_1, q_2) = (D_1, D_2)$; but when $S_d < D_1 + D_2$, the solution can be any point on the line segment AB . For the latter situation, Daganzo defined two (non-negative) distribution fractions α_1 and α_2 , which satisfy $\alpha_1 + \alpha_2 = 1$ and may be related to D_1 , D_2 , S_d , and other characteristics of the merge. Then, the total flow q is distributed by $q_i = \alpha_i q$ ($i = 1, 2$). One example when $S_d < D_1 + D_2$ is depicted in the figure, with given fractions α_1 and α_2 . Figure 3.1 also shows that α_1 or α_2 are restricted by D_1 , D_2 , and S_d . For instance, for S_d given in the figure, α_1 can not be 1.

Lebacque suggested another supply-demand method: the supply of the downstream cell is first distributed to the two upstream cells with two fractions α_1 and α_2 , and it is assumed that the flows q_1 and q_2 reaches their individual maximums. i.e., we can compute the flow q_i ($i = 1, 2$) as the following:

$$\begin{aligned}
 S_i &= \alpha_i S_d, \\
 q_i &= \min\{D_i, S_i\}.
 \end{aligned} \tag{3.11}$$

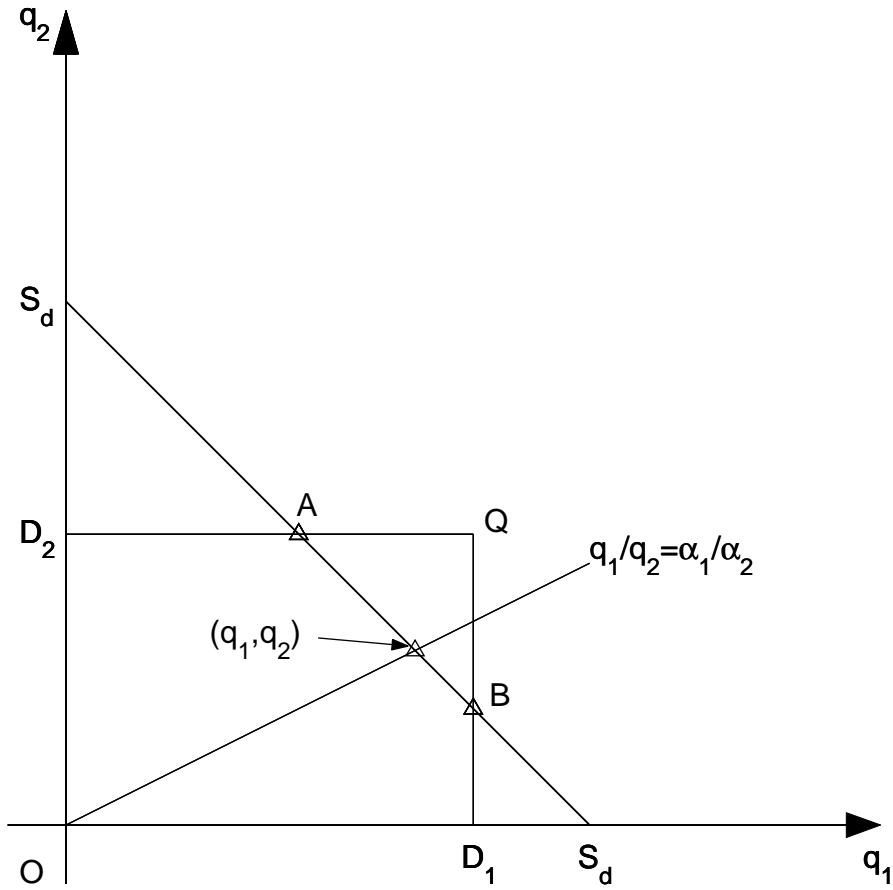


Figure 3.1: Feasible solutions in Daganzo's supply-demand method

The feasible solutions of Lebacque's method without fixed fractions are shown in Figure 3.2. As shown, in this model, when $S_d \geq D_1 + D_2$, (q_1, q_2) can be any point on D_1BQAD_2 ; when $S_d < D_1 + D_2$, (q_1, q_2) can be any point on D_1BAD_2 . In Lebacque's formulation, therefore, α_1 and α_2 are not restricted by D_1 , D_2 , or S_d , and the total flow q may not reach its maximum $\min\{D_1 + D_2, S_d\}$ in this method.

Comparing Daganzo's and Lebacque's methods, we can see that: 1) when the fractions are the same, the two methods give the same flows; 2) for given D_1 , D_2 , and S_d , the feasible solution domain of Daganzo's method is contained by that of Lebacque's

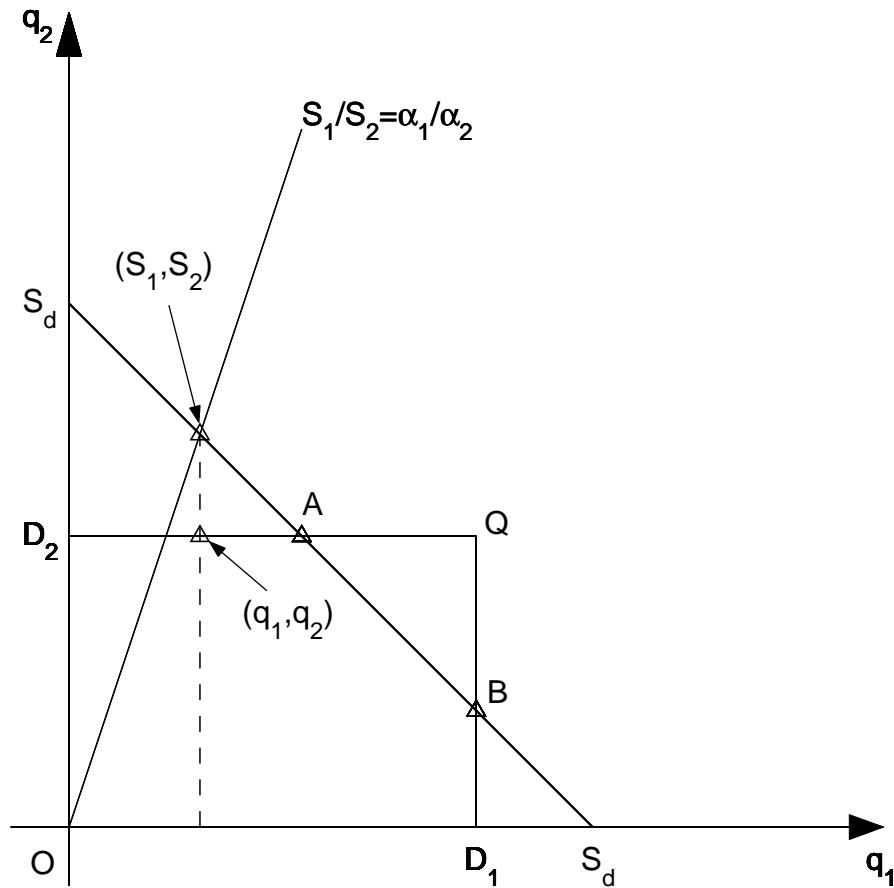


Figure 3.2: Feasible solutions in Lebacque's supply-demand method

since the distribution fractions in Daganzo's method (but not in Lebacque's) are confined by the supplies and the demand.

From the above analysis, we can see that both Daganzo's and Lebacque's models in the supply-demand framework are based on reasonable assumptions, and Lebacque's method Equation 3.11 yields a larger set of feasible solutions than Daganzo's. In addition, we think that both formulations are clear and general enough to contain physical solutions. Thus, in this chapter, we do not intend to investigate further the formulations. Instead, we are interested in the distribution schemes used in these

models.

The reasons why distribution schemes are worth further, deeper discussions are as follows. First, we can see from Figure 3.1 and Figure 3.2 that distribution schemes play a key role in uniquely determining flows through a merge. Thus whether solutions of flows are physical is highly dependent on the distribution scheme used. Therefore, in order to apply these models to simulate traffic dynamics at a merge, we need a better understanding of their distribution schemes. Second, the distribution fractions can be affected by travelers' merging behaviors, the geometry of a merge, differences between the upstream cells, traffic conditions, and possible control strategies imposed on an on-ramp. On the surface, a distribution scheme that models all these factors may be extremely complicated. A closer look at various distribution schemes is needed to find a simple yet physically meaningful one. Third, it is possible that many valid distribution schemes are available. When this happens, a distribution scheme that is easy to calibrate and computationally efficient is always preferred.

3.3 Investigation of various distribution schemes

In this section, we take a closer look at various distribution schemes and see how their distribution fractions are affected by traffic conditions, i.e., D_1 , D_2 , and S_d , and other characteristics of a merge. We start with a review and a discussion on the existing distribution schemes of Daganzo and Lebacque, then propose a simple distribution scheme and demonstrate that the supply-demand method incorporating this scheme is capable of addressing all factors that we concern about.

3.3.1 Discussion of existing distribution schemes

As we know, different types of links have different characteristics. As a result, even when an upstream highway and an on-ramp have the same number of lanes and traffic density, the downstream link usually receives more vehicles from the upstream highway than from the on-ramp due to differences in design speeds and geometry. For example, when vehicles queues up on both a L -lane highway and 1-lane on-ramp that merge together, the ratio of flow from the on-ramp to that from the highway is about $1/(2L - 1)$ (Daganzo, 1996). From these observations, Daganzo (1995a) suggested that different upstream links bear different priorities and proposed a distribution scheme including parameters for priorities.

Figure 3.3 shows how Daganzo's distribution scheme is defined. In the figure, the priorities of the highway and the on-ramp are denoted as p_1 and p_2 ($p_1 + p_2 = 1$), respectively. Here the upstream link u_1 is assumed to have higher priority than u_2 ; i.e., $p_1/p_2 > D_1/D_2$. Then the solution (q_1, q_2) can be shown to be one of three cases: i) when $S_d \leq D_1/p_1$; i.e., S_d is x - and y -intercept of line i, the solution $(q_1, q_2) = (p_1 S_d, p_2 S_d)$ is at point 1; ii) when $S_d \in (D_1/p_1, D_1 + D_2)$; i.e., S_d is the x - and y - intercept of line ii, the solution $(q_1, q_2) = (D_1, S_d - D_1)$ is at point 2; iii) when $S_d \geq D_1 + D_2$; i.e., S_d is the x - and y - intercept of line iii, the solution $(q_1, q_2) = (D_1, D_2)$ is at point 3.

Thus in Daganzo's distribution scheme, we can find that the fraction α_1 is defined as

$$\alpha_1 = \begin{cases} p_1, & S_d \leq D_1/p_1, \\ \frac{D_1}{S_d}, & D_1/p_1 < S_d \leq D_1 + D_2, \\ \frac{D_1}{D_1 + D_2}, & S_d > D_1 + D_2; \end{cases} \quad (3.12)$$

and $\alpha_2 = 1 - \alpha_1$. From this definition and Figure 3.3, we can see that the priorities p_1 and p_2 have to satisfy $p_2/p_1 < D_2/D_1$. i.e., they have to change with respect to traf-

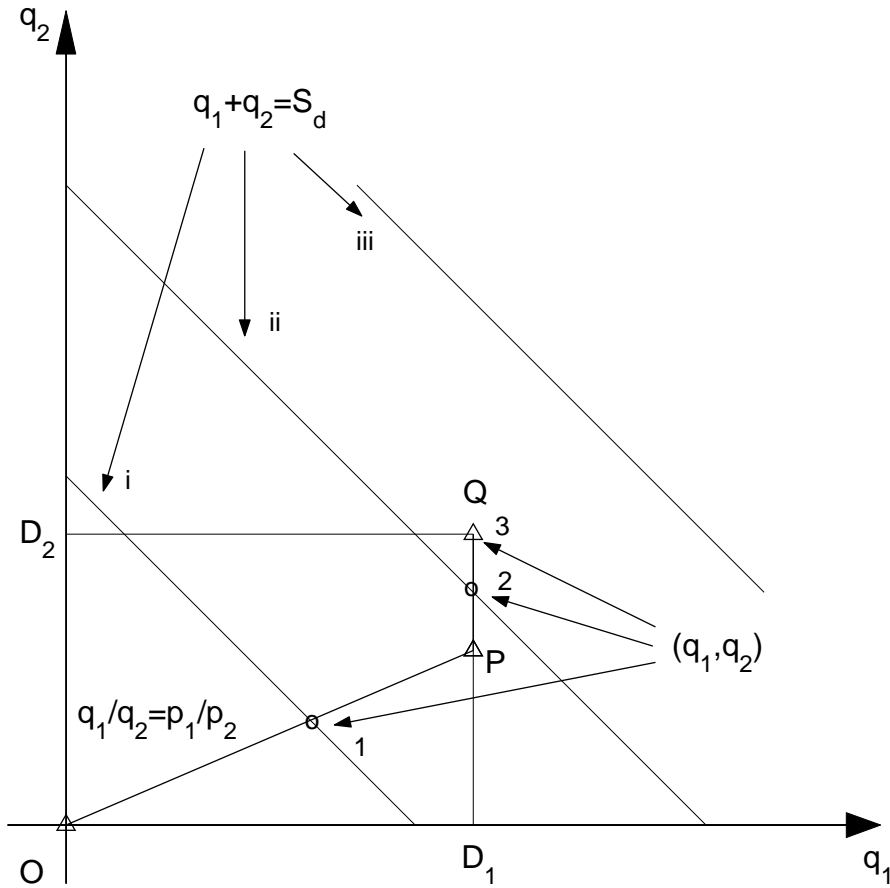


Figure 3.3: Solutions of flows in Daganzo's distribution scheme

fic conditions D_2 and D_1 . Therefore, such “priorities” are not uniquely determined by road characteristics, as one would expect. This property makes this distribution scheme less attractive. Moreover, even we allow non-constant priorities, the distribution scheme with fractions defined in Equation 3.12 becomes quite complicated when considering a merge with more than two upstream links.

Lebacque (1996) suggested another distribution scheme, in which α_i equals to the ratio of the number of lanes of link u_i to that of link d . When all branches of a merge are highways with the same characteristics, and the traffic conditions of upstream

links are overcritical, the demand of each upstream link is equal to its lane capacity times the number of lanes. In this case, it is reasonable that outflow from each upstream link is proportional to the number of lanes; i.e., the distribution scheme by Lebacque works well. However, when the upstream links are not similar, e.g., one is highway and the other on-ramp, the fractions are obviously not proportional to the number of lanes. Lebacque's distribution scheme fails in another case when $\alpha_1 + \alpha_2 > 1$ and $S_i \leq D_i$, because it may yield invalid solutions of $q = q_1 + q_2 > S_d$.

3.3.2 A simple distribution scheme and its interpretation

Our above analysis has revealed certain drawbacks of the existing distribution schemes, here we propose a simple distribution scheme, which, as we will see later, removes these drawbacks yet is capable of capturing characteristics of a merge. In this distribution scheme, the distribution fractions are only related to the demands D_1 and D_2 , as defined in Equation 3.13.

$$\begin{aligned}\alpha_1 &= \frac{D_1}{D_1 + D_2}, \\ \alpha_2 &= \frac{D_2}{D_1 + D_2}.\end{aligned}\tag{3.13}$$

As shown in Figure 3.4, combining the distribution scheme Equation 3.13 with models Equation 3.10 or Equation 3.11, we are able to uniquely determine the flows: the solution (q_1, q_2) with this distribution scheme is simply the intersection of $q_1 + q_2 = S_d$ and $q_1/q_2 = D_1/D_2$ when $D_1 + D_2 \geq S_d$, and the point Q otherwise.

A distribution scheme is in fact equivalent to an additional entropy condition, which helps identify q_1 and q_2 . Thus we also call the distribution scheme Equation 3.13 the “fairness” condition, because the distribution fractions are proportional to traffic demands of upstream links; i.e., the upstream cell with more “sending” flow is given more chances. This “fairness” condition, to some extent, is supported by

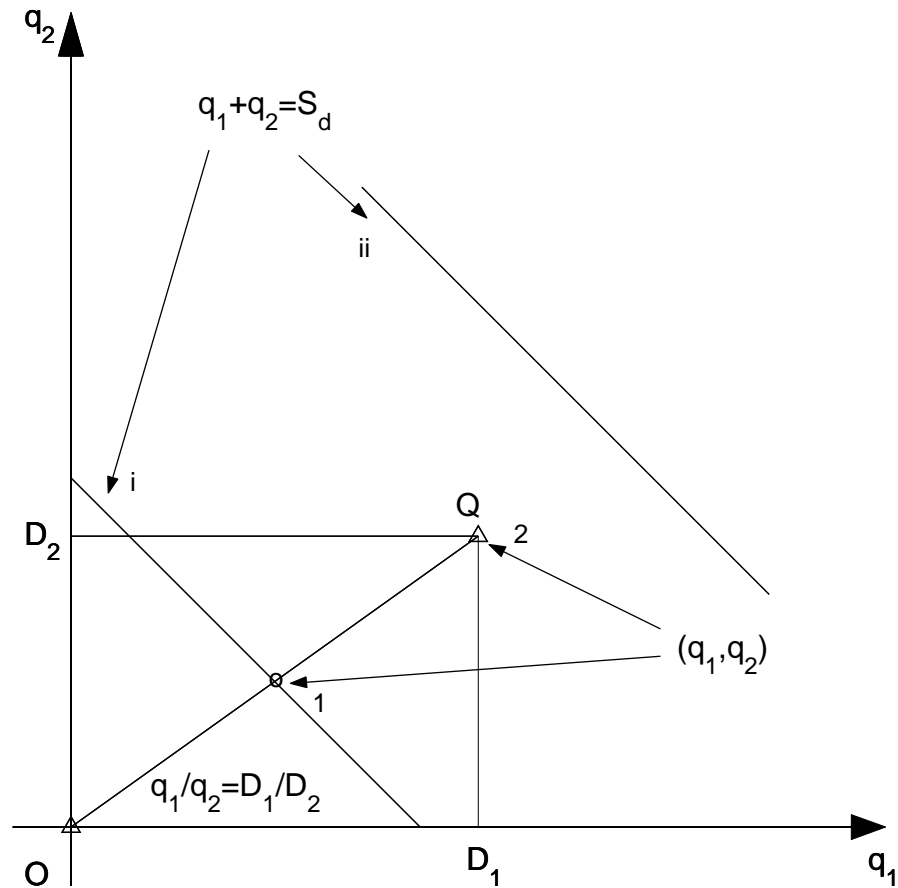


Figure 3.4: Solutions of flows in the simple distribution scheme

observations at crowded merges, e.g., vehicles from an on-ramp generally wait until there is a big enough gap to merge when traffic is fluid. When many vehicles from the on-ramp cannot merge and queue up, they may squeeze in and force vehicles from the upstream mainline freeway to slow down or switch lanes to give way to them (Kita, 1999). These observations show that vehicles from the upstream cells compete “fairly” with each other for admission into the downstream cell.

From Equation 3.13, we can see that the distribution scheme is not *directly* related to capacities, number of lanes, the difference between upstream links, or control of

on-ramps. Thus we can say that this distribution scheme uses the fewest parameters. Therefore, it will be easy to calibrate and efficient to compute. Indeed, it is the simplest distribution scheme that we can have. Besides, note that the fractions are independent of the downstream traffic supply S_d , although the flows are related to S_d . As a mathematical exercise, the following theorem shows the fractions in this scheme are in fact the only fractions that are independent of S_d .

Theorem 3.3.1 *Suppose that the fractions α_1 and α_2 are independent of the downstream supply S_d , then the fractions will be as in Equation 3.13.*

Proof. We have $q_1 = \alpha_1 q$ and $q_2 = \alpha_2 q$. From Equation 3.11, we then obtain

$$\alpha_1 q \leq D_1, \quad (3.14)$$

$$\alpha_2 q \leq D_2. \quad (3.15)$$

Since α_1 and α_2 are independent of S_d , set $S_d = D_1 + D_2$, we obtain $q = D_1 + D_2$. Thus, both Equation 3.14 and Equation 3.15 have to take the “=” sign, and we have Equation 3.13. ■

On the other hand, characteristics of a merge can be *indirectly* captured in the simplest distribution scheme Equation 3.13 since capacities, number of lanes, design speeds, and on-ramp control can be included in the definition of traffic demands, Equation 3.6. For example, when upstream links have the same per lane capacity and are congested, Equation 3.13 will give fractions proportional to the number of lanes. Thus this distribution scheme coincides with Lebacque’s scheme based on the number of lanes. As to Daganzo’s “priorities”, they are embedded in the simple distribution scheme as follows: when the freeway and the on-ramp have the same number of lanes and density, the freeway generally admits higher free flow speed, has higher flow-rate and higher demand, and therefore has larger outflow that reflects its higher priority.

In addition, the resultant supply-demand method can be applied to determine flows through a merge with a controlled on-ramp (Daganzo, 1995a): when the metering rate of the on-ramp, whose real traffic demand is D_2 , is r , we can apply the controlled traffic demand of the on-ramp $\min\{r, D_2\}$ in the supply-demand method. Therefore, although the distribution scheme plays “fairly”, the resultant supply-demand method of merges can address the characteristics of a merge by incorporating them into the computation of traffic demands and traffic supply.

From discussions above we can see that, in this simple distribution scheme, characteristics of upstream links, the control of on-ramps, and other properties of a merge are captured in the definitions of demand and supply. This is why distribution fractions depends only on demands in this scheme. Although demand functions of upstream cells are related to many factors and may not be easily obtained, they have to be found in all supply-demand methods. In this sense, the simple distribution scheme and, therefore, the supply-demand method with this scheme, are the easiest to calibrate and the most computationally efficient.

3.3.3 Properties of the discrete kinematic wave model of merges with the simplest distribution scheme

With the distribution scheme Equation 3.13, the supply-demand method has the following further properties:

Equivalence of models by Daganzo and Lebacque: With the distribution scheme

Equation 3.13, as shown in Figure 3.4, the solution (q_1, q_2) will be on the line segment OQ . We can see that Daganzo’s model Equation 3.10 and Lebacque’s model Equation 3.11 are equivalent with these fractions. Both yield the following

fluxes through the merge:

$$\begin{aligned} q &= \min\{D_1 + D_2, S_d\}, \\ q_1 &= q \cdot \frac{D_1}{D_1 + D_2}, \\ q_2 &= q \cdot \frac{D_2}{D_1 + D_2}. \end{aligned} \tag{3.16}$$

Extensibility: The supply-demand method incorporating the simplest distribution scheme produces qualitatively similar results for merges with different number of upstream links. When a merge has $U > 2$ upstream links, the method Equation 3.16 can be easily extended as

$$\begin{aligned} q &= \min\{\sum_{i=1}^U D_i, S_d\}, \\ q_i &= q \frac{D_i}{\sum_{i=1}^U D_i}, \quad i = 1, \dots, U. \end{aligned} \tag{3.17}$$

Convergence of the merge model: The discrete LWR model is considered as a good approximation to the continuous LWR model since it converges as $\Delta x \rightarrow 0$ while $\Delta x/\Delta t$ is constant. Although analytical convergence analysis of the merge model with the simplest distribution scheme has not yet been performed, numerical results in section 3.2 do show that it is convergent in the L_1 norm.

Consistency of the merge model with the LWR model: Here we conceptually consider the consistency of the merge model Equation 3.16 with the LWR model for a link with multiple lanes. In the LWR model for a multi-lane link, all lanes are assumed to be identical; i.e., given the same initial and boundary conditions for each lane, flows at the same location on each lane are identical and the link's flow-rate or density at a location is simply the number of lanes times the flow-rate or density at the location of each lane, respectively. i.e., the LWR model does not model lane-changing and traffic in different lanes is treated as the same. Therefore a multi-lane link can be considered as an artificial merge:

for a boundary inside the link, we separate its upstream part into two links with identical flow characteristics, while keep the downstream part intact. Next we check if traffic dynamics of this artificial merge is indeed the same as those of the original link. Assuming the two upstream links of the artificial merge have N and M lanes, respectively, traffic demand of each lane is D , and traffic supply of the downstream link is S_d . Since the lanes are identical in the upstream links, traffic demands for the upstream links are $D_1 = ND$, $D_2 = MD$; from Equation 3.16, we have

$$\begin{aligned} q &= \min\{(N + M)D, S_d\}, \\ q_1 &= q \frac{N}{N + M}, \\ q_2 &= q \frac{M}{N + M}. \end{aligned}$$

Hence, as expected, flow from each upstream lane is $\min\{D, S_d/(N+M)\}$, which is the same as the original boundary flow computed from the LWR model.

The above analyses indicate that the merge model with the simplest distribution scheme is well-defined and qualitatively sound, although the ultimate test of its validity rests on empirical validation.

3.4 Numerical simulations

In this section, we present our numerical studies of the discrete kinematic wave model of merges using the simple distribution scheme. Here we apply Godunov's method discussed in Subsection 3.2.1 for each link, and the supply-demand method is used to find flows through link boundaries and merging boundaries. In particular, the simple distribution scheme is used for computing fluxes through the merge. The resulted numerical solution method is described as follows: in each cell, Equation 3.4 is used

to update traffic density; we compute flows through link boundaries with Equation 3.9; flows through a merge are computed from Equation 3.17.

In the numerical studies, we introduce a unit time $\tau = 5$ s and a unit length $l = 0.028$ km. Here we study a merge formed by a two-lane mainline freeway and a one-lane on-ramp. The three branches of the merge have the same length, $L = 400l = 11.2$ km. The upstream mainline freeway, the on-ramp, and the downstream mainline freeway are labeled as links u_1 , u_2 , and d , respectively. The simulation starts from $t = 0$ and ends at $t = 500\tau = 41.7$ min. In the following numerical simulations, we partition each link into N cells and the time interval into K steps, with $N/K = 1/10$ always; e.g., if $N = 50$ and $K = 500$, the cell length is $\Delta x = 8l$ and the length of each time step $\Delta t = 1\tau$.

For both the mainline freeway and the on-ramp, we use the triangular fundamental diagram; i.e., the flow-density relationships are triangular. For the mainline freeway, the free flow speed is $v_{f,m} = 65$ mph = $5.1877 l/\tau$; the jam density is $\rho_{j,m} = 2\rho_j = 360$ veh/km, where $\rho_j = 180$ veh/km/lane is the jam density of a single lane; and the critical density $\rho_{c,m} = 0.2\rho_{j,m} = 0.4\rho_j = 72$ veh/km. Therefore, the speed- and flow-density relationships can be written as follows:

$$V_m(\rho) = \begin{cases} v_{f,m}, & 0 \leq \rho \leq \rho_{c,m}; \\ \frac{\rho_{c,m}}{\rho_{j,m} - \rho_{c,m}} \frac{\rho_{j,m} - \rho}{\rho} v_{f,m}, & \rho_{c,m} < \rho \leq \rho_{j,m}. \end{cases}$$

$$Q_m(\rho) = \rho V_m(\rho) = \begin{cases} v_{f,m} \rho, & 0 \leq \rho \leq \rho_{c,m}; \\ \frac{\rho_{c,m}}{\rho_{j,m} - \rho_{c,m}} v_{f,m} (\rho_{j,m} - \rho), & \rho_{c,m} < \rho \leq \rho_{j,m}. \end{cases}$$

For the on-ramp, the free flow speed $v_{f,r} = 35$ mph = $2.7934 l/\tau$; the jam density is ρ_j ; and the critical density $\rho_{c,r} = 0.2\rho_j$. Similarly, we can have the following speed- and flow-density relationships:

$$V_r(\rho) = \begin{cases} v_{f,r}, & 0 \leq \rho \leq \rho_{c,r}; \\ \frac{\rho_{c,r}}{\rho_j - \rho_{c,r}} \frac{\rho_j - \rho}{\rho} v_{f,r}, & \rho_{c,r} < \rho \leq \rho_j. \end{cases}$$

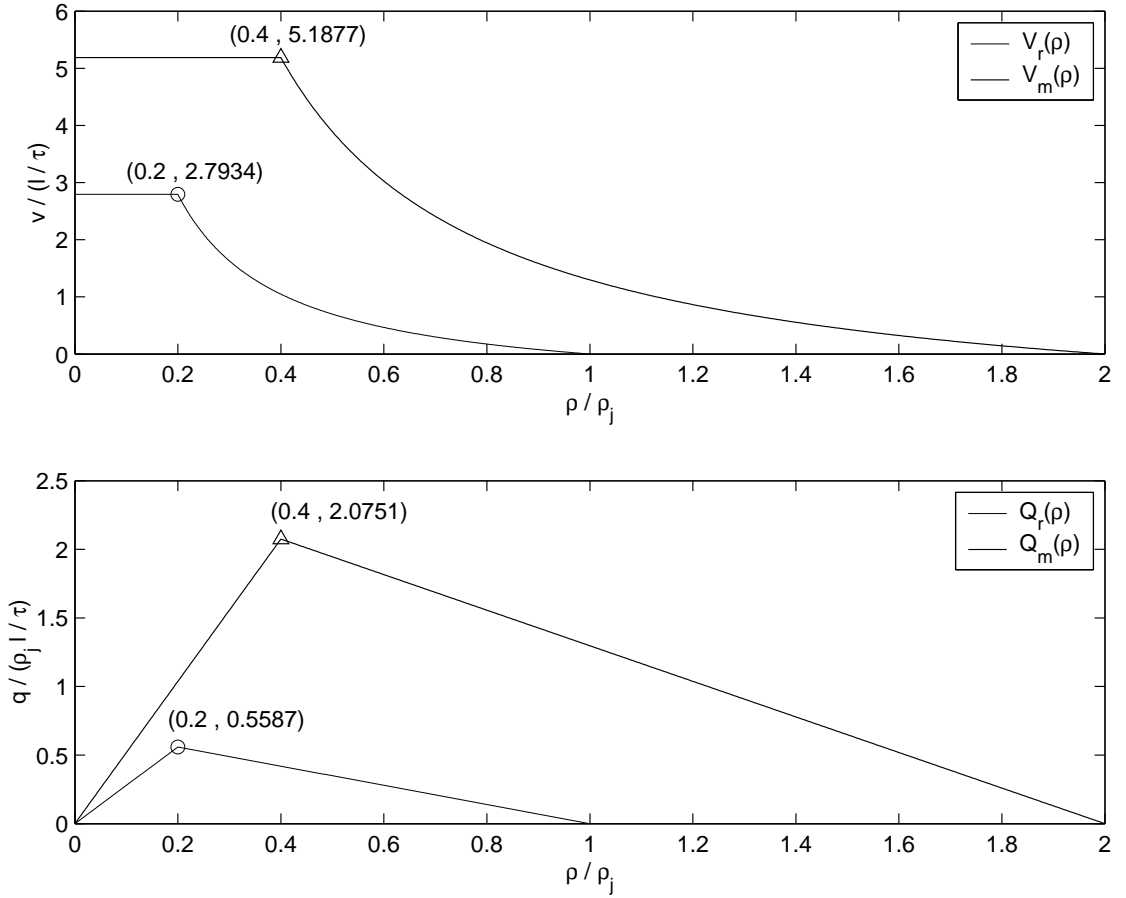


Figure 3.5: The triangular fundamental diagrams for the mainline freeway and the on-ramp

$$Q_r(\rho) = \rho V_r(\rho) = \begin{cases} v_{f,r}\rho, & 0 \leq \rho \leq \rho_{c,r}; \\ \frac{\rho_{c,r}}{\rho_j - \rho_{c,r}} v_{f,r}(\rho_j - \rho), & \rho_{c,r} < \rho \leq \rho_j. \end{cases}$$

The above relationships are depicted in Figure 3.5.

Since $|\lambda_{*,m}| \leq v_{f,m} = 5.1877l/\tau$, where $\lambda_{*,m}(\rho) = V_m(\rho) + \rho V'_m(\rho)$ is the characteristic speed of Equation 3.3 on the mainline freeway, we find the CFL (Courant et al., 1928) condition number

$$|\lambda_{*,m}| \frac{\Delta t}{\Delta x} \leq 0.65 < 1.$$

Since the characteristic speed on the on-ramp is smaller than that on the mainline freeway, the CFL condition is also satisfied for the on-ramp.

3.4.1 Simulation of merging traffic without control

In this subsection, we study the following merging traffic. Initially, the mainline freeway carries a constant flow: traffic densities on the upstream and downstream freeway are the same, $\rho_{u_1} = \rho_{u_2} = 0.36\rho_j$, which is under-critical. After time $t = 0$, a constant flow with density $\rho_{u_2} = 0.175\rho_j$ arrives at the on-ramp, and the on-ramp remains uncontrolled. In our simulation, the Riemann boundary condition is imposed for the upstream boundaries of link u_1 and u_2 and the downstream boundary of link d ; i.e. the spatial derivatives of traffic density at these boundaries are assumed to be zero.

After partitioning each of the three links into $N = 500$ cells and discretizing the time duration into $K = 5000$ steps, we obtain simulation results as shown in Figure 3.6. Figure 6(a) illustrates the evolution of traffic density on the freeway upstream of the merge: at time $t = 0\tau$, traffic density is uniformly at $\rho_A = 0.36\rho_j$; after the arrival of the on-ramp flow, freeway traffic immediately upstream of the merging point² becomes congested and reaches a new state $\rho_B = 0.7394\rho_j$; then a shock wave forms and travels upstream in a constant speed $s_1 \approx -0.61l\tau = -7.6$ mph. Figure 6(b) shows the evolution of traffic on the freeway downstream of the merge: initially, traffic density is also uniformly at ρ_A . After $t = 0$, traffic immediately downstream of the merging point reaches capacity flow at density $\rho_C = 0.4\rho_j$, and a contact wave³ appears since ρ_C and ρ_A are both on the free-flow side of the triangular fundamental

²Traffic density at the merging point is multiple-valued.

³A contact wave is a flow/density discontinuity traveling at the same speed of traffic on both sides of it.

diagram. It travels downstream at the speed $s_2 = 5.2l/\tau = v_{f,m}$. Figure 6(c) shows that a backward shock wave also forms on the on-ramp: traffic upstream of the shock has density $\rho_D = 0.175\rho_j$ and downstream of the shock density $\rho_E = 0.3697\rho_j$. This shock travels at $s_3 \approx -0.25l/\tau = -3.1$ mph. The shock waves and the contact wave observed on the three branches are shown in Figure 6(d) on the $\rho - q$ plane, in which line AB represents the shock wave on the freeway upstream of the merge and the slope of AB is its speed; line CA represents the contact wave on the freeway downstream of the merge and its travel speed is the slope of CA , which is also the free flow speed; finally line DE represents the shock wave on the on-ramp and the slope of DE is its travel speed.

Comparing the congested states on the upstream freeway (point B in Figure 3.6(d)) and that on the on-ramp (point E in Figure 3.6(d)), we have the following observations: 1) the ratio of the outflows from the upstream branches (freeway: $q_B = 1.6349\rho_j l/\tau = 5933$ veh/hr and on-ramp: $q_E = 0.4402\rho_j l/\tau = 1597$ veh/hr) are not proportional to the lane ratio, owing to the different geometric and flow characteristics of the two upstream branches, as reflected in their respective fundamental diagrams and 2). as long as the freeway downstream of the merge is not congested, and the total demand is greater than the total supply at the merging point, traffic states surrounding the merge, ρ_B , ρ_E , and ρ_C , are constant (i.e., stationary) states regardless of the initial traffic conditions. This unique characteristics of the merge model with our suggested distribution scheme offers a way to validate the model and the fairness assumption.

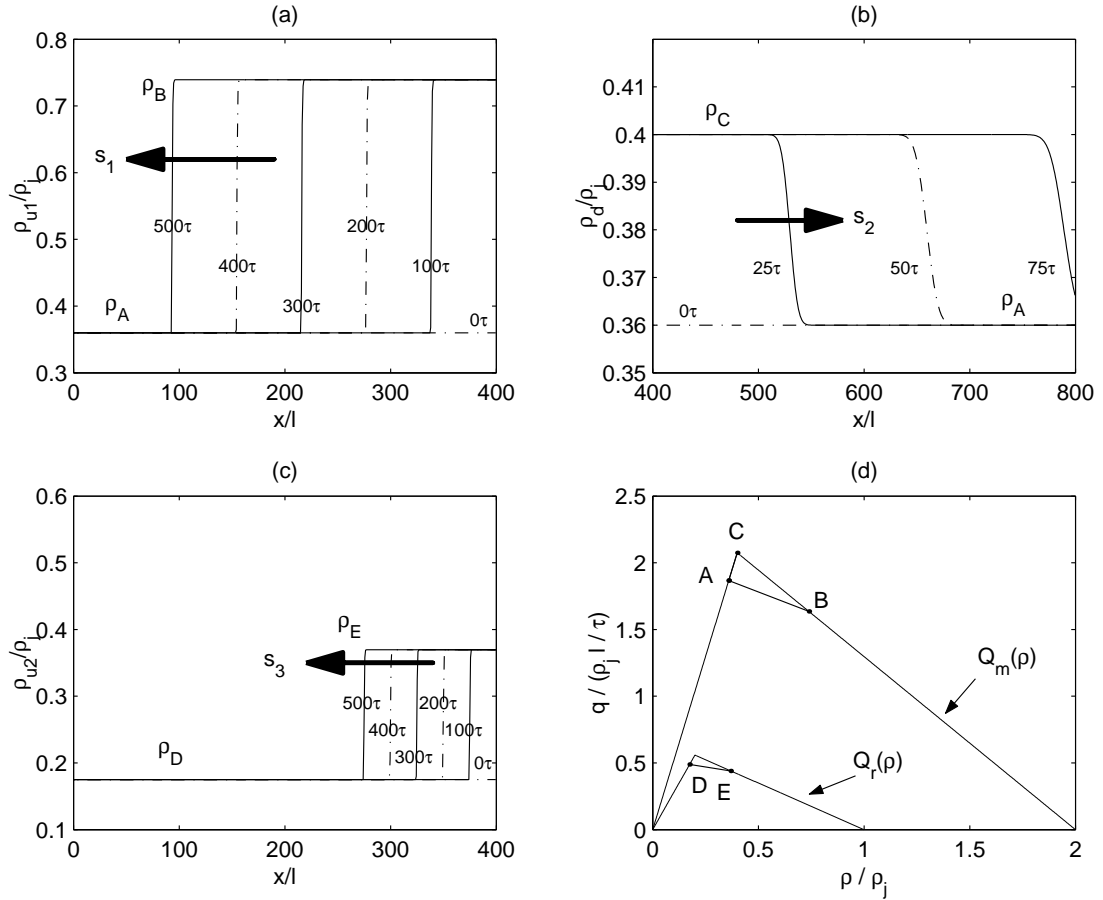


Figure 3.6: Simulation of merging traffic without control

3.4.2 Simulation of merging traffic when the on-ramp is controlled

In this subsection, we have the same initial/boundary conditions as in the preceding subsection, but with the on-ramp controlled by a ramp meter. For simplicity we take a constant metering rate $r = 0.3445\rho_j l / \tau = 1250$ veh/hr. The simulation results are shown in Figure 3.7. From Figure 3.7(a), we can see that a backward traveling shock wave forms on the freeway upstream of the merge, traveling at $s_1 \approx -0.33l/\tau = -4.1$ mph. Traffic densities besides the shock are $\rho_A = 0.36\rho_j$ (upstream) and $\rho_B =$

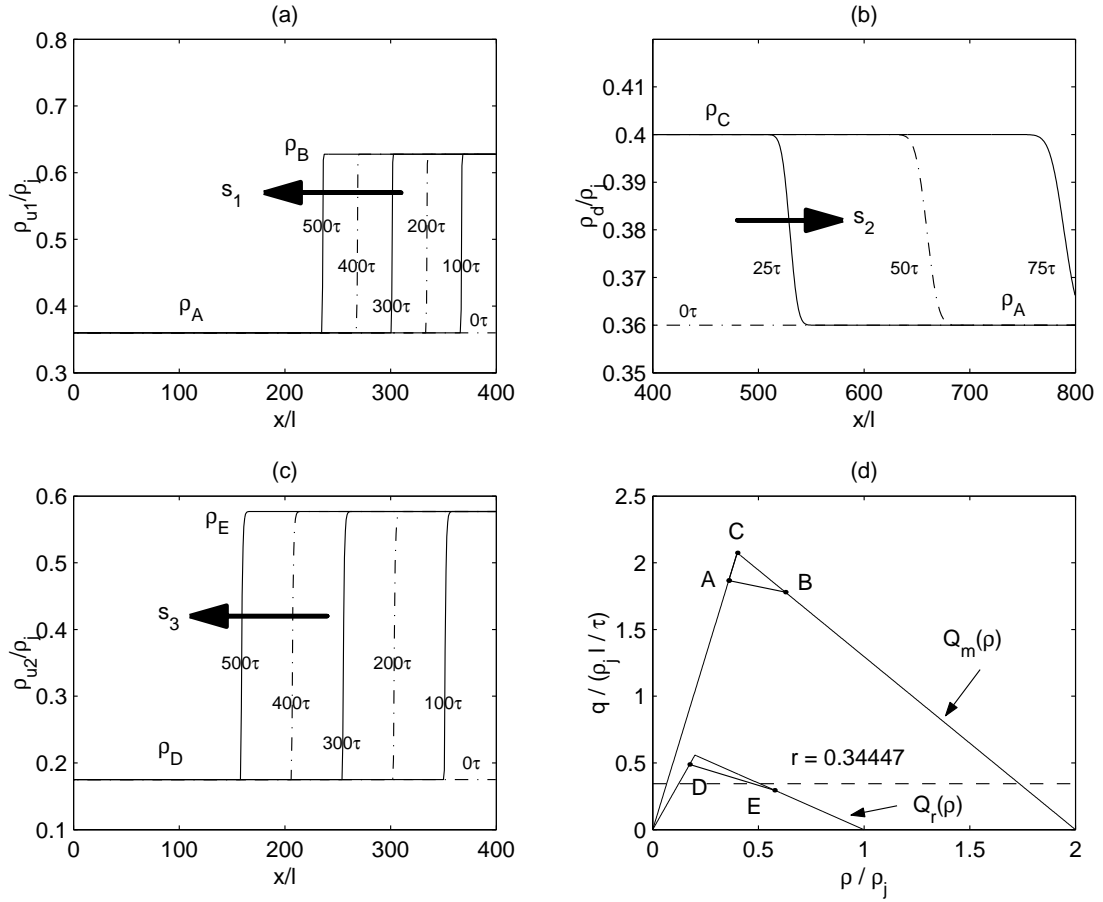


Figure 3.7: Simulation of merging traffic with on-ramp control

$0.6278\rho_j$ (downstream), respectively. Figure 3.7(b) shows the evolution of traffic on the freeway downstream of the merge, which is identical to the case without ramp control. From Figure 3.7(c), we can see that a backward traveling shock wave also forms on the on-ramp, traveling at $s_3 \approx -0.48l/\tau = -6.0$ mph. On the ramp, traffic densities besides the shock are $\rho_D = 0.175\rho_j$ (upstream) and $\rho_E = 0.577\rho_j$ (downstream), respectively. Again, Figure 3.7(d) shows the the initial and congested states in the $\rho - q$ plane.

We note that with ramp control, the freeway upstream of the merge becomes less

congested (ρ_B is lower) while the on-ramp becomes more congested (ρ_E is higher). Furthermore, the freeway queue grows slower while the ramp queue grows faster with ramp control than without. Finally, the ramp control also affects the stationary states (ρ_B, ρ_C, ρ_E) and the distribution fractions, in favor of discharging higher flow from the freeway.

3.4.3 Computation of convergence rates

In this subsection we will check the convergence of the merge model with the distribution scheme Equation 3.13, when the on-ramp is not controlled. Here, this is done by computing convergence rates of traffic density over the whole network.

First, we compare traffic density solutions at time $T_0 = 500\tau$ for two different number of cells into which the network is partitioned and obtain their difference. Denote solutions as $(U_i^{2N})_{i=1}^{2N}$ for $2N$ cells and $(U_i^N)_{i=1}^N$ for N cells respectively, and define a difference vector $(e^{2N-N})_{i=1}^N$ between these two solutions as

$$\mathbf{e}_i^{2N-N} = \frac{1}{2}(U_{2i-1}^{2N} + U_{2i}^{2N}) - U_i^N, i = 1, \dots, N. \quad (3.18)$$

Then, the relative error with respect to L^1 -, L^2 - or L^∞ -norm can be computed as

$$\epsilon^{2N-N} = \|\mathbf{e}^{2N-N}\|. \quad (3.19)$$

Finally, a convergence rate is obtained when we compare two relative errors:

$$r = \log_2\left(\frac{\epsilon^{2N-N}}{\epsilon^{4N-2N}}\right). \quad (3.20)$$

Here the vector of U contains the densities of all three links which are weighted by the number of lanes of each link.

We will compute convergence rate with the following conditions. For link u_1 , the

number of lanes $a(u_1) = 2$, we define its initial condition as

$$\begin{aligned}\rho(x, 0) &= a(u_1)(0.18 + 0.05 \sin \frac{\pi x}{L})\rho_j, & x \in [0, L], \\ v(x, 0) &= V_m(\rho(x, 0)), & x \in [0, L].\end{aligned}\tag{3.21}$$

For link u_2 , the number of lanes $a(u_2) = 1$, we define its initial condition as

$$\begin{aligned}\rho(x, 0) &= a(u_2)(0.175 + 0.05 \sin \frac{2\pi x}{L})\rho_j, & x \in [0, L], \\ v(x, 0) &= V_r(\rho(x, 0)), & x \in [0, L].\end{aligned}\tag{3.22}$$

For link d , the number of lanes $a(d) = 2$, we define its initial condition as

$$\begin{aligned}\rho(x, 0) &= a(d)(0.18 - 0.05 \sin \frac{\pi x}{L})\rho_j, & x \in [L, 2L], \\ v(x, 0) &= V_m(\rho(x, 0)), & x \in [L, 2L].\end{aligned}\tag{3.23}$$

In addition, we impose the Riemann boundary condition for the upstream boundaries of link u_1 and u_2 and the downstream boundary of link d ; i.e., ρ has zero derivative at these boundaries.

From Table 3.1, convergence rates of the merge model with the simple distribution scheme are of order one in L^1 norm. The convergence rate is of order one is expected because the Godunov method used here is a first-order method, in which traffic density on a link is approximated by piece-wise constant functions. Unlike the Godunov discretization of the LWR model, which we know is convergent to the LWR model, we do not yet know what differential equations the discrete model converges to. Nevertheless, the numerical convergence analysis gives us comfort in applying the discrete merge model in the sense that we know the properties of the computed solutions will not change over discretization scales.

3.5 Discussions

In this chapter, we studied the discrete kinematic wave model of merges in the supply-demand framework, probed the supply-demand merge models by Daganzo

ρ/ρ_j	128-64	Rate	256-128	Rate	512-256	Rate	1024-512
L^1	3.31e-03	1.00	1.65e-03	1.00	8.27e-04	1.00	4.13e-04

Table 3.1: Convergence rates of the discrete merge model

and Lebacque, and gained a better understanding of various distribution schemes in merge models. More importantly, we proposed the simplest distribution scheme, equivalent to the so-called “fairness” condition, in which the distribution fractions are proportional to the upstream demands. We demonstrated with both analytical discussions and numerical studies that the discrete merge model with the simplest distribution scheme is well-defined.

The simple distribution scheme can also be easily extended to diverges in single-commodity traffic flow. In reality, a diverge is not simply a reverse of a merge: in a merge, vehicles advance in the same direction and once they travel into the downstream link, their origins no longer affect traffic dynamics; while in a diverge, traffic dynamics in the upstream link are affected by the combination of vehicles with different destinations. However, for single-commodity traffic flows, in which vehicles have no predefined routes and can choose any downstream links when diverging, we can have similar supply-demand method for computing fluxes through a diverge: assuming that a diverge has K downstream links, the upstream link and the downstream links are properly discretized, the traffic demand of the upstream link is D_u , and traffic supply of downstream link d_i ($i = 1, \dots, K$) is S_i , the supply-demand method with the “fairness” condition, in which the influx into a downstream link is proportional

to its accommodation S_i , can be written as:

$$\begin{aligned} q &= \min\{D_u, \sum_i^K S_i\}, \\ q_i &= p_i q, \\ p_i &= \frac{S_i}{\sum_i^K S_i}, \quad i = 1, \dots, K, \end{aligned} \tag{3.24}$$

where q_i is influx into the downstream link d_i .

Further, for a general junction with J upstream links and K downstream links, we can compute fluxes as

$$\begin{aligned} q &= \min\{\sum_{j=1}^J D_j, \sum_{k=1}^K S_k\}, \\ q_j^u &= \alpha_j q, \\ q_k^d &= \beta_k q, \\ \alpha_j &= \frac{D_j}{\sum_{j=1}^J D_j}, \quad j = 1, \dots, J \\ \beta_k &= \frac{S_k}{\sum_{k=1}^K S_k}, \quad k = 1, \dots, K, \end{aligned} \tag{3.25}$$

where D_j is the traffic demand of the upstream link u_j , S_k is the traffic supply of the downstream link d_k , q_j^u is the out-flux from u_j , and q_k^d the influx into d_k . Although this model may not be proper for realistic traffic flow, it could be helpful for the study of other unidirectional flows.

With a complete picture of the merge model, we can now simulate how a traffic disturbance propagates through a merge. In particular, since merges are well recognized as locations where congestion often initiates (Daganzo, 1999b), this study will help traffic engineers understand how congestion start and propagate at a merge. Moreover, with the complete discrete kinematic wave merge model, we are able to develop and evaluate local ramp metering strategies, e.g., the ALINEA algorithm (Papageorgiou et al., 1997). In the future, we will be also interested in the limit of the discrete kinematic wave model with the simple distribution scheme. In particular, we will be interested in kinematic wave solutions for a general Riemann problem

of this model. Finally, and more importantly, the supply-demand method and the “fairness” condition needs to be checked against observed merging phenomena.

Chapter 4

Kinematic wave traffic flow model of diverging traffic

4.1 Introduction

Diverges have been well recognized as a major type of bottlenecks (Daganzo, 1999b; Daganzo et al., 1999), where congestion of one downstream branch can propagate to the upstream branch and further blocks vehicles traveling to other directions. Observations of diverging traffic (Muñoz and Daganzo, 2002, 2003) have shown that vehicles to different downstream branches tend to segregate themselves at a point, called the actual diverging point, as far as 2 km upstream of the physical diverging point. In addition, traffic upstream of the actual diverging point is in the so-called “1-pipe” regime in the sense that vehicles that appear at the same time and location have the same speed even they have different destinations; while between the actual and physical diverging points traffic is in a “2-pipe” regime, since vehicles to different directions are separated and travel independently. In certain cases, however, the actual and physical diverging points may be the same (Newell, 1999). Although it is

an interesting problem to determine the location of an actual diverging point, here we only intend to study traffic dynamics at an actual diverging point or simply a highway diverge; i.e., we want to know, under certain traffic conditions, how much traffic will flow into each downstream branch.

Due to its simplicity in representation and efficiency in computation, the kinematic wave theory developed by (Lighthill and Whitham, 1955b; Richards, 1956) has played an important role in understanding traffic dynamics on road networks. In the framework of the kinematic wave theory of diverging traffic, there have been two major lines of research in the framework of the kinematic wave theory. In the first line of research, the effect of diverging traffic to the mainline freeway is incorporated by considering an off-ramp as a sink (Kuhne and Michalopoulos, 1992). In these models, only part of the interaction between the diverging traffic and the main highway traffic, i.e., the impact of diverging traffic to the mainline traffic, is taken into account. In addition, the characteristics of sinks are not trivial to obtain. In contrast, in the second line of research, the complete dynamics at diverges is studied by treating each branch equally. When vehicles do not have predefined routes and can choose any downstream branches at a diverge, Holden and Risebro (1995) determined the flow to each branch by solving an optimization problem, and Jin and Zhang (2003c) proposed a distribution scheme based on the definitions of traffic supply and demand. For more realistic situations when vehicles have predefined route choices, Daganzo (1995a) and Lebacque (1996) proposed the so-called supply-demand method for computing traffic flows through a diverge. In this method, each branch is partitioned into a number of cells and a duration of time is discretized into time steps. Then a diverge connects an upstream cell and a number of downstream cells, and the flow to a downstream cell during a time period is assumed to be proportional to the fraction of vehicles in the upstream cell that wish to travel to this downstream cell. In addition, the flows

to the downstream cells are assumed to reach their maxima subject to the constraint of traffic demand of the upstream cell and supplies of the downstream cells.

Although the supply-demand method is quite straightforward in computing flows through a diverge, it fails to provide a system-wide picture of how a small traffic perturbation on one branch will propagate through the diverge. That is, it gives no answer to what kind of kinematic waves will initiate in diverging traffic. In this chapter, we intend to study the kinematic waves (more specifically, the instantaneous kinematic waves) at a diverge. In our study, we still partition each branch into a number of cells and discretize a duration of time into some time steps. Then in a (short) time step¹, we compute the in-flow to a downstream branch by holding traffic conditions of vehicles to the other destinations constant in the upstream cell and, after obtaining all flows, update traffic conditions in all the upstream and downstream cells. We can see that, in this theory, dynamics of traffic traveling to different destinations are first decoupled during a short time period and then combined together in an alternating manner. With this decoupling, corresponding to each downstream branch, we can obtain a hyperbolic system of conservation laws, which is independent of the systems corresponding to the other downstream branches. To the best of our knowledge, this decoupling approach in solving complicated dynamics of diverging traffic is the first of its kind in traffic flow.

Moreover, we will show that the decoupled systems are nonlinear resonant systems in the sense of Isaacson and Temple (1992) and can be solved by combinations of shock, rarefaction, and standing waves. Here, these waves are considered instantaneous since they only exist in a short time interval, and waves corresponding to different downstream branches interact with each other at the end of each time inter-

¹The length of this “short” time step Δt , theoretically, can be infinitely small and, practically, can be obtained through a calibration exercise.

val. Thus, after a long time, the asymptotic kinematic waves arising from diverging traffic can be totally different from the instantaneous waves. In this chapter, we will focus on the instantaneous waves arising from each branch, and the interaction between these waves and the asymptotic kinematic waves will be further studied in a following chapter.

The rest of this chapter is organized as follows. In Section 4.2, we first formulate the kinematic wave theory of diverges in the framework of the LWR model, and introduce the instantaneous kinematic wave theory for dynamics of diverging traffic. In Section 4.3, we solve in detail for the instantaneous kinematic waves. In Section 4.4, we present a new definition of traffic demand for diverging vehicles and the supply-demand method based on this new definition. In Section 4.5, we carry out simulations of the new model for two cases. In Section 4.6, we make our conclusions and propose some follow-up research.

4.2 A kinematic wave theory for diverges

As we know, in a traffic stream, traffic dynamics can be affected by characteristics such as vehicle types and destinations, and drivers' behavior. Here vehicles of the same characteristics are considered to belong to a commodity. In this study we are only interested in the impact of vehicles' destinations on traffic dynamics at a highway diverge. Therefore, for a diverge with D downstream branches and one upstream branch, we can differentiate vehicles into D commodities.

Here we consider an ideal diverge: on the upstream branch, traffic is considered in 1-pipe regime; once through the diverge, vehicles completely segregate. Therefore, we have a D -commodity flow on the upstream link and a single-commodity flow on each downstream link, and traffic dynamics on a road network with a diverge consists

of three parts: dynamics of the single-commodity flow on each downstream branch, dynamics of the D -commodity flow on the upstream branch, and dynamics at the diverge. In the following part, after reviewing the kinematic wave models of single-commodity and D -commodity traffic, we will focus on the study of traffic dynamics at the diverge.

4.2.1 The kinematic wave theory of single-commodity traffic flow

For dynamics of single-commodity traffic, the seminal LWR (Lighthill and Whitham, 1955b; Richards, 1956) kinematic wave theory can be applied. In the LWR model for traffic flow on a long crowded road, two equations are used to describe traffic dynamics of aggregate quantities such as traffic density ρ , flow-rate q and travel speed v :

$$\text{Traffic conservation: } \rho_t + q_x = 0, \quad (4.1)$$

$$\text{Fundamental diagram: } q = Q(a, \rho). \quad (4.2)$$

In Equation 4.2, $a(x)$ is an inhomogeneity factor depending on road characteristics such as the number of lanes at x . Since $q = \rho v$, we also have a speed-density relation: $v = V(a, \rho) = Q(a, \rho)/\rho$; for vehicular traffic, generally, v is nonincreasing and the equilibrium flow-density relation is assumed to be concave. From Equation 4.1 and Equation 4.2, the LWR model can be written as

$$\rho_t + Q(a, \rho)_x = 0. \quad (4.3)$$

When the road is homogeneous; i.e., $a(x)$ is constant, the LWR model is called homogeneous; otherwise, when $a(x)$ is dependent on location, Equation 4.3 is called an inhomogeneous LWR model.

The homogeneous LWR model is nothing but a scalar conservation law and has been well studied both analytically and numerically. It is solved by combinations of shock and expansion (rarefaction) waves. In contrast, the inhomogeneous LWR model Equation 4.3 can be considered as a nonlinear resonant system and has an additional type of kinematic waves - standing waves, which initiate and stay at the inhomogeneity (Jin and Zhang, 2003b). Therefore, for a single-commodity flow on a road branch, traffic dynamics can be considered as the evolution of a combination of shock, rarefaction, and standing waves.

4.2.2 The kinematic wave theory of multi-commodity traffic flow

For traffic on the upstream link, it is assumed that vehicles with different destinations have no differences in dynamics; i.e., the speed-density relation is independent of commodities. Let $\rho_i(x, t)$, $v_i(x, t)$, and $q_i(x, t)$ ($i = 1, \dots, D$) denote, at place x and time t , the density, speed, and flow-rate of commodity i , respectively. In contrast, $\rho(x, t)$, $v(x, t)$, and $q(x, t)$ are the aggregate density, speed, and flow-rate. Then we have (with (x, t) suppressed hereafter)

$$\rho = \sum_{i=1}^D \rho_i, \quad (4.4)$$

$$v = v_i = V(a, \rho), \quad i = 1, \dots, D, \quad (4.5)$$

$$q = \sum_{i=1}^D q_i, \quad (4.6)$$

where $q = \rho v$, $q_i = \rho_i v_i$ ($i = 1, \dots, D$), $V(a, \rho)$ is the aggregate speed-density relation. We also call this kind of multi-commodity traffic as additive. In additive traffic, the flow of each commodity is called a partial flow and the flow containing all commodities the total flow.

Therefore, in additive traffic, dynamics of each partial flow can be written as

$$(\rho_i)_t + (\rho_i V(a, \rho))_x = 0, \quad i = 1, \dots, D. \quad (4.7)$$

Note that these D equations are coupled through the aggregate speed-density relation. By introducing the fraction of vehicles of commodity i , $\xi_i = \rho_i/\rho$, which satisfies $\sum_{i=1}^D \xi_i = 1$, Lebacque (1996) showed that traffic dynamics of additive traffic can also be written as

$$\rho_t + (\rho V(a, \rho))_x = 0, \quad (4.8)$$

$$(\xi_i)_t + V(a, \rho) (\xi_i)_x = 0, \quad i = 1, \dots, D - 1. \quad (4.9)$$

We can see that the fractions travel in the same speed as vehicles. This shows that the First-In-First-Out principle is guaranteed in the kinematic wave theory of additive traffic (Lebacque, 1996). In addition, we can see that, for multi-commodity traffic, the aggregate traffic dynamics can be described by the (inhomogeneous) LWR model and is still a combination of shock waves, rarefaction waves, and/or standing waves, and traffic dynamics of a commodity is of the similar pattern.

4.2.3 A kinematic wave theory of diverging traffic

To model traffic dynamics on a network with a diverge, the harder problem is to find the number of vehicles traveling from the upstream link to each downstream link during a time interval. This is an important problem to answer since flows from the upstream link to the downstream links are the necessary boundary conditions for the connected links. Here we propose a new approach to finding the approximate flows through a diverge. This new theory is different from the supply-demand method of (Daganzo, 1995a; Lebacque, 1996) in that this theory can be analytically solved by a combination of kinematic waves.

Like the supply-demand method of (Daganzo, 1995a; Lebacque, 1996), the new kinematic wave theory is also in a discrete form: we partition each branch into a number of cells of length Δx , discretize the time duration into time steps of length Δt , and assume that the aggregate and partial traffic densities are constant in each cell at a time step. The discretization of space-time plane in this model is required to satisfy the CFL condition (Courant et al., 1928), which guarantees that the flows through the diverge are only dependent on traffic densities in the adjacent cells and are independent of traffic conditions farther upstream or downstream.

In the discrete model, connected to the diverge with D downstream branches are an upstream cell and D downstream cells, denoted as downstream cell i ($i = 1, \dots, D$). Assume that, at $t = 0$, partial densities in the upstream cell are ρ_i^L and the aggregate density $\rho^L = \sum_{i=1}^D \rho_i^L$, and density in downstream cell i is ρ_i^R . With these initial traffic conditions, we will show how traffic dynamics will evolve from $t = 0$ till $t = \Delta t$. In addition, we will be able to compute the in-flow to downstream cell i ($i = 1, \dots, D$), q_i . Then from traffic conservation, the out-flow from the upstream cell is $\sum_{i=1}^D q_i$. With these flows, traffic conditions at the next time step $t = \Delta t$ can be obtained.

In this new model, to study the traffic dynamics of commodity i through the diverge from $t = 0$ to $t = \Delta t$, we hold partial densities of vehicles of the other commodities in the upstream cell constant during this time interval. That is, ρ_j^L , where $j = 1, \dots, D$ and $j \neq i$, are all constant. Here we assume that traffic densities of commodities other than i are constant during the short time interval. This assumption is equivalent to saying that the change of traffic conditions of commodity i is, in a short time interval, independent of traffic dynamics in the other directions. This assumption appears to be a natural and reasonable way to decouple the interactions between traffic in different directions. This approach can be considered as an attempt to answer an important question: how do vehicles of different destinations segregate

themselves at a diverge?

We set the diverging point at $x = 0$ and vehicles travel in the positive direction of x -axis. Thus, $x < 0$ for the upstream link and $x > 0$ for the downstream link. Also, to simplify the notations, we rewrite ρ_i as ρ and the total traffic densities of other commodities as k . Therefore, traffic dynamics of vehicles of commodity i in the upstream cell can be written as $\rho_t + (\rho V(a(x), \rho + k))_x = 0$ for $x < 0$, and $\rho_t + (\rho V(a(x), \rho))_x = 0$ for $x > 0$. Since k is held constant during the time interval $[0, \Delta t]$, and $k = 0$ in downstream cell i , we have the following equation and conditions for traffic dynamics of commodity i :

$$\rho_t + (\rho V(a(x), \rho + k))_x = 0, \quad (4.10)$$

with the following initial traffic conditions

$$\begin{aligned} \rho &= \begin{cases} \rho_L & x < 0, \\ \rho_R & x > 0; \end{cases} & t = 0, \\ k &= \begin{cases} k_L & x < 0, \\ 0 & x > 0; \end{cases} & t \in [0, \Delta t]. \end{aligned} \quad (4.11)$$

Here we extend our x -axis to both positive and negative infinity since, with the CFL condition, the traffic dynamics only depend on the conditions above.

Thus, Equation 4.10 with Equation 4.11 is a description of traffic dynamics of commodity i during a short time interval. This new model will be shown to be solved by instantaneous kinematic waves in the following section.

4.3 The instantaneous kinematic waves

In this section, we discuss the instantaneous kinematic waves of Equation 4.10 with initial conditions Equation 4.11. For the purpose of exposition, we here assume that

both the upstream and downstream branches share the same speed-density relation; i.e., we exclude the road characteristics $a(x)$. We also assume that q is concave and v non-increasing in $\rho \in [0, \rho_j]$, where ρ_j is the jam density. With modifications, the results here are applicable to the case when the upstream and downstream branches have different characteristics.

Since we assume that k is time independent, we have another conservation equation: $k_t = 0$. Therefore Equation 4.10 with Equation 4.11 can be rewritten as a 2×2 system:

$$\begin{aligned} \rho_t + (\rho V(\rho + k))_x &= 0, \\ k_t &= 0, \end{aligned} \tag{4.12}$$

together with initial conditions

$$\begin{aligned} \rho(x, t = 0) &= \begin{cases} \rho_L & x < 0, \\ \rho_R & x > 0, \end{cases} \\ k(x, t = 0) &= \begin{cases} k_L & x < 0, \\ 0 & x > 0. \end{cases} \end{aligned} \tag{4.13}$$

Next, we will show that Equation 4.12 is indeed a nonlinear resonant system studied by Isaacson and Temple (1992). Consequently, we can use their technique to solve this system, which describes traffic dynamics of one commodity during a short time period. Note that here we do not restrict our time domain to be $[0, t_1]$. This is because Equation 4.12 with Equation 4.13 has self-similar solutions, which means that the flow $f(x = 0, t)$ is constant for any time $t > 0$.

4.3.1 The properties of Equation 4.12 as a nonlinear resonant system

Denote the state $U = (k, \rho)$, the flux vector $F(U) = (0, \rho V(\rho + k))$, Equation 4.12 can be written as a hyperbolic system of conservation laws:

$$U_t + F(U)_x = 0, \quad (4.14)$$

where $x \in (-\infty, \infty)$, $t \geq 0$. This system can be written in the following form of a quasi-linear system

$$U_t + \partial F(U)U_x = 0, \quad (4.15)$$

where the Jacobian matrix $\partial F(U)$ is

$$\partial F = \begin{bmatrix} 0 & 0 \\ \rho V'(\rho + k) & V(\rho + k) + \rho V'(\rho + k) \end{bmatrix}. \quad (4.16)$$

Thus the two eigenvalues of $\partial F(U)$ are

$$\lambda_0 = 0, \quad \lambda_1 = V(\rho + k) + \rho V'(\rho + k),$$

and their corresponding right eigenvectors are

$$\vec{R}_0 = \begin{bmatrix} V(\rho + k) + \rho V'(\rho + k) \\ -\rho V'(\rho + k) \end{bmatrix}, \quad \vec{R}_1 = \begin{bmatrix} 0 \\ 1 \end{bmatrix}.$$

System Equation 4.14 is a non-strictly hyperbolic system, since it may happen that

$$\lambda_1(U_*) = \lambda_0(U_*) = 0. \quad (4.17)$$

When Equation 4.17 is satisfied, we say that traffic state U_* is partially critical. If denoting the partial fundamental diagram as $Q(\rho; k) = \rho V(\rho + k)$, we can define

other partial quantities of the commodity that we are interested in, partial capacity $Q^{\max}(k)$ and partial critical density $\gamma(k)$, as follows:

$$Q(\rho; k) \leq Q^{\max}(k), \quad \forall \rho \in [0, \rho_j - k], \quad (4.18)$$

$$Q^{\max}(k) = Q(\gamma(k); k). \quad (4.19)$$

Since $V' \leq 0$ and $d^2(\rho V(\rho))/d\rho^2 < 0$, we have

$$\begin{aligned} \frac{\partial^2 Q(\rho; k)}{\partial \rho^2} &< 0, \\ \frac{\partial Q(\rho; k)}{\partial k} &\leq 0; \end{aligned}$$

therefore, $Q^{\max}(k)$ and $\gamma(k)$ are unique for given $k \in [0, \rho_j]$. Thus the partially critical state $U_* = (k_*, \rho_*) = (k_*, \gamma(k_*))$. We call the collection of the partially critical states, $\Gamma = \{U_* | k \in [0, r_j]\}$, the transition curve.

Moreover, at a partially critical state U_* , Equation 4.12 is genuinely nonlinear; i.e.,

$$\frac{\partial}{\partial \rho} \lambda_1(U_*) = \frac{\partial^2}{\partial \rho^2} (\rho V(\rho + k)) < 0, \quad (4.20)$$

since $q = \rho V(\rho + k)$ is concave in ρ , and $\partial F(U)$ is nondegenerate; i.e.,

$$\frac{\partial}{\partial k} (\rho_* V(\rho_* + k_*)) = \rho_* V'(\rho_* + k_*) = -V(\rho_* + k_*) < 0. \quad (4.21)$$

With conditions Equation 4.17-Equation 4.21 satisfied, Equation 4.12 is a nonlinear resonant system in the sense of (Isaacson and Temple, 1992), and it is guaranteed that, in a neighborhood of the state U_* , the Riemann problem for Equation 4.12 with Equation 4.13 has a unique solution with a canonical structure.

4.3.2 The instantaneous kinematic waves of Equation 4.12 with Equation 4.13

The Riemann problem for Equation 4.12 with initial conditions Equation 4.13 is solved by two families of basic waves, associated with the two eigenvalues. The 0-waves with wave speed $\lambda_0 = 0$, also called standing waves, are the integral curves of \vec{R}_0 in U -space, and therefore are given by $Q(\rho; k) = \text{const}$. Similarly, the 1-waves with wave speed $\lambda_1(U)$ are integral curves of \vec{R}_1 in U -space, and are given by $k = \text{const}$. As shown in Figure 4.1, the 0-curve is concave and tangent to the 1-curve at the critical state U_* ; states left to the transition wave $\Gamma(k)$ are undercritical (UC), and overcritical (OC) right to the transition wave.

Isaacson and Temple (1992) showed that wave solutions to the Riemann problem are formed by no more than three basic waves, including standing waves, shock waves, and rarefaction waves, and these waves satisfy two entropy conditions: Lax's entropy condition (1972), i.e., that these waves increase their wave speeds from left (upstream) to right (downstream), and an additional condition that an UC state and an OC state can not be connected by a standing wave. With these conditions, wave solutions exist and are unique: when U_L is UC, wave solutions in U -space are shown in Figure 4.2, and in Figure 4.3 when U_L is OC. Note that the solutions can also be categorized according to whether ρ_R is OC or UC. Also recall that U_R always lies on $k = 0$.

In the remaining part of this subsection, we will discuss the Riemann solutions of Equation 4.12 with Equation 4.13, and compute the boundary flux $q(x = 0, t)$.

1. When U_L is UC; i.e., $\rho_L < \gamma(k_L)$, we denote the intersection between $Q(U_L)$ and $k = 0$ by ρ_1 and ρ_2 , where $\rho_1 \leq \gamma(0) \leq \rho_2$. Hence, we obtain three types of solutions when $\rho_R \in [0, \rho_1]$, (ρ_1, ρ_2) , or $[\rho_2, \rho_j]$ as shown in Figure 4.2.

Type 1 When $\rho_R \in [0, \rho_1]$; i.e., $Q(\rho_R; 0) \leq Q(U_L)$ and U_R is UC, wave solutions

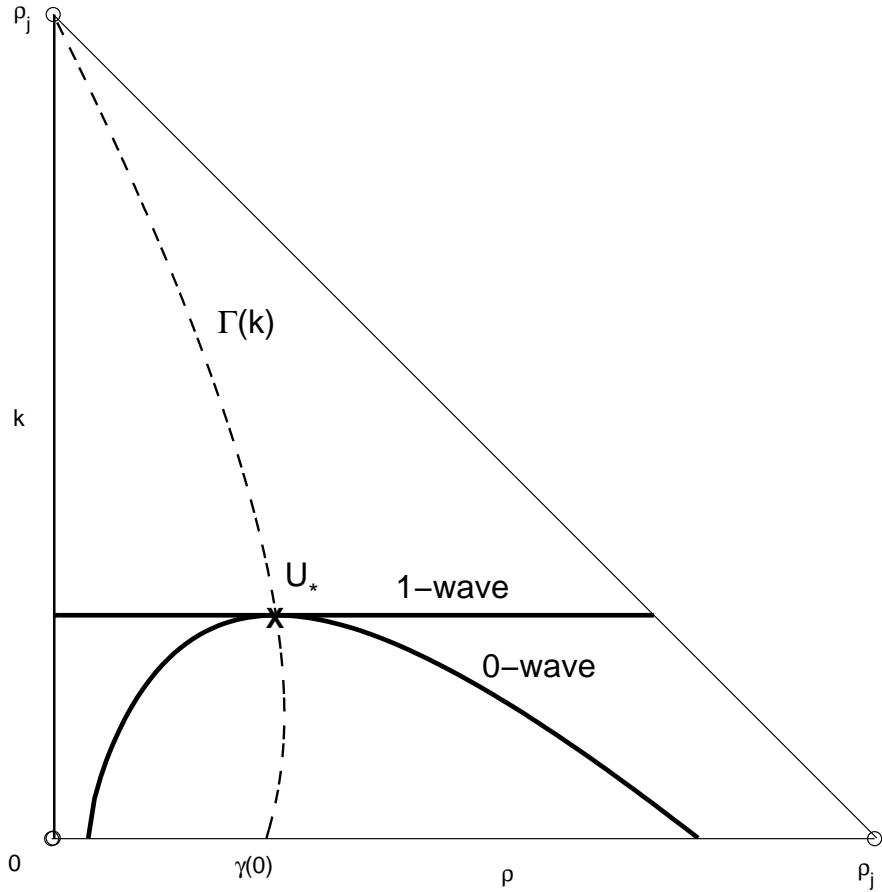


Figure 4.1: Integral curves in (ρ, k) -space

to the Riemann problem consist of two basic waves with the intermediate state, $U_1 = (\rho_1, 0)$: the left wave (U_L, U_1) is a standing wave and the right wave (U_1, U_R) is a rarefaction wave with characteristic velocity $\lambda_1(U) > 0$. As shown in Figure 4.4, the boundary flux $q(x = 0, t > 0) = Q(U_L)$.

Type 2 When $\rho_R \in (\rho_1, \rho_2)$; i.e., $Q(\rho_R; 0) > Q(U_L)$, wave solutions to the Riemann problem consist of two basic waves with the intermediate state, $U_1 = (\rho_1, 0)$: the left wave (U_L, U_1) is a standing wave and the right wave (U_1, U_R) is a shock wave with positive wave speed $s(U_1, U_R) = (Q(\rho_R; 0) -$

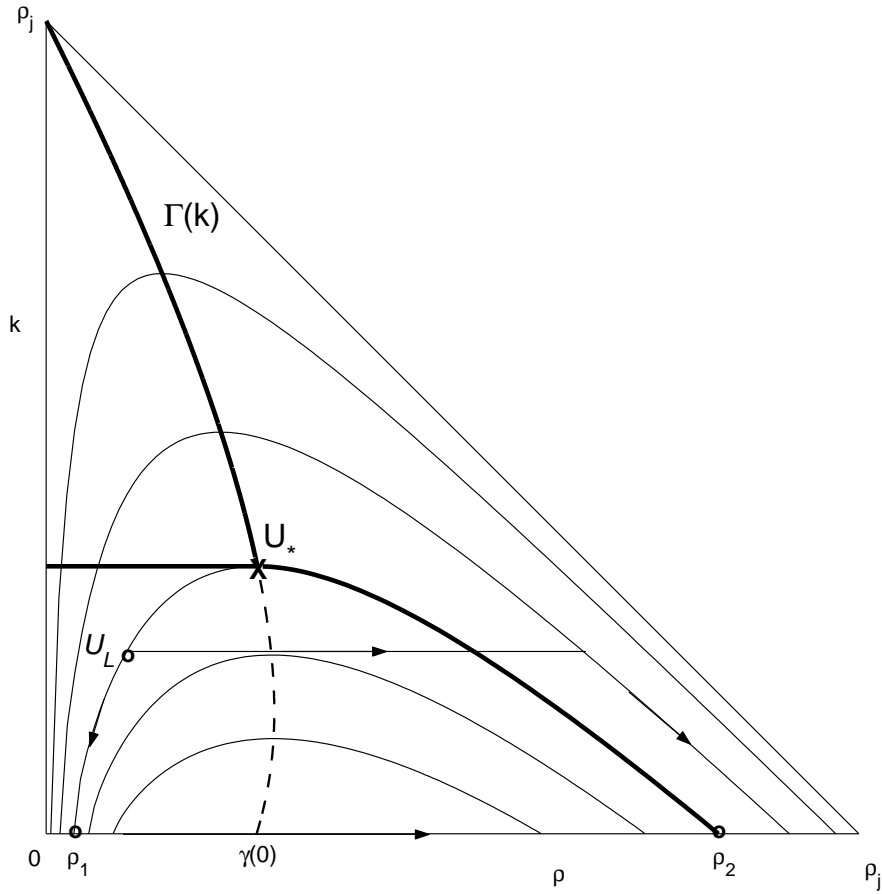


Figure 4.2: The Riemann solutions when U_L is UC

$Q(U_L)/(\rho_R - \rho_1)$. As shown in Figure 4.5, the boundary flux $q(x = 0, t > 0) = Q(U_L)$.

Type 3 When $\rho_R \in [\rho_2, \rho_j]$; i.e., $Q(\rho_R; 0) \leq Q(U_L)$ and U_R is OC, wave solutions to the Riemann problem consist of two basic waves with the intermediate state, $U_1 = (\rho_1, \rho_L)$ and $Q(U_1) = Q(\rho_R; 0)$: the left wave (U_L, U_1) is a shock wave with negative wave speed $s(U_L, U_1) = (Q(U_L) - Q(U_1))/(\rho_L - \rho_1)$ and the right wave (U_1, U_R) is a standing wave. As shown in Figure 4.6, the boundary flux $q(x = 0, t > 0) = Q(U_L)$.

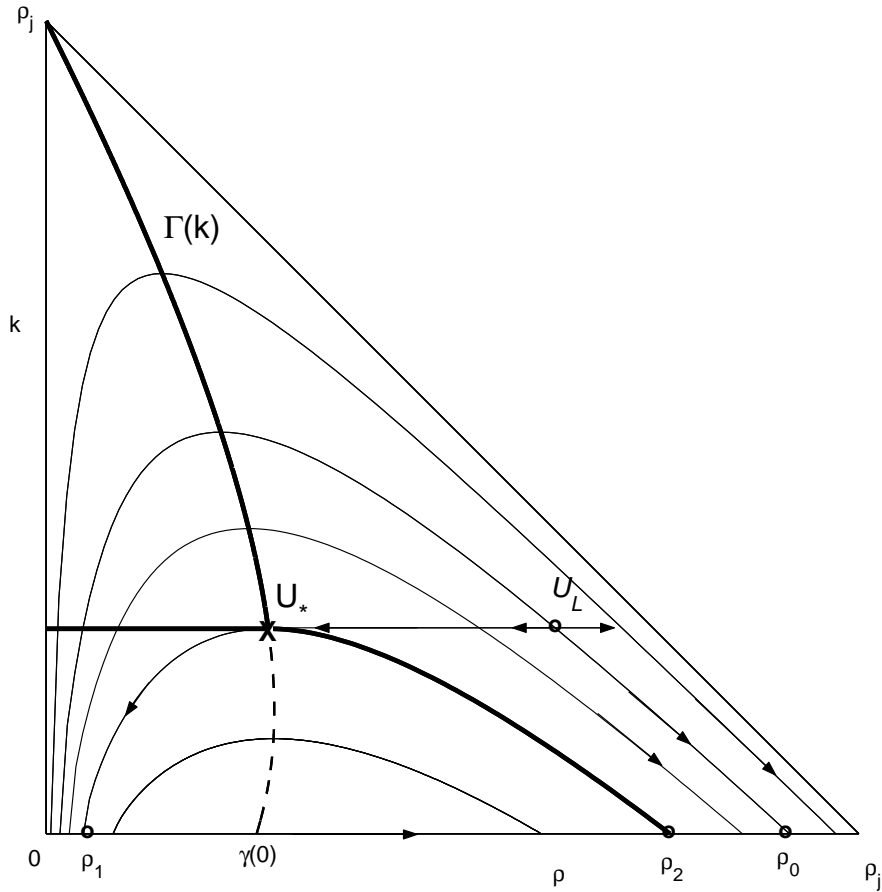


Figure 4.3: The Riemann solutions when U_L is OC

2. When U_L is OC; i.e., $\rho_L > \gamma(k_L)$, we define U_* by $U_* \in \Gamma(k)$ and $k_* = k_L$. Therefore, $Q(U_*)$ is the partial capacity $Q^{\max}(k_L)$. Denoting the intersection between $Q(\rho; k) = Q(U_L)$ and $(\rho \geq \gamma(0), k = 0)$ by ρ_0 and the intersections between $Q(\rho; k) = Q(U_*)$ and $k = 0$ by ρ_1 and ρ_2 , where $\rho_1 \leq \gamma(0) \leq \rho_2$, we can obtain four types of solutions when $\rho_R \in [0, \rho_1]$, (ρ_1, ρ_2) , $[\rho_2, \rho_0]$, or $(\rho_0, \rho_j]$, as shown in Figure 4.3.

Type 4 When $\rho_R \in [0, \rho_1]$; i.e., $Q(\rho_R; 0) \leq Q(U_*)$ and U_R is UC, wave solutions to the Riemann problem consist of three basic waves with two intermedi-

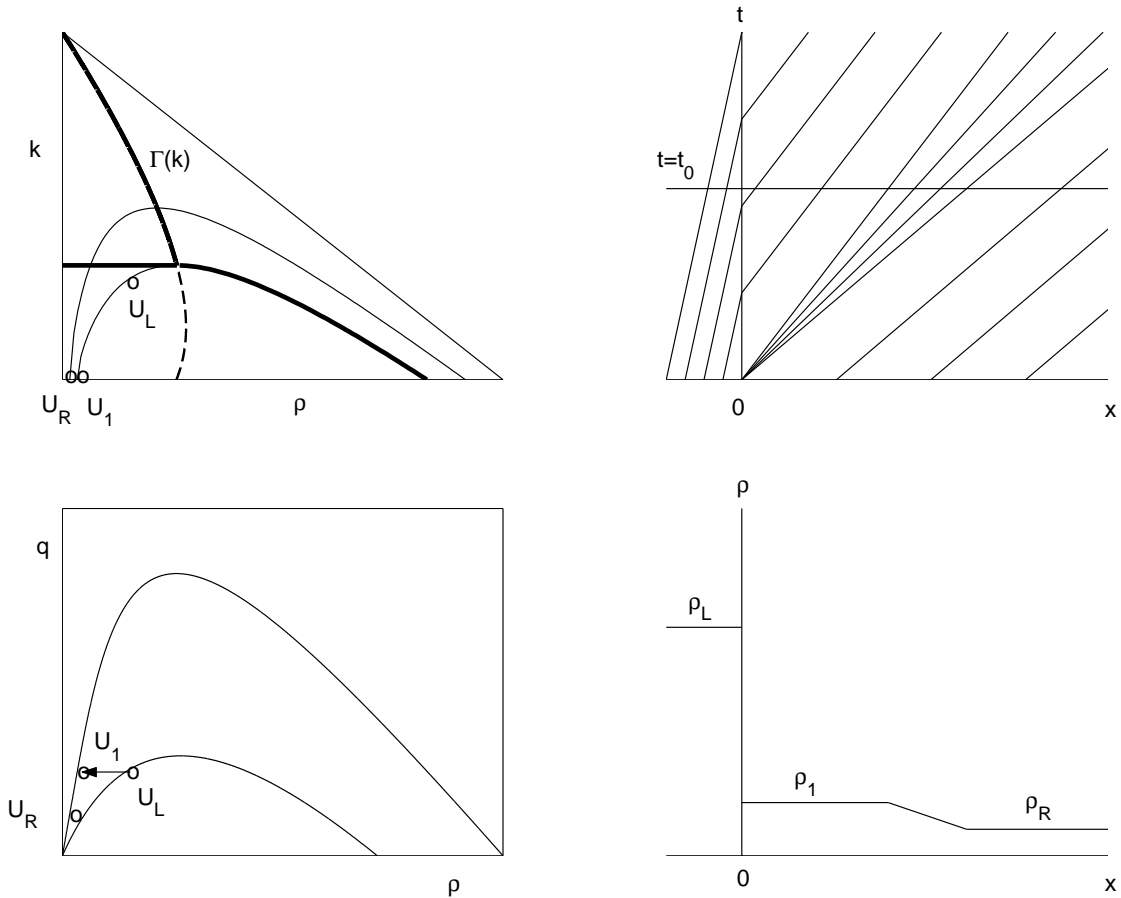


Figure 4.4: An example for wave solutions of type 1 for Equation 4.12 with initial conditions Equation 4.13

ate states, U_* and U_1 , where $Q(U_1) = Q(U_*)$ and $k_1 = 0$: the left wave (U_L, U_*) is a rarefaction wave with non-positive characteristic velocity, the center wave (U_*, U_1) is a standing wave, and the right wave (U_1, U_R) is a rarefaction wave with positive characteristic velocity. As shown in Figure 4.7, the boundary flux $q(x = 0, t > 0) = Q(U_*) = Q^{\max}(k_L)$.

Type 5 When $\rho_R \in (\rho_1, \rho_2)$; i.e., $Q(\rho_R; 0) > Q(U_*)$, wave solutions to the Riemann problem consist of three basic waves with two intermediate states, U_* and

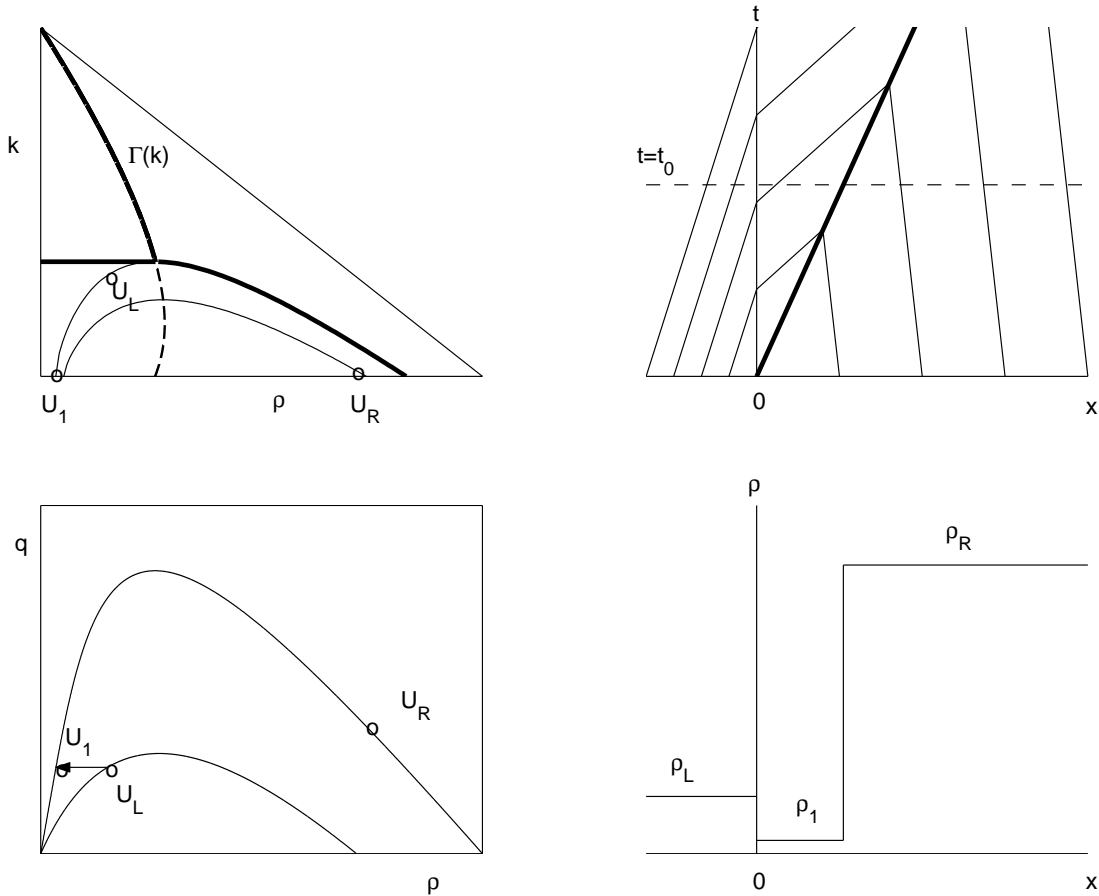


Figure 4.5: An example for wave solutions of type 2 for Equation 4.12 with initial conditions Equation 4.13

U_1 , where $Q(U_1) = Q(U_*)$ and $k_1 = 0$: the left wave (U_L, U_*) is a rarefaction wave with non-positive characteristic velocity, the center wave (U_*, U_1) is a standing wave, and the right wave (U_1, U_R) is a shock wave with positive speed. As shown in Figure 4.8, the boundary flux $q(x = 0, t > 0) = Q(U_*) = Q^{\max}(k_L)$.

Type 6 When $\rho_R \in [\rho_2, \rho_0]$; i.e., $Q(U_L) \leq Q(\rho_R; 0) \leq Q(U_*)$ and U_R is OC, wave solutions to the Riemann problem consist of two basic waves with the

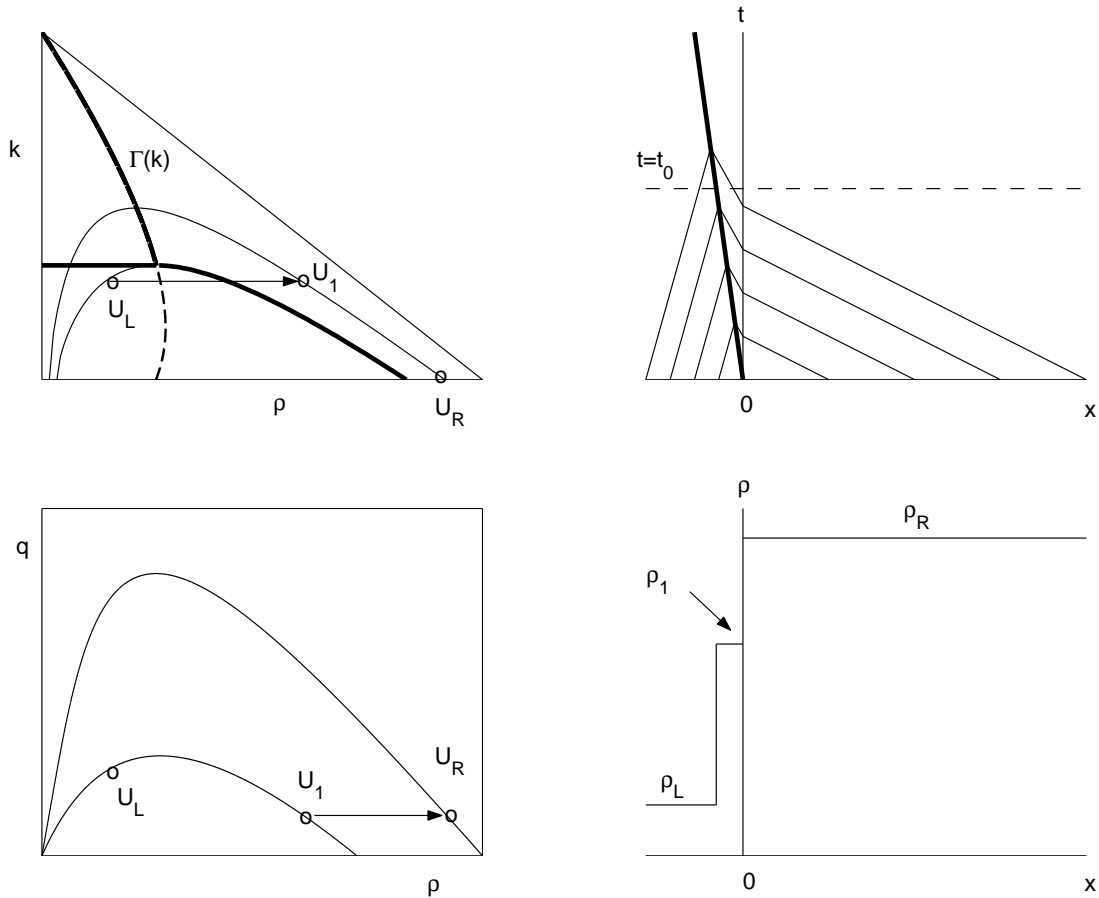


Figure 4.6: An example for wave solutions of type 3 for Equation 4.12 with initial conditions Equation 4.13

intermediate state U_1 , where $Q(U_1) = Q(U_R)$ and $k_1 = k_L$: the left wave (U_L, U_1) is a rarefaction wave with negative characteristic velocity and the right wave (U_1, U_R) is a standing wave. As shown in Figure 4.9, the boundary flux $q(x = 0, t > 0) = Q(U_R)$.

Type 7 When $\rho_R \in (\rho_0, \rho_j]$; i.e., $Q(\rho_R; 0) < Q(U_L)$ and U_R is OC, wave solutions to the Riemann problem consist of two basic waves with the intermediate state U_1 , where $Q(U_1) = Q(U_R)$ and $k_1 = k_L$: the left wave (U_L, U_1) is a

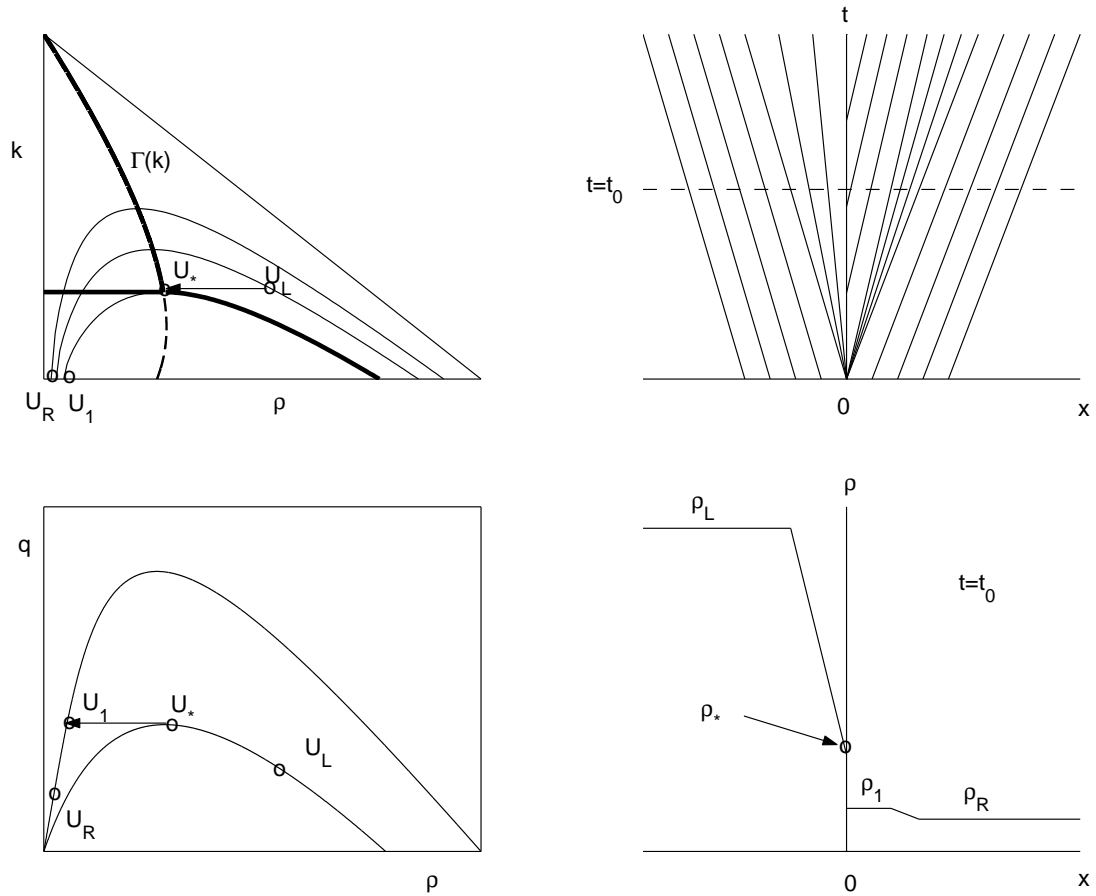


Figure 4.7: An example for wave solutions of type 4 for Equation 4.12 with initial conditions Equation 4.13

shock wave with negative speed and the right wave (U_1, U_R) is a standing wave. As shown in Figure 4.10, the boundary flux $q(x = 0, t > 0) = Q(U_R)$.

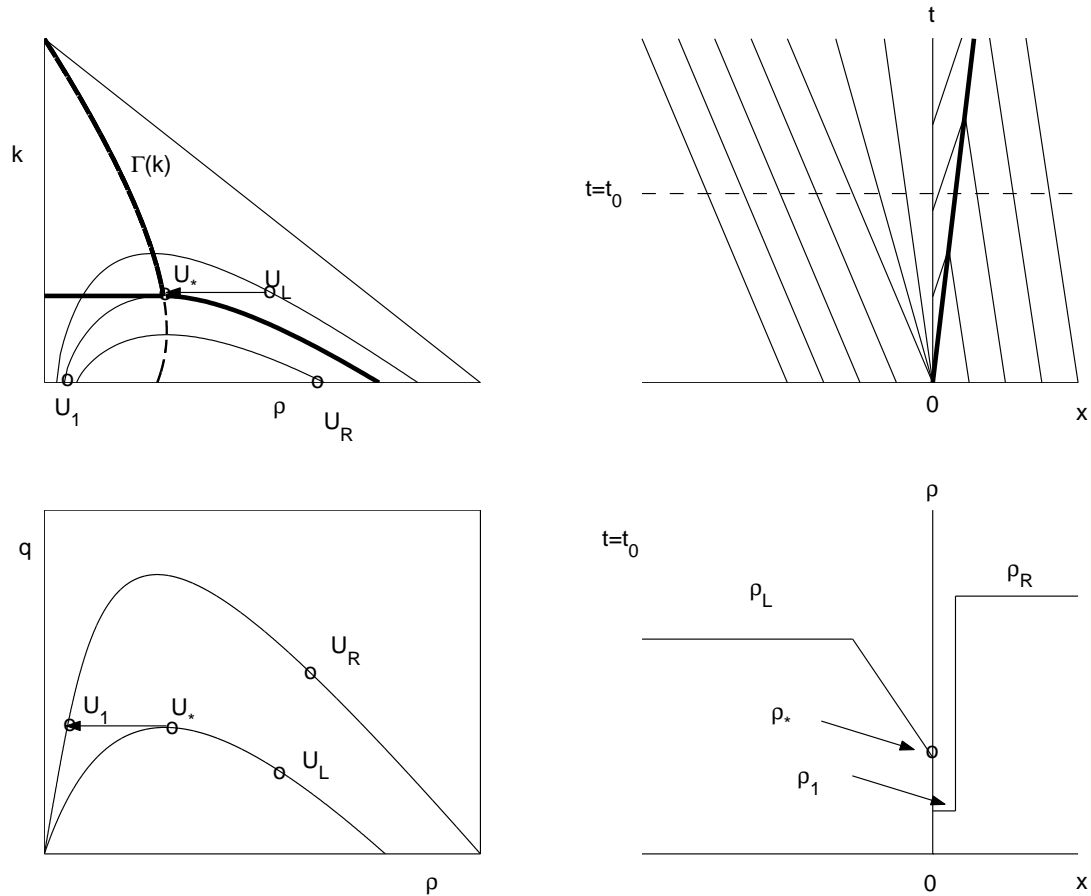


Figure 4.8: An example for wave solutions of type 5 for Equation 4.12 with initial conditions Equation 4.13

4.4 The supply-demand method with a new definition of traffic demand

Based on the discussions in the previous section, we summarize solutions of boundary flux $q(x = 0, t > 0)$ in Table 4.1.

Further, if we introduce a new definition of partial traffic demand for commodity

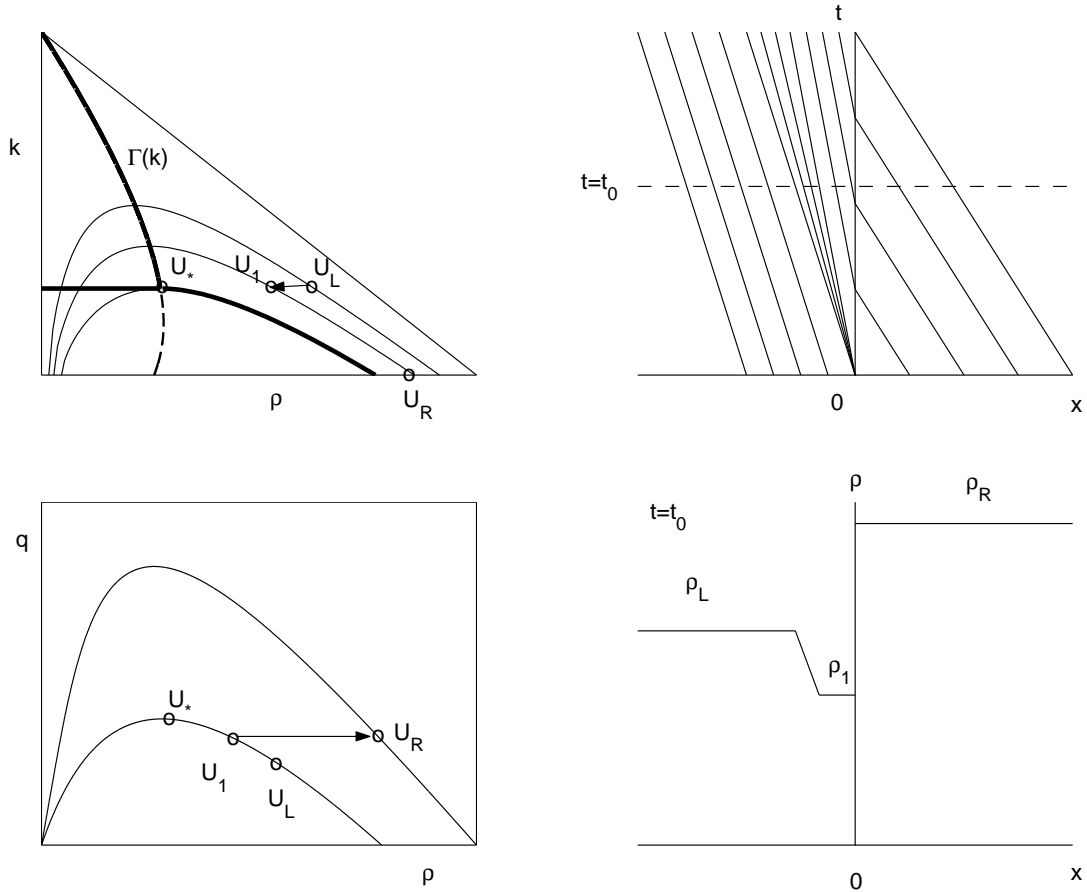


Figure 4.9: An example for wave solutions of type 6 for Equation 4.12 with initial conditions Equation 4.13

1 in the upstream link as

$$D(\rho_L; k_L) = \begin{cases} Q(U_L) & U_L \text{ is UC} \\ Q^{\max}(k_L) & \text{otherwise} \end{cases}, \quad (4.22)$$

the boundary flux $q(x = 0, t > 0)$ can then be computed by

$$q(x = 0, t > 0) = \min\{S_1, D(\rho_L; k_L)\}, \quad (4.23)$$

where the supply of the downstream link, S_1 , is the same as in (Daganzo, 1995a;

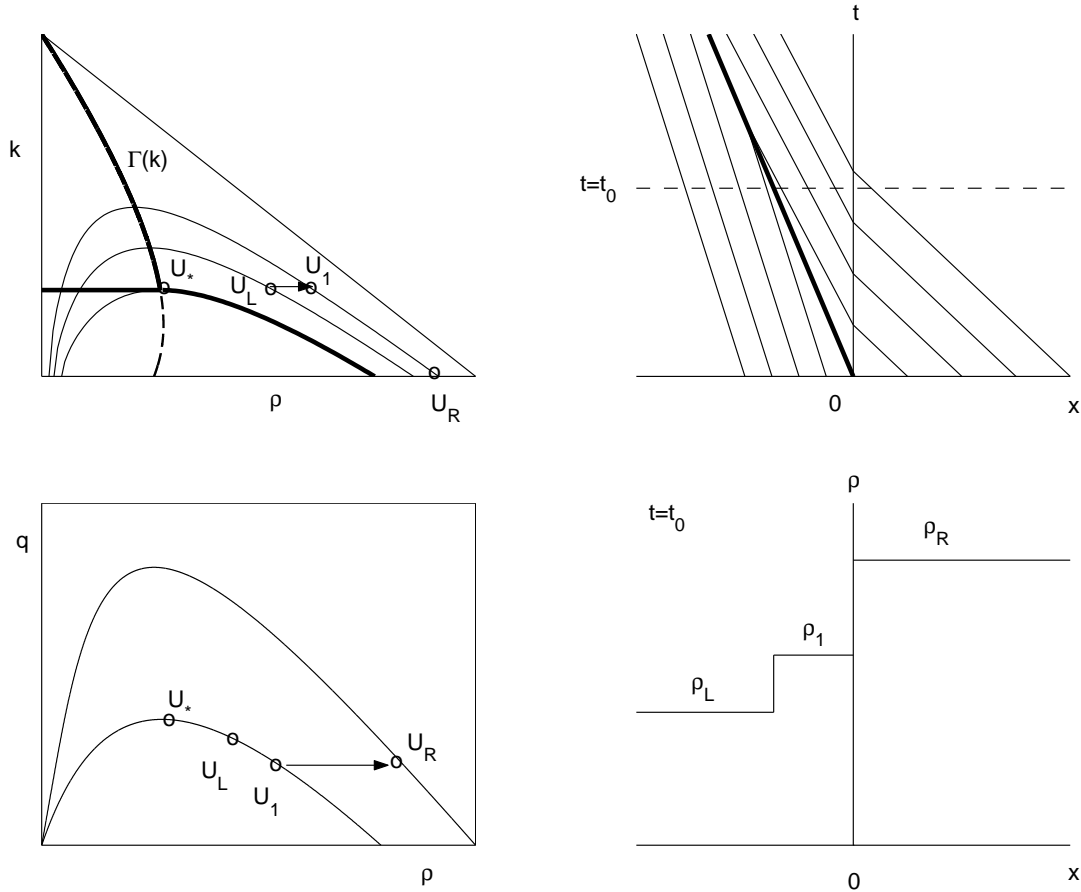


Figure 4.10: An example for wave solutions of type 7 for Equation 4.12 with initial conditions Equation 4.13

Lebacque, 1996); i.e.,

$$S_1 = \begin{cases} Q(U_R) & U_R \text{ is OC} \\ Q^{\max}(0) & \text{otherwise} \end{cases} . \tag{4.24}$$

The supply-demand method Equation 4.23 can also be used to calculate the boundary fluxes of other commodities. It yields the same solutions to the Riemann problem of Equation 4.12 with Equation 4.13 as the analytical solution method. Moreover, it is much simpler in computation and can be easily extended to the more

Solution type	left state U_L	right state ρ_R	$q(x = 0, t > 0)$
1	UC	$Q(\rho_R; 0) \leq Q(U_L), \rho_R < \gamma(0)$	$Q(U_L)$
2	UC	$Q(\rho_R; 0) > Q(U_L)$	$Q(U_L)$
3	UC	$Q(\rho_R; 0) \leq Q(U_L), \rho_R > \gamma(0)$	$Q(U_R)$
4	OC	$Q(\rho_R; 0) \leq Q(U_L), \rho_R > \gamma(0)$	$Q^{\max}(k_L)$
5	OC	$f(U_R) < f_L^{\max}, a_R > a_L, \rho_R/a_R < \alpha$	$Q^{\max}(k_L)$
6	OC	$f(U_R) > f_L^{\max}$	$Q(U_R)$
7	OC	$f(U_R) < f(U_L), \rho_R/a_R < \alpha, a_R < a_L$	$Q(U_R)$

Table 4.1: Solutions of the boundary flux $q(x = 0, t > 0)$

complicated cases when the upstream and downstream branches have different road characteristics.

4.5 Numerical simulations

In this section, we carry out numerical simulations of the instantaneous kinematic wave model presented in this chapter. We will study a small diverging network consisting of two downstream links and one upstream link: the lengths of three links are the same, $L = 400l = 11.2$ km, with unit length $l = 0.028$ km; one downstream link, labeled as link d_1 , has $a(d_1) = 2$ lanes, another downstream link, link d_2 , has $a(d_2) = 1$ lane, and the upstream link, link u , has $a(u) = 2$ lanes. The simulation starts from $t = 0$ and ends at $t = 500\tau = 41.7$ min, with unit time $\tau = 5$ s. In the following simulations, we partition each link into N cells and the time interval into K steps, with $N/K = 1/10$ always; e.g., if $N = 50$ and $K = 500$, the cell length is $\Delta x = 8l$ km and the length of each time step $\Delta t = 1\tau$ s.

We will use the exponential fundamental diagram (Del Castillo and Benitez, 1995b),

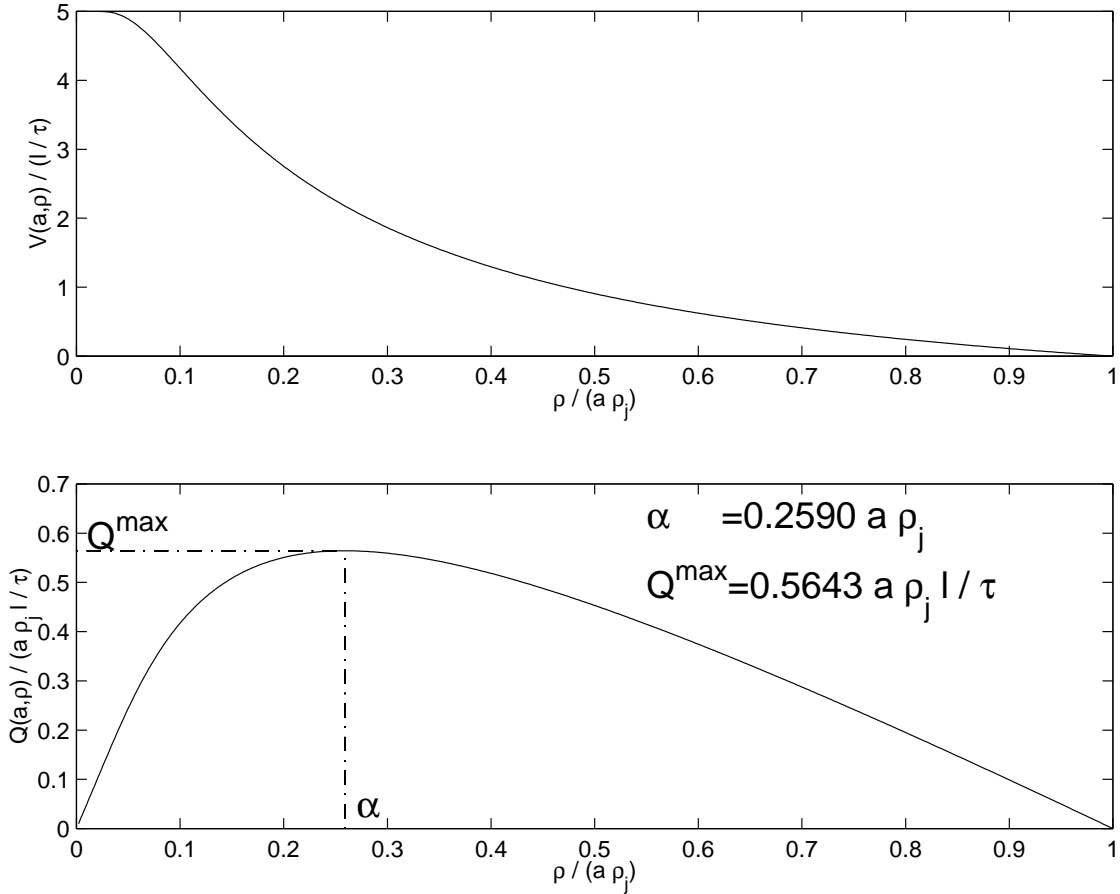


Figure 4.11: The Newell model of speed-density and flow-density relations

and the parameters are given as follows: the free flow speed $v_f = 5.0l/\tau = 0.028 \text{ km/s} = 100.8 \text{ km/h}$; the jam density of a single lane $\rho_j = 180 \text{ veh/km/lane}$; the wave velocity for jam traffic $c_j = -1.0l/\tau = -0.0056 \text{ km/s} = -20.16 \text{ km/h}$; and the equilibrium speed-density relationship

$$V(a, \rho) = 5 \left[1 - \exp \left\{ \frac{1}{5} \left(1 - \frac{a \rho_j}{\rho} \right) \right\} \right] l/\tau,$$

where $a(x)$ is the number of lanes at location x . The equilibrium functions $V(a, \rho)$ and $Q(a, \rho)$ are shown in Figure 4.11, in which the critical traffic density is $\alpha = 0.259a\rho_j$.

Here we apply the first-order Godunov method (Godunov, 1959), in which the

traffic conditions are updated for each cell based on traffic conservation, and boundary fluxes are computed with the supply-demand method described in Section 4. Since $\lambda_* \leq v_f = 5l/\tau$, we find the CFL condition number

$$\lambda_* \frac{\Delta t}{\Delta x} \leq 0.625 < 1.$$

Therefore, the first-order Godunov method can solve the instantaneous kinematic wave model efficiently.

4.5.1 Simulation I: A general case

In this simulation, we study a general case of diverging traffic. Initially, the upstream branch carries a constant flow with traffic density $\rho_u = 1.1111\rho_j = 200$ veh/km and the proportion of vehicles traveling to downstream branch d_1 is 80%; downstream link d_1 is empty; traffic density on downstream link d_2 is $\rho_{d_2} = 0.5556\rho_j = 100$ veh/km. In addition, we impose the Neumann boundary conditions on the boundary of this diverging network; i.e., the spatial derivatives of traffic densities at the boundary are set to be zero.

With $N = 500$ and $K = 5000$, we obtain simulation results as shown in Figure 4.12. Fig. 4.12(a) illustrates the evolution of traffic on the upstream link: at time $t = 0\tau$, traffic density is uniformly at $\rho_A = 1.11\rho_j$; after the beginning of diverging process, traffic immediately upstream of the diverging point reaches a new state $\rho_B = 0.69\rho_j$, which keeps propagating on the upstream link; as a result, an expansion wave forms and travels upstream. Fig.4.12(b) shows the evolution of traffic on downstream link d_1 : initially, this link is empty; after $t = 0$, traffic immediately downstream of the diverging point reaches state $\rho_C = 0.22\rho_j$; along with the propagation of ρ_C , on this link, another expansion wave forms and travels downstream; after around 200τ , traffic density on this link is uniformly ρ_C . Fig. 4.12(c) presents the evolution of traffic on

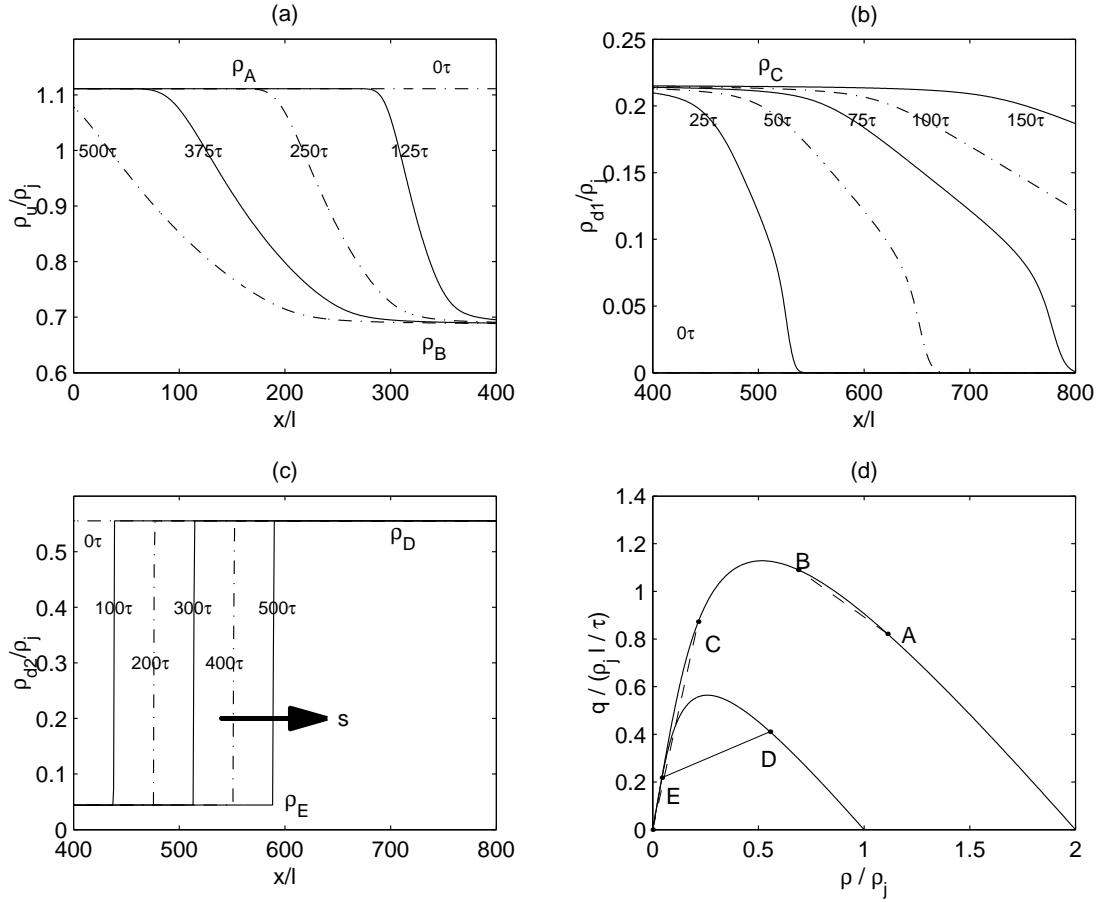


Figure 4.12: Simulation I: A general case

downstream link d_2 : initially, traffic density is $\rho_D = 0.56\rho_j$; after vehicles start to diverge at $t = 0$, traffic immediately downstream of the diverging point reaches $\rho_E = 0.04\rho_j$; then a shock forms and travels downstream in a constant speed $s = 0.38l/\tau$. The expansion waves and the shock wave observed on the three branches can be shown on the $\rho - q$ plane as in Fig. 4.12(d), in which dashed line AB represents the expansion wave on the upstream link u , dashed line OC represents the expansion wave on downstream link d_1 , and solid line DE represents the shock wave on downstream link d_2 , whose slope gives the shock speed.

As shown in Figure 4.12, at the diverging point, there are three traffic states, represented by B , C , and E in Fig. 4.12(d). Flow rates at these states are $q_B = 1.09\rho_j l/\tau$, $q_C = 0.87\rho_j l/\tau$, and $q_E = 0.22\rho_j l/\tau$ respectively. We can see that $q_B = q_C + q_E$. Note that q_B is the outflow of link u , q_C inflow to link d_1 , and q_E inflow to link d_2 . Thus traffic is conserved at the diverge. Further, $q_C/q_B = 80\%$, which is the proportion of vehicles on the upstream link traveling to d_1 . Therefore, this is consistent with a general observation that diverging flows are proportionally determined by the composition of traffic on the upstream link (Papageorgiou, 1990). This property of diverging flows guarantees that the composition of vehicles on the upstream link never changes as observed in our simulation.

4.5.2 Simulation II: An extreme case

In this subsection, an extreme case is studied. Initially, like in the previous simulation, the upstream branch carries a constant flow with traffic density $\rho_u = 1.1111\rho_j = 200$ veh/km, the proportion of vehicles on the upstream link traveling to downstream branch d_1 is 80%, and downstream link d_1 is empty. However, traffic on downstream link d_2 is jammed; i.e., $\rho_{d_2} = \rho_j = 180$ veh/km. Still, we impose the Neumann boundary conditions on the boundary of the diverging network and have the same discretization to the three links and the time duration: $N = 500$ and $K = 5000$.

Simulation results are shown in Figure 4.13. In this simulation, traffic density on link d_2 is uniformly ρ_j as expected and not shown. Fig. 4.13(a) demonstrates traffic evolution on the upstream link u : initially traffic density is $\rho_A = 1.11\rho_j$; after the beginning of the diverging process, traffic density immediately upstream of the diverging point reaches the jammed density $\rho_B = 2\rho_j$; then, jammed traffic propagates upstream as a back-traveling shock at a speed $s = -0.92l/\tau$. Fig. 4.13(b) shows traffic dynamics on link d_1 . In this figure, we can observe small spikes of

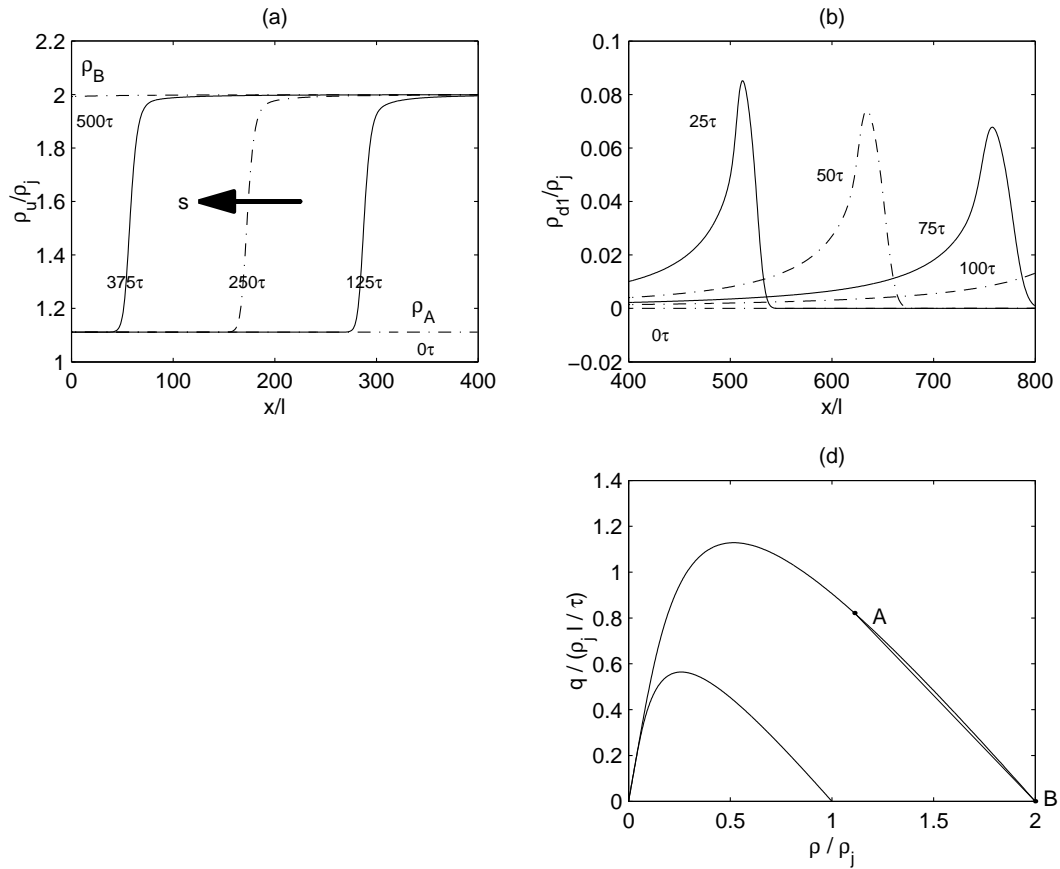


Figure 4.13: Simulation II: An extreme case

density, which travel downstream and shrink along time. After around $t = 200\tau$, link d_1 is almost empty as initially. Fig. 4.13(d) presents traffic states on the diverging network on the $\rho - q$ plane. Here line AB represents the shock wave on the upstream link, and its slope gives the shock wave speed.

From these figures, we can see that, if a downstream link is blocked, the upstream link and the other downstream link(s) will be blocked, as expected. However, the small spikes in Fig. 4.13(b) suggests there is still a small number of vehicles get out of the upstream link at the very beginning. Although this phenomenon seems

interesting, the appearing of small spikes in our model is due to numerical error of finite difference, caused by the finite number of cells, and are expected to disappear if we partition the links into fine enough cells.

4.6 Discussions

In this chapter, we have introduced a new approach to modeling diverging traffic dynamics, which is represented by instantaneous kinematic waves. We presented analytical solutions to these waves and found these solutions are consistent with the supply-demand method if the traffic demand is modified as in Section 4.4. With numerical simulations, we assert that this model satisfies two important properties: (1) diverging flow to a downstream link is proportional to the fraction of vehicles traveling to this link, and (2) the upstream link is blocked after a downstream link is blocked.

The instantaneous kinematic wave theory of diverging traffic is different from existing models since it provides more details on diverging traffic dynamics and sheds more light at the aggregate level how vehicles segregate themselves at a diverge. In the follow-up studies, we would like to discuss the convergent kinematic wave solutions when all branches are partitioned into infinite number of cells. We will also be interested in finding the location of actual diverging point and how it is related to traveler's behavior, the geometry of a diverge, and traffic conditions. Finally we will test this model with field data and discuss possible applications.

Chapter 5

Kinematic wave traffic flow model for mixed traffic

5.1 Background

Vehicular traffic on highways often comprises different types of vehicles with varying driving performances. This heterogeneity affects traffic flow characteristics in significant ways, a fact that has long been recognized by the transportation engineering profession. For example, in the computation of flow capacity on a highway or at a signalized intersection, the Highway Capacity Manual recommends a series of adjustments to take account of the capacity reduction caused by heavy vehicles (i.e., trucks/buses/recreational vehicles). If one is interested in the effects of heavy vehicles on traffic flow over space and time, however, the Highway Capacity Manual procedures are not adequate. For this one needs a dynamic model for mixed traffic.

Mixed traffic can be modeled at three different levels—microscopic, mesoscopic and macroscopic. It is perhaps most straightforward to model mixed traffic on a microscopic level—one simply endow, at one extreme, each individual vehicle with

different performance and behavior characteristics. Many commercially available simulation packages, such as CORSIM, PARAMICS, and VISSIM allow the specification of multiple vehicle classes. Major challenges arise when one models mixed traffic on a mesoscopic level, mainly due to the correlation between various probability distributions of vehicular speeds. Nevertheless, a number of mesoscopic models of mixed traffic have been developed in recent years (Helbing, 1997; Hoogendoorn and Bovy, 2000). Aggregation of mesoscopic models of mixed traffic through expectation operations lead to multi-class traffic flow models in the macroscopic level. There is, however, another approach to develop macroscopic mixed traffic flow models. This is the approach of continuum modeling. It is this approach that we shall adopt in developing a traffic flow model for mixed traffic.

In the continuum description of traffic flow, vehicular traffic is described as a special kind of fluid that are characterized by its concentration (density, ρ), mean velocity (v), and vehicle flux (flow rate q), all are functions of space (x) and time (t). The starting point of any continuum model of traffic flow is the conservation of vehicles

$$\frac{\partial}{\partial t} \int_{x_1}^{x_2} \rho(x, t) dx = q(x_1, t) - q(x_2, t), \quad (5.1)$$

and the relation between flow, density, and mean velocity $q = kv$.

Equation 5.1 is an integral form of traffic conservation. When the road segment $[x_1, x_2]$ shrinks to a point in space, one obtains the familiar differential form of traffic conservation:

$$\rho_t + q_x = 0, \text{ or } \rho_t + (\rho v)_x = 0. \quad (5.2)$$

If one introduces a relation between vehicle concentration and traffic speed $v = V(\rho)$, one obtains the classic kinematic wave model developed by Lighthill, Whitham

(Lighthill and Whitham, 1955b) and Richards (Richards, 1956):

$$\rho_t + (\rho V(\rho))_x = 0, \quad \rho V(\rho) \equiv Q(\rho). \quad (5.3)$$

The classic kinematic wave model of Lighthill and Whitham was formulated for homogeneous flows on a long crowded road. It does not consider the effects of performance differences among different types of vehicles. Recently, Daganzo extended the theory to treat a freeway system with two types of lanes, special lanes and regular lanes, and two types of vehicles, priority vehicles and regular vehicles (Daganzo, 1997; Daganzo et al., 1997; Daganzo, 2002). Priority vehicles are allowed to travel on either regular lanes or special lanes, whereas regular vehicles can only travel on the regular lane. The two types of vehicles in Daganzo's special lane model have different vehicle performances in free-flow traffic, but are indistinguishable in heavy traffic, where both types of vehicles travel at the same speed.

In this chapter, we extend the kinematic wave model to vehicular traffic with a mixture of vehicle types. In the mixed flow each vehicle type is conserved and travels at the group velocity, but the differences among vehicle types are accounted for in determining the states of the collective flow. This model can be used to study traffic evolution on long crowded highways where low performance vehicles entrap high performance ones. It can also give a more accurate description of the I-pipe state in Daganzo's special lane model.

The remaining parts of the chapter are organized as follows. In Section 5.2 we give the extended KW model and its basic properties. In Section 5.3 we analyze the Riemann problem for this model. In Section 5.4 we propose a fundamental diagram of mixed traffic and discuss its properties. In Section 5.5 we provide numerical examples and in Section 5.6 we conclude the chapter.

5.2 The extended KW model for mixed traffic

Let us assume that there are $i = 1, \dots, n$ types of vehicles in the traffic stream ($n \geq 2$), each type has concentration $\rho_i(x, t)$ and velocity $v_i(x, t)$. By conservation of each vehicle type, we have

$$(\rho_i)_t + (\rho_i v_i)_x = 0, \quad i = 1, \dots, n; \quad (5.4)$$

As in the development of the classic KW model, we postulate that equilibrium relations exist between vehicular speeds and traffic densities:

$$v_i = V_i(\rho_1, \dots, \rho_n), \quad (5.5)$$

with $v_i(0) = v_{fi}$, the free-flow speed of each vehicle type and $\partial_{\rho_j} V_i < 0$, $i = 1, \dots, n$; $j = 1, \dots, n$.

Equations 5.4 and 5.5 are the general governing equations of mixed traffic flow without special lanes. Note that if one adopts $v_i = V(\sum_{i=1}^n \rho_i)$, one recovers the I-pipe state in Daganzo's special lane model. In this chapter we study a special case of the general equations for mixed traffic in which we consider two types of vehicles—one represents passenger cars (ρ_1) and the other represents heavy vehicles such as trucks (ρ_2), and two traffic flow regimes—free-flow and congested traffic.

When traffic is light and there are adequate opportunities for passing, different classes of vehicles would travel at their own free-flow speeds v_{fi} . The traffic flow in this case can be described by

$$(\rho_i)_t + v_{fi}(\rho_i)_x = 0, \quad i = 1, 2; \quad (5.6)$$

By defining $\rho = \sum_{i=1}^n \rho_i$, and $v_f = \frac{\sum_{i=1}^n \rho_i v_{fi}}{\sum_{i=1}^n \rho_i}$, we can use

$$\rho_t + (\rho v_f)_x = 0, \quad (5.7)$$

to approximately model the average behavior of light traffic.

When traffic concentration reaches a critical value ρ_c , passing opportunities diminish and vehicles of lower performance (e.g. trucks) start to entrap vehicles of higher performance (e.g., passenger cars). Under such conditions it is assumed that the various classes of vehicles are completely mixed and move at the group velocity V . That is, mixed traffic flow in this regime is described by

$$(\rho_i)_t + (\rho_i V)_x = 0, \quad i = 1, 2. \quad (5.8)$$

Through the definition of a proper average free-flow speed and the selection of a suitable critical density, we combine Equation 5.6 (for free-flow traffic) and Equation 5.8 (for congested traffic) into one modeling equation:

$$\begin{pmatrix} \rho_1 \\ \rho_2 \end{pmatrix}_t + \begin{pmatrix} \rho_1 V(\rho_1, \rho_2) \\ \rho_2 V(\rho_1, \rho_2) \end{pmatrix}_x = 0, \quad (5.9)$$

where

$$V(\rho_1, \rho_2) = \begin{cases} \frac{\sum_{i=1}^2 \rho_i v_{fi}}{\sum_{i=1}^2 \rho_i}, & \gamma_1 \rho_1 + \gamma_2 \rho_2 < 1 \\ V_*(\rho_1, \rho_2), & \gamma_1 \rho_1 + \gamma_2 \rho_2 \geq 1 \end{cases}.$$

Here γ_1 and γ_2 are parameters that determine the critical density in (ρ_1, ρ_2) coordinates. V_* is a two-dimensional speed-density relation for congested traffic. It is understood that $\partial_{\rho_i} V_* < 0$, $i = 1, 2$.

Equation 5.9 is a system of conservation laws with characteristic velocities:

$$\lambda_1 = V + \rho_1 V_1 + \rho_2 V_2, \quad \lambda_2 = V(\rho_1, \rho_2).$$

Here we used a special notation for partial derivatives of V with respect to ρ_1 and ρ_2 : $\partial_{\rho_1} V \equiv V_1$ and $\partial_{\rho_2} V \equiv V_2$. Owing to the nature of $V(\rho_1, \rho_2)$, we have $\lambda_1 \leq \lambda_2 = V$, that is, both characteristics travel no faster than *average traffic*. In fact, the second characteristic travels at precisely the speed of traffic. When the free-flow speeds of

both types of vehicles are identical, the extended KW model preserves the anisotropic property of the KW model. Otherwise, the extended model is not anisotropic in light traffic (the nature of this violation of anisotropy is explained in detail in (Zhang)). Moreover, it can be shown that

$$\left(\frac{\rho_2}{\rho_1}\right)_t + V \left(\frac{\rho_2}{\rho_1}\right)_x = 0,$$

from which one obtains $\frac{d}{dt} \left(\frac{\rho_2}{\rho_1}\right) = 0$, that is, the level curves of $\left(\frac{\rho_2}{\rho_1}\right)$ in the $t - x$ plane coincide with vehicle trajectories. The separation of $\left(\frac{\rho_2}{\rho_1}\right)$ level curves therefore implies first-in-first-out traffic flow behavior between vehicle classes.

Furthermore, the corresponding eigenvectors of the flow Jacobian matrix are

$$r_1 = \begin{pmatrix} \frac{\rho_1}{\rho_2} \\ 1 \end{pmatrix}, \quad r_2 = \begin{pmatrix} -\frac{V_2}{V_1} \\ 1 \end{pmatrix}$$

and the Riemann invariants (w, z) , defined as $\nabla w \bullet r_1 = 0$, $\nabla z \bullet r_2 = 0$, are

$$w = \frac{\rho_2}{\rho_1}, \quad z = V.$$

They are used here to obtain the expansion wave solutions of a Riemann problem (see next section. For more details on Riemann problems and Riemann invariants, refer to (Whitham, 1974)).

It can be shown that the first characteristic field is nonlinear and the second characteristic field is linearly degenerate. We therefore have both shock and smooth expansion waves in the first field and contact waves (or slips) in the second field. We shall derive the expressions for these waves related to Riemann data in the next section.

5.3 The Riemann problem and basic wave solutions

In this section we discuss the solutions of the extended KW model, Equation 5.9, with the following so-called Riemann data:

$$\rho(x, 0) = \begin{cases} \rho^l, & x < 0 \\ \rho^r, & x > 0 \end{cases} \quad \rho = \begin{pmatrix} \rho_1 \\ \rho_2 \end{pmatrix} \quad (5.10)$$

To solve the above Riemann problem, we first study the right (downstream) states that can be connected to the left (upstream) states by an elementary wave, i.e., a smooth expansion (rarefaction) wave, a contact, or a shock (readers are referred to (LeVeque, 2002) and Aw and Rascle (2000); Zhang (2000, 2002, 2001b) for a more detailed discussion of Riemann problems related to systems of conservation laws in general and traffic flow in particular). Throughout the remaining sections, we assume that $v_{f1} = v_{f2} = v_f$. This assumption ensures that our proposed $V(\rho_1, \rho_2)$ function is continuous over the entire feasible (ρ_1, ρ_2) region. The Riemann problem of Equation 5.9 with discontinuous $V(\rho_1, \rho_2)$ is more involved and will be discussed elsewhere. Nevertheless, the analysis of the model, Equation 5.9, with $v_{f1} = v_{f2} = v_f$ still reveals many key features of mixed traffic flow.

The 1-expansion waves: An upstream state ρ^l can be connected to a downstream state ρ^r by a 1-expansion wave if and only if the downstream state satisfies

$$w(\rho^l) = w(\rho^r), \quad \rho^l > \rho^r,$$

i.e.,

$$\frac{\rho_2^l}{\rho_1^l} = \frac{\rho_2^r}{\rho_1^r}. \quad (5.11)$$

This means that in the ρ -plane the two states are on a ray from the origin. Clearly

across an expansion wave traffic composition does not change, that is, vehicles observe the first-in-first-out rule.

The contact waves:

A contact wave is a slip that separates two traffic regions of different traffic densities and vehicle compositions but the same travel speed. That is,

$$V(\rho^l) = V(\rho^r). \quad (5.12)$$

In the ρ -plane, all states on a level curve of $V(\rho)$ are connected by a contact wave.

The shock waves:

The shock waves in the extended KW model are given by the jump condition:

$$s(\rho_1^l - \rho_1^r) = \rho_1^l V(\rho_1^l, \rho_2^l) - \rho_1^r V(\rho_1^r, \rho_2^r) \quad (5.13)$$

$$s(\rho_2^l - \rho_2^r) = \rho_2^l V(\rho_1^l, \rho_2^l) - \rho_2^r V(\rho_1^r, \rho_2^r) \quad (5.14)$$

After elimination of s from the equations and some algebraic manipulations one obtains

$$(\rho_1^l \rho_2^r - \rho_1^r \rho_2^l)(V(\rho_1^l, \rho_2^l) - V(\rho_1^r, \rho_2^r)) = 0.$$

Two possibilities exist: $V(\rho_1^l, \rho_2^l) - V(\rho_1^r, \rho_2^r) = 0$ which gives the contact waves that we have already discussed, or

$$\rho_1^l \rho_2^r - \rho_1^r \rho_2^l = 0, \quad (5.15)$$

this gives the downstream states ρ^r that can be connected to the upstream state ρ^l by a shock. Note that all these states also fall on a ray originating from the origin of the ρ -plane. This implies that across a shock vehicle composition also does not change, that is, vehicles observe first-in-first-out rule. Moreover, we have the following entropy conditions

$$\rho^l < \rho^r.$$

to ensure the stability of the shock.

Now we can state the procedure to solve a Riemann problem for the extended KW model. Note that for any state ρ^l , the two curves/lines given by Equations 5.11 and 5.12 divide the feasible ρ -plane into four regions (Figure 5.1). If the downstream state ρ^r falls on any of these two curves/lines, it can be connected to the upstream state by an elementary wave. If it falls on any of the four regions, however, an intermediate state ρ^m is generated on the line given by Equation 5.11, which is connected with the upstream state by a 1-wave (i.e., an expansion or shock wave) and with the downstream state by a contact (Figure 5.1. Figure 5.2 shows a few examples of Riemann solutions.

5.4 Fundamental diagrams for mixed traffic

We propose the following $\rho - V$ relation, which can be derived from a car-following model under steady-state conditions (Zhang and Kim, 2000), to be used in the mixed traffic flow model.

$$V = \begin{cases} \frac{\rho_1 v_{f1} + \rho_2 v_{f2}}{\rho_1 + \rho_2}, & (l_1 + \tau_1 v_{f1})\rho_1 + (l_2 + \tau_2 v_{f2})\rho_2 < 1 \\ \frac{1 - \rho_1 l_1 - \rho_2 l_2}{\rho_1 \tau_1 + \rho_2 \tau_2}, & (l_1 + \tau_1 v_{f1})\rho_1 + (l_2 + \tau_2 v_{f2})\rho_2 \geq 1 \end{cases}$$

This fundamental diagram is shown in Figure 5.3.

We call the above relation the extended speed-density relation for the triangular fundamental diagram. The parameters are: free flow speeds for both types of vehicles v_{f1} and v_{f2} , effective vehicle lengths for type-1 and type-2 vehicles l_1 and l_2 , and response times of type-1 and type-2 vehicles τ_1 and τ_2 . The last two parameters capture, to a certain degree, the acceleration/deceleration differences between the two classes of vehicles.

The capacity of mixed flow depends on vehicle composition. For example, in the

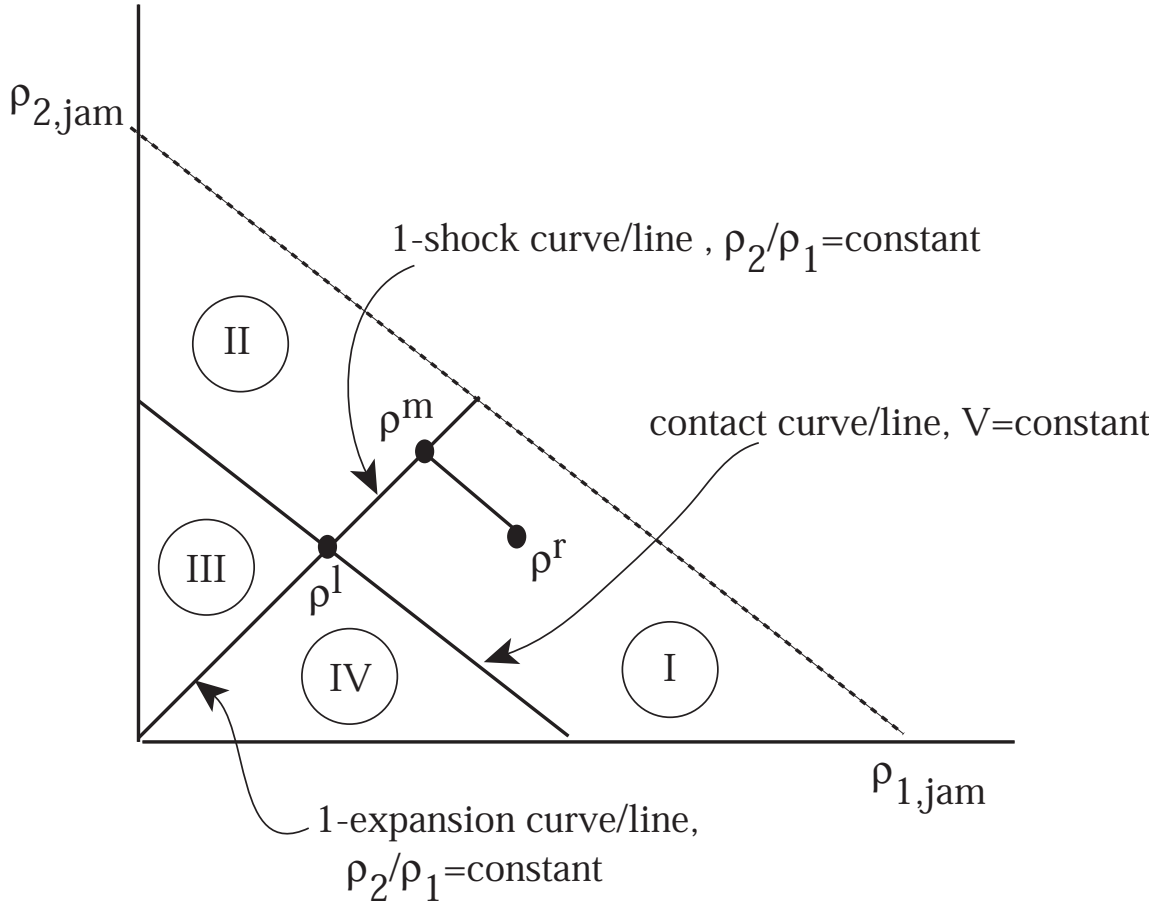


Figure 5.1: Phase diagram for determining elementary and simple waves

case of $v_{f1} = v_{f2} = v_f$, let $\frac{\rho_2}{\rho_1} = p < \infty$, then the critical densities of the proposed speed-density relation are

$$\rho_{1c} = \frac{1}{(l_1 + pl_2) + v_f(\tau_1 + p\tau_2)}, \quad \rho_{2c} = p\rho_{1c}$$

Note that when $p = 0$, i.e., there are no type-2 vehicles in the traffic stream, we recover the critical density for type-1 vehicles

$$\rho_{1c} = \frac{1}{l_1 + v_f\tau_1}$$

and when $p = \infty$, i.e., no type-1 vehicles present in the traffic stream, we can switch

the positions of p in relation to l 's and τ 's in the above formulas and replace it with $\frac{1}{p} = 0$. Again we recover the critical density for type-2 vehicles

$$\rho_{2c} = \frac{1}{l_2 + v_f \tau_2}$$

For any vehicle mixture (i.e. $0 < p < \infty$), the capacity flow is $\left(\frac{v_f}{l_2 + v_f \tau_2}, \frac{v_f}{l_1 + v_f \tau_1}\right)$.

5.5 Numerical solution method and simulations

5.5.1 The Godunov method

We approximate the mixed traffic KW model with the Godunov method (Godunov, 1959):

$$\begin{aligned} \frac{\rho_{1,i}^{j+1} - \rho_{1,i}^j}{\Delta t} + \frac{\rho_{1,i+1/2}^{*j} V(\rho_{1,i+1/2}^{*j}, \rho_{2,i+1/2}^{*j}) - \rho_{1,i-1/2}^{*j} V(\rho_{1,i-1/2}^{*j}, \rho_{2,i-1/2}^{*j})}{\Delta x} &= 0, \\ \frac{\rho_{2,i}^{j+1} - \rho_{2,i}^j}{\Delta t} + \frac{\rho_{2,i+1/2}^{*j} V(\rho_{1,i+1/2}^{*j}, \rho_{2,i+1/2}^{*j}) - \rho_{2,i-1/2}^{*j} V(\rho_{1,i-1/2}^{*j}, \rho_{2,i-1/2}^{*j})}{\Delta x} &= 0, \end{aligned}$$

in which $\rho_{k,i}^j$ is the average of ρ_k over cell i at time t_j ; i.e., $\rho_{k,i}^j = \int_{x=x_{i-1/2}}^{x_{i+1/2}} \rho_k(x, t_j) dx / \Delta x$, and $\rho_{k,i-1/2}^{*j}$ is the average over time interval $[t_j, t_{j+1}]$ at the boundary $x_{i-1/2}$ between cells i and $i-1$; i.e., $\rho_{k,i-1/2}^{*j} = \int_{t=t_j}^{t_{j+1}} \rho_k(x_{i-1/2}, t) dt / \Delta t$. Given (ρ_1, ρ_2) at t_j , we hence can compute traffic states at the following time t_{j+1} .

In the above equations, the boundary average $\rho_{k,i-1/2}^{*j}$ can be found by solving the Riemann problem for the extended KW model, Equation 5.9, with the following initial condition $(\rho^l = (\rho_{1,i-1}^j, \rho_{2,i-1}^j))$ and $\rho^r = (\rho_{1,i}^j, \rho_{2,i}^j)$

$$\rho = \begin{cases} \rho^l, & \text{if } x - x_{i-1/2} < 0, \\ \rho^r, & \text{if } x - x_{i-1/2} \geq 0. \end{cases}$$

As shown in section 2, the Riemann solutions consist of a shock or rarefaction wave with an intermediate state ρ^m and a contact wave. Since all the waves are self-similar,

	s given in Equation 5.18	$\rho_{1,i-1/2}^{*j}$	$\rho_{2,i-1/2}^{*j}$
Shock	$s > 0$	ρ_1^l	ρ_2^l
	$s \leq 0$	ρ_1^m	ρ_2^m

Table 5.1: Shock wave solutions in mixed traffic

we have $\rho_{i-1/2}^{*j} = \rho(x_{i-1/2}, t) = \text{const}$ for all $t > 0$, which is determined by the shock or rarefaction wave connecting ρ^l and ρ^m since the contact wave has non-negative velocity and is not involved.

From Equations 5.11 and 5.15, we have

$$\frac{\rho_2^l}{\rho_1^l} = \frac{\rho_2^m}{\rho_1^m}, \quad (5.16)$$

and from Equation 5.12

$$V(\rho^m) = V(\rho^r). \quad (5.17)$$

Combining Equations 5.16 and 5.17, we can find the intermediate state ρ^m , from which we can compute $\rho_{i-1/2}^{*j}$ as described in the following cases.

Case 1 When $\rho^l < \rho^m$, they are connected by a shock, and the shock speed is

$$s = \frac{\rho_1^l V(\rho_1^l, \rho_2^l) - \rho_1^m V(\rho_1^m, \rho_2^m)}{\rho_1^l - \rho_1^m}. \quad (5.18)$$

In this case, solutions of $\rho_{i-1/2}^{*j}$ are summarized in the Table 5.1.

Case 2 When $\rho^l > \rho^m$, they are connected by a rarefaction wave, in which the characteristic velocity is $\lambda_1(\rho_1, \rho_2)$, and $\lambda_1(\rho^l) < \lambda_1(\rho^m)$. If $\lambda_1(\rho^l) \geq 0$, $\rho_{i-1/2}^{*j}$ is the same as the left state ρ^l ; if $\lambda_1(\rho^m) \leq 0$, it is the same as the intermediate state ρ^m . Otherwise, $\rho_{i-1/2}^{*j}$ satisfies

$$\begin{aligned} \lambda_1(\rho_{1,i-1/2}^{*j}, \rho_{2,i-1/2}^{*j}) &= 0, \\ \rho_{2,i-1/2}^{*j} / \rho_{1,i-1/2}^{*j} &= \rho_2^l / \rho_1^l, \end{aligned} \quad (5.19)$$

Rarefaction	λ_1	$\rho_{1,i-1/2}^{*j}$	$\rho_{2,i-1/2}^{*j}$
	$\lambda_1(\rho^l) \geq 0$	ρ_1^l	ρ_2^l
	$\lambda_1(\rho^m) \leq 0$	ρ_1^m	ρ_2^m
	o.w.	given in Equation 5.19	

Table 5.2: Rarefaction wave solutions in mixed traffic

which implies that $\rho_{i-1/2}^{*j}$ maximizes the total flow $(\rho_1 + \rho_2)V(\rho_1, \rho_2)$ along the line $\rho_2/\rho_1 = \rho_2^l/\rho_1^l$.

In this case, therefore, solutions of $\rho_{i-1/2}^{*j}$ are summarized in Table 5.2.

5.5.2 Numerical simulations

In our simulations, we will use the extended triangular fundamental diagram (Figure 5.3), in which the parameter values are: free flow speed for both types of vehicles $v_{f1} = v_{f2} = v_f = 65 \text{ mph} = 95.3333 \text{ ft/sec}$, effective vehicle lengths for type-1 and type-2 vehicles: $l_1 = 20 \text{ ft}$, $l_2 = 40 \text{ ft}$, and response times of type-1 and type-2 vehicles: $\tau_1 = 1.5 \text{ s}$, $\tau_2 = 3 \text{ s}$. Therefore, we have $\rho_{1,jam} = 1/l_1 = 0.05 \text{ veh/ft}$ and $\rho_{2,jam} = 1/l_2 = 0.025 \text{ veh/ft}$. Moreover, since $l_1/l_2 = \tau_1/\tau_2$, we have that in the extended triangular fundamental diagram $V(\rho_1, \rho_2)$ is a function of $\rho_1/\rho_{1,jam} + \rho_2/\rho_{2,jam}$. Thus, as we will see later, the evolution pattern of travel speed is the same as that of $\rho_1/\rho_{1,jam} + \rho_2/\rho_{2,jam}$.

We will conduct numerical simulations for a ring road, whose length $L = 2000l_1=40,000$ ft, during a time interval from $t = 0$ to $T = 100\tau_1=150$ s. In order to apply the Godunov method, we partition the ring road into $N = 1000$ cells with length $\Delta x = L/N=40$ ft, and discretize the time interval to $M = N/2$ steps with the duration of each time step $\Delta t = T/M=0.3$ s. Since the CFL condition number

(Courant et al., 1928)

$$\max\{|\lambda_1|, |\lambda_2|\} \frac{\Delta t}{\Delta x} \leq v_f \frac{\Delta t}{\Delta x} = 0.715 < 1,$$

the Godunov method yields convergent solutions.

For the numerical simulations, we use the following global perturbation as initial traffic conditions,

$$\begin{aligned} \rho_1(x, 0) &= (0.2 + 0.16 \sin(2\pi x/L))\rho_{1,jam}, \\ \rho_2(x, 0) &= (0.15 + 0.1 \sin(2\pi x/L))\rho_{2,jam}, \end{aligned} \tag{5.20}$$

in which the density of the 1-type vehicles, i.e., has higher average but smaller oscillation.

With these conditions, the solutions of the mixed traffic flow model are depicted as contour plots and shown in Figure 5.4. The horizontal axis in each of the sub figures represents space and the vertical axis time. These figures depict the traffic conditions (speed and density). As shown in the contour plots of v and $\rho_1/\rho_{1,jam} + \rho_2/\rho_{2,jam}$, there are roughly two traffic regions along the ring road initially. In one region $(l_1 + \tau_1 v_f)\rho_1 + (l_2 + \tau_2 v_f)\rho_2 \geq 1$, waves initiated from this region travel backward in the same speed, which is $\lambda_1(\rho_1, \rho_2) = -(\rho_1 l_1 + \rho_2 l_2)/(\rho_1 \tau_1 + \rho_2 \tau_2) = -l_1/\tau_1 = -40/3$ ft/sec. In another region, $(l_1 + \tau_1 v_f)\rho_1 + (l_2 + \tau_2 v_f)\rho_2 < 1$, waves initiated from this region travel forward at free-flow speed. Two waves separate the two regions: an expansion wave on the left and a shock wave on the right. The shock wave travels forward initially but eventually travel at $-l_1/\tau_1$ as traffic density increases to critical density in the second (free-flow) region. The patterns of the solutions of ρ_1 and ρ_2 , however, are not the same as that of v because the change of the overall traffic conditions affect each vehicle class differently.

The contour plot of ρ_2/ρ_1 is given in Figure 5.5, from which we can see that the level curves do not intersect. Remembering that the level curves of ρ_2/ρ_1 coincide with

vehicle trajectories, the solutions shown here indicate that under the given conditions first-in-first-out rule is respected by the mixed flow model. From this figure we can also see the expansion and shock waves as they move through traffic, which are marked by changes in the slopes of the level curves.

5.6 Concluding remarks

In this chapter we extend the Lighthill-Whitham-Richards kinematic wave traffic flow model to describe traffic with different types of vehicles, where all types of vehicles are completely mixed and travel at the same group velocity. A study of such a model with two vehicle classes (e.g., passenger cars and trucks) shows that, when both classes of traffic have identical free-flow speeds, the model 1) satisfies first-in-first-out rule, 2) is anisotropic, and 3) has the usual shock and expansion waves, and a family of contact waves. Different compositions of vehicle classes in this model propagate along contact waves. Such models can be used to study traffic evolution on long crowded highways where low performance vehicles entrap high performance ones.

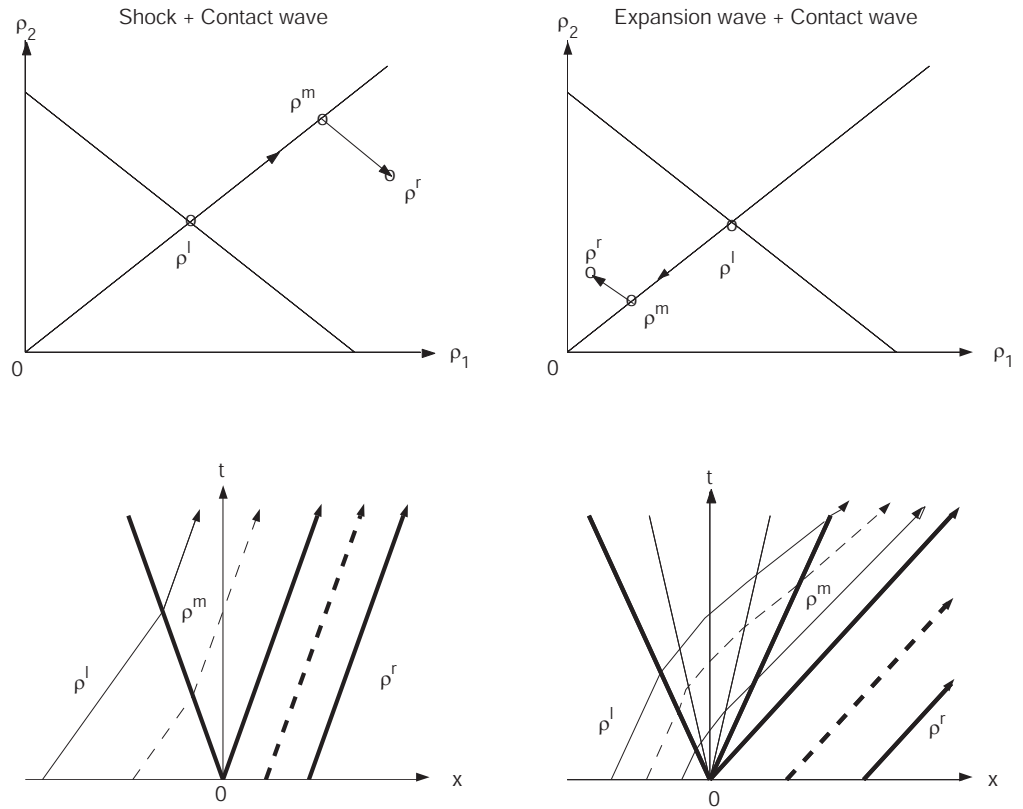


Figure 5.2: Wave solutions to the Riemann problem: Shock + Contact wave (left) and Expansion wave + Contact wave (right) (In the bottom figures, thick (dashed) lines are characteristics, and lines with arrows are vehicles' trajectories.)

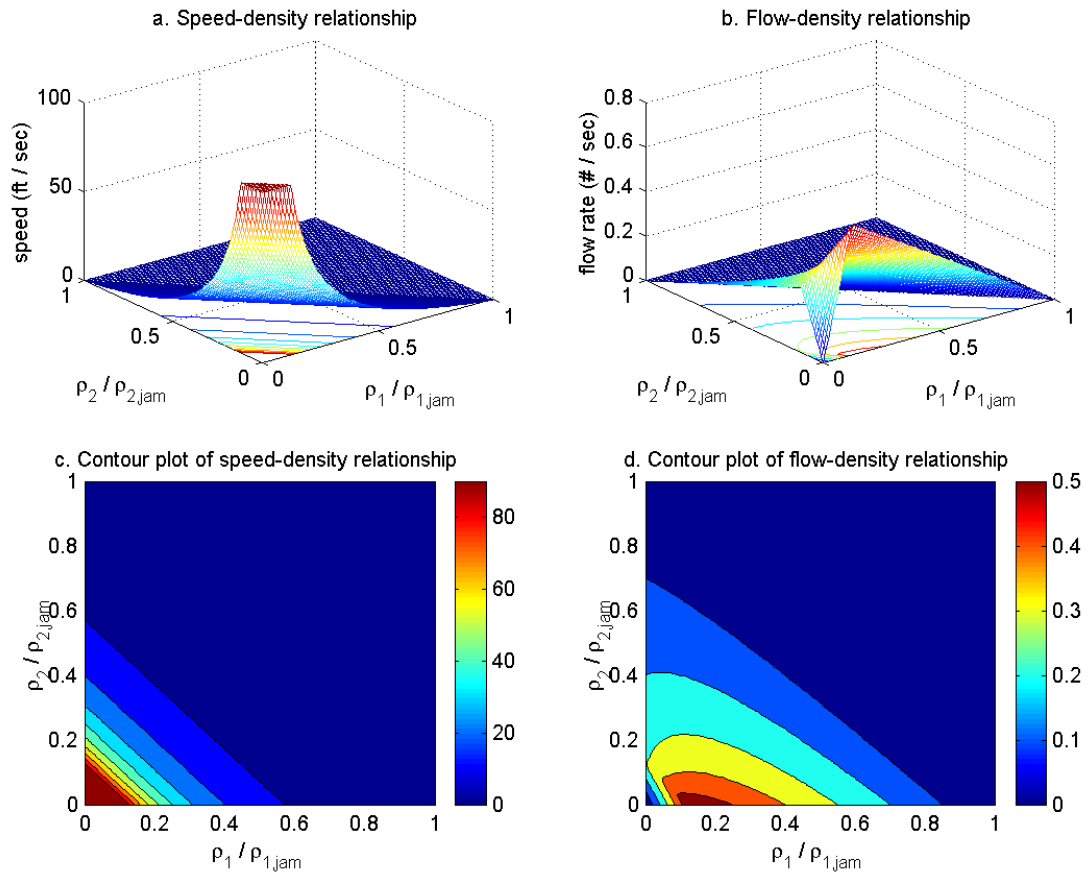


Figure 5.3: The extended triangular fundamental diagram

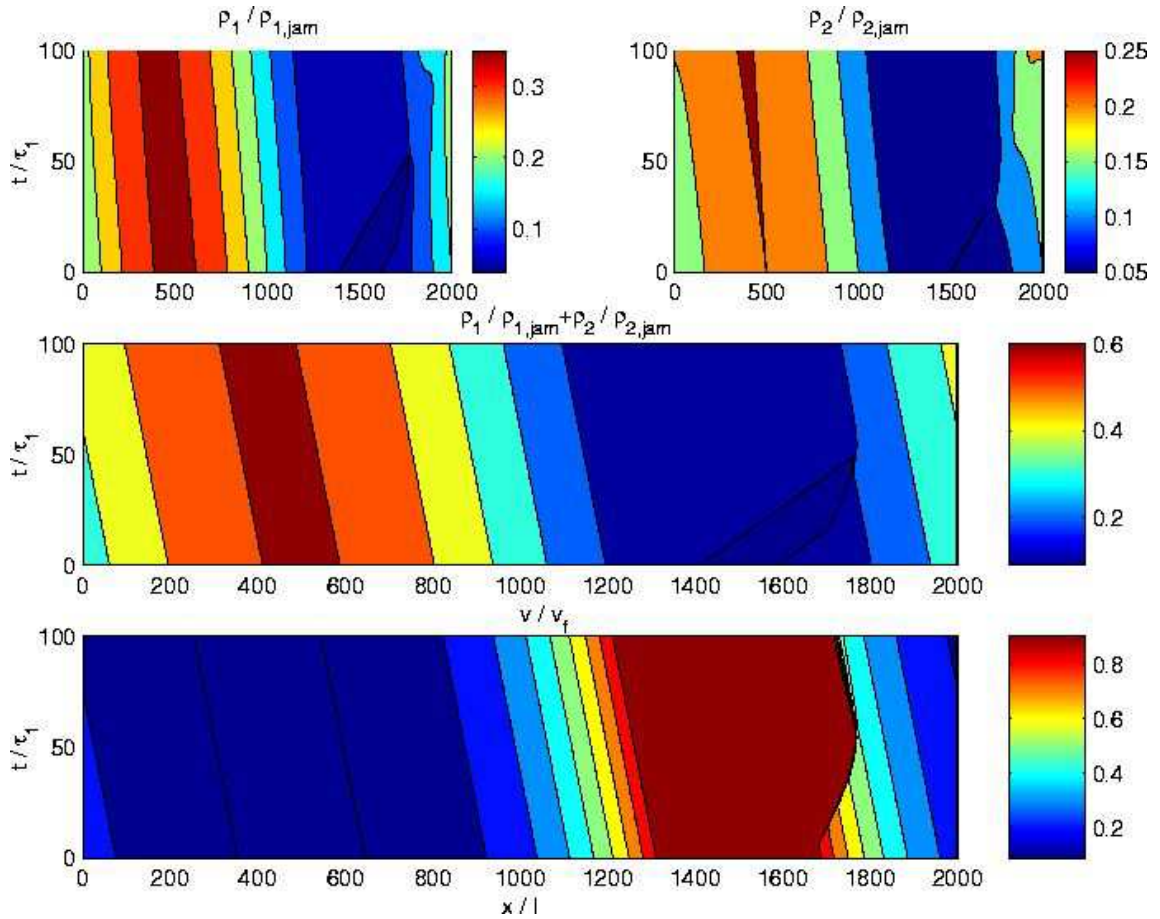


Figure 5.4: Contour plots of solutions on the $x - t$ space with the extended triangular fundamental diagram

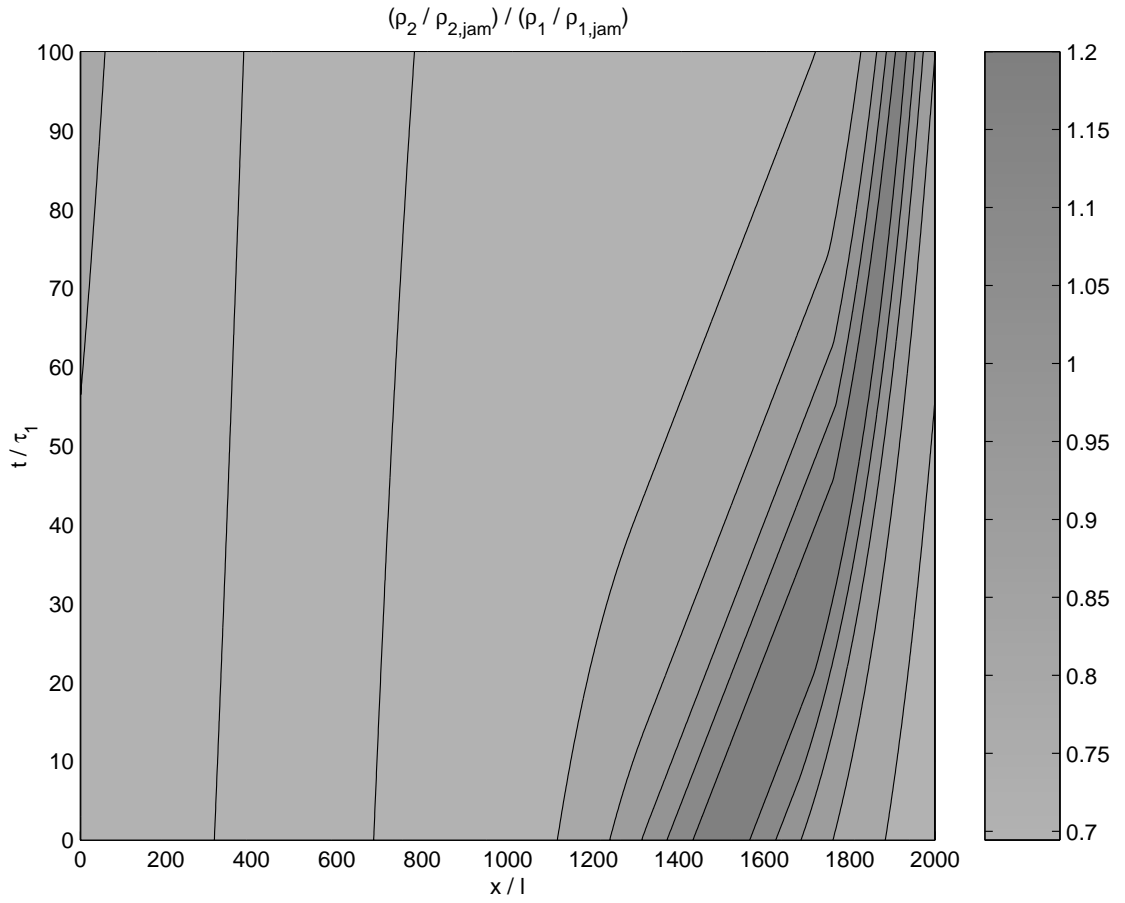


Figure 5.5: Contour plot of ρ_2/ρ_1 on the $x - t$ space with the extended triangular fundamental diagram

Chapter 6

Kinematic wave simulation model for multi-commodity network traffic flow

6.1 Introduction

Recurrent or non-recurrent traffic congestion in many major metropolitan areas have seriously deteriorated the mobility, convenience, and productivity of highway transportation. To tackle the congestion problem, traffic engineers and scientists are facing a number of challenges, including: 1) the evaluation of the performance of a road network (e.g. total travel time or the level of service (LOS)), 2) the prediction of occurrence of incidents, 3) the development of traffic control schemes (e.g. ramp metering) and management strategies (e.g. traffic guidance) in Advanced Transportation Management and Information Systems (ATMIS) or other Intelligent Transportation Systems (ITS), and 4) the estimation of traffic demand associated with a given origin/destination (i.e. O/D information). As we all know, a fundamental and essential

issue in addressing all these challenges is the understanding of traffic dynamics on a road network, i.e., the evolution of traffic on a road network under initial and boundary conditions, for which traffic flow models of road networks play an important role.

Among many traffic flow models, the kinematic wave models are advantageous in studying traffic dynamics in a large-scale road network, due to their inherent compliance with ITS applications, theoretical rigor, and computational efficiency. Practically, people are more interested in aggregate-level traffic conditions such as average travel speeds, densities, flow-rates, and travel times, which are directly concerned or can be easily derived in the kinematic wave models. Theoretically, the evolution of traffic conditions on a link can be studied as hyperbolic conservation laws, given the fundamental diagram, which defines a functional relationship between density and flow-rate or travel speed, and traffic conservation, which means that the change of the number of vehicles in a section in a time interval equals to the number of vehicles entering the section minus the number of vehicles leaving it. Computationally, the kinematic wave models can be solved with the Godunov method, in which influx and out-flux of a cell can be computed through kinematic wave solutions or the supply-demand method (Daganzo, 1995a; Lebacque, 1996).

In literature, the following approaches can be considered as typical when modeling network traffic flow in the framework of kinematic wave theory. First, Vaughan et al. (1984) studied network traffic flow with two continuous equations: a “local equation”, which ensures traffic conservation and is consistent with the traditional LWR model on a link at the aggregate level, and a “history equation”, which computes the trajectory of each vehicle at the disaggregate level. Since the trajectories of all vehicles are not always required for many applications, this model tends to waste significant amount of computational resources. Second, Jayakrishnan (1991) introduced a discrete network flow model, in which each link is partitioned into a number of cells, vehicles adjacent

to each other and with the same O/D and path are called a “macroparticle”, and the position of a macroparticle at each time step is determined by its travel speed and the cell’s length. However, with the given mechanism, this model may not be consistent with the LWR model since traffic conservation can be violated. Third, Daganzo (1995a) introduced a network flow model based on his Cell Transmission Model (Daganzo, 1994), which is a numerical approximation of the LWR model with a special fundamental diagram — a triangle. In this discrete model, macroparticles in the sense of Jayakrishnan (1991) in a cell are ordered according to their waiting times and moved to the downstream cell when their waiting times are greater than a threshold minimum waiting time, which is computed from traffic flow at the aggregate level. However, the determination of the threshold minimum waiting time is quite tedious. Fourth, in the KWave98 simulation package (Lenonard II, 1998), which is based on the simplified kinematic wave theory by Newell (1993), vehicles on a link are considered to be ordered as a queue. Then, with the in-queue and out-queue of the link determined, one can easily update the link queue. However, in-queues and out-queues at typical highway junctions such as merges and diverges create difficulties for this model.

In many applications, such as dynamic traffic assignment (DTA), First-In-First-Out (FIFO) principle is a key concern. Consequently, all the aforementioned models order vehicles but in different fashions. Vehicles are ordered according to their trajectories in (Vaughan et al., 1984), locations in (Jayakrishnan, 1991), waiting times in (Daganzo, 1995a), and positions in a link queue in (Lenonard II, 1998). That is, these simulation models track either vehicles’ trajectories, or positions, or waiting times, or queue orders.¹ In these models, therefore, traffic conditions are also considered

¹In (Jayakrishnan, 1991), although the introduction of macroparticles save a certain amount of memory in computation, this saving is diminished when vehicles of different classes are evenly mixed.

at the vehicle level. As a result, the computational efficiency of the kinematic wave models is not fully utilized.

In order to fully explore the computational efficiency inherited in the kinematic wave theory, we propose a new network traffic flow simulation model, in which traffic dynamics are studied at the aggregate level with commodity specified densities and flow-rates. Traffic of a commodity has the same characteristics, which can be vehicle type, destination, path, or any classification criterion. We hereafter refer to this model as multi-commodity kinematic wave (MCKW) simulation model. In this dissertation research, we start with a simple traffic system, where vehicles are categorized into multiple commodities according to their paths and no differentiations are made in vehicle types, driver classes, or lane types, such as high-occupancy-vehicles (HOV's) or HOV lanes. In the MCKW simulation platform, besides link characteristics such as free flow speed, capacity, and number of lanes, traffic dynamics are highly related to geometrical characteristics of a road network including link inhomogeneities, merges, diverges, and other junctions. Although it does not give a complete, detailed picture of traffic dynamics, this model is still of importance for many applications, in which the difference in vehicles, drivers, or lanes are negligible not interested or can be averaged out without major loss of accuracy.

In the MCKW simulation platform, the Godunov-type approximation is applied, and fluxes through boundaries inside a link and junctions such as merges and diverges are computed systematically in the framework of the supply-demand method. In addition, since vehicles are categorized by vehicles' origins, destinations, and paths, traffic dynamics are also differentiated for different commodities in the MCKW simulation platform. We will show that FIFO is observed in the commodity specific kinematic wave theory.

In the rest of this chapter, we will discuss theories underlying the MCKW model

in Section 6.2, and the data, network, and program structures in the MCKW model in Section 6.3. In Section 6.4, we will discuss the process of output from the MCKW model to obtain interested data of a road network, such as travel times. In Section 6.5, we carry out some numerical simulations of a simple road network. In Section 6.6, we will draw some conclusions and provide further discussions about the calibration of the MCKW model.

6.2 Underlying theories of the MCKW simulation model

In the multi-commodity kinematic wave (MCKW) simulation of network traffic flow, dynamics of total traffic, i.e., the evolution of traffic conditions of all commodities, are studied at the aggregate level and governed by the kinematic wave theories. These theories have been studied in the previous chapters for fundamental network components such as inhomogeneous links, merges, and diverges. They provide the underlying algorithms and building blocks for the MCKW simulation platform. At the disaggregate level, traffic of each commodity in the form of proportions is studied with its proportion, and First-In-First-Out property on a link will be discussed.

6.2.1 Kinematic wave theories at the aggregate level

In the MCKW model, we use the discrete form of the kinematic wave theories, which can be obtained through the first-order² Godunov method (Godunov, 1959) of the continuous versions. In the discrete form, each link is partitioned into N cells, of equal length or not, and the time interval is discretized into K time steps. Then, we

²A second-order method was discussed in (Daganzo, 1999a).

obtain the Godunov-type finite difference equation for total flow in cell i from time step j to time step $j + 1$ as follows:

$$\frac{\rho_i^{j+1} - \rho_i^j}{\Delta t} + \frac{f_{i-1/2}^{j*} - f_{i+1/2}^{j*}}{\Delta x} = 0, \quad (6.1)$$

where Δx is the length of cell i , Δt is the time from time step j to time step $j + 1$, and the choice of $\frac{\Delta t}{\Delta x}$ is governed by the CFL (Courant et al., 1928) condition. In Equation 6.1, ρ_i^j is the average of traffic density ρ in cell i at time step j , similarly ρ_i^{j+1} is the average of ρ at time step $j + 1$; $f_{i-1/2}^{j*}$ is the flux through the upstream boundary of cell i from time step j to time step $j + 1$, and similarly $f_{i+1/2}^{j*}$ is the downstream boundary flux. Given traffic conditions at time step j , we can calculate the traffic density in cell i at time step $j + 1$ as

$$\rho_i^{j+1} = \rho_i^j + \frac{\Delta x}{\Delta t} (f_{i-1/2}^{j*} - f_{i+1/2}^{j*}). \quad (6.2)$$

Defining $\mathbf{N}_i^j = \rho_i^j \Delta x$ as the number of vehicles in cell i at time step j , $\mathbf{N}_i^{j+1} = \rho_i^{j+1} \Delta x$ as the number of vehicles at time step $j + 1$, $F_{i-1/2}^j = f(\rho_{i-1/2}^{j*}) \Delta t$ as the number of vehicles flowing into cell i from time step j to $j + 1$, and $F_{i+1/2}^j$ as the number of vehicles flowing out of cell i , Equation 6.2 can be written as:

$$\mathbf{N}_i^{j+1} = \mathbf{N}_i^j + F_{i-1/2}^j - F_{i+1/2}^j, \quad (6.3)$$

which is in the form of traffic conservation.

Given the initial and boundary conditions, we will use the supply-demand method (Daganzo, 1995a; Lebacque, 1996) for computing fluxes through cell boundaries: $F_{i-1/2}^j$ or $f_{i-1/2}^{j*}$. In a general road network, there are the following types of boundaries: boundaries inside a link, merges, diverges, and more complicated intersections.

1. When the boundary at $x_{i-1/2}$ is a boundary inside a link, whose upstream cell is denoted as u and downstream cell d , we follow the supply-demand method

discussed in (Daganzo, 1995a; Lebacque, 1996; Jin and Zhang, 2003b). I.e., if we define the upstream demand as

$$D_u = \begin{cases} Q(U_u), & \text{when } U_u \text{ is under-critical} \\ Q_u^{max}, & \text{when } U_u \text{ is over-critical} \end{cases} \quad (6.4)$$

and define the downstream supply as

$$S_d = \begin{cases} Q_d^{max}, & \text{when } U_d \text{ is under-critical} \\ Q(U_d), & \text{when } U_d \text{ is over-critical} \end{cases} \quad (6.5)$$

then the boundary flux can be simply computed as

$$f_{i-1/2}^{j*} = \min\{D_u, S_d\}, \quad (6.6)$$

where U_d and U_u are traffic conditions including density ρ and road inhomogeneity a at j th time step, of the downstream and upstream cells, respectively. As discussed in (Jin and Zhang, 2003b), this method is consistent with analytical solutions of the Riemann problem for inhomogeneous roadway.

2. When $x_{i-1/2}$ is a merging junction with P upstream merging cells, which are denoted as u_p ($p = 1, \dots, P$), and a downstream cell d . The demand of upstream cell u_p , D_p , is defined in Equation 6.4, and the supply of the downstream cell, S_d , is defined in Equation 6.5. Then, we apply the simplest distribution scheme (Jin and Zhang, 2003c) and compute the boundary fluxes as

$$\begin{aligned} f_{i-1/2,d}^{j*} &= \min\{\sum_{p=1}^P D_p, S_d\}, \\ f_{i-1/2,u_p}^{j*} &= q \frac{D_p}{\sum_{p=1}^P D_p}, \quad p = 1, \dots, P, \end{aligned} \quad (6.7)$$

where $f_{i-1/2,d}^{j*}$ is the in-flow of the downstream cell, and $f_{i-1/2,u_p}^{j*}$ is the out-flow of upstream cell u_p .

In addition, if an upstream cell, e.g. u_p , is signalized and denote r as the proportion of green light in a cycle (i.e. green ratio), then we can apply the

controlled traffic demand of u_p , $\min\{rQ_p^{max}, D_p\}$, in the supply-demand method above (Daganzo, 1995a; Jin and Zhang, 2003c). Note that r can be a continuous function when considering the average effect or a piece-wise constant function when the simulation interval Δt is smaller than a signal cycle.

3. When $x_{i-1/2}$ is a diverging junction with P downstream cells, which are denoted as d_p ($p = 1, \dots, P$), and an upstream cell u . In the model proposed in (Jin and Zhang, 2002), we introduced a new definition of partial traffic demand of vehicles traveling to D_p in cell u as follows,

$$D_p = \begin{cases} Q(\rho_p; \hat{\rho}_p) & \rho_p \text{ is UC} \\ Q^{\max}(\hat{\rho}_p) & \text{otherwise} \end{cases}, \quad (6.8)$$

where $\hat{\rho}_p$ is equal to the density of vehicles not traveling to d_p , and at critical density $Q(\rho; \hat{\rho}_p)$ reaches its maximum. The traffic supply for d_p , S_p , is defined by Equation 6.5. Then, the boundary flux to d_p , $f_{i-1/2,d_p}^{j*}$, can be computed by

$$f_{i-1/2,d_p}^{j*} = \min\{S_p, D_p\}, \quad (6.9)$$

and the out-flow of u , $f_{i-1/2,u}^{j*}$, is the sum of these flows,

$$f_{i-1/2,u}^{j*} = \sum_{p=1}^P f_{i-1/2,d_p}^{j*}. \quad (6.10)$$

Another model of traffic diverging to D downstream links we will implement in the MCKW simulation was proposed in (Daganzo, 1995a; Lebacque, 1996):

$$\begin{aligned} f_{i-1/2,u}^{j*} &= \min_{d=1}^D \{D_u, S_d/\xi_d\}, \\ f_{i-1/2,d}^{j*} &= \xi_d f_{i-1/2,u}^{j*}, \quad d = 1, \dots, D, \end{aligned} \quad (6.11)$$

where ξ_d is the proportion of commodity d in total traffic, and here D_u is the demand of the upstream cell as defined in Equation 6.4.

When vehicles have no predefined route choice and can choose every downstream link at a diverge, we use the model proposed in (Jin and Zhang, 2003c):

$$\begin{aligned} f_{i-1/2,u}^{j*} &= \min\{D_u, \sum_{d=1}^D S_d\}, \\ f_{i-1/2,d}^{j*} &= \frac{S_d}{\sum_{d=1}^D S_d} f_{i-1/2,u}^{j*}, \quad d = 1, \dots, D. \end{aligned} \quad (6.12)$$

4. For intersections with two or more upstream and downstream links, we can combine the merge and diverge models together. Note that only the computation of demands and supplies may change, and the supply-demand method is still the same.

For example, when we combine the supply-demand methods in Equation 6.7 and Equation 6.11 for an intersection with U upstream branches and D downstream branches, we can compute fluxes by

$$\begin{aligned} f_{i-1/2}^{j*} &= \min_{d=1}^D \left\{ \sum_{u=1}^U D_u, S_d / \left(\frac{\sum_{u=1}^U D_u \xi_{u,d}}{\sum_{u=1}^U D_u} \right) \right\}, \\ f_{i-1/2,d}^{j*} &= \frac{\sum_{u=1}^U D_u \xi_{u,d}}{\sum_{u=1}^U D_u} f_{i-1/2}^{j*}, \quad d = 1, \dots, D, \\ f_{i-1/2,u}^{j*} &= \frac{D_u}{\sum_{u=1}^U D_u} f_{i-1/2}^{j*}, \quad u = 1, \dots, U, \end{aligned} \quad (6.13)$$

where $\xi_{u,d}$ is the proportion of traffic heading downstream link d in upstream link u , $f_{i-1/2}^{j*}$ is the total flux through the boundary, $f_{i-1/2,d}^{j*}$ flux heading downstream link d , and $f_{i-1/2,u}^{j*}$ flux from upstream link u . In this model, the intersection is considered as a combination of a merge with U upstream branches and a diverge with D downstream links in the fashion of (Daganzo, 1995a). Note that the merge model, Equation 6.7, and the diverge model, Equation 6.11, are specific cases of Equation 6.13.

6.2.2 Commodity-based kinematic wave theories

In the MCKW simulation platform, commodities are differentiated by origin/destination or path. We assume that a road network has P' origin/destination (OD) pairs and P

paths ($P \geq P'$). When vehicles have predefined paths, we then have a P -commodity traffic flow on the road network and label vehicles taking p th path as p -commodity. When vehicles of an O/D have no predefined paths, we have P' -commodity traffic flow.

In the kinematic wave theories of multi-commodity traffic, we denote total traffic density, travel speed, and flow-rate respectively by ρ , v , and q , which are all functions of location x and time t . In contrast, these quantities for p -commodity vehicles are ρ_p , v_p , and q_p respectively. The fundamental diagram of total traffic defines a functional relationship between density and travel speed or flow-rate: $q = Q(a, \rho)$ and $v = V(a, \rho) \equiv Q(a, \rho)/\rho$, where $a(x)$ stands for road inhomogeneities at location x such as changes in the number of lanes, curvature, and free flow speed. Further, we assume traffic on all links is additive in the following sense (Jin and Zhang, 2002):

$$\rho = \sum_{p=1}^P \rho_p, \quad (6.14)$$

$$v = v_p = V(a, \rho), \quad p = 1, \dots, P, \quad (6.15)$$

$$q = \sum_{p=1}^P q_p, \quad (6.16)$$

The kinematic wave theory of additive multi-commodity traffic on a link can be described by the following theory (Jin and Zhang, 2003b),

$$\begin{aligned} \rho_t + Q(a, \rho)_x &= 0, \\ (\rho_p)_t + (\rho_p V(a, \rho))_x &= 0, \quad p = 1, \dots, P. \end{aligned} \quad (6.17)$$

If denoting the local proportion of p -commodity ($p = 1, \dots, P$) by $\xi_p = \rho_p/\rho$, we then have the following advection equations (Lebacque, 1996)

$$(\xi_p)_t + V(a, \rho)(\xi_p)_x = 0, \quad p = 1, \dots, P. \quad (6.18)$$

From Equation 6.18, we can see that proportions of all commodities travel forward in a link along with vehicles in traffic flow, as the change of ξ_p in material space,

$(\xi_p)_t + V(a, \rho)(\xi_p)_x$, equals to zero. This is also true for all kinds of junctions, in particular diverges, in their supply-demand models in the preceding subsection ³ Therefore, Equation 6.18 also means that the profile of proportions coincides with vehicles' trajectories on a link. That is, if two or more commodities initially completely are divided by an interface, this interface will move forward along with vehicles on both sides of, and these commodities will never mix. Since each single vehicle can considered as a commodity, all vehicles' trajectories keep disjoint in the commodity-based kinematic wave models. Therefore, FIFO principle is respected in this continuous model.

In the previous subsection, we studied the discrete kinematic wave theory for total traffic. Here, we will present the discrete kinematic wave theory for each commodity. Given traffic conditions of p -commodity at time step j , i.e., $\rho_{p,i}^j$ in all cells, we can calculate the traffic density of p -commodity in cell i at time step $j + 1$ as

$$\rho_{p,i}^{j+1} = \rho_{p,i}^j + \frac{\Delta t}{\Delta x} (f_{p,i-1/2}^{j*} - f_{p,i+1/2}^{j*}), \quad (6.19)$$

where $f_{p,i-1/2}^{j*}$ is the in-flux of p -commodity through the upstream boundary of cell i during time steps j and $j + 1$, and $f_{p,i+1/2}^{j*}$ out-flux. Furthermore, since the profile of the proportion of a commodity always travels forward at traffic speed, the proportion of a commodity in out-flux of cell i compared to all commodities is equal to the proportion of the commodity in the cell. I.e. (Lebacque, 1996),

$$f_{p,i+1/2}^{j*} \cdot \rho_i^j = f_{i+1/2}^{j*} \cdot \rho_{p,i}^j, \quad p = 1, \dots, P. \quad (6.20)$$

This is true for cells right upstream of merging junctions (Jin and Zhang, 2003c) and diverging junctions (Papageorgiou, 1990; Daganzo, 1995a; Lebacque, 1996; Jin and Zhang, 2001a).

³That traffic is anisotropic is believed to regulate this property.

During time steps j and $j + 1$ at a boundary $x_{i+1/2}$, which has U upstream cells and D downstream cells, if we know the out-flux from upstream cell u ($u = 1, \dots, U$), $f_{p,u,i+1/2}^{j*}$ ($p = 1, \dots, P$), we can obtain the in-flux of downstream cell d ($d = 1, \dots, D$), $f_{p,d,i+1/2}^{j*}$ ($p = 1, \dots, P$), from traffic conservation in p -commodity:

$$\sum_{u=1}^U f_{p,u,i+1/2}^{j*} = \sum_{d=1}^D f_{p,d,i+1/2}^{j*}. \quad (6.21)$$

However, when p -commodity vehicles can take more than one downstream cells, we have

$$\sum_{p=1}^P f_{p,d,i+1/2}^{j*} = f_{d,i+1/2}^{j*}. \quad (6.22)$$

Note that, in Equation 6.17, the kinematic wave solutions are determined by those of total traffic, which are obtained by the first-order convergent Godunov method. Also from Equation 6.18, we can see that Equation 6.20 yields an up-wind method for ξ_p in Equation 6.19. Therefore, the discrete model for the commodity-based kinematic wave model, Equation 6.17, converges in first order to continuous version, whose solutions observe FIFO principle. That is, in numerical solutions, error in travel time of any vehicle is in the order of Δt . That is, in the MCKW simulation, FIFO is accurate to the order of Δt and Δx . Therefore, when we decrease Δt , this approximation becomes more accurate.

6.3 Network structure, data structure, and program flow-charts in the MCKW simulation platform

In this section, we will discuss the programming details of the MCKW simulation of an illustrative road network.

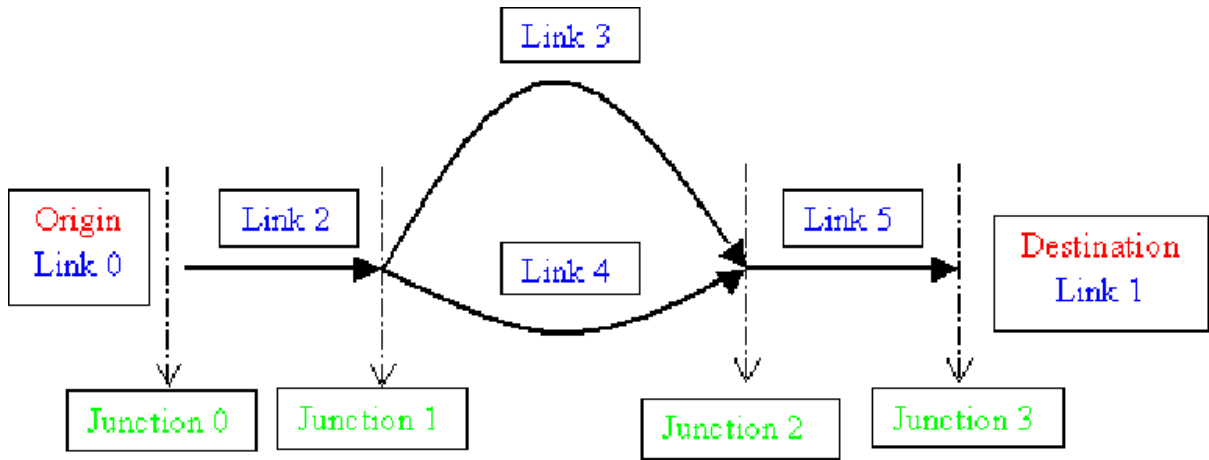


Figure 6.1: A demonstration road network

6.3.1 Network structure

For the purposes of exposition, a simple traffic network, shown in Figure 6.1, is considered, and these discussions can be extended to more general road networks.

The road network in Figure 6.1, where the arrows show traffic direction, consists of one origin/destination (O/D) pair and four links. In this network, there are two paths. Furthermore, we assume vehicles have predefined paths.⁴ Thus, traffic flow on this road network consists of two commodities.

In the MCKW simulation, origins and destinations have the same data structure as regular links and are treated as links. For a road network with `num_origin` origins, `num_od` origins and destinations, and `num_link` links, all links are numbered: origins from 0⁵ to `num_origin-1`, the number of origins; destinations from `num_origin` to `num_od-1`; and regular links from `num_od` to `num_links-1`. In the sample network, links are numbered as shown in Figure 6.1.

With these numbers, the paths or commodities are denoted as follows: commodity

⁴When vehicles have no predefined paths, these discussions are also applicable.

⁵The numbering starts from 0 rather than 1 according to C/C++ conventions.

0 takes links 0, 2, 3, 5, and 1, and commodity 1 takes links 0, 2, 4, 5, and 1. This is equivalent to saying that links 0, 2, 5, and 1 carry 0-commodity and 1-commodity flows, link 3 carries only 0-commodity flow, and link 4 carries only 1-commodity flow. Further, the network structure and traffic flow direction is represented by the upstream and downstream links of each link. For example, the upstream links of link 5 and the downstream links of link 2 are links 3 and 4, respectively.

In the MCKW simulation, each link is partitioned into a number of cells.⁶ Since fluxes through cell boundaries are important in computation in the kinematic wave theories, cell boundaries are also included in the structure of a link.⁷ In the MCKW simulation platform, cells and boundaries are ordered according to traffic direction: adjacent cells and boundaries are either upstream or downstream to a cell.

In the MCKW simulation, therefore, network can be constructed if we know the structures of all links, commodities on a link, and the upstream and downstream links of all links. That is, junctions are not used to store network structure although they are also numbered in Figure 6.1. The representation of network structure in the MCKW simulation largely simplifies the data structure, in which only links are used.

6.3.2 Data structure

In the MCKW simulation platform, the structure and characteristics of a road network and traffic conditions are all represented by links as well as cells and boundaries inside a link. Therefore, the major data structure is `linkType`, through which network and traffic conditions are dealt with, together with sub-structures for cells, `cellType`, and boundaries, `boundaryType`. The data structures are shown in Figure 6.2 and explained in detail as below.

⁶Origins and destinations have only one cell.

⁷Note that there are one more cell boundaries than cells.

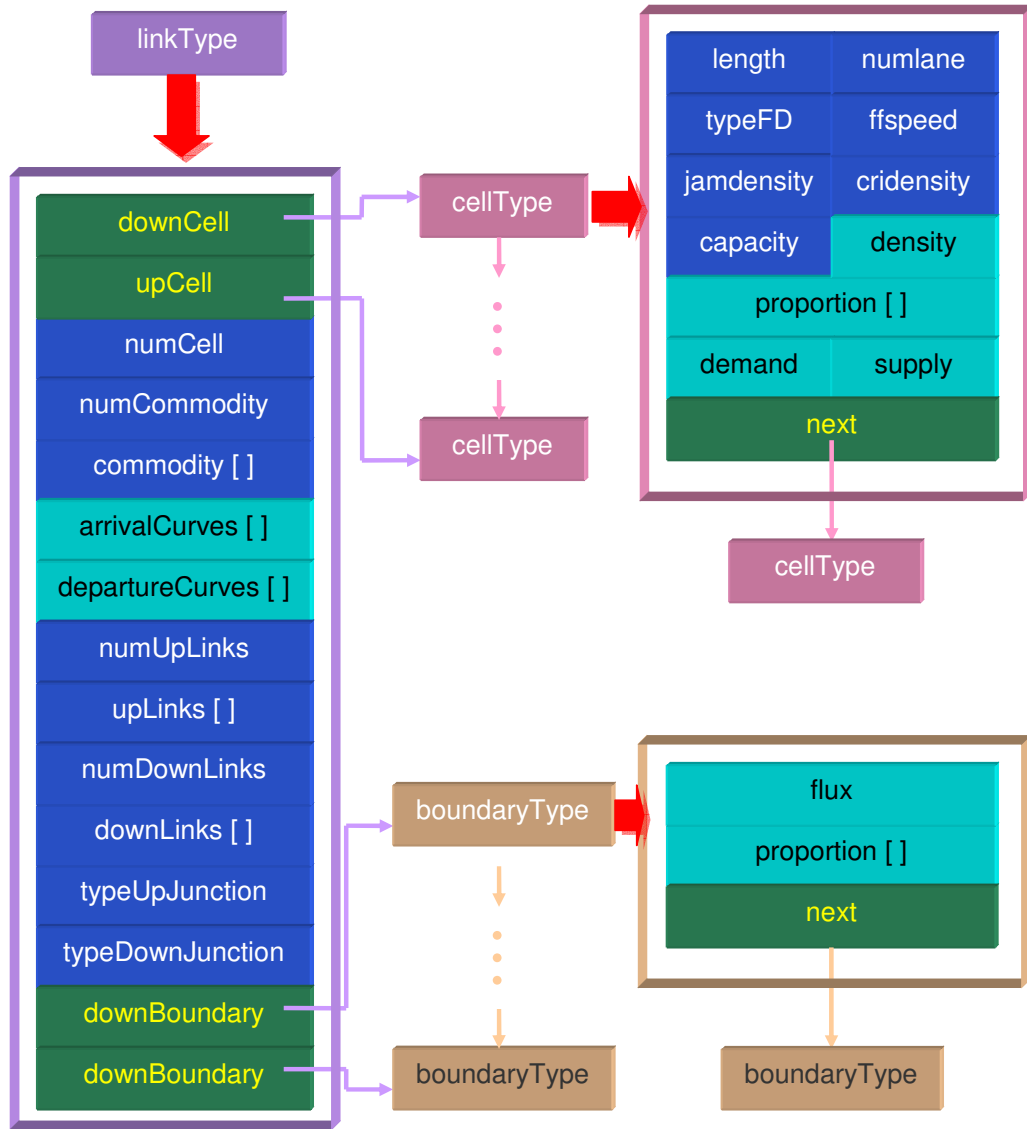


Figure 6.2: Data structure in the MCKW mckw platform

In Figure 6.2, the data structure for a link, `linkType`, is shown in the left box. Its fields are explained as follows:

`downCell` is an address pointing to the furthest downstream cell of a link.

`upCell` is an address pointing to the furthest upstream cell of a link.

`numCell` is the number of cells in a link.

`numCommodity` is the number of commodities traveling on the link.

`commodity []` is an array of commodities, whose length is `numCommodity`. Commodities are ordered increasingly for all links.

`arrivalCurves []` is an array of accumulative flow entering the link. Its length is `numCommodity+1`. The first `numCommodity` entries store the cumulative flows of corresponding commodities, and the last entry stores total cumulative flow.

`departureCurves []` is the same as `arrivalCurves []` except that we consider exiting flows.

`numUpLinks` is the number of upstream links adjacent to a link.

`upLinks []` stores all the adjacent upstream links. Its length is `numUpLinks`.

`numDownLinks` is the number of downstream links adjacent to a link.

`downLinks []` stores all the adjacent downstream links. Its length is `numDownLinks`.

`typeUpJunction` denotes the type of the upstream junction incident to a link. Here, type 0 stands for a linear junction connecting one upstream link and one downstream link, type 1 for a merging junction, type 2 for a diverging junction as described by Equation 6.11, type 3 for a diverging junction by Equation

6.8-Equation 6.10, and type 4 for a diverging junction by Equation 6.12. For different types of junctions, traffic flow models are different, as shown in Section 6.2.

`typeDownJunction` denotes the type of the downstream junction incident to a link.

The definition of junction types are the same as in `typeUpJunction`.

`downBoundary` is an address pointing to the furthest downstream boundary of a link.

`upBoundary` is an address pointing to the furthest upstream boundary of a link.

In these cells, four fields in dark green are pointers with no physical meaning, two fields in cyan are time-dependent quantities, and the rest in blue represent quantities that determine network structure and are time invariant.

As exhibited by the top right box of Figure 6.2, `cellType`, has the following fields, which characterize a cell.

`length` is the length of a cell.

`numlane` is the number of lanes of a cell.

`typeFD` denotes the type of fundamental diagrams in a cell. Type 0 stands for the triangular fundamental diagram (Newell, 1993). For other types of fundamental diagrams, refer to (Del Castillo and Benitez, 1995b; Kerner and Konhäuser, 1994). With the number of lanes considered, we can have the fundamental diagram for the cell.

`ffspeed` is the cell free flow speed.

`jamdensity` is the cell jam density of each lane.

`cridensity` is the cell critical density of each lane, at which traffic flow reaches capacity.

`capacity` is the cell maximum flow-rate of a lane.

`density` is the cell total density.

`proportion []` is an array of proportions of commodities in a cell. Its length is `numCommodity` of the corresponding link.

`demand` is the cell traffic demand during a time interval, as defined in Equation 6.4.

`supply` is the cell traffic supply, as defined in Equation 6.5.

`next` is the address pointing to the upstream cell.

As in `linkType`, the dark green field is a pointer, seven blue fields are for time-independent quantities, which denote major characteristics of a cell, and four cyan fields are for time-dependent quantities. Note that the number of lanes, free flow speed, and, therefore, the critical density and capacity may change when accidents occur. Besides, if there are signals on the boundaries of a cell, the demand and supply may be restricted (Daganzo, 1995a; Jin and Zhang, 2003c).

The data structure for cell boundaries, `boundaryType`, is illustrated by the bottom right box in Figure 6.2 and has the following fields:

`flux` is the flux through the boundary during a time interval.

`proportion []` stores the proportions of all commodities in the total flux. Its length is `numCommodity` of the corresponding link.

`next` is the address pointing to the upstream boundary.

As we can see, both **flux** and **proportion** [] are time dependent.

In the MCKW simulation, cells and boundaries are ordered in the direction opposite to traffic's. However, it is also straightforward to order them in the traffic direction. Besides, ordering will not affect computation efficiency significantly.

6.3.3 Program flow-chart

The program flow chart in the MCKW simulation platform is shown in Figure 6.3. The modules in the program are explained below in the same order as they appear in the chart.

1. **Create network.** Network structure and characteristics are created. That is, we provide values for the blue fields of each link and cell in Figure 6.2. We also assign all locations of the pointers.
2. **Initialize traffic.** Traffic density and proportions of all commodities are initialized for each cell. One typical initialization is to set network empty; i.e., traffic density of each cell is zero.
3. **Compute supply/demand.** Given traffic density of a cell, we are able to compute traffic demand and supply according to Equation 6.4 and Equation 6.5.
4. **Resolve boundary conditions.** Several types of boundary conditions can be used. The first and most important type of boundary conditions is conditions for origins and destinations. In the MCKW simulation, we use traffic demand, specified for all commodities, for origins and traffic supply for destinations. This is different from the boundary conditions used in the previous chapters, where the Dirichlet, Neumann, and periodic boundary conditions are generally used.

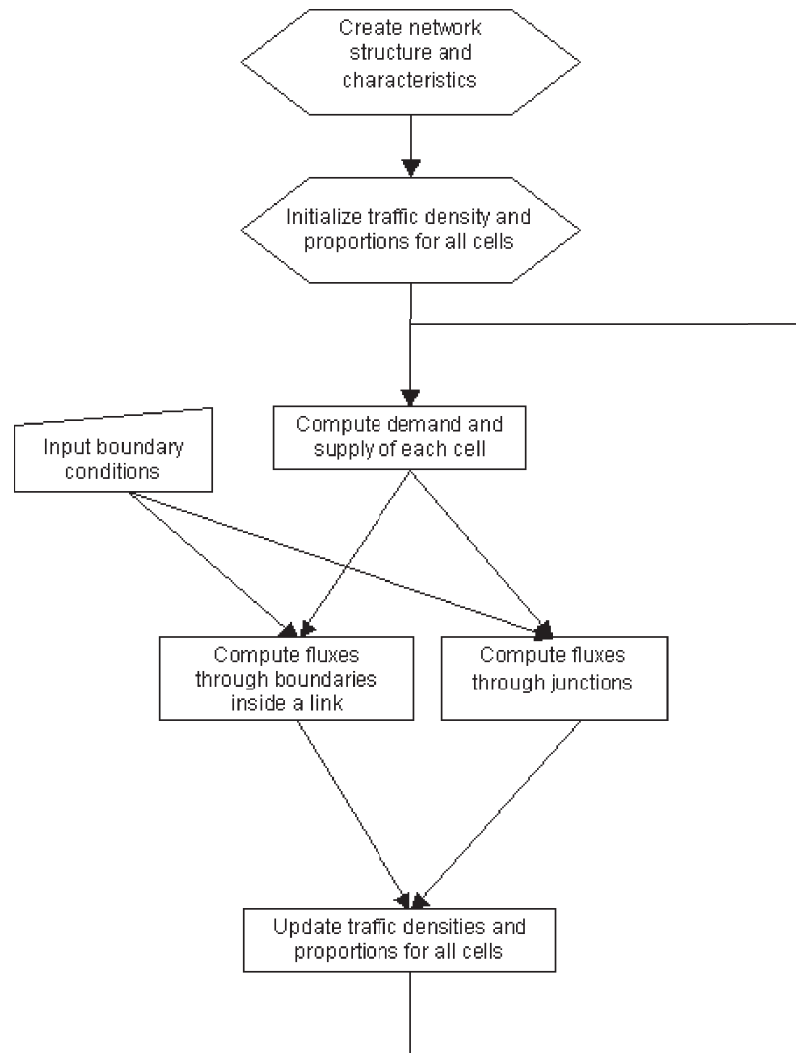


Figure 6.3: The program flow chart in the MCKW simulation

However, from those boundary conditions, we can easily compute the supply and demand according to Equation 6.4 and Equation 6.5. Moreover, these boundary conditions are different from the O/D flow matrix in dynamic loading studies in the sense that we cannot determine in-flow, which is also affected by current traffic conditions on a link incident to an origin. Therefore, with the same pattern in origin demand, we may have totally different O/D flows. This observation suggests a criteria for evaluating the level of service of a road network: the amount of time for loading a number of vehicles. In addition, the effect of assignment algorithms can be studied through the proportions of origin demands. Second, signals and accidents are considered as boundary conditions in the MCKW simulation: signals acting at cell boundaries put a constraint on supplies of the downstream cells and demands of the upstream cells (Daganzo, 1995a; Jin and Zhang, 2003c), and accidents will change the number of lanes and free flow speed in a cell. From the discussions above, we can see that the influence of incidents and accidents can be studied through imposing different boundary conditions.

5. **Compute link flows.** From Equation 6.6, we are able to compute fluxes through boundaries inside a link. From the FIFO principle of traffic flow in the kinematic wave theories, the proportion of a commodity in fluxes is equal to that in density in the upstream cells.
6. **Compute junction flows.** From Equation 6.7, Equation 6.8-Equation 6.10, Equation 6.11, and Equation 6.12, we can compute fluxes through different types of junctions. The proportions of different commodities can be obtained from the FIFO property and traffic conservation of each commodity, Equation 6.21. Since links share junctions, we only need compute junction fluxes for a

set of links. For example, for the road network in Figure 6.1, we only compute junction fluxes at the upstream and downstream junctions of links 2 and 5.

7. **Update traffic conditions.** Traffic densities of all commodities in a cell can be updated by Equation 6.19. However, one has to be careful when computing the proportions since total density, as a divider, may be very small. Although the proportions may not be accurate for very small densities, it rarely matters.

6.4 Cumulative flow, travel time, and other properties of a road network

In the MCKW simulation, we keep track of the change of traffic densities of all cells and fluxes through all boundaries. Besides, these quantities are specified for commodities. In this section, we will discuss how to obtain other traffic information from these quantities.

6.4.1 Cumulative flow and vehicle identity

Cumulative flow at a boundary $x_{i-1/2}$ from time t_0 to t , $N(x_{i-1/2}; [t_0, t])$, is the total number of vehicles passing the spot during the time interval. If the flux is $f^*(x_{i-1/2}, s)$ at time s , then we have

$$N(x_{i-1/2}; [t_0, t]) = \int_{s=t_0}^t f^*(x_{i-1/2}, s) ds. \quad (6.23)$$

Correspondingly, the discrete cumulative flow, $N(x_{i-1/2}; [J_0, J])$, which is from time steps J_0 to J , is defined as

$$N(x_{i-1/2}; [J_0, J]) = \sum_{j=J_0}^{J-1} f_{i-1/2}^{j*} \Delta t, \quad (6.24)$$

where $f_{i-1/2}^{j*}$ is the flux at $x_{i-1/2}$ during time steps j and $j + 1$.

A curve of cumulative flow versus time is also known as a Newell-curve or simply N-curve (Daganzo, 1994), since Newell (1993) developed a simplified version of the LWR kinematic wave theory based on this concept.

From the definition of cumulative flow, we can see that an N-curve is non-decreasing in time. Further, it is increasing when passing flow is not zero.

Although densities and fluxes are quantities at the aggregate level, the MCKW model is capable of tracking traffic information at the disaggregate level. This can be done also with cumulative flows: a vehicle passing a cell boundary at a time step can be labeled by the corresponding cumulative flow. If all cumulative flows are synchronized; for example, when the initial traffic in a road network is empty, then the same cumulative flow of a commodity refer to the same vehicle. This fact is due to the FIFO property in all commodities.⁸

Therefore, in the MCKW simulation, with curves of cumulative flows as a bridge between the aggregate and disaggregate quantities, we are able to keep track of vehicle trajectories, accurate to the order of Δx and Δt , from cumulative flows at all cell boundaries. Further, with finer partition of each link, we can obtain more detailed information at the disaggregate level.

6.4.2 Travel time

For a vehicle, which can be identified by its commodity cumulative flow number under FIFO, its travel time across a link or from the origin to the destination can be inferred from N-curves. For example, when we know its arrival and departure times to a link from the corresponding N-curves, we can easily compute its travel time across the link.

⁸When type 4 diverge appears, this has to be checked.

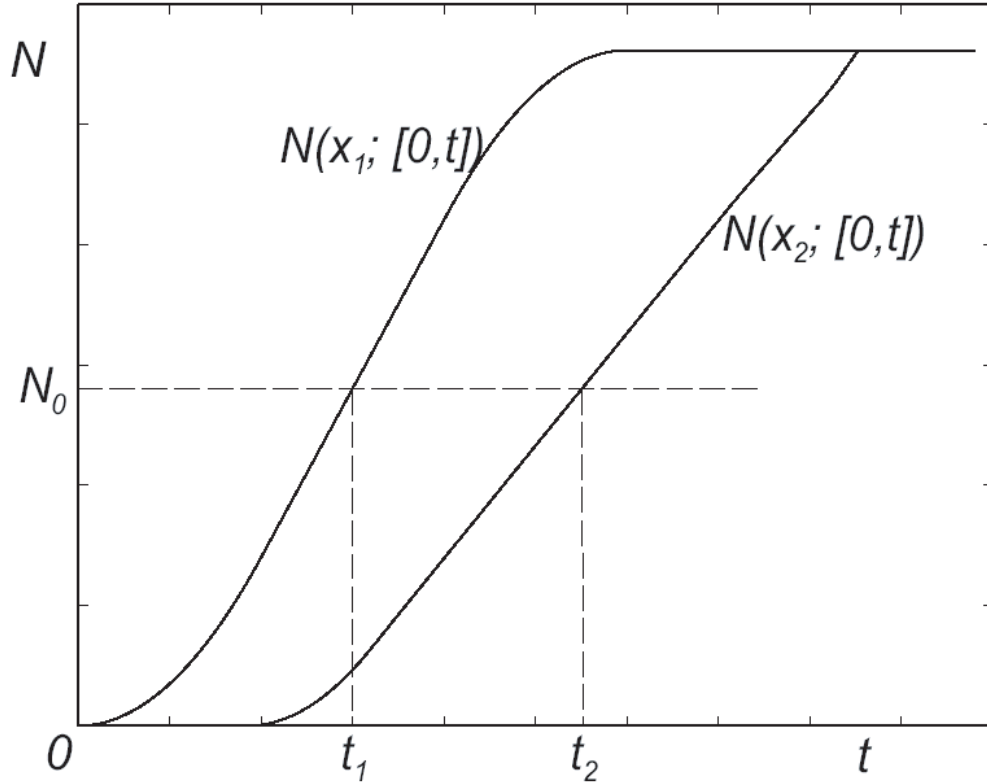


Figure 6.4: Cumulative flows and travel time

This can be demonstrated in Figure 6.4. In this figure, the left curve is the N -curve at location x_1 , and the right curve at x_2 . These two curves are synchronized in the sense that the vehicles between x_1 and x_2 at $t = 0$ are not counted in $N(x_2; [0, t])$. Therefore, from FIFO, we can see that the N_0 vehicle on the left N -curve is the same as the N_0 vehicle on the right N -curve. Then, from the curve, we know that the times of the N_0 passing x_1 and x_2 are t_1 and t_2 respectively. Thus, its travel time from x_1 to x_2 is $t_2 - t_1$.

In Figure 6.4, the left N -curve reaches a maximum at some time and stop in-

creasing after that. This means that no flow passes x_1 after that time. The right N-curve has the same pattern. In such cases, one has to be cautious when computing travel time for the last vehicle, identified by the maximum cumulative flow, which corresponds to multiple values in time. Rigorously, therefore, the time for a vehicle N_0 passing a location x , where the N-curve is $N(x; [t_0, t])$, can be defined by

$$T(N_0; x) = \min_s \{s \mid \text{when } N(x; [t_0, s]) = N_0\}. \quad (6.25)$$

Further, the travel time for the N_0 vehicle from x_1 to x_2 is

$$T(N_0; [x_1, x_2]) = T(N_0; x_2) - T(N_0; x_1). \quad (6.26)$$

With the definition of passing time in Equation 6.25, at x , the vehicle identity N_0 has a one-to-one relationship with its passing time $T(N_0; x)$. Therefore, the passing time can be considered as another identity of a vehicle. For a vehicle N_0 , if we know its passing time at any location in a road network, we then obtain its trajectory.

From the travel times of individual vehicles, we are able to compute the total travel time between two locations, in particular between an O/D pair, as follows:

$$T([N_1, N_2]; [x_1, x_2]) = \sum_{M=N_1}^{N_2} T(M; [x_1, x_2]), \quad (6.27)$$

where N_1 is the first vehicle and N_2 the last. We can see that, in Figure 6.4, the total travel time is equal to the area between the two N-curves. Then the average travel time for each vehicle will be

$$\bar{T}([N_1, N_2]; [x_1, x_2]) \equiv \frac{T([N_1, N_2]; [x_1, x_2])}{N_2 - N_1} = \frac{\sum_{M=N_1}^{N_2} T(M; [x_1, x_2])}{N_2 - N_1}. \quad (6.28)$$

Moreover, for a road network, we can integrate travel times for all O/D pairs and, therefore, obtain the total travel time and the average travel time for the whole road network. These quantities are important indicators of the performance of a road

network. Besides, we consider the loading time for an amount of flow to be released from an origin as another performance indicator.

Hence, the MCKW simulation platform can be applied to evaluate traffic management and control strategies, such as route assignment and ramp metering algorithms. These applications will be discussed in the next chapter.

6.5 Numerical simulations

In this section, we investigate the properties of the MCKW simulation model through numerical simulations. We will show the evolution of traffic and examine the convergence of solutions. In this section, the diverge connecting links 2, 3, and 4 is modeled by Equation 6.11.

6.5.1 Simulation set-up

For these simulations, the network has the structure as shown in Figure 6.1. In this network, links 2, 3, and 5 have the same length, 20 miles, and the length of link 4 is 40 miles (not drawn to proportion); link 2 has three lanes, and the other links has two lanes; all links have the same triangular fundamental diagram (Newell, 1993):

$$Q(a, \rho) = \begin{cases} v_f \rho, & 0 \leq \rho \leq a\rho_c; \\ \frac{\rho_c}{\rho_j - \rho_c} v_f (a\rho_j - \rho), & a\rho_c < \rho \leq a\rho_j; \end{cases} \quad (6.29)$$

where ρ is the total density of all lanes, a the number of lanes, the jam density $\rho_j=180$ vpmpl, the critical density $\rho_c=36$ vpmpl, the free flow speed $v_f=65$ mph, the capacity of each lane $q_c = \rho_c v_f=2340$ vphpl, and the corresponding shock wave speed of jam traffic is $c_j = -\rho_c/(\rho_j - \rho_c)v_f \approx -17$ mph.

Initially, the road network is empty. Boundary conditions are defined as follows. Traffic supply at the destination is always $2q_c$. At origin, traffic demand at the origin

is $3q_c$ during $[0, 6.0]$ and zero after that, and the proportion of commodity 0, which takes link 3 instead of 4, is always $\xi = 70\%$.

Links 2, 3, and 5 are partitioned into N cells each, and link 4 into $2N$ cells, with each cell of the same length, $\Delta x = 20/N$ miles. The total simulation time of 8.4 hours is divided into K time steps, with the length of a time step $\Delta t = 8.4/K$. In our simulations, we set $N/K = 1/30$. Thus the CFL (Courant et al., 1928) number is no larger than $v_f \Delta t / dx = 0.91$, which is valid for Godunov method (Godunov, 1959).

6.5.2 Traffic patterns on the road network

We let $N = 400$ and $K = 12000$. Hence $\Delta x = 0.05$ miles=80 meters, and $\Delta t = 0.0007$ hours=2.52 seconds. Here the sizes of road cells and time steps are relatively small, in order for us to obtain results closer to those of the kinematic wave theories with the Godunov method.

The contour plots of the solutions are shown in Figure 6.5. From these figures, we can divide the evolution of traffic dynamics on the road network into three stages.

In the first stage starting from 0, vehicles embark link 2 with the free flow speed, prevail the link in its critical density $3\rho_c$, and arrive junction 1 at $t_1 = 20/65$ hr. At the diverge, junction 1, fluxes are computed from Equation 6.11: out-flux of link 2 is

$$f_{2,out} = \min\left\{3q_c, \frac{2q_c}{0.7}, \frac{2q_c}{0.3}\right\} = \frac{20}{7}q_c,$$

which is slightly smaller than the in-flux of link 2, in-flux of link 3 is $f_3 = 0.7f_2 = 2q_c$, which is its capacity, and in-flux of link 4 is $f_4 = 0.3f_2 = \frac{6}{7}q_c$, which is less than half of its capacity. After t_1 , two streams of free flow form on links 3 and 4, and a backward travelling shock wave forms on Link 2, and the shock wave speed is

$$v_j = -\frac{1}{4}v_f.$$

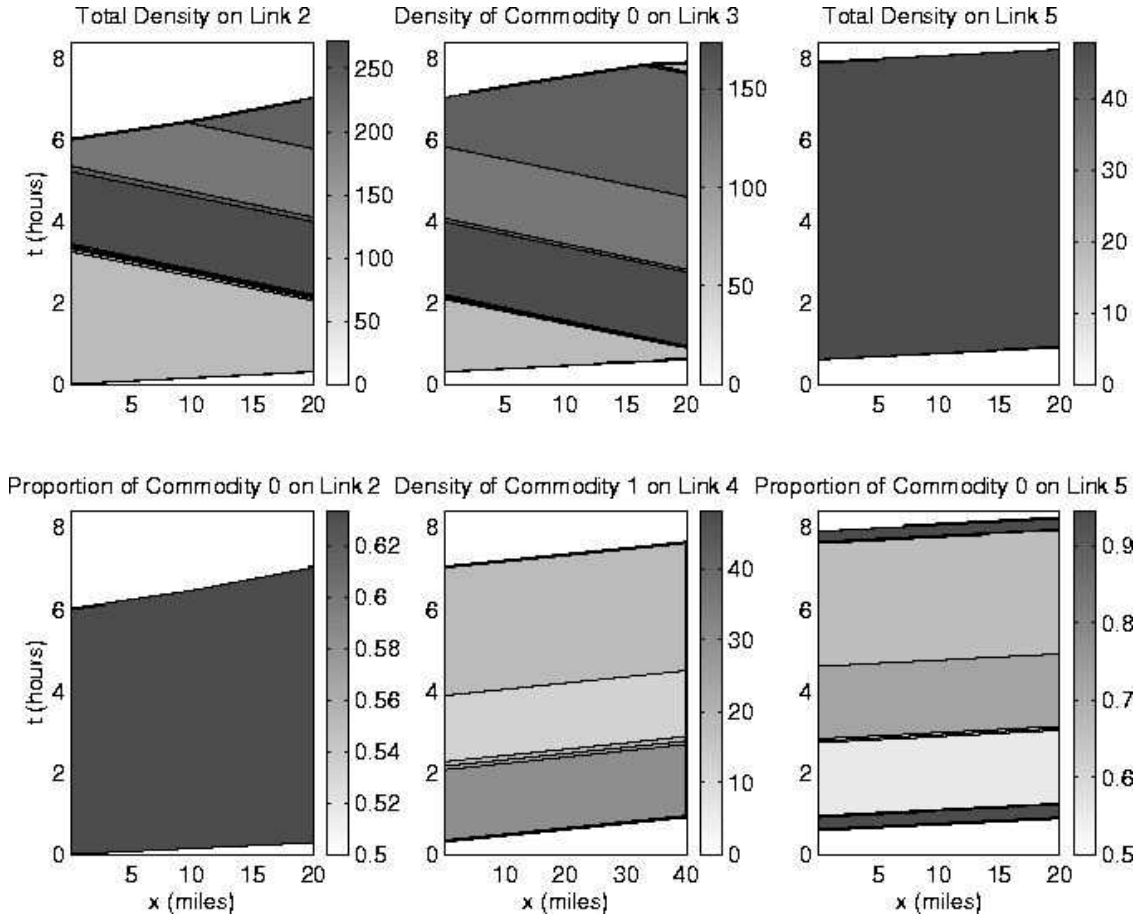


Figure 6.5: Contour plots of network traffic flow

At $t_2 = t_1 + 20/v_f$, the first vehicle on link 3 reaches junction 2, which is a merge. At t_2 , the first vehicle on link 4 is half way back since the length of link 4 is double of link 3's. From the merge traffic flow model, Equation 6.7, we have the in-flux of link 5 as

$$f_{5,in} = \min\{2q_c, 2q_c\} = 2q_c,$$

which is also the out-flux of link 3. After t_2 , the proportion of commodity 0 on link 5 is 1, as we can see on the bottom right figure.

The second stage starts at $t_3 = t_1 + 40/v_f = 60/65$ hr, when the first vehicle

on link 4 reaches junction 2. After that, the in-flux of link 5 is still $2q_c$, but the proportion of commodity 0 reduces to 0.5714 since commodity 1 also contributes; on link 3, a new state forms at $\rho = 195.4290$ vpm, which is over-critical, and a shock wave travels upstream at the speed of $|c_j| \approx 17$ mph; on link 4, $\rho = 30.8571$ vpm, which is under-critical. At $t_4 = t_3 + 20/|c_j| = 140/65$ hr, the back-traveling shock on link 3 hits junction 1, and the traffic supply on link 3 is reduced. Therefore, the out-flux of link 2 is further reduced, and link 2 becomes more congested, as shown in the top left picture. This also reduces traffic flow on link 4, and the reduced flow reaches junction 2 at $t_5 = t_4 + 40/v_f = 180/65$ hr. After t_4 , link 3 becomes less congested, and a rarefaction wave travels backward on it at $|c_j| \approx 17$ mph; the proportion of commodity on link 5 gets higher. From the bottom middle figure, we can see that at $t_5 = t_4 + 20/|v_j|$, traffic density on link 4 swings back a little due to the back traveling rarefaction on link 3. This shift is transported to junction 2 at $t_6 = t_5 + 40/v_f$ and oscillates traffic density on link 3 and the proportion of commodity 0 on link 5.

The third stage starts at $t_7 = 6$, when traffic demand from origin subsides to zero. After that, a shock forms on link 2 and travels forward, and propagates to link 4 and link 3. On link 4 the shock travels at v_f , and on link 3 it travels slower. This is why the proportion of commodity 0 on link 5 becomes 1 before it is emptied.

This simulation indicates that oscillation of traffic conditions can be caused by network merges and diverges even the initial and boundary conditions are very nice. The traffic flow pattern on this road network suggests that, if we keep the same demand from the origin, an equilibrium state will be reached after some time. This equilibrium state will be further investigated in the following chapter.

The traffic patterns in Figure 6.5 can be partially observed from the top left figure in Figure 6.6, where the thicker four curves give cumulative flows for commodity 0, the thinner for commodity 1, and solid, dashed, dotted, and dash-dot curves are for

	Total Number of Vehicles	TTT	ATT
Commodity 0	23,8585	4.7291×10^4	1.9822
Commodity 1	10,2251	1.7372×10^4	1.6989

Table 6.1: Total travel time (TTT) and average travel time (ATT) for two commodities

cumulative flows at junction 0, 1, 2, and 3, respectively. In the bottom left figure, the solid lines are cumulative flows of commodity 0 at origin/destination, i.e., junction 0 and 3, the dashed curve is the number of commodity 0 vehicles in the network at a time, the dashed line shows the average number, the dotted curve is the travel time of a commodity 0 vehicle identified by its cumulative flow, and the dotted line is the average travel time. The bottom right figure has the same curves and lines as the bottom left figure, except that they are for commodity 1. Here travel time of individual vehicle is computed by Equation 6.26, total travel time by Equation 6.27, and average travel time by Equation 6.28. Although the formulas were developed for link travel times, it is valid for a network as long as vehicles of each commodity observe FIFO principle. Total (TTT) and average (ATT) travel times are listed in Table 6.1 (unit=hours).

Thus, vehicles that take link 4 on average use shorter time, which is still longer than the free flow travel time, 80/65 hr. Obviously, if all vehicles at origin decide to take link 3, the travel time, 60/65 will be the shortest possible travel time between the origin and destination. Therefore, this assignment fraction, 70%, is not an optimum one. More detailed analysis of the influence of the assignment fraction on travel times will be engaged in the following chapter.

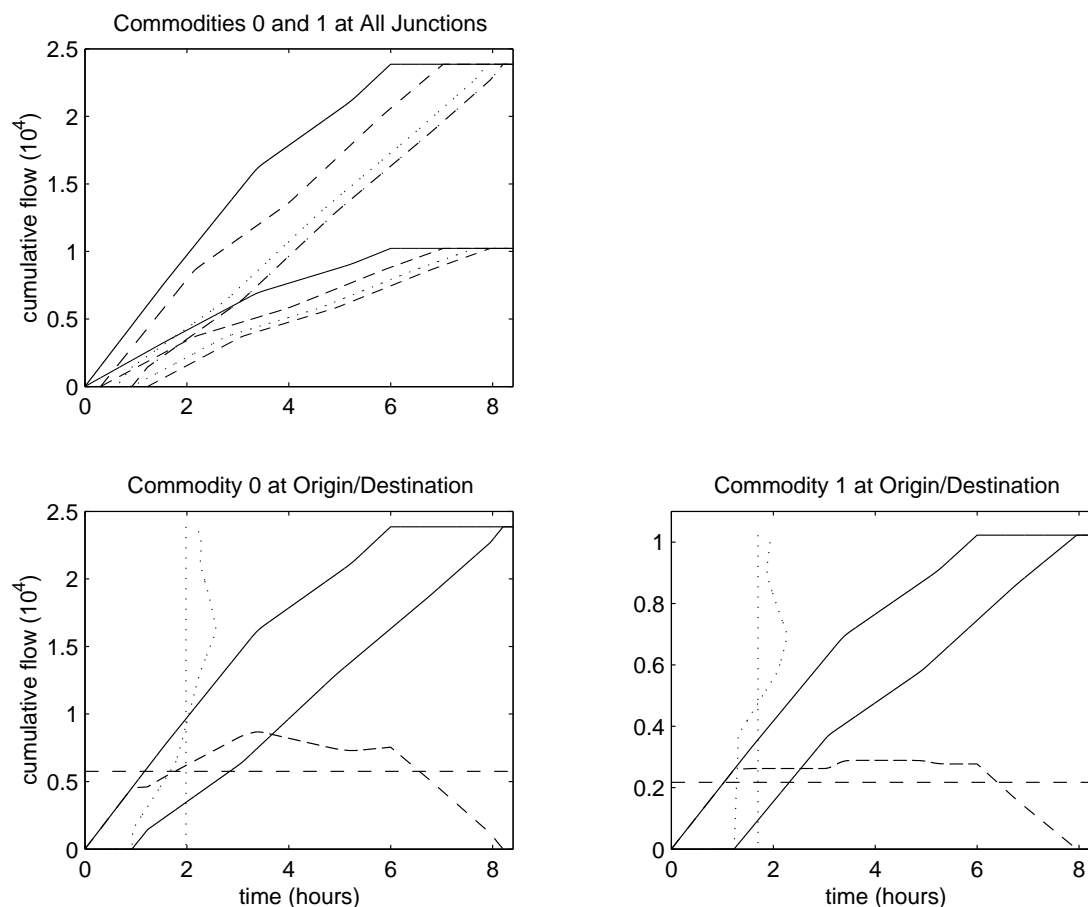


Figure 6.6: N-curves and travel times of each commodity in the road network

6.5.3 Convergence of the MCKW simulation model

In this subsection, we study the convergence of the MCKW simulation platform with increasing number of cells. Here we use the same road network, initial and boundary conditions as in the preceding subsection.

As we show in the previous chapters, the discrete forms of kinematic wave theories converge to their continuous counterparts as we partition each link into finer cells (Jin and Zhang, 2003c). In those studies, we generally check convergence in terms of traffic densities. Here we intend to show convergence in average travel times of both

Commodity 0	N=200	N=400	N=800	N=1600	N=3200
ATT	1.98189893	1.98215215	1.98227240	1.98234941	1.98239377
Error [10^{-3}]		0.2532	0.1202	0.07700	0.0444
Rate			1.074	0.6430	0.7958
Commodity 1	N=200	N=400	N=800	N=1600	3200
ATT	1.69922958	1.69892887	1.69877593	1.69871236	1.69868722
Error [10^{-3}]		-0.3007	-0.1529	-0.0636	-0.0251
Rate			0.9755	1.2664	1.3384

Table 6.2: Convergence rates for the MCKW simulation platform

commodities.

Denoting the average travel time of a commodity, T , as a function of the number of cells, N ; i.e., $T = T(N)$, we can define the relative error, from N to $2N$, by

$$\epsilon^{2N-N} = |T(2N) - T(N)|. \tag{6.30}$$

Then a convergence rate is computed by

$$r = \log_2\left(\frac{\epsilon^{2N-N}}{\epsilon^{4N-2N}}\right). \tag{6.31}$$

The convergence rates of the average travel times are given in Table 6.2.

From the table, we can see that average travel times are also convergent in first order. Note that this convergence is different from the aforementioned traffic conditions converging to certain equilibrium state. Moreover, we can see that the results with $N = 200$ is already accurate enough in this case. Since the computation time of the MCKW simulation platform is quadrupled when N is doubled, in later simulations, we use $\Delta x = 0.1$ mile=160 meters and $\Delta t = 0.0014$ hours= 5.04 seconds with the same simulation period.

6.6 Discussions

In this chapter, we proposed the Multi-Commodity Kinematic Wave (MCKW) simulation model. In this simulation model, we integrated the kinematic wave theories studied in the previous three chapters to form the foundation of the algorithms, carefully discussed commodity-based kinematic wave theories, and presented the data structure and program structure for implementation. We further demonstrated how to obtain cumulative flows and travel times from outputs of the MCKW simulation model. Simulations show that numerical results converge to FIFO solutions although the FIFO condition is not strictly enforced in the discrete form of commodity-based kinematic wave theories.

Different from many existing simulation packages, where traffic is tracked down to vehicle level, the MCKW simulation concerns traffic conditions down to commodity level. The simulation model is designed for handling very large road networks and can be applied in studies of Intelligent Transportation Systems, such as dynamic traffic assignment, dynamic O/D estimation, and so on. However, as pointed out earlier, the effects of “departure from FIFO” should be carefully considered in these applications.

In the future, the MCKW simulation model can be enhanced in three aspects. Theoretically, vehicle types and special lanes can be incorporated (Daganzo, 2002), and nonequilibrium continuum models (Jin and Zhang, 2003d) may also be integrated. Numerically, parallel algorithms can be applied to improve computational speed since traffic conditions on different links can be updated simultaneously, and consumption of computer memory will be checked. Finally, for different applications, we also plan to design different input/out interfaces. For example, the network structure can be imported from GIS (Geographic Information System) data, and boundary conditions and output can be manipulated for different applications.

Chapter 7

Studies of network vehicular traffic with kinematic wave simulations

7.1 Introduction

As discussed in the preceding chapter, the Multi-Commodity Kinematic Wave (MCKW) simulation model is based on the kinematic wave theories of traffic dynamics at various road network components, including link bottlenecks, merges, and diverges. After vehicles are differentiated into commodities by their paths or origin/destination (O/D) pairs, we can then keep track of the evolution of traffic densities of all commodities on a road network over time. Further, information of individual vehicles can be obtained through cumulative flows. Therefore, compared to some other simulation models based on the kinematic wave theory (e.g., Daganzo (1995a); Vaughan et al. (1984)), the MCKW simulation is a pure macroscopic simulation program. As such, the MCKW simulation model is expected to be less costly in computation but adequate for many applications in Advanced Transportation Information Systems (ATIS) and Advance Transportation Management Systems (ATMS).

In this chapter, we will explore traffic dynamics in a road network with the MCKW simulation model and its implications in applications. First in Section 7.2, we are interested in equilibrium states of a road network under a given O/D demand pattern and the influence of different assignment strategies. Then in Section 7.3, we study the formation mechanism of periodic oscillations in a network and their properties.

These simulations are studied on a small, demonstration network, where traffic dynamics at diverges obey Equation 6.11. The major purpose of these studies is to show the capabilities of the MCKW simulation model. Moreover, these studies can be considered as initial steps to the understanding of more complicated traffic phenomena in a large-scale road network and practical applications.

7.2 Equilibrium states of a road network and preliminary examination of traffic assignment

In Subsection 6.5.2, we show that traffic flow on a road network can reach a certain pattern after sufficient amount of time. We call these time-invariant traffic patterns as equilibrium states.

For the equilibrium states, we are interested in the following questions: 1) how are the equilibrium states related to the boundary conditions? 2) what is the effect of changing proportions in origin demand? 3) do these equilibrium states have anything to do with the so-called User Equilibrium States?

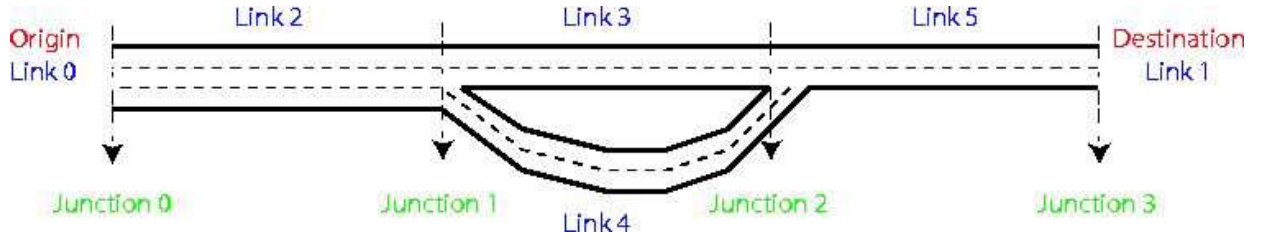


Figure 7.1: Network for studying equilibrium state and traffic assignment

7.2.1 The simulated network

In this section, we study a demonstration network shown in Figure 7.1. In this network, links 2, 3, and 5 have the same length, 20 miles, and the length of link 4 is 40 miles; link 2 has three lanes, and the other links has two lanes; all links have the same fundamental diagram:

$$Q(a, \rho) = \begin{cases} v_f \rho, & 0 \leq \rho \leq a \rho_c; \\ \frac{\rho_c}{\rho_j - \rho_c} v_f (a \rho_j - \rho), & a \rho_c < \rho \leq a \rho_j; \end{cases}$$

where ρ is the total density of all lanes, a the number of lanes, the jam density $\rho_j=180$ vpmpl, the critical density $\rho_c=36$ vpmpl, the free flow speed $v_f=65$ mph, and the capacity of each lane $q_c = \rho_c v_f=2340$ vphpl.

Initially, the road network is empty. Traffic supply at the destination is always the capacity of two lanes. For studying equilibrium states, we assume traffic demand at the origin is always the capacity of link 2, $3q_c$.

Links 2, 3, and 5 are partitioned into 200 cells each, and link 4 into 400 cells. Therefore, all cells have the same length, 0.1 miles. The total simulation time of 8.4 hours is divided into 6000 time steps, with the length of a time step $\Delta t = 0.0014$ hours=5.04 seconds. Thus the CFL (Courant et al., 1928) number is no bigger than $v_f \Delta t / dx = 0.91$, which is valid for Godunov method (Godunov, 1959). As we show in subsection 6.5.3, the simulation results are numerically convergent.

In the following simulations, we will study the equilibrium states and the performance of the road network for a proportion of commodity 0, ξ .

7.2.2 Equilibrium states

When $\xi = 0.5$, and commodity 1 vehicles have the same proportion, $1 - \xi = 0.5$, solutions of traffic dynamics on the road network are shown in Figure 7.2. The traffic pattern evolves as follows. From $t_0 = 0$ to $t_1 = 20/65 \text{ hr}^1$, the first vehicle traverses link 2 and reaches junction 1, where fluxes can be computed from Equation 6.11 as

$$\begin{aligned} f_{2,out} &= \min\{3q_c, 2q_c/0.5, 2q_c/0.5\} = 3q_c, \\ f_{3,in} &= 1.5q_c, \\ f_{4,in} &= 1.5q_c, \end{aligned}$$

where subscript *in* denotes in-flux, and *out* out-flux. After t_1 , links 2, 3, and 4 all carry free flow. At $t_2 = t_1 + 20/65$, traffic on link 3 arrives at the merge, junction 2, where from Equation 6.7 fluxes are the following:

$$\begin{aligned} f_{5,in} &= \min\{2q_c, 2q_c\} = 2q_c, \\ f_{3,out} &= 2q_c, \\ f_{4,out} &= 0. \end{aligned}$$

At $t_3 = t_2 + 20/65$, vehicles on link 4 also reaches junction 2, and fluxes become

$$\begin{aligned} f_{5,in} &= \min\{2q_c + 2q_c, 2q_c\} = 2q_c, \\ f_{3,out} &= q_c, \\ f_{4,out} &= q_c. \end{aligned}$$

¹Hereafter, the unit of time is always hour except if otherwise mentioned.

Thus, after t_3 , shock waves form on both links 3 and 4 and travel upstream in the speed of $-v_f/4$. At $t_4 = t_3 + 80/65$, the shock wave on link 3 reaches junction 1, and fluxes become

$$\begin{aligned} f_{2,out} &= \min\{3q_c, q_c/0.5, 2q_c/0.5\} = 2q_c, \\ f_{3,in} &= q_c, \\ f_{4,in} &= q_c. \end{aligned}$$

After this, link 3 equilibrates at $q_3 = q_c$ and $\rho_3 = 1.2\rho_j$, a shock travels backward on link 2 at $v_f/4$, and a shock travels forward at the free flow speed. At $t_5 = t_4 + 20/65$, the two shock waves on link 4 meet at the middle of the link and form a stable zero-speed shock wave, where the upstream half is at $0.2\rho_j$ and the downstream half at $1.2\rho_j$. After $t_6 = t_4 + 80/65$, traffic on link 2 is uniformly at $q_2 = 2q_c$ and $\rho_2 = 1.4\rho_j$.

Therefore, the whole road network reaches an equilibrium state after t_6 . In the equilibrium state, links 2 and 5 both carry flow-rate $2q_c$, which is the capacity of the road network, links 3 and 4 carry flow rate q_c corresponding to the proportion of each commodity. Besides, links 2 and 3 are congested, and link 4 has a zero-speed shock, which, however, is unstable in the sense that a small oscillation in the upstream or downstream flow will make the zero-shock disappear. The instability of this equilibrium state on the road network can also be seen later when we consider ξ away from 0.5.

When $\xi = 0.6$, the contour plots of traffic densities on four links are given in Figure 7.3. The traffic evolution pattern is similar to that in subsection 6.5.2. Here we directly go into the discussion of the equilibrium state, in which, from Figure 7.3, we can see that all links carry uniform flows. The equilibrium flow-rate is determined by the network bottleneck, link 5, and is $2q_c$. From observations for $\xi = 0.5$, the equilibrium density on link 5 is always $0.4\rho_j$, and traffic density on link 2 is $1.4\rho_j$, which

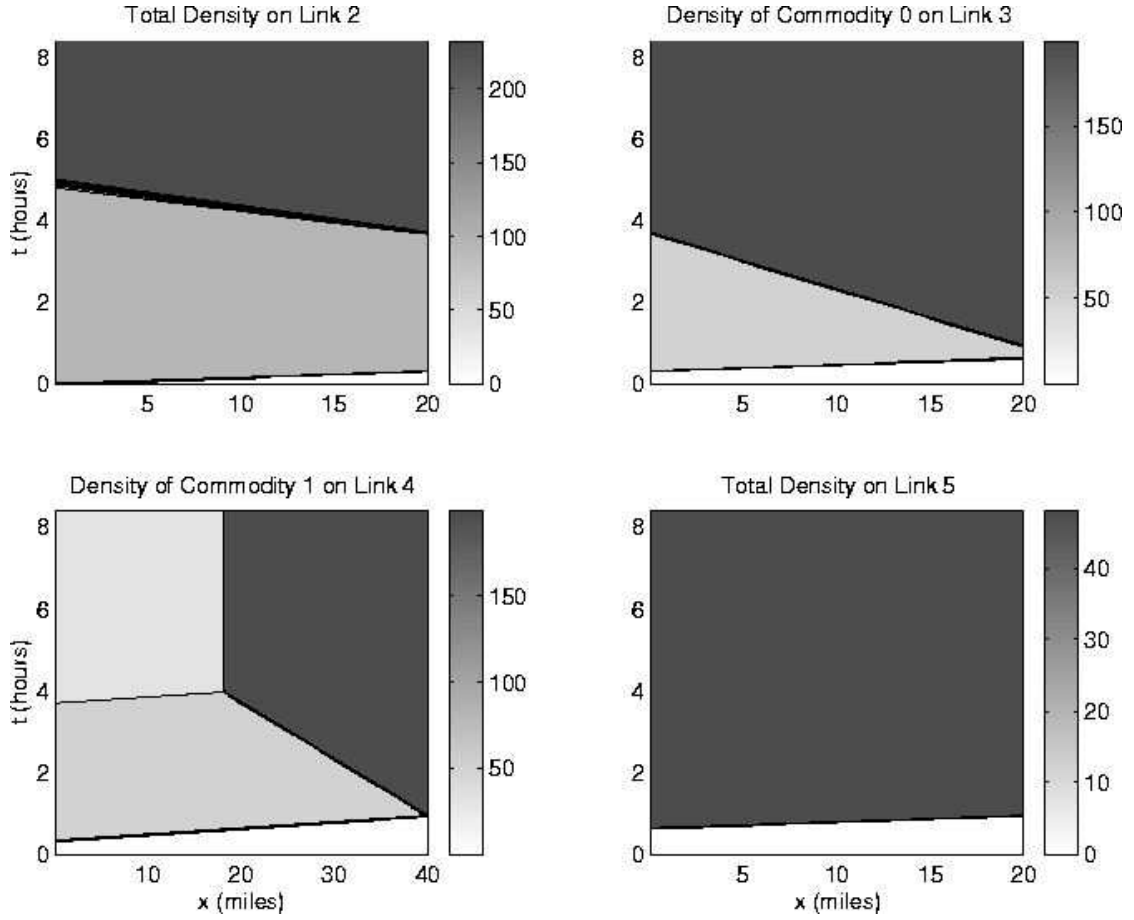


Figure 7.2: Solutions when $\xi = 0.5$

is brought by a back-traveling shock wave. Then, determined by traffic proportions, the flow-rate on links 3 and 4 are $1.2q_c$ and $0.8q_c$, respectively. The remaining task is to determine the traffic densities on links 3 and 4.

We denote traffic demand and supply on these links as $D_3, S_3, D_4,$ and S_4 . Then $(D_3, S_3) = (1.2q_c, 2q_c)$ when link 3 is under-critical, and $(D_3, S_3) = (2q_c, 1.2q_c)$ otherwise. Similarly, $(D_4, S_4) = (0.8q_c, 2q_c)$ when link 4 is under-critical, and $(D_4, S_4) = (2q_c, 0.8q_c)$ otherwise. Since at junction 1

$$f_{2,out} = \min\{3q_c, S_3/0.6, S_4/0.4\} = 2q_c,$$

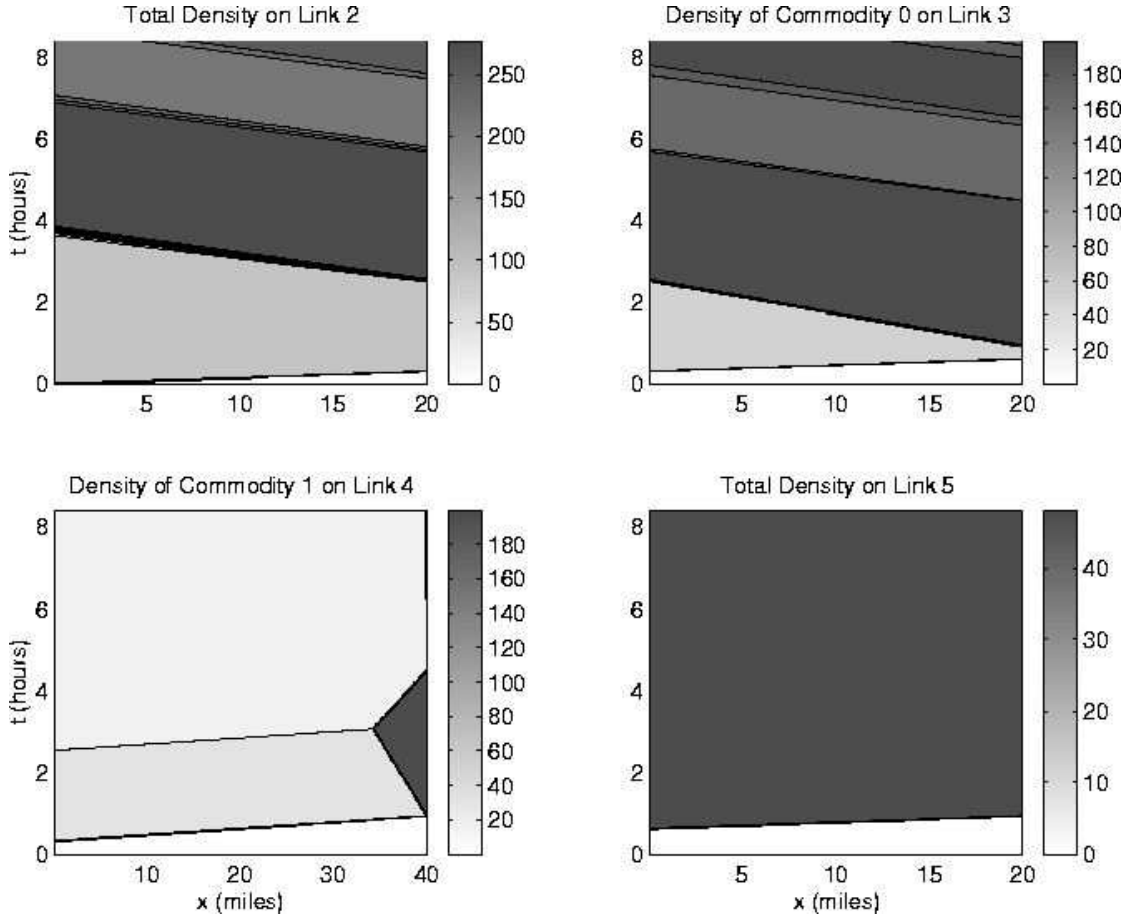


Figure 7.3: Solutions when $\xi = 0.6$

links 3 and 4 cannot be under-critical at the same time. Moreover, since at junction 2

$$\begin{aligned} f_{3,out} &= \frac{D_3}{D_3+D_4} 2q_c = 1.2q_c, \\ f_{4,out} &= \frac{D_4}{D_3+D_4} 2q_c = 0.8q_c, \end{aligned} \tag{7.1}$$

links 4 cannot be over-critical at the same time. Therefore, the only possible case is that link 3 is over-critical and link 4 under-critical. Thus, the equilibrium densities on links 3 and 4 are $\rho_3 = 1.04\rho_j$ and $\rho_4 = 0.32\rho_j$. The solutions in Figure 7.3 support these solutions.

$(\rho/\rho_j, q/q_c)$	$0 \leq \xi < 0.5$	$\xi = 0.5$	$0.5 < \xi \leq 1$
Link 2	(1.4, 2)	(1.4, 2)	(1.4, 2)
Link 3	$(0.4\xi, 2\xi)$	(1.2, 1)	$(2 - 1.6\xi, 2\xi)$
Link 4	$(0.4 + 1.6\xi, 2(1 - \xi))$	(0.2, 1) and (1.2, 1)	$(0.4(1 - \xi), 2(1 - \xi))$
Link 5	(0.4, 2)	(0.4, 2)	(0.4, 2)

Table 7.1: Equilibrium density and flow-rate v.s. ξ

However, $D_3 = 2q_c$ and $D_4 = 0.8q_c$ do not satisfy Equation 7.1 exactly. In fact, there is an intermediate state at the downstream boundary of link 4 (Jin et al., 2002). At the intermediate state, also under-critical, the demand is $\bar{D}_4 = \frac{4}{3}q_c$, which satisfies Equation 7.1, and $\bar{\rho}_4 = \frac{0.8}{3}\rho_j$. This intermediate state, theoretically, only exists at a point, but is stable since its in-flux and out-flux is equal. This kind of intermediate state unlikely exists on a single link (Jin and Zhang, 2003b).

When $\xi = 0.4$, the solutions are shown in Figure 7.4. Although the evolution process is different from that for $\xi = 0.6$, the equilibrium state is exactly the same as before if links 3 and 4 are switched.

For a general proportion $\xi \in [0, 1]$, the equilibrium states are listed in Table 7.1. In this table, we omit the tenuous (unstable) intermediate states, on link 3 when $0 < \xi < 0.5$ and on link 4 when $0.5 < \xi < 1$.

7.2.3 Travel times at equilibrium states

For equilibrium states of different proportion ξ , Table 7.2 shows travel speed and travel time on each link as well as average travel times of commodity 0 (ATT_0), commodity 1 (ATT_1), and all commodities ($ATT = \xi ATT_0 + (1 - \xi)ATT_1$). In the table, travel times during the establishment of equilibrium states are not considered.

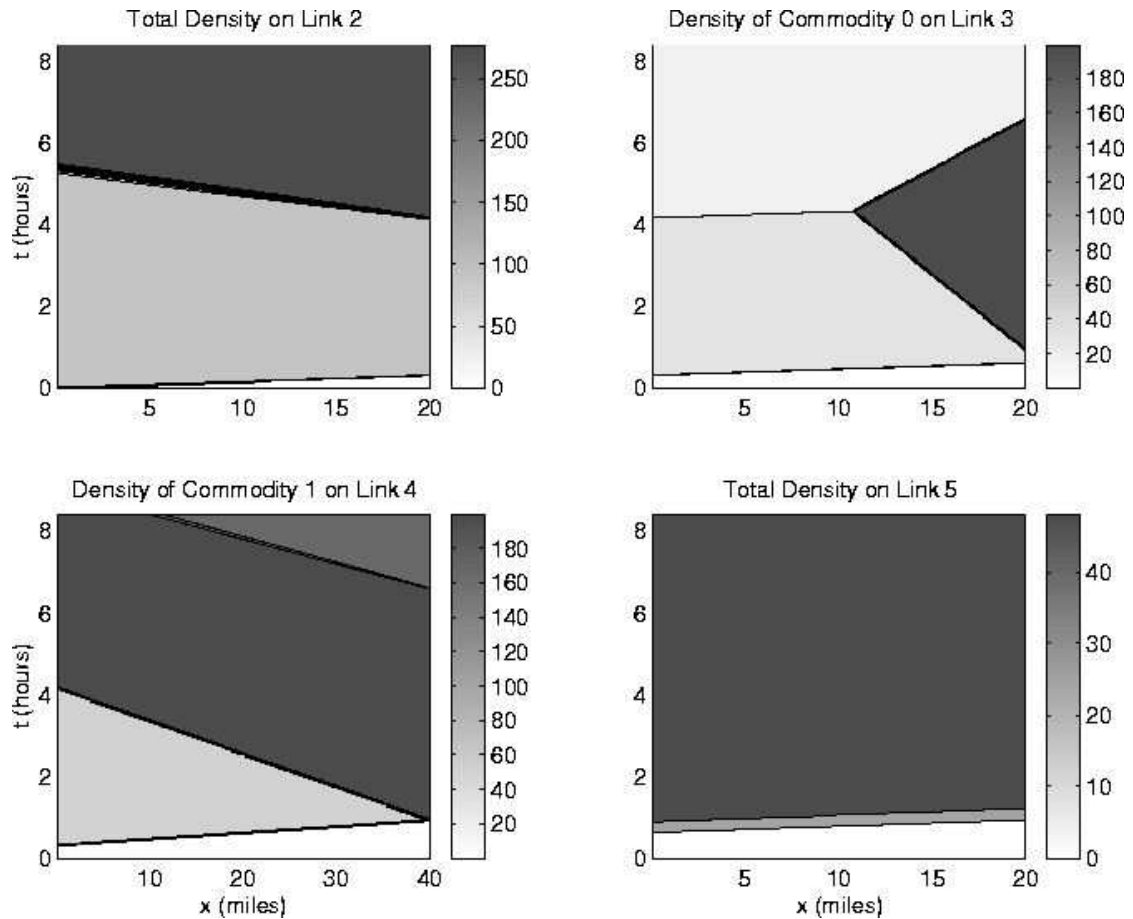


Figure 7.4: Solutions when $\xi = 0.4$

The relationship between these travel times and proportion ξ is illustrated in Figure 7.5.

From the table and figure, we can see the following properties of travel times. First, the average travel time of all commodities, which can be considered the performance function of the whole road network, consists of two pieces of lines and jumps when $\xi = 0.5$. This discontinuity asserts the fact that the equilibrium state when $\xi = 0.5$ is not stable. Third, the minimum average travel time ATT attains its minimum when $\xi = 1$; i.e., when all vehicles take the shorter path. Third, the travel

$(v/v_f, T/\text{hours})$	$0 \leq \xi < 0.5$	$\xi = 0.5$	$0.5 < \xi \leq 1$
Link 2	$(\frac{2}{7}, 1.0769)$	$(\frac{2}{7}, 1.0769)$	$(\frac{2}{7}, 1.0769)$
Link 3	$(1, 0.3077)$	$(\frac{1}{6}, 1.8462)$	$(\frac{\xi}{5-4\xi}, \frac{20-16\xi}{13\xi})$
Link 4	$(\frac{1-\xi}{1+4\xi}, \frac{8(1+4\xi)}{13(1-\xi)})$	$(1 \text{ or } \frac{1}{6}, 2.1538)$	$(1, 0.6154)$
Link 5	$(1, 0.3077)$	$(1, 0.3077)$	$(1, 0.3077)$
ATT_0	1.6923	3.2308	$\frac{20-16\xi}{13\xi} + 1.3846$
ATT_1	$\frac{8(1+4\xi)}{13(1-\xi)} + 1.3846$	3.5384	2
ATT	$2 + 2.7692\xi$	3.3846	$3.5385 - 1.8462\xi$

Table 7.2: Equilibrium speed and travel times v.s. ξ

times of commodities 0 and 1 are equal when $\xi = 5/6$. However, ATT is not at its minimum when $\xi = 5/6$.

7.2.4 Discussions

In the previous subsections, we examine equilibrium states for the road network in Figure 7.1 and its performance at these states against the proportion ξ . The determination of ξ is really part of a traffic assignment process. Therefore, this study provides another angle for checking the user-equilibrium property (Wardrop, 1952). For this network, it is shown to have two user equilibrium states, one at $\xi = 5/6$ and the other at $\xi = 1$, with the latter has smaller path travel times. This is a clear evidence that the inclusion of physical queues destroys the uniqueness property of traffic assignment with other commonly used models, in which queues do not take up space (Wardrop, 1952). Note that, in our discussions, the performance function is the average path travel time, which is different from the link performance function used in static traffic assignment studies (Sheffi, 1984).

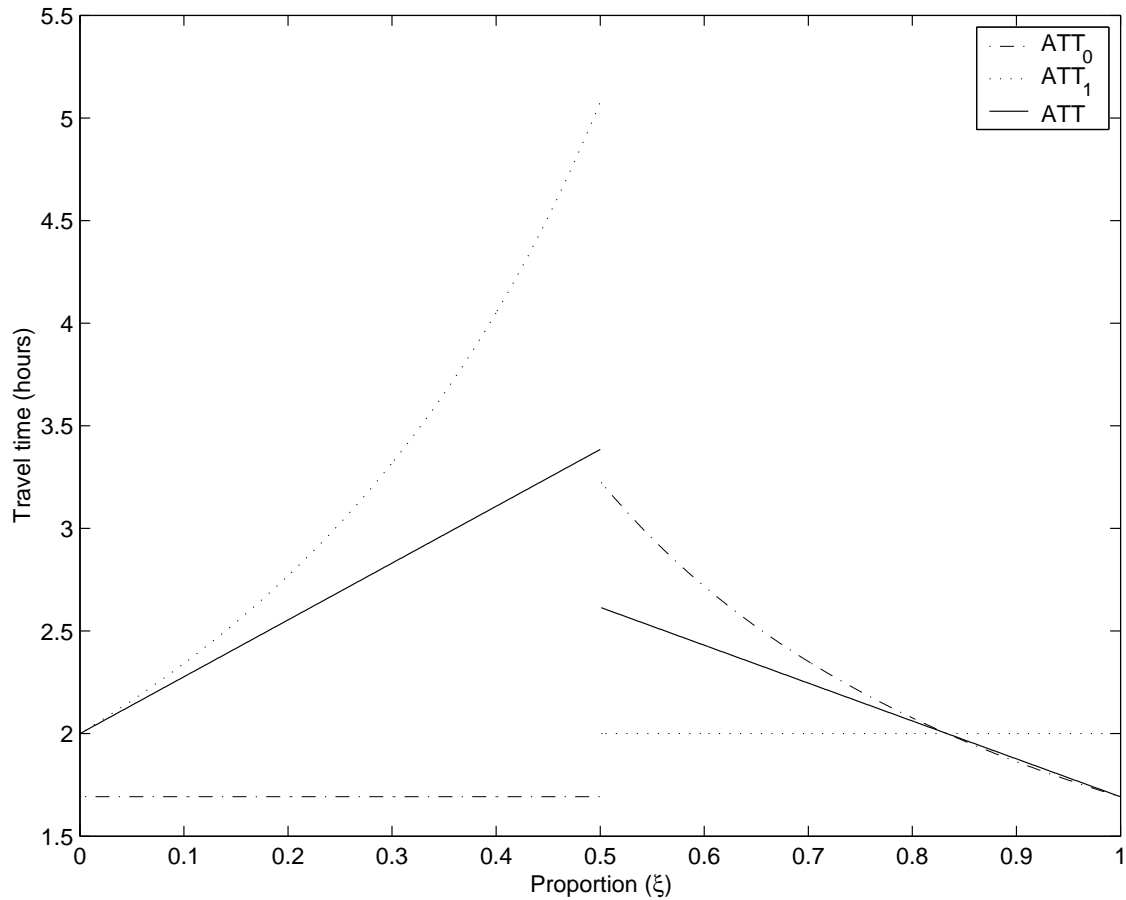


Figure 7.5: Travel times at equilibrium states v.s. proportion ξ

Although the connection between equilibrium states from a dynamic point of view and the user-equilibrium is still premature, these studies shed light on solving dynamic traffic assignment problems, in which the choice of a proper link performance function is still in debate (Daganzo, 1995b). From the MCKW simulation, we can obtain average origin/destination (O/D) travel times under an assignment strategy and use these travel times to evaluate the strategy. To make the performance function of an O/D flow more accurate, one can include the loading time at the origin, which is defined as the average waiting time before a vehicle enters the road network. If

departure (or loading) flow-rate at the origin is $f(t)$ ($t \in [0, T]$), then the average loading time is

$$LT = \frac{\int_{t=0}^T f(t) t \, dt}{\int_{t=0}^T f(t) \, dt}. \quad (7.2)$$

In the examples above, since the loading flow-rate is the same for all ξ , there is no difference between the loading times.

7.3 The formation and structure of periodic oscillations in the kinematic wave model of road networks

In (Jin and Zhang, 2003b) it is shown that there are three types of basic kinematic waves on a road link: shock (decelerating) waves, rarefaction (accelerating) waves, and transition (standing) waves. Further, for a single merge or diverge, we still have these three types of waves on each branch (Jin and Zhang, 2003c; Jin et al., 2002; Jin and Zhang, 2002, 2001a). In this section, we show with MCKW simulation an interesting type of solutions, periodic oscillations, which can be observed in real traffic. We show that these solutions can exist in a small road network with a diverge and a merge and check their formation and structure against network characteristics.

7.3.1 Network for studying periodic solutions

In this section, we study periodic solutions on a road network shown in Figure 7.6. In this network, lengths of links 2, 3, 4, and 5 are $L_2 = 10$ miles, $L_3 = 1$ mile, $L_4 = 2$ miles, and $L_5 = 1$ mile, respectively; the number of lanes of these links are 3, 1, 2,

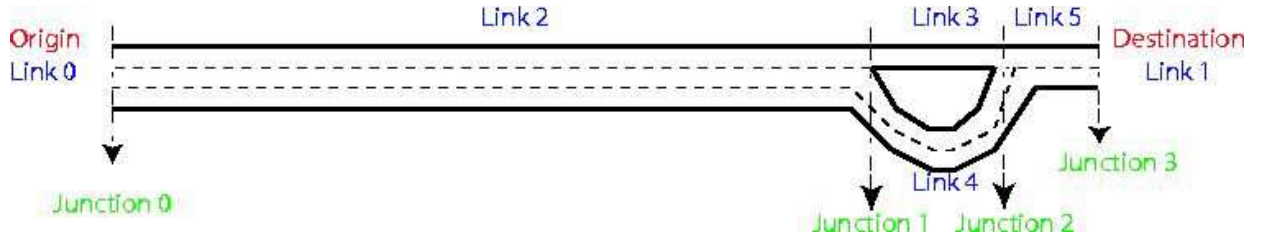


Figure 7.6: Network for studying periodic oscillations

and 2, correspondingly; all links have the same fundamental diagram for each lane:

$$Q(a, \rho) = \begin{cases} v_f \rho, & 0 \leq \rho \leq a\rho_c; \\ \frac{\rho_c}{\rho_j - \rho_c} v_f (a\rho_j - \rho), & a\rho_c < \rho \leq a\rho_j; \end{cases}$$

where ρ is the total density of all lanes, a the number of lanes, the jam density $\rho_j=180$ vpmpl, the critical density $\rho_c=36$ vpmpl, the free flow speed $v_f=65$ mph, and the capacity of each lane $q_c = \rho_c v_f=2340$ vphpl.

Initially, the road network is empty. Traffic supply at the destination is always capacity of two lanes. Here, traffic demand at the origin is always the capacity of link 2, $3q_c$.

Links 2, 3, 4, and 5 are partitioned into 800, 80, 160, and 80 cells respectively, with the length of all cells as 0.0125 miles. The total simulation time of 1.4 hours is divided into 8000 time steps, with the length of a time step $\Delta t = 1.75 \times 10^{-4}$ hours=0.63 seconds. Thus the CFL (Courant et al., 1928) number is no bigger than $v_f \Delta t / dx = 0.91$, which is valid for Godunov method (Godunov, 1959). As we show in subsection 6.5.3, the simulation is numerically convergent. Therefore, with this very fine partition of links, we are able to obtain results closer to theoretical solutions.

Link 3	under-critical	over-critical	Link 4	under-critical	over-critical
S_3	q_c	q_3	S_4	$2q_c$	q_4
D_3	$\leq q_c$	q_c	D_4	$\leq 2q_c$	$2q_c$

Table 7.3: Constraints on equilibrium states

7.3.2 Periodic oscillations

As in the preceding section, we also consider the equilibrium states for a proportion of commodity 0, ξ . In equilibrium states, at junction 1, we have

$$\begin{aligned}
 f_{2,out} &= \min\{3q_c, S_3/\xi, S_4/(1-\xi)\}, \\
 f_{3,in} &= \xi f_{2,out}, \\
 f_{4,in} &= (1-\xi)f_{2,out},
 \end{aligned} \tag{7.3}$$

and at junction 2

$$\begin{aligned}
 f_{5,in} &= \min\{D_3 + D_4, 2q_c\}, \\
 f_{3,out} &= \frac{D_3}{D_3 + D_4} f_{5,in}, \\
 f_{4,out} &= \frac{D_4}{D_3 + D_4} f_{5,in},
 \end{aligned} \tag{7.4}$$

where D_i and S_i are traffic demand and supply of link i ($i = 2, 3, 4, 5$) respectively, $D_2 = 3q_c$, and $S_5 = 2q_c$. Moreover, we have

$$\begin{aligned}
 f_{3,in} &= f_{3,out}, \\
 f_{4,in} &= f_{4,out},
 \end{aligned} \tag{7.5}$$

and constraints defined in Table 7.3, where q_3 and q_4 are flow-rates in the upstream cells of links 3 and 4.

Since links 3 and 4 are initially empty, $S_3 = q_c$ and $S_4 = 2q_c$. Therefore, when $\xi = 0$ or $0.5 \leq \xi \leq 1$, $f_{2,out} \leq 2q_c$ according to Equation 7.3. Note that the capacity of link 5 is $2q_c$. Under this circumstance, solutions are trivial. When $0 < \xi < 0.5$,

from Equation 7.3, we have $f_{2,out} > 2q_c$. This means that at least one of links 3 and 4 has to be over-critical. When both links are over-critical, we have from Equation 7.3-Equation 7.5 and Table 7.3 that $\xi = \frac{1}{3}$. When $0 < \xi < \frac{1}{3}$, link 4 is congested in equilibrium state, and the solution pattern is similar to Figure 7.3 and Figure 7.4. Refer to subsection 7.2.2 for an analysis of the equilibrium states.

For the network in Figure 7.6, interesting solutions occur for $\frac{1}{3} < \xi < \frac{1}{2}$, when link 3 is over-critical and link 4 under-critical. When $\xi = 0.45$, contour plots of traffic densities on the four links are shown in Figure 7.7. This figure shows the formation of periodic solutions as follows: (i) During $t_0 = 0$ and $t_1 = L_3/v_f$, capacity flow travels forward on link 2. When the first vehicle reaches junction 1 at t_1 , we obtain from Equation 7.3 that $f_{2,out} = q_c/0.45$, $f_{3,in} = q_c$, and $f_{4,in} = \frac{11}{9}q_c$. (ii) Thus, after t_1 , a back-traveling shock wave forms on link 2, capacity flow travels on link 3, and free flow travels on link 4. At $t_2 = t_1 + L_3/v_f$, the first vehicle on link 3 reaches junction 2. Since the first commodity-1 vehicle is still half way on link 4, from Equation 7.4, we obtain $f_{5,in} = q_c$, $f_{3,out} = q_c$, and $f_{4,out} = 0$. Therefore, there is no change in traffic patterns on links 2 or 3 at t_2 . (iii) AT $t_3 = t_1 + L_4/v_f$, vehicles on link 4 reach junction 2. From Equation 7.4, we have $f_{5,in} = 2q_c$, $f_{3,out} = 0.9q_c$, and $f_{4,out} = 1.1q_c$. (iv) After t_3 , a back-traveling shock forms on link 3 and the over-critical traffic state, whose flow-rate is $0.9q_c$, propagates upstream. On link 4, there exists a flimsy intermediate area, which is still under-critical. Thus there is no backward wave on link 4. The shock wave on link 3 travels at the speed $\frac{1}{4}v_f$ and hits junction 1 at $t_4 = t_3 + 4L_3/v_f$. (v) At t_4 , we have $S_3 = 0.9q_c$, which yields from Equation 7.3 that $f_{2,out} = 2q_c$, $f_{3,in} = 0.9q_c$, and $f_{4,in} = 1.1q_c$. Therefore, a forward shock wave forms on link 4, whose upstream flow-rate is $1.1q_c$ and downstream flow-rate $\frac{11}{9}q_c$. (vi) At $t_5 = t_4 + L_4/v_f$, the new traffic state reaches junction 2. Consequently, $f_{3,out} = 2/2.1q_c > 0.9q_c$, and $f_{4,out} = 2.2/2.1q_c < 1.1q_c$. Thus the downstream of link 3 becomes less congested, and

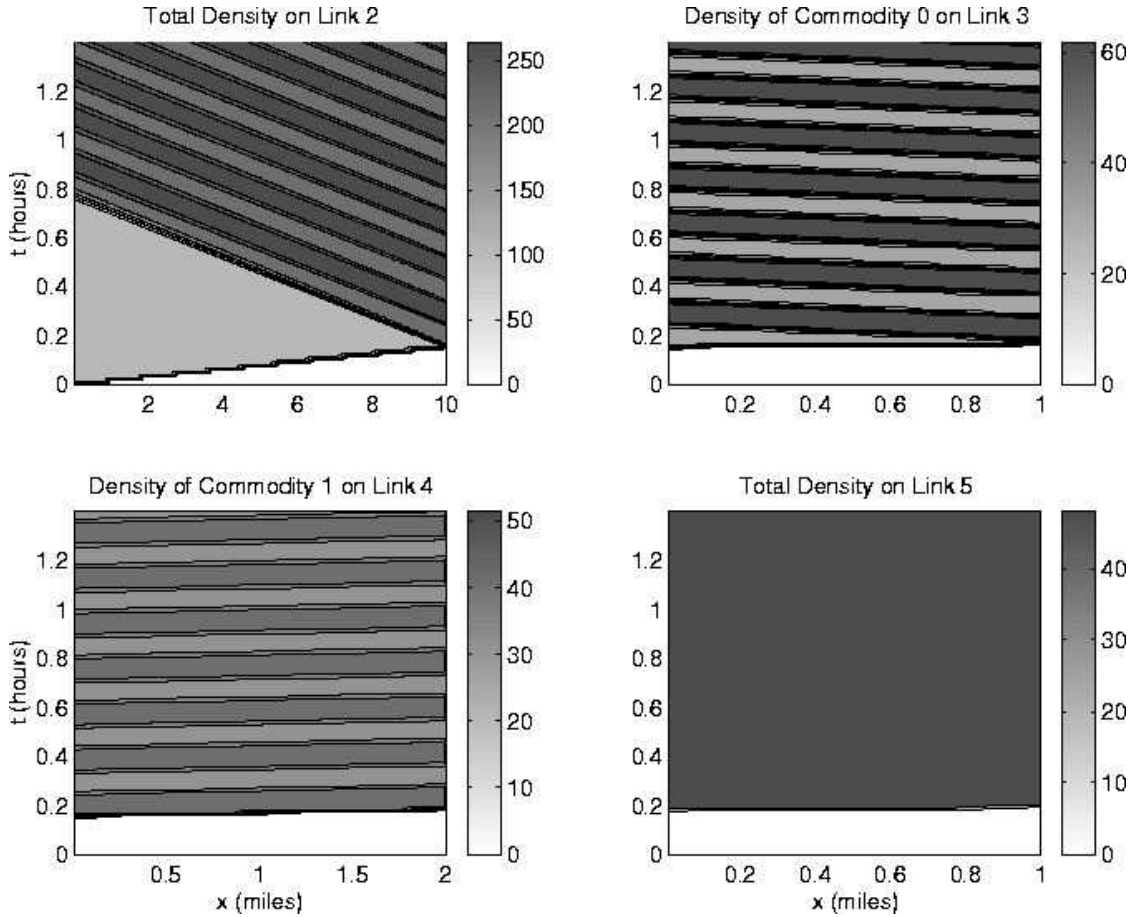


Figure 7.7: Contour plots of periodic oscillations

a rarefaction wave travels upstream. Note that there is no back-traveling wave on link 4. (vii) At $t_6 = t_5 + 4L_3/v_f$, the rarefaction wave reaches junction 1 and increases out-flux of link 2, $f_{2,out} = 2.1164q_c$, and $f_{4,in} = 1.164q_c > 1.1q_c$. (viii) When the new flow on link 4 reaches junction 2 at $t_7 = t_6 + L_4/v_f$, link 3 becomes more congested again. After another time period, $(4L_3 + L_4)/v_f$, link 4 will go back to lower congestion. This process repeats in a periodic manner with the period $T = 2(4L_3 + L_4)/v_f = 0.1846$ hours. After a number of periods, traffic conditions on links 2, 3, and 4 reach a stable pattern, a period of which is explained as follows.

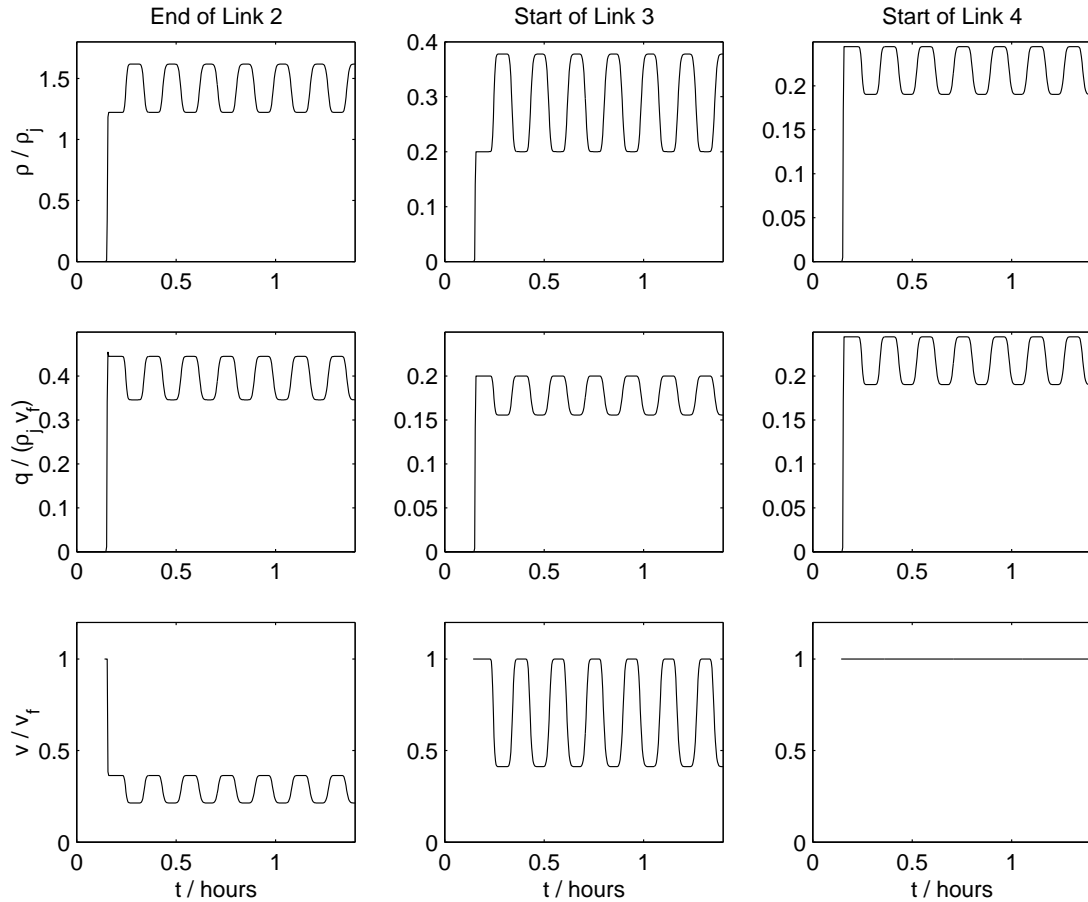


Figure 7.8: Density, flow-rate, and speed at the end of link 2, start of link 3, and start of link 4

The formation of periodic solutions can also be observed at certain locations, such as the end of link 2, start of link 3, and start of link 4, as shown in Equation 7.8. From Figure 7.7, we can see that, most of the time, wave speeds on links 2, 3, and 4 are $-\frac{1}{4}v_f$, $-\frac{1}{4}v_f$, and v_f , respectively. Thus, from curves in Figure 7.8, we can derive traffic pattern at other locations.

In a period, traffic conditions evolve in the following five stages. (i) Assuming the period starts at $t_0 = 0$ when the downstream of link 3 becomes less congested at $\bar{\rho}_3$,

which is always over-critical, at t_0 , link 4 has a smaller density $\bar{\rho}_4$. (ii) At $t_1 = 4L_3/v_f$, traffic density on link 4 starts to increase to $\hat{\rho}_4$. (iii) After $t_2 = t_1 + L_4/v_f$, traffic density on link 3 increased to $\hat{\rho}_3$. This finishes the half period. (iv) At $t_3 = t_2 + 4L_3/v_f$, traffic density on link 3 decreases to $\bar{\rho}_3$. (v) At $t_4 = T$, traffic density on link 3 gets back to $\hat{\rho}_3$.

7.3.3 The structure of periodic solutions

In half a period, solutions at the end of link 2, start of link 3, and start of link 4 in the (ρ, q) -plane are shown in Figure 7.9, in which lines are for fundamental diagrams and dots for solution data. From the figure, we can see that solutions in each period is highly symmetric, with transition layer evenly distributed in the (ρ, q) -plane. In half a period, ρ decreases and approximately satisfies the following equation:

$$\frac{d\rho}{dt} = \alpha(\rho - \hat{\rho})(\rho - \bar{\rho}), \tag{7.6}$$

where $\hat{\rho}$ and $\bar{\rho}$ are the maximum and minimum of ρ respectively, and α is a constant to be determined, and the other half satisfies

$$\frac{d\rho}{dt} = \alpha(\hat{\rho} - \rho)(\rho - \bar{\rho}), \tag{7.7}$$

which is increasing.

In a period, the solutions can be approximated by

$$\rho(t) = \begin{cases} \hat{\rho} - (\hat{\rho} - \bar{\rho}) / \{1 + \exp[-\alpha(\hat{\rho} - \bar{\rho})(t - T/4)]\} & \text{when } t \in [0, \frac{T}{2}), \\ \hat{\rho} - (\hat{\rho} - \bar{\rho}) / \{1 + \exp[\alpha(\hat{\rho} - \bar{\rho})(t - 3T/4)]\} & \text{when } t \in [\frac{T}{2}, T). \end{cases} \tag{7.8}$$

The corresponding v and q are solved by

$$v(t) = \begin{cases} \hat{v} - (\hat{v} - \bar{v}) / \left\{1 + \frac{\hat{v}}{\bar{v}} \exp[\alpha(\hat{\rho} - \bar{\rho})(t - T/4)]\right\} & \text{when } t \in [0, \frac{T}{2}), \\ \hat{v} - (\hat{v} - \bar{v}) / \left\{1 + \frac{\hat{v}}{\bar{v}} \exp[-\alpha(\hat{\rho} - \bar{\rho})(t - 3T/4)]\right\} & \text{when } t \in [\frac{T}{2}, T), \end{cases} \tag{7.9}$$

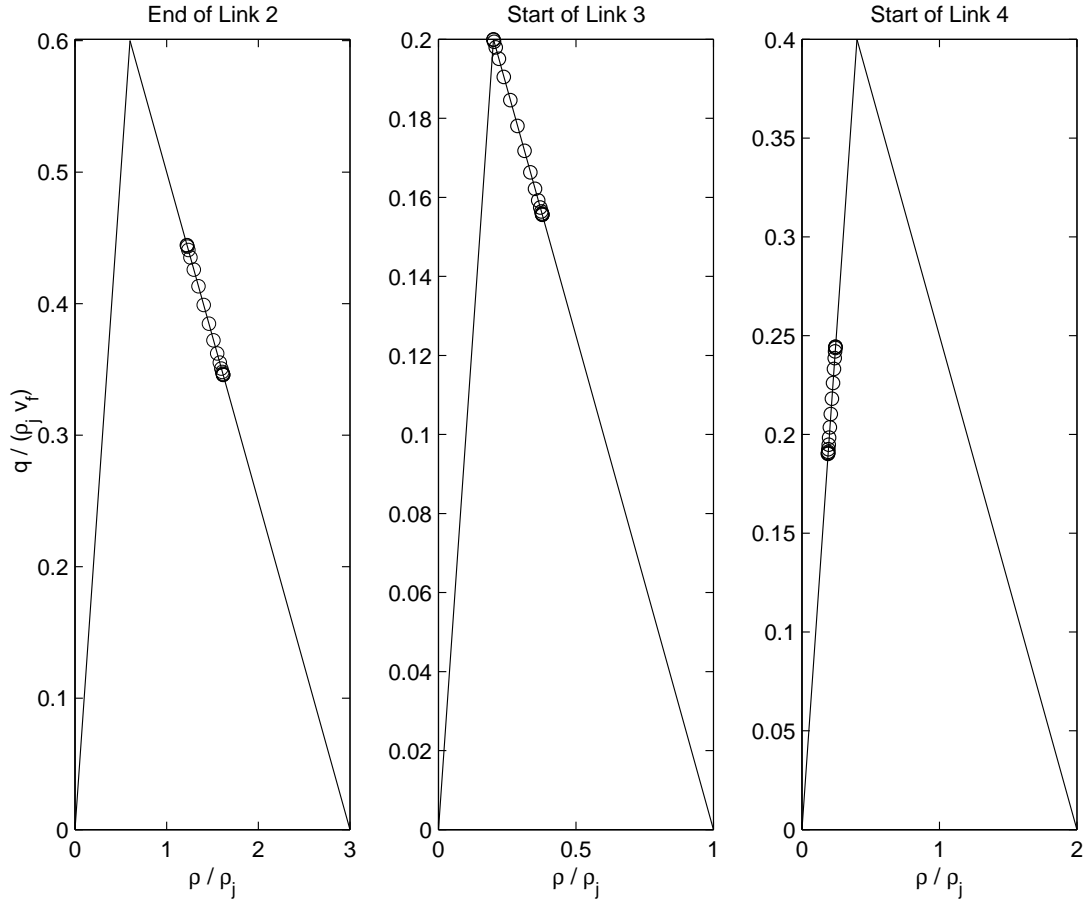


Figure 7.9: Periodic solutions at the end of link 2, start of link 3, and start of link 4 in the (ρ, q) -plane

$$q(t) = \begin{cases} \bar{q} + (\hat{q} - \bar{q}) / \{1 + \exp[-\alpha(\hat{\rho} - \bar{\rho})(t - T/4)]\} & \text{when } t \in [0, T/2), \\ \bar{q} + (\hat{q} - \bar{q}) / \{1 + \exp[\alpha(\hat{\rho} - \bar{\rho})(t - 3T/4)]\} & \text{when } t \in [T/2, T). \end{cases} \quad (7.10)$$

As shown in Figure 7.10, density, flow-rate, and travel speed at the end of link 2 can be well approximated with $\alpha = 500$, and the average of q_2 in a period is equal to $0.4\rho_j v_f \approx 2q_c$. Therefore, this pattern is stable.

Solutions at other locations on link 2, or locations on links 3 and 4 share similar structure as in Equation 7.8-Equation 7.10, but the phase or amplitude may be

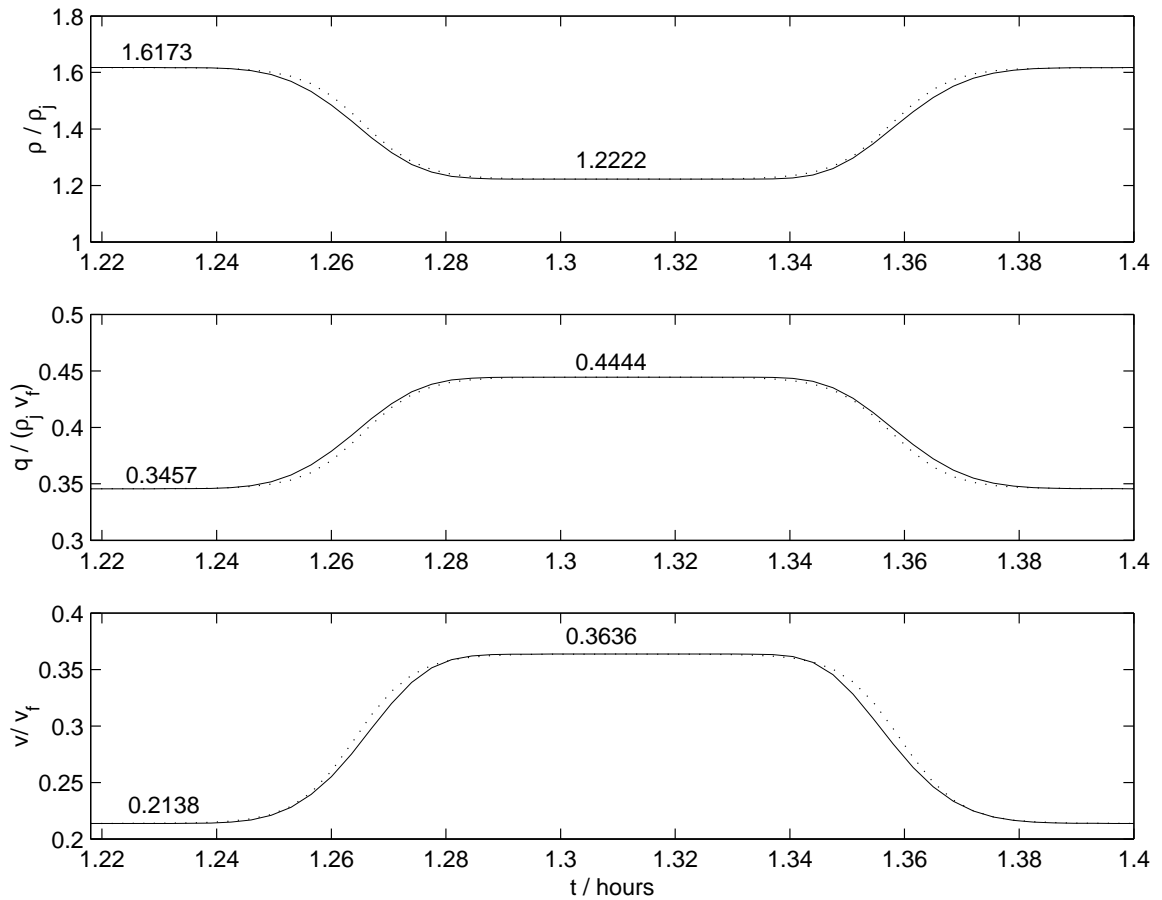


Figure 7.10: Structure of periodic solutions on link 2

different.

7.3.4 Discussions

From Figure 7.7, we can see that we can observe several periods at the same time only on link 2, although traffic on links 3 and 4 are also periodic. Therefore, these periodic waves can be considered to exist on the link upstream to a diverge and a merge when the proportion satisfies a certain condition. The special road structure, i.e., a diverge and a merge, can be considered as the generator of periodic solutions.

We can also see that the period is determined by the length of links between the diverge and merge. In addition, possible approximation of the periodic solutions are provided.

This study shows the effect of network structure on traffic dynamics. We expect more un-revealed solutions patterns exist in more complicated road networks. In the future, it will also be interesting to study the propagation of periodic solutions in road networks. It is not hard to check that when traffic demand decreases, the periodic solutions will disappear.

Since periodic solutions have important negative impact on driver's behavior and vehicles' emission, this study will help to resolve such kind of solutions.

7.4 Conclusions

In this chapter, with the MCKW simulation model, we studied equilibrium states in a demonstration network and oscillations caused by a special network structure.

In Section 7.2, we showed that traffic dynamics on a network approach equilibrium states with constant boundary conditions. Against different combination of traffic commodities, solutions of equilibrium states and the performance of the road network were carefully examined. We further discussed possible relationship between these equilibrium states and the user-equilibrium. Traffic equilibrium states in a road network can be used pursuing important concepts in many network traffic studies, such as traffic assignment, origin demand estimation, etc.

In Section 7.3, we revealed the existence of periodic solutions in a road network. We showed the structure of periodic solutions, whose period is solely dependent on the network structure. This study shows that, in a road network, special network

structure may cause stop and go oscillatory waves.² The periodic oscillations are in fact a new type of kinematic waves initiated from simple, jump initial conditions. From this study, we expect more complicated kinematic waves when more complicated networks are considered.

Studies in this chapter show that, with the MCKW simulation, we are able to study more complicated kinematic waves in a road network. This is important for understanding traffic dynamics as demonstrated that complicated traffic phenomena can be caused by network topology and O/D demand pattern. However, other factors may also contribute to stop and go waves in a realistic network.

²Another type of vehicle clusters are shown to exist in higher-order models (Kerner and Konhäuser, 1994; Jin and Zhang, 2003a).

Chapter 8

Conclusions

8.1 Summary

The original kinematic wave theory, also known as the Lighthill-Whitham-Richards theory (Lighthill and Whitham, 1955b; Richards, 1956), explains traffic dynamics of single origin/destination traffic on a linear road with kinematic waves, including decelerating (shock) waves and accelerating (expansion or rarefaction) waves. In this dissertation, we study traffic phenomena in a road network within the framework of kinematic waves. We have theoretically and numerically investigate traffic dynamics for link inhomogeneities, junctions, and mixed-type vehicles. Furthermore, we have developed a simulation platform of multi-commodity network traffic and studied some network traffic phenomena.

The major results of this dissertation are as follows.

1. In Chapter 2, we reformulate the Lighthill-Whitham-Richards model into a non-linear resonant system for link bottlenecks such as lane-drops. We then show that there is an additional type of kinematic waves, namely, standing (transition) waves. A standing wave always stays at the inhomogeneity spot, and

traffic on its both sides has the same flow-rate but different velocities. We further solve the Riemann problem by ten combinations of shock, rarefaction, and transition waves. The wave solutions are summarized and shown to be consistent with solutions by the supply-demand method. Using numerical simulations, we have also shown how traffic queues up in the region upstream to a link bottleneck.

2. In Chapter 3, we take a closer look at existing kinematic wave models for merging traffic within the supply-demand framework. In particular, we study the distribution scheme, which helps to uniquely determine traffic flow from each upstream branch to the downstream link. Further, we propose a “fairness” condition, under which the out-flow from each upstream branch is proportional to its demand. This condition yields the simplest distribution scheme, which is the only valid distribution independent of downstream conditions. We also show that it can capture the key characteristics of a merge and leads to a merge model that is computationally efficient and easy to calibrate. Furthermore, we show that the new distribution scheme is well-defined and qualitatively sound. With numerical simulations, we demonstrate that the distribution scheme produce convergent solutions.
3. In Chapter 4, we propose a new kinematic wave model for highway diverges. Based on the assumption that, in a short time interval, diverging traffic flows are independent of each other, dynamics of traffic to a downstream link can be described by a system of non-strict conservation laws, or a nonlinear resonant system, whose Riemann problem can be solved by seven types of wave combinations. These waves are called as instantaneous kinematic waves. Further, we show that this model is equivalent to a supply-demand method with modified

definitions of traffic demands of diverging traffic. With numerical simulations, we show that this model is consistent with some existing rules on diverging traffic.

4. In Chapter 5, we study traffic dynamics with mixed-type vehicles, for which we find an additional family of kinematic waves, contact waves. We carefully study the wave solutions of the Riemann problem and develop a Godunov method for solving the model. Using simulations, we demonstrate how mixed traffic evolves on a road link and show that the First-In-First-Out (FIFO) principle is always observed.
5. In Chapter 6, we propose a multi-commodity kinematic wave (MCKW) model of network traffic flow. In this model, we apply the models studied in the previous chapters for different network components and classify vehicles into a number of commodities according to their paths. The proportions of commodities in a road cell are updated based on the fact that traffic is anisotropic. We then show that this model yields solutions, whose departure from the FIFO principle is in the order of a time interval. This model is macroscopic, but is able to provide individual vehicles' trajectories and travel times by using cumulative curve. We also propose an implementation of the MCKW simulation and carefully design the data structure for network topology, traffic characteristics, and simulation algorithms. Our numerical simulations demonstrate that the numerical results converge to FIFO solutions.
6. In Chapter 7, we first study equilibrium states in a road network with a single origin-destination (O/D) pair and two routes. We demonstrate the formation of an equilibrium state. After examining the relationship between equilibrium states and the distribution of vehicles to different routes, we find that multiple

equilibrium status may exist for the same O/D flow but different route distributions. We then show the formation of periodic oscillations for certain network structure and route distributions. The periodic oscillations are in fact a new type of kinematic wave in a road network. We then discuss their structure and properties.

The kinematic wave models of network vehicular traffic studied in this dissertation are theoretically rigor, numerically reliable, and computational efficient. These studies help better understand traffic dynamics in a road network, in particular the formation and propagation of traffic congestion, and establish a solid foundation for applications in traffic control and management.

8.2 Future research directions

There are three directions in which we could extend this dissertation research: further investigation of the kinematic wave theories, enhancement of the MCKW simulation model, and applications of the MCKW simulation model to solve real-world problems.

8.2.1 Further investigations of the kinematic wave theories

In studies of inhomogeneous links (Chapter 2) and diverges (Chapter 4), the kinematic wave theories are shown to yield consistent results with the supply-demand method given proper definitions of traffic supply and demand. That is, the supply-demand method can be considered as the discrete form of the corresponding continuous kinematic wave theory. It is also interesting to directly prove that the discrete model in the supply-demand method converge to the corresponding kinematic wave theory. For the inhomogeneous LWR model under jump initial conditions, for example, we can find solutions by the supply-demand method and obtain a time series for each

cell. Then will these series get closer to the wave solutions predicted in Chapter 2 as the length of a time interval keeps decreasing? The answer to this problem will help to understand the continuous kinematic wave model of merging traffic, whose discrete model is simple and clear (Chapter 3). In addition, the diverging model (Chapter 4) is an instantaneous approximation, also in discrete form, whose continuous counterpart is another interesting topic. One probable alternative approach is to introduce appropriate fundamental diagram as in (Daganzo, 1997).

The kinematic wave models studied in this dissertation are deterministic. However, these models can be extended to include randomness in a road network. For example, non-recurrent traffic congestion is generally caused by accidents or work zones, which are reflected by a change in the number of lanes. Since the number of lanes has been included in the models we studied, these stochastic effects could be considered in the kinematic waves. As another example, weaving effects on traffic dynamics could also be studied in a similar fashion.

Finally, it is of interest to study kinematic waves that arise from the traffic dynamics of other traffic systems, such as those with special lanes, special vehicles, and so on.

8.2.2 Calibration, validation, and enhancement of the MCKW simulation model

The enhancement of MCKW simulation model will be carried out in three aspects. First, we can incorporate new kinematic wave theories so that it is capable of simulating traffic systems with more components, such as different types of vehicles and special lanes. To achieve this, traffic has to be categorized into more commodities, and more complicated data and program structures are expected. Second, we can

improve the computational efficiency of the MCKW simulation for large-scale road networks. In this dissertation, the solution methods, either the supply-demand methods or the Godunov methods, are of first order. One improvement can be made by applying higher-order methods in the MCKW model (e.g., Daganzo, 1999a; Colella and Puckett, 2000), which are more efficient. Another approach is to incorporate parallel algorithms and more efficient memory management methods. Finally, we can design the programming of the simulation model in order to satisfy different requirements of different applications. For example, we need very detailed information when studying traffic dynamics and phenomena, but need less information in traffic assignment. Thus it will be better to use two different programming structure for these two applications.

The MCKW simulation model, as other simulation models, is also subject to calibration and validation with observed traffic dynamics. A conceptual approach is to calibrate and validate the simulation model first for inhomogeneous links, merges, and diverges and then for a whole road network. We can check existing databases or collect data by ourselves in the calibration and validation process. In many data sets collected by loop detectors, however, volumes (the number of vehicles passing a detector) are not conserved over a link. This inconsistency will be fatal for calibrating the kinematic wave models, since the fundamental assumption in these models is traffic conservation. Thus, it may be necessary to seek advanced measures, such as video-taping or by satellite sensing techniques, to provide the ideal accuracy in data in these studies.

8.2.3 Applications of the MCKW simulation model

First, using the MCKW simulation model, we can better understand the formation and characteristics of traffic congestion. This will form a foundation to alleviate it

by either expansion of infrastructure or traffic control and management.

Second, the MCKW simulation model can be applied in evaluating strategies in infrastructure expansion and traffic operations and management. For example, we could develop and evaluate on-ramp metering and arterial signal control algorithms by using the MCKW model, in which signals have been incorporated in the computation of traffic demand (see Chapter 3). In addition, in simulation-based dynamic traffic assignment, the MCKW model can be used as a loading model.

Finally, the MCKW simulation model can be used to estimate the travel demands in a road network with observed traffic conditions at a number of locations and can be further applied in regional and transportation plan.

Bibliography

- A. Aw and M. Rascle. Resurrection of “second order” models of traffic flow. *SIAM Journal on Applied Mathematics*, 60(3):916–938, 2000.
- J. H. Banks. The two-capacity phenomenon: some theoretical issues. *Transportation Research Record*, 1320:234–241, 1991.
- G. Cameron and G. Duncan. Paramics: parallel microscopic simulation of road traffic. *Journal of Supercomputing*, 10:25–53, 1996.
- D. Chowdhury, L. Santen, and A. Schadschneider. Statistical physics of vehicular traffic and some related systems. *Physics Reports*, 329(4-6):199–329, 2000.
- P. Colella and E. G. Puckett. *Modern Numerical Methods for Fluid Flow*. 2000. In draft.
- K. Courage and C. Wallace. *TRANSYT/7F User’s Guide*. Federal Highway Administration, Washington, DC, 1991.
- R. Courant, K. Friedrichs, and H. Lewy. ber die partiellen differenzgleichungen der mathematischen physik. *Mathematische Annalen*, 100:32–74, 1928.
- C. F. Daganzo. The cell transmission model: a dynamic representation of highway

- traffic consistent with hydrodynamic theory. *Transportation Research B*, 28(4): 269–287, 1994.
- C. F. Daganzo. The cell transmission model II: Network traffic. *Transportation Research B*, 29(2):79–93, 1995a.
- C. F. Daganzo. Properties of link travel time functions under dynamic loads. *Transportation Research Part B*, 29(2):95–98, April 1995b.
- C. F. Daganzo. Requiem for second-order fluid approximations of traffic flow. *Transportation Research B*, 29(4):277–286, 1995c.
- C. F. Daganzo. The nature of freeway gridlock and how to prevent it. In *The International Symposium on Transportation and Traffic Theory*, Lyon, France, 1996.
- C. F. Daganzo. A continuum theory of traffic dynamics for freeways with special lanes. *Transportation Research B*, 31(2):83–102, 1997.
- C. F. Daganzo. The lagged cell-transmission model. In *The 14th International Symposium on Transportation and Traffic Theory*, Jerusalem, Israel, 1999a.
- C. F. Daganzo. Remarks on traffic flow modeling and its applications. In *Proc. Traffic and Mobility - Simulation*, Aachen, Germany, 1999b.
- C. F. Daganzo. A behavioral theory of multi-lane traffic flow. Part I: Long homogeneous freeway sections. II: Merges and the onset of congestion. *Transportation Research B*, 36:131–169, 2002.
- C. F. Daganzo, M. J. Cassidy, and R. L. Bertini. Possible explanations of phase transitions in highway traffic. *Transportation Research A*, 33:365–379, 1999.

- C. F. Daganzo, W.-H. Lin, and J. M. Del Castillo. A simple physical principle for the simulation of freeways with special lanes and priority vehicles. *Transportation Research B*, 31(2):103–125, 1997.
- J. M. Del Castillo and F. G. Benitez. On the functional form of the speed-density relationship - I: General theory. *Transportation Research B*, 29(5):373–389, 1995a.
- J. M. Del Castillo and F. G. Benitez. On the functional form of the speed-density relationship - II: Empirical investigation. *Transportation Research B*, 29(5):391–406, 1995b.
- J. S. Drake, J. L. Schofer, and A. D. May. A statistical analysis of speed-density hypotheses. *Highway Research Record*, 156:53–87, 1967.
- Federal Highway Administration. *NETSIM User Manual*. Department of Transportation, USA, 1998.
- D. C. Gazis, R. Herman, and R. W. Rothery. Nonlinear follow-the-leader models of traffic flow. *Operations Research*, 9(4):545–567, 1961.
- S. K. Godunov. A difference method for numerical calculations of discontinuous solutions of the equations of hydrodynamics. *Matematicheskii Sbornik*, 47:271–306, 1959. In Russian.
- H. Greenberg. An analysis of traffic flow. *Operations Research*, 7(1):79–85, January - February 1959.
- B. D. Greenshields. A study in highway capacity. *Highway Research Board Proceedings*, 14:448–477, 1935.
- F. L. Hall, B. L. Allen, and M. A. Gunter. Empirical analysis of freeway flow-density relationships. *Transportation Research A*, 20:197, 1986.

- D. Helbing. *Verkehrsdynamik: Neue physikalische Modellierungskonzepte*. Springer, Berlin, 1997.
- M. Herrmann and B. S. Kerner. Local cluster effect in different traffic flow models. *Physica A*, 255:163–198, 1998.
- H. Holden and N. H. Risebro. A mathematical model of traffic flow on a network of unidirectional roads. *SIAM Journal on Mathematical Analysis*, 26(4):999–1017, 1995.
- S. P. Hoogendoorn and P. H. L. Bovy. Continuum modeling of multiclass traffic flow. *Transportation Research B*, 34(2):123–146, 2000.
- E. I. Isaacson and J. B. Temple. Nonlinear resonance in systems of conservation laws. *SIAM Journal on Applied Mathematics*, 52(5):1260–1278, 1992.
- R. Jayakrishnan. *In-vehicle information systems for network traffic control: a simulation framework to study alternative guidance strategies*. PhD thesis, The University of Texas at Austin, 1991.
- R. Jayakrishnan, H. S. Mahmassani, and T.-Y. Hu. An evaluation tool for advanced traffic information and management systems in urban networks. *Transportation Research C*, 2:129, 1994.
- R. Jiang, Q.-S. Wu, and Z.-J. Zhu. A new continuum model for traffic flow and numerical tests. *Transportation Research B*, 36:405–419, 2002.
- W. L. Jin and H. M. Zhang. A kinematic wave traffic flow model for diverges, Part II: The coupled version. 2001a. Working paper.
- W. L. Jin and H. M. Zhang. Solving the payne-whitham traffic flow model as a hyperbolic system of conservation laws with relaxation. 2001b. In draft.

- W. L. Jin and H. M. Zhang. An instantaneous kinematic wave theory of diverging trac. 2002. Submitted.
- W. L. Jin and H. M. Zhang. The formation and structure of vehicle clusters in the payne-whitham traffic flow model. *Transportation Research B*, 37(3):207–223, March 2003a.
- W. L. Jin and H. M. Zhang. The inhomogeneous kinematic wave traffic flow model as a resonant nonlinear system. *Transportation Science*, 37(3):294–311, August 2003b.
- W. L. Jin and H. M. Zhang. On the distribution schemes for determining flows through a merge. *Transportation Research B*, 37(6):521–540, July 2003c.
- W. L. Jin and H. M. Zhang. Studies on a nonequilibrium continuum traffic flow model with frozen “sound wave” speed. January 2003d. Presented at TRB 2003 Annual Meeting.
- W. L. Jin, H. M. Zhang, and E. G. Puckett. Continuum traffic flow model of highway merges. *Transportation Research B*, 2002. Working paper, UC Davis.
- B. S. Kerner and P. Konhäuser. Structure and parameters of clusters in traffic flow. *Physical Review E*, 50(1):54–83, 1994.
- H. Kita. A merging-giveaway interaction model of cars in a merging section : a game theoretic analysis. *Transportation Research Part A*, 33(3):305–312, 1999.
- M. Koshi, M. Iwasaki, and I. Ohkura. Some findings and an overview on vehicular flow characteristics. In V. F. Hurdle, R. Hauer, and G. N. Stewart, editors, *Proceedings of the Eighth International Symposium on Transportation and Traffic Theory*, pages 403–426, Toronto, Ontario, 1983. University of Toronto Press.

- R. Kuhne and P. Michalopoulos. Continuum flow models. In *Traffic flow theory: A state-of-the-art report*, chapter 5. 1992.
- P. D. Lax. *Hyperbolic systems of conservation laws and the mathematical theory of shock waves*. SIAM, Philadelphia, Pennsylvania, 1972.
- J. Lebacque. Two-phase bounded acceleration traffic flow model: analytical solutions and applications. *TRB Annual Meeting*, 2003.
- J. P. Lebacque. The godunov scheme and what it means for first order traffic flow models. In *The International Symposium on Transportation and Traffic Theory*, Lyon, France, 1996.
- H. Y. Lee, H.-W. Lee, and D. Kim. Traffic states of a model highway with on-ramp. *Physic A*, 281:78–86, 2000.
- J. D. Lenonard II. A tool for evaluating freeway congestion. Technical report, Georgia Institute of Technology, January 1998.
- R. J. LeVeque. Some traffic flow models illustrating interesting hyperbolic behavior. In *SIAM Annual Meeting*, San Diego, CA, 2001.
- R. J. LeVeque. *Finite volume methods for hyperbolic problems*. Cambridge University Press, Cambridge; New York, 2002.
- T. Li. Global solutions of nonconcave hyperbolic conservation laws with relaxation arising from traffic flow. *Journal of Differential Equations*, 190(1):131–149, 2003.
- M. J. Lighthill and G. B. Whitham. On kinematic waves: I. Flood movement in long rivers. *Proceedings of the Royal Society of London A*, 229(1178):281–316, 1955a.

- M. J. Lighthill and G. B. Whitham. On kinematic waves: II. A theory of traffic flow on long crowded roads. *Proceedings of the Royal Society of London A*, 229(1178): 317–345, 1955b.
- L. Lin, J. B. Temple, and J. Wang. A comparison of convergence rates for godunov’s method and glimm’s method in resonant nonlinear systems of conservation laws. *SIAM Journal on Numerical Analysis*, 32(3):824–840, 1995.
- G. Liu, A. S. Lyrintzis, and P. G. Michalopoulos. Modelling of freeway merging and diverging flow dynamics. *Applied Mathematical Modelling*, 20, 1996.
- Massachusetts Institute of Technology. *DYNAMIT/MITSIM*. Cambridge, MA, 1999. <http://its.mit.edu>.
- J. C. Muñoz and C. Daganzo. Structure of the transition zone behind freeway queues. *Transportation Science*, 37(3):312–329, August 2003.
- J. C. Muñoz and C. F. Daganzo. The bottleneck mechanism of a freeway diverge. *Transportation Research Part A*, 36(6):483–505, 2002.
- G. F. Newell. Nonlinear effects in the dynamics of car following. *Operations Research*, 9(2):209, March - April 1961.
- G. F. Newell. A simplified theory of kinematic waves in highway traffic I: General theory. II: Queuing at freeway bottlenecks. III: Multi-destination flows. *Transportation Research B*, 27:281–313, 1993.
- G. F. Newell. Delays caused by a queue at a freeway exit ramp. *Transportation Research B*, 33:337–350, 1999.
- M. Papageorgiou. Dynamic modelling, assignment and route guidance in traffic networks. *Transportation Research B*, 24(6):471–495, 1990.

- M. Papageorgiou, H. Hadj-Salem, and F. Middelham. ALINEA local ramp metering - summary of field results. *Transportation Research Record*, 1603:90–98, 1997.
- H. Payne. FREFLO: a macroscopic simulation model of freeway traffic. *TRB Transportation Research Board*, 722:68–77, 1979.
- H. J. Payne. Models of freeway traffic and control. In *Mathematical Models of Public Systems*, volume 1 of *Simulation Councils Proceeding Series*, pages 51–60, 1971.
- L. A. Pipes. Car-following models and the fundamental diagram of road traffic. *Transportation Research*, 1:21–29, 1967.
- P. I. Richards. Shock waves on the highway. *Operations Research*, 4:42–51, 1956.
- S. Schochet. The instant response limit in whitham’s nonlinear traffic model: uniform well-posedness and global existence. *Asymptotic Analysis*, 1:263–282, 1988.
- D. Schrank and T. Lomax. The 1999 annual mobility report: information for urban america. Technical report, Texas Transportation Institute, The Texas A&M Universtiy System, 1999.
- Y. Sheffi. *Urban Transportation Networks: Equilibrium Analysis with Mathematical Programming Methods*. Prentice Hall, Englewood Cliffs, NJ, 1984.
- E. Smith and E. Noel. Assessment of the impact of an automated lane on freeway operations. *Institute of Transportation Engineers 1995 Compendium of Technical Papers*, pages 41–47, 1995.
- J. Smoller. *Shock waves and reaction-diffusion equations*. Springer-Verlag, New York, 1983.

- Texas Transportation Institute (TTI). *PASSER II-90 Microcomputer User's Guide*. Texas A&M University, College Station, Texas, 1991.
- TRANSIMS. *TRansportation ANalysis and SIMulation System*. (since 1992) see <http://transims.tsasa.lanl.gov>.
- R. T. Underwood. *Speed, volume and density relationships*, pages 141–188. Yale Bureau of Highway Traffic, New Haven, Connecticut, 1961.
- M. Van Aerde and the Transportation Systems Research Group. *INTEGRATION - Release 2.0, Users Guide*, December 1995.
- R. Vaughan, V. F. Hurdle, and E. Hauer. A traffic flow model with time dependent O-D patterns. In *Ninth International Symposium on Transportation and Traffic Theory*, pages 155–178. VNU Science Press, 1984.
- J. G. Wardrop. Some theoretical aspects of road traffic research. *Proceedings of the Institute of Civil Engineers, Part II*, 1:325–378, 1952.
- G. B. Whitham. *Linear and nonlinear waves*. John Wiley and Sons, New York, 1974.
- G. C. K. Wong and S. C. Wong. A multi-class traffic flow model: an extension of lwr model with heterogeneous drivers. *Transportation Research Part A: Policy and Practice*, 36(9):827–841, November 2002.
- H. M. Zhang. Anisotropic property revisited—when is it violated in traffic flow?
- H. M. Zhang. A theory of nonequilibrium traffic flow. *Transportation Research B*, 32(7):485–498, 1998.
- H. M. Zhang. An analysis of the stability and wave properties of a new continuum theory. *Transportation Research B*, 33(6):387–398, 1999.

- H. M. Zhang. Structural properties of solutions arising from a non-equilibrium traffic flow theory. *Transportation Research B*, 34:583–603, 2000.
- H. M. Zhang. A finite difference model of nonequilibrium traffic flow. *Transportation Research B*, 35(5):337–365, 2001a.
- H. M. Zhang. New perspectives on continuum traffic flow models. *Journal of Networks and Spatial Economics*, 1(1):9–33, 2001b. Special issue on traffic flow theory.
- H. M. Zhang. A non-equilibrium traffic model devoid of gas-like behavior. *Transportation Research B*, 36(3):275–290, 2002.
- H. M. Zhang and T. W. Kim. Transient and steady state behavior of car-following in mixed traffic on a ring road. Working paper, Institute of Transportation Studies, Davis, 2000.